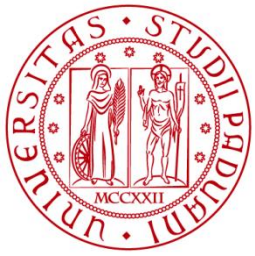

UNIVERSITÀ DEGLI STUDI DI PADOVA

Universita degli Studi di Padova

Dipartimento di Biologia

SCUOLA DI DOTTORATO DI RICERCA in BIOSCIENZE E BIOTECHNOLOGIE

INDIRIZZO: BIOLOGIA CELLULARE

CICLO XXVIII

A FRET based high content screen identifies DMPK as a novel tether of ER and mitochondria

Direttore: Ch.mo Prof. Paolo Bernardi

Coordinatore: Ch.mo Prof. Paolo Bernardi

Supervisore: Ch.mo Prof.sse Vera Bianchi

Co-supervisore: Ch.mo Prof. Luca Scorrano

Dottoranda: Sowmya Lakshminarayanan

31 Gennaio **2016**

Table of Contents

1. Riassunto dell'attività svolta

La comunicazione tra organelli cellulari è una delle principali funzioni delle cellule eucariotiche e di numerosi processi di segnalazione (Bravo-Sagua et al., 2014). Uno dei cross-talk intracellulari maggiormente caratterizzati è quello tra reticolo endoplasmatico (ER) e mitocondri (Lopez-Crisosto et al., 2015). Definiti anche come “Membrane ER Associate ai Mitocondri” (MAMs), l’esistenza dei contatti tra mitocondri ed ER è stata scoperta più di 50 anni fa tramite studi di microscopia elettronica (Copeland and Dalton, 1959). Gli anni 90 videro poi il primo punto di svolta per la comprensione del significato funzionale dei MAMs quando Vance e Rizzuto et al., dimostrarono che lo scambio di fosfolipidi ed il trasferimento di ioni calcio avviene proprio nei punti di giunzione tra questi due organelli. Malgrado l’importanza di questi contatti nei processi metabolici e patologici, finora solo per poche proteine è stata descritta la funzione di mantenimentodell’integrità strutturale dei MAMsnei mammiferi (Lopez-Crisosto et al., 2015). MFN2 è stato il primo componente strutturale dei MAMs ad essere identificato. La componente di Mfn2localizzata sulla membrana dell’ER è in grado di formare interazioni omo- ed eterotipiche con molecole di MFN2 e MFN1 presenti nella membrana mitocondriale, formando così un ponte tra i due organelli. Poiché una residua giustapposizione tra mitocondri ed ER è stata osservata anche in cellule $Mfn2^{-/-}$, ne consegue che devono esistere altre molecoleancora da scoprire coinvolte nella modulazione dei contatti tra i due organelli. Abbiamo quindi voluto eseguire uno screening genomico su larga scala per identificare i componenti strutturali delle giunzioni tra mitocondri ed ER in fibroblasti embrionali murini (MEF). Per fare ciò, abbiamo sfruttato al meglio un biosensore basato sulla FRET sviluppato da Csordas et al., in cui la proteina CFP è fusa con il dominio funzionale FRB, e la proteina YFP con il dominio funzionale FKBP. Queste proteine andranno a legarsi rispettivamente all’ER (tramite la sequenza di localizzazione Sac1) ed ai mitocondri (tramite la sequenza di localizzazione Akap) (Csordas et al., 2010). Abbiamo modificato questo biosensore affinchéentrambe le molecole fluorescenti si trovassero su unico

mRNA e la loro espressione fosse guidata da un singolo promotore, tramitel'introduzione tra i loro cDNA del peptide auto-catalitico Tav2a (Luke et al., 2008). Grazie ai domini di legame FKBP e FRB, che interagiscono dopo l'aggiunta di rapamicina, siamo stati in grado di misurare sia il livello basale sia il massimo livello di giustapposizione tra i due organelli. Abbiamo poi utilizzato questo biosensore così modificato per seguire uno screening genetico su larga scala in modo da identificare le molecole che avvicinano o allontanano ER e mitocondri, definite rispettivamente come "tethers" e "spacers". Abbiamo analizzato le immagini non processate ottenute tramite lo screening e calcolato per ogni gene il numero massimo di contatti possibili. A seguito dell'analisi automatizzata delle immagini e successivamente dell'analisi statistica, effettuata utilizzando il pacchetto cellHTS2 tramite la programmazione in R,dei dati dello screening primario effettuato su ~10000 geni, abbiamo classificato il 14.4% dei geni come tethers tra ER e mitocondri (i.e., geni che una volta rimossi aumentano la distanza tra i due organelli) e il 5.3% come spacers (i.e., geni che una volta rimossi diminuiscono la distanza tra i due organelli). L'analisi dei processi cellulari in cui questi geni risultano coinvolti tramite i programmi Reactome ePanther ha evidenziato sia pathways già noti sia altri che devono ancora essere esplorati in termini di comunicazione tra mitocondri ed ER. L'analisi della localizzazione subcellulare delle proteine classificate come "tethers" ha rivelato otto proteine per cui è stata predetta la localizzazione sia all'ER sia nella membrana mitocondriale esterna (OMM). Una di queste otto proteine è DMPK (myotonicdystrophyproteinkinase), abbiamo quindi ulteriormente caratterizzato come DMPK tether tra ER e mitocondri. DMPK risulta mutata nella distrofia miotonica 1 (DM1) (Cho and Tapscott, 2007). Questa proteina presenta sei isoforme note dovute asplicing alternativo sia nell'uomo sia nel topo (Wansink et al., 2003). Il ruolo di DMPK nella distrofia miotonica non è ancora completamente chiarito, in quanto il modello animale KO per questo gene sviluppa tardivamente miopatia e disfunzioni cardiache contrattili (Reddy et al., 1996). La localizzazione subcellulare delle varie isoformeè stata riportata ai mitocondri o all'ER, tuttavia molta meno enfasi è stata data alla sua rilevanza funzionale.

In conclusione, abbiamo sviluppato un nuovo metodo per determinare la prossimità tra ER e mitocondri ed abbiamo utilizzato questa tecnologia in uno screening genetico su larga scala per identificare nuovi componenti strutturali che regolano i contatti tra i due organelli. I dati ricavati da questo screening mettono in evidenza anche molti processi cellulari in cui le giunzioni tra mitocondri ed ER erano state implicate, ma il loro ruolo non è stato ancora completamente compreso. Le molecole identificate tramite il nostro screen aiuteranno quindi a svelare i componenti molecolari in questi pathways cellulari.

2. Summary

Inter-organelle communication is a key feature of basic eukaryotic cells functions and of numerous cell signaling events(Bravo-Sagua et al., 2014). One of the best-characterized inter-organelle cross talk is that between Endoplasmic Reticulum (ER) and mitochondria(Lopez-Crisosto et al., 2015). Also referred to as mitochondria associated ER-membranes (MAMs), the existence of mitochondria-ER contacts was uncovered 50 years ago through electron microscopic studies(Copeland and Dalton, 1959). The 90s saw the first break-through in functional significance of the MAMs, when Vance and Rizzuto et al., showed that exchange of phospholipids and calcium transfer occurs between the two organelles(Rizzuto et al., 1998; Vance, 1990). Despite the importance of the tether in metabolism and disease(Cali et al., 2013; Giorgi et al., 2015; Vance, 2014), only few proteins have so far been described to maintain the structural integrity of the tether in mammals (Lopez-Crisosto et al., 2015). MFN2was the firststructural tether to be identified. ER localized MFN2 forms homo and heterotypic interactions with mitochondrialMFN2 and MFN1, thus tethering the two organelles. As residual juxtapositionexist in $Mfn2^{-/-}$cells, yet to be discovered tethersmust exist (de Brito and Scorrano, 2008). Hence, we set out to perform a genome wide screening to identify the structural components of the tether in mouse embryonic fibroblasts (MEFs). In order to perform the genome wide screening, we capitalized on the FRET based biosensor developed by Csordaset al., where CFP fused with FRB domain and YFP fused with FKBP domain were targeted to ER (by a Sac 1 signaling sequence) and mitochondria (by an Akap signaling sequence) respectively (Csordas et al., 2010). We modified this biosensor by driving expression of both fluorescent molecules from a single mRNA, introducing between their cDNAs a self-cleaving Tav2A peptide(Luke et al., 2008). This modification allows expressing equimolar level of the proteins. Thanks to FKBP and FRB binding domain, which interacts upon addition of rapamycin, we were

able to study the basal and maximal level of juxtaposition between the two organelles. We then utilized this

modified biosensor to perform a high content screen to identify molecules that either tether or space ER and mitochondria. We termed them as **tethers** and **spacers** respectively. We analyzed raw images from the screen and calculated the maximum number of contacts possible for every gene. Following automated image analysisand statistical analysis using R programming in cellHTS2 package of the primary screen performed on ~10,000 genes, we identified 14.4% genes as ER-mitochondria tethers (i.e., genes that once ablated increase the distance between the two organelles) and 5.3% genes as spacers (i.e., genes that once ablated decrease the distance between the two organelles). Pathway analysis using reactome and Panther predicted both existing and new pathways that are yet to explored in terms of ER-mitochondria communication. Subcellular localization analysis of the tethers revealed eight proteins predicted to be present in both ER and outer mitochondrial membrane (OMM). One of the eight is myotonic dystrophy protein kinase (DMPK) and we have further characterized how DMPK tethers ER and mitochondria. DMPK is mutated in myotonic dystrophy 1 (DM1) (Cho and Tapscott, 2007). Having six known isoforms based on alternate splicing in humans and mouse (Wansink et al., 2003), DMPK's role in myotonic dystrophy is not yet understood completely since the KO model of this gene developed late onset of myopathy and cardiac contractile dysfunction (Reddy et al., 1996). The subcellular localization either to ER or to mitochondria of the isoforms have been identified, although very less emphasis has been given to the functional relevance of different sub-cellular localizations.

In conclusion, we have developed a new method to assess the proximity of ER and mitochondria and we have utilized this technology in a high content screen to identify novel structural components of the tether. The data from the screen has also spanned several existing pathways where ER-mitochondria junction has been implicated but not completely understood.

Hence, the molecules identified from our screen, will help in unraveling the molecular players in these cellular pathways.

3. Introduction

Mitochondria play a fundamental role in several cellular processes ranging from bioenergetics to the amplification of signals necessary for programmed cell death to calcium homeostasis, differentiation, cell division and autophagy(Ferri and Kroemer, 2001; Rizzuto and Pozzan, 2006). Not surprisingly therefore mitochondria are involved in several human diseases, including neurodegenerative disorders and cancer (Schapira A.H. (2000*)*.

The shape of ER is continuous, its membranes occupying nearly 10% of entire cell volume. The ER network can be distinguished into the nuclear envelope and the peripheral ER comprising the ribosome- bound rough ER (RER) and the ribosome-free smooth ER (SER) (Goyal and Blackstone, 2013). The shape and dynamics of ER is with the membrane occupied by both sheet like cisternae and highly curved tubules (Friedman and Voeltz, 2011). The cisternae are thought to be the sites of protein synthesis, while highly curved membrane of tubules is thought to contribute to other functions of ER including calcium and lipid transfer and communicate with other organelles.

One such inter-organelle communication occurs between ER and mitochondria(Bravo-Sagua et al., 2014). The first proposal of the existence of juxtaposition between the ER and mitochondrial outer membrane (OMM) dates back to the sixties (Copeland and Dalton, 1959). Subcellular fractionation studies and electron microscopy (EM) observations identified ER membranes co-purifying with mitochondria (Elgass et al., 2015, Rusinol et al., 1994, Vance 1990). Wide- field digital 3D deconvolution microscopy and electron tomography indicated that ~20% of the mitochondrial surface is in direct contact with the ER at a distance of about 10-

25nm (Csordas et al., 2006). In recent years, several functions including calcium regulation, lipid transfer, apoptosis, cell survival, organelle dynamics, autophagy and inflamasomes formation have been attributed to the tether (Bui et al., 2010; Friedman et al., 2011; Lang et al., 2015; Lopez-Crisosto et al., 2015; Naon and Scorrano, 2014). Yet, the molecular composition of the tether itself is not completely understood. In this thesis, we set out to explore the structural components of ER-mitochondria tether in mammalian cells by means of high content screening.

3.1 Mitochondria

Million years of evolution and yet, carrying still the traits of its bacterial originin its genome, mitochondria as an organelle has taken a center place in eukaryotic cells. The observations that these organelles carry their own DNA and have distinct translation machinery when compared to the major one in the cell led to the theory of endo-symbiosis of alpha-proteobacteria emerging into mitochondria(Margulis, 1971).

The mitochondrial genome (16Kb) encodes 13 protein sub-units linked to respiratory complexes (OXPHOS), rRNA and tRNA component of the mitochondrial translation machinery. Being nicknamed as the “Power house of the cell”, mitochondria was and has been continuously researched for the multitude of functions it carries out other than its major role as ATP producer.

The ultra structure of mitochondria is extremely complex, with the organelle bound by two distinct membranes: the outer membrane (OMM) and the inner membrane (IMM). The IMM is organized into peripheral inner membrane and the *cristae* that are separated from the peripheral inner membrane by narrow tubular junction. The cristae are key mitochondrial structures where the complexes of respiratory chain are localized and oxidative phosphorylation takes place.

Mitochondria have been implicated in several key cellular functions. Their main role in maintenance and utilization of calcium has been well studied. Mitochondria are also involved in apoptosis where they amplify the apoptotic signals once the cell has been committedto die. Recent evidences also bestows on them yet another function of providing membrane for autophagosomes formation upon certain stimuli of stress. Last but not the least, mitochondria is also known to participate in cell division and maintenance of correct organelle shape is a requisite to complete cell division. Dysfunction in any of these processes is associated with several metabolic diseases including cancer and neuro-degenerative diseases.

In recent years, it has been demonstrated that mitochondria reaches out to other organelles in exchange of calcium andother molecules such as lipids. In this thesis, we have investigated the molecules that are involved in tethering mitochondria to ER. Hence the focus of this part of introduction will be on the morphology and dynamics of the organelle.

3.2 Mitochondria dynamics and morphology

The shape of mitochondria in living cells is very heterogeneous and depending on the cell type and energy needs, can either be fragmented or tubular (Bereiter-Hahn and Voth, 1994). Infact the term mitochondrion originates from two Greek words, mitos meaning “thread” and chondron meaning “grain” and was given to this organelle owing to the heterogeneity in its shape as visualised under light microscope. Real-time imaging revealed that individual mitochondrionare dynamic and continuouslymove. The ability of mitochondria to move and fuse is required by the cell to distribute ATP and mitochondrial DNA, whereas mitochondrial division allows the correct redistribution of mitochondrial DNA(Youle and van der Bliek, 2012). It is important to note that mitochondrial dynamics is a complicated process and alterations in

mitochondrial morphology have been implicated in embryonic development, metabolism, apoptosis, and autophagy.

3.2.1 Mitochondrial shaping proteins: Fusion

The key players of mitochondrial fusion are MFN1/MFN2 (Fzo1) and OPA1. Outer mitochondrial fusion protein, Fuzzy onions protein (Fzo1) was the first described fusion protein in Drosophila and was shown to be essential for the genesis of the giant mitochondrial derivative during spermatogenesis (Hales and Fuller, 1997). The yeast ortholog, Fzo1p was shown to be involved in mitotic growth and mating(Hermann et al., 1998). Santel and Fuller discovered its mammalian homologs, Mitofusin 1 and 2 in 2001 (Santel et al., 2003). Mitofusins are large transmembrane GTPasesthat share a high degree of structural similarity (81%) and reside on the outer mitochondrial membrane (OMM) (Chen et al., 2003; Rojo et al., 2002; Santel et al., 2003; Santel and Fuller, 2001). Structural studies revealed an N-terminal GTP binding domain, a coiled-coil domain 1 (HR1) twotransmembrane domains and a coiled-coil domain 2 (HR2). The HR2 domain has been implicated in homo and heterotypic interaction between the mitofusins during the fusion event (Santel et al., 2003). The domain arrangement and fusion mechanism is depicted in the following cartoon:

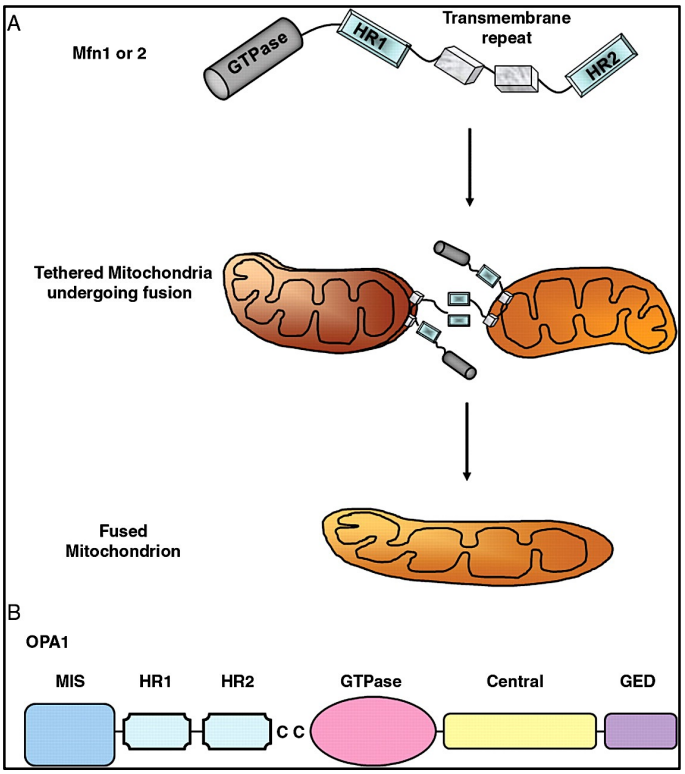

Figure 1: Mitochondrial fusion. The cartoon depicts the molecular structure of MFNs and OPA1 and the process of mitochondrial fusion. Adapted from (Ong and Hausenloy, 2010)

The expression levels of the two mitofusins differ considerably,MFN2being predominantly expressed in brain, skeletal muscle and heart while MFN1 predominantly in heart and testis (Chen et al., 2003). Amongst the two mitofusins, MFN1 was found to have higher GTPase activity (8 fold more active) thanMFN2 and hence to drive fusion (Ishihara et al., 2004). MFN2additionallywas the first identifiedER to mitochondriaphysical tether(de Brito and Scorrano, 2008). A fraction of MFN2, localized on ER membrane undergoes homo/heterotypic interaction with MFN2/MFN1 to form the structural bridge between the two organelles. The juxtaposition was shown to be essential for direct transfer of calcium from ER to mitochondria and to maintain lipid homeostasis (de Brito and Scorrano, 2008). MFN2 also binds and inhibits the proto-oncogene Ras(de Brito and Scorrano, 2009). This inhibition is independent of its role

in tethering the two organelles, thereby emphasizing its role as more than only a fusion protein(de Brito and Scorrano, 2009) .

The fusion of IMM is carried out by Optic atrophy 1 (OPA1), another dynamin-related protein(Alexander et al., 2000; Delettre et al., 2000; Praefcke and McMahon, 2004; Satoh et al., 2003). The *Opa1*gene encodes eight mRNA splice variants (Satoh et al., 2003). Common to all the 8 variants are an N-terminal mitochondrial localization sequence responsible for importing the protein into the mitochondrial inner membrane, a transmembrane domain that anchors OPA1tothe mitochondrial inner membrane; afirst coiled-coil domain involved in protein-protein interactions; theGTPase domain crucial for protein activity; amiddle domain, which participates in tetramerizationand higher-order assembly of OPA1(Ishihara et al., 2006; Zorzano et al., 2010); and a second coiled-coil domain in the C-terminus (the GTPase effector domain, also called the assembly domain) that is crucial for protein activity and mediates the interaction between OPA1 and MFN1/2(Zorzano et al., 2010).The biological function of OPA1 had been elusive since both its over-expression and silencing caused mitochondrial fragmentation (Misaka et al., 2002; Olichon et al., 2003). Our laboratory identified that OPA1 is a core component of mitochondrial fusion and that the fragmentation observed upon its overexpression was a paradoxical consequence of too high OPA1 levels. Indeed, when OPA1 is expressed at moderate-low levels, it drives MFN1-dependent mitochondrial fusion (Cipolat et al., 2004).

In addition to the complexity of the genetic locus, OPA1 also undergoes to refined posttranslational modification that further complicates its biology. Three types of mammalian proteases, presenilin-associated rhomboid-like protease (PARL), i-AAA metalloprotease (YmelL), and m-AAA metalloprotease (paraplegin), are the main regulators of OPA1 cleavagethereby generating the long and the short forms of OPA1 that can be operationally identified on a Western blot(Cipolat et al., 2006, Duvezin-Caubet et al., 2007; Frezza et al., 2006, Song et al., 2007).

3.2.2 Mitochondrial shaping proteins: Fission

Mitochondrial fission process is mediated again by dynamin-likeGTPases that are well conserved amongst yeast, flies and mammals. In mammals, Dynamin related protein (DRP1) carries out mitochondrial fission (Smirnova et al., 2001; Smirnova et al., 1998). DRP1is a cytosolic GTPase, which upon cues for mitochondrial fragmentation, forms oligomers and constrict both outer and inner mitochondrial membrane, thus fragmenting the organelle (Smirnova et al., 2001). Structurally it containsaN -terminal GTPase domain, a central domain and a C-terminal GTPase effector domain (GED). Intramolecular interaction between the GTPase and GED regions appear to be required for full GTPase activity and mitochondrial targeting (Zhu et al., 2004). Mitochondrial fission is prevented in cells expressing the kinase dead mutant K38A suggesting the importance of GTPase activity in fission.

The translocation of DRP1 to mitochondria depends on its phosphorylation status. Phosphorylation of Serine 637 of human DRP1 by cyclic AMP dependent protein kinase (PKA) retains the protein in cytoplasm while dephosphorylation by Calceneurin leads to its recruitment to mitochondria followed by constriction and fission (Cereghetti et al., 2008; Cribbs and Strack, 2007). DRP1 translocation to mitochondria is regulated by other post-translational modifications such as sumoylation and nitrosylation. SUMO-1 and its conjugating enzyme Ubc9 induce mitochondrial fission by stabilizing DRP1 while SUMO-specific protease, SENP5, reduces DRP1 levels (Harder et al., 2004; Zunino et al., 2007).DRP1 may also be subject to *S*-nitrosylation, a post-translational modification, which enhances its pro-fission activity by inducing dimerization and GTPase activity(Cho et al., 2009).

Once translocated onto mitochondria,DRP1 must bind to specific receptor(s). The first identified such receptors in mammals was FIS1(James et al., 2003). FIS1is homologous to the S. cerevisiae protein Fis1p that works as a receptor for yeast DRP1. Human FIS1 (hFis1)

contains an N-terminal domain with five alpha helices (first one essential for oligomerisation and fission and the remaining four forming two tetratrico-peptide repeats), which is exposed to cytoplasm, and a C-terminal domain, which consists of transmembrane domain and a short stretch of amino acids facing the inter-mitochondrial space (Dohm et al., 2004; Yoon et al., 2003).FIS1 is evenly distributed on the outer mitochondrial membrane (OMM) and recruitsDRP1 during mitochondrial fission in yeast(Cerveny, K.M et al., 2001). In mammalian cells, overexpression of hFis1 induces mitochondrial fragmentation, which can result in DRP1 mediated cytochrome c release and apoptosis (Lee et al., 2004). However, reduction of FIS1 levels by siRNA does not disrupt DRP1 localization to mitochondria, even if the residual level of FIS1 could still be sufficient to recruit DRP1 to mitochondria (Lee et al., 2004). The process of how DRP1 and hFis1 lead to mitochondria constriction is depicted in the following figure:

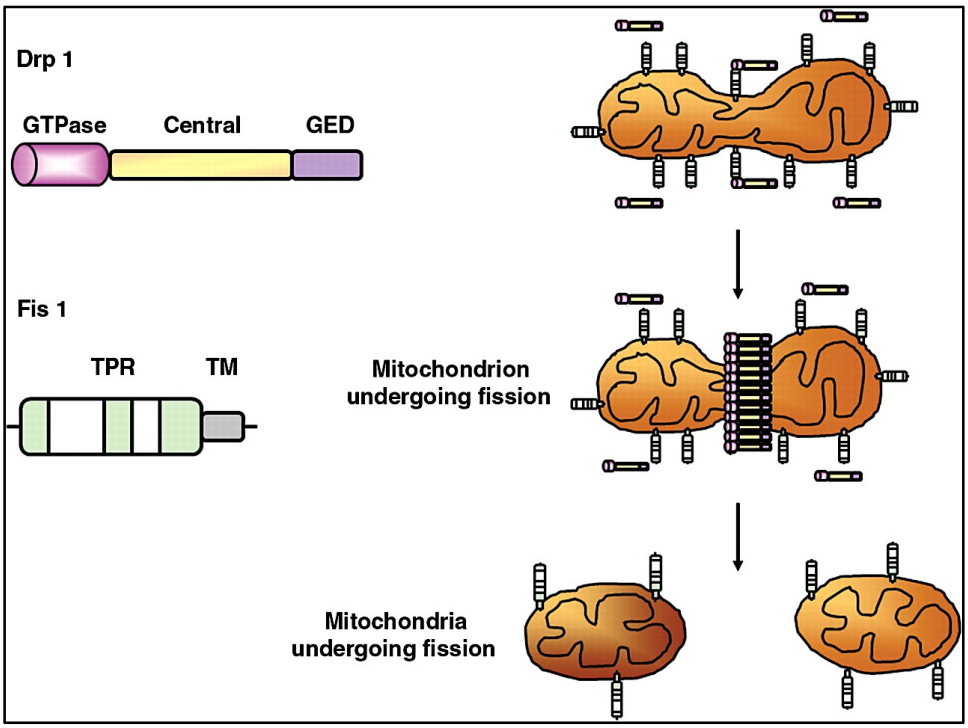

Figure 2: Mitochondrial fission. The cartoon depicts the molecular structure of DRP1 and hFIS1 and the process of mitochondrial fragmentation. Adapted from (Ong and Hausenloy, 2010)

The concept of mitochondrial fission is not completely understood even though its key molecular players have been identifiedDRP1and FIS1 seem to interact, as observed by crosslinking and co-immunoprecipitation(Yoon et al., 2003). Indeed, downregulation of FIS1 only partially diminishes DRP1recruitment to mitochondria (Lee et al., 2004b). This pointed out whether FIS1 isthe only protein needed for DRP1-dependent fission. In 2008 Van der Bliek and colleagues identified a new fission regulator proteinnamed mitochondrial fission factor (MFF). This protein is anchored to the OMMwith the C-terminal trans membrane domain, extruding the bulk of the N-terminalportion containing two short amino acids repeats in the N-terminal half and acoiled-coil domain just upstream of the trans membrane domain into the cytosol.The N-terminal cytosolic region is the one required for Drp1 recruitment, similarlyto Fis1. It is able to both control mitochondrial and peroxisome elongation(Gandre-Babbe and van der Bliek, 2008) and its downregulation is able to diminishthe number of Drp1 puncta on mitochondrial surface (Otera et al., 2010). Thisindicates that Mff and Fis1 share a similar function but act independently.Other components of the mitochondrial fission machinery are the MiD49 andMiD51 (also called mitochondrial elongation factor 1) of 49 and 51 KDarespectively (Palmer et al., 2013). They are amino-terminally anchored in themitochondrial outer membrane with a cytosolic C-terminus. Two independent studies have demonstratedthat MiD49/51 are able to recruit Drp1 to the mitochondrial surface independentlyof other anchor proteins such as Fis1 and Mff (Loson et al., 2013; Palmer et al.,2013). Moreover MiD overexpression causes mitochondrial elongation which isdue to a sequestration and consequent inactivation of Drp1 at the OMM withconsequent unopposed fusion events (Palmer et al., 2013). Finally Fis1, Mff andMID49/51 can promote mitochondrial fission by recruiting Drp1 to the OMM.These proteins can act independently, but it remains possible that they canfunction together in orchestrating this process. Recent evidences reach out to actin-mediated constriction of mitochondrial outer membrane before the recruitment of DRP1 (Korobova et al., 2014; manor et al., 2015). It was also shown that these sites were marked by ER, thus increasing the complexity in this arena

(Friedman et al., 2011). How ER marked tubules undergo scission is discussed later in this thesis.

3.3 ER dynamics and morphology

Mammalian endoplasmic reticulum (ER) is a continuous membrane organelle that comprises the nuclear envelope and peripheral ER, which is composed of ribosome studded sheets called roughER and a network of highly interconnected tubules called smooth ER extending throughout the cell(Goyal and Blackstone, 2013). In yeast, the ER is composed of sheets of varying sizes interspersed with tubules and is located closer to the plasma membrane of the cell. Known for its storage of calcium ions, ER has been bestowed with several different functions including protein and lipid biosynthesis, protein modification, vesicular transport, calcium dynamics and protein quality control(Friedman and Voeltz, 2011).

The ER is a highly dynamic organelle undergoing constant fusion of tubular ER to form three way junctions and sheetsrearrangements(Friedman and Voeltz, 2011). The extent of sheets and tubules vary according to the cellularneeds. For instance, sheets, which are regions where polysomes are bound, are prominent in secretory cells such as pancreatic cells, thus aiding in synthesizing proteins; Tubules, which have highly curved surface and considered to take part in lipid and calcium signaling, on the other hand are predominant in adrenal cells. The organelle has also been studied for its interaction with cytoskeletal structure and other organelles including mitochondria, plasma membrane, vacuole, lipid droplets and peroxisomes(English and Voeltz, 2013; Klopfenstein et al., 1998).

Defects in ER shaping mechanisms have been associated with neurologic disorders such as spastic paraplegias and amyotrophic lateral sclerosis (ALS)(Salinas et al., 2008). In this thesis, we have analyzed the functional capacity of ER to interact with mitochondria leading to a plethora of cellular outcomes. We have specifically addressed the proteins that are involved in maintaining the structural integrity of such juxtaposition between the two organelles.

3.4 ER shape and function

To perform its plethora of functions the ERspecialized in a complex structure, which includes nuclear envelope (NE), cytoplasmic sheets and tubules in the peripheral ER extending until plasma membrane. The NE is by itself a complex structure with outer nuclear membrane (ONM), inner nuclear membrane (INM) and peri-nuclear space. Peripheral ER branches from ONM and has a lumen continuous with peri-nuclear space (Hetzer et al., 2005). Majority of ER is comprised of tubules and cisternae, although their main functions are completely understood. It is suggested that cisternae are the preferred sites for protein translation while tubules perform calcium and lipid transfers. ER tubules are characterized by a high membrane curvature, which is given by reticulon family proteins also known as REEP family (DP1/YOP1). These are large integral membrane proteins with reticulons containing RHD domain, two long transmembrane domains separated by a soluble linker. These domains insert as hairpins, thus increasing the membrane curvature.

In mammalian cells, ER interacts with microtubules (MT) to maintain its shape (Klopfenstein et al., 1998; Terasaki et al., 1986). CLIMP63, an integral membrane protein, anchors ER to MT, thereby maintaining the organelle shape (Klopfenstein et al., 1998). ER tubules also grow along MT by two mechanisms: tip attachment complex (TAC) and ER sliding. TAC events occur when STIM1 and the MT protein EB1 interact and this allows the ER to grow or shrink in accordance with the attached microtubule (Grigoriev et al., 2008). In case of ER sliding, Kinesin 1 and dynein along acetylated MTs pull ER tubules out of the ER membrane (Friedman et al., 2010; Wozniak et al., 2009). The association of ER to microtubules allows the organelle to change its shape depending on cellular events; for instance, during cell migration, differentiation, polarization and cell division (Friedman and Voeltz, 2011). The significance of maintenance of proper distribution and shape has been implicated in several neurological

diseases including Alzheimer's, HSP and during viral infections (Park et al., 2010; Zhao et al., 2001).

3.4.1 Mechanism of ER membrane fusion

ER is a continuous membrane organelle that constantly undergoes fission and fusion to generate or break three way junctions (Goyal and Blackstone, 2013). The dynamic nature of the network and its spread across the cell was attributed to its association with microtubules (Terasaki et al., 1986). An initial observation in yeast that actin-depolymerizing agents didn't entirely disrupt the tubular network led to the finding that Atlastins (Yeast ortholog Sey1) is involved in homotypic fusion of the ER membranes (Hu et al., 2009; Terasaki et al., 1986). Two reports in 2009 found that Atlastins are involved in homotypic membrane fusion in mammals and in Drosophila (Hu et al., 2009; Orso et al., 2009). Atlastins are a class of dynamin related GTPases and are integral membrane proteins (Hu et al., 2009). They consist of two transmembrane domains with the N-terminal GTPase and C-terminal domain facing the cytosol. The localization of Atlastins to the ER tubules is credited to its transmembrane domains, which particularly senses the high curvature of the tubules. In yeast, it was shown that Sey1 interacts with the reticulons to maintain the tubular structure of ER (Hu et al., 2009).Mechanism of Atlastin mediated fusion was deciphered after the crystal structure of the protein in its initial state and GDP bound state was solved in 2011(Bian et al., 2011; Byrnes and Sondermann, 2011). The homotypic fusion mechanism is shownin the following figure.

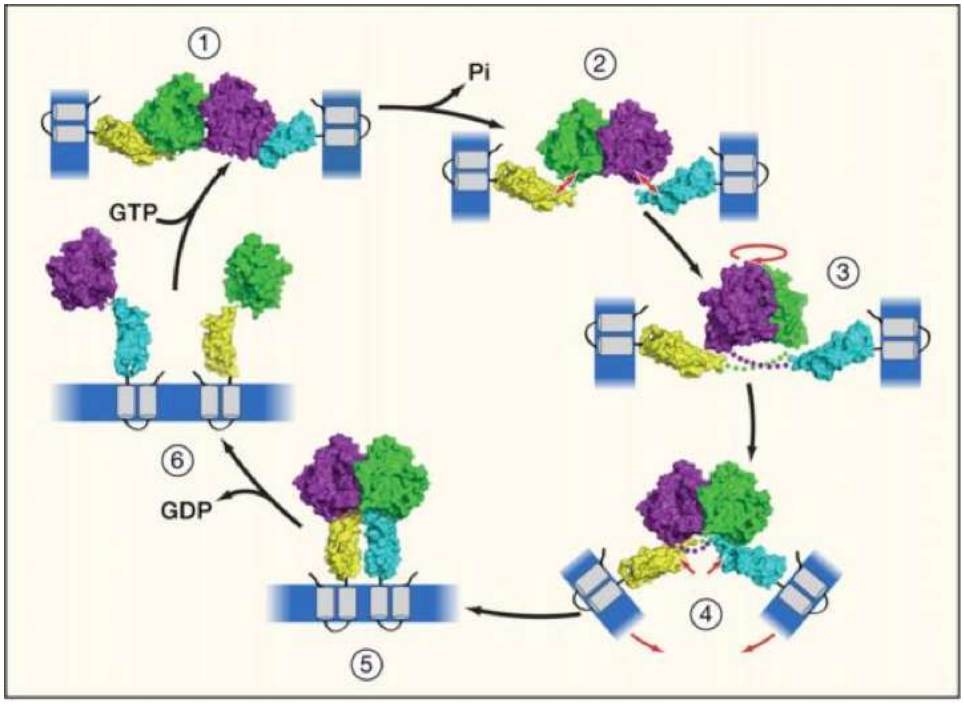

Figure 3: Mechanism of membrane fusion by Atlastins. Membrane fusion starts with hydrolysis of GTP by oppositely oriented Atlastins (step 1) until the exchange of helix bundles in their GDP bound state (step 5). Adapted from (Hu et al., 2011)

Atlastins, sitting on opposite membranes, upon GTP hydrolysis (Prefusion, step 1) undergoes conformational change in their helix bundles and exchanges helix bundles with the opposite membranes in an energy dependent manner, thereby fusing the two membranes in the process (Post fusion, step 5). This process leads to the formation of three-way junctions (Chen et al., 2013). At these junctions, the Lunapark protein, Lnp1p, works in conjunction with the reticulons, DP1/Yop1p, and in antagonism to Atlastin/Sey1p to maintain the network in a dynamic equilibrium(Chen et al., 2015). This transition is conserved amongst Drosophila as well. It is also believed that the C-terminal tail might contribute to the membrane fusion(Orso et al., 2009). The mechanism of ER fusion by Atlastins is thought to be similar to that of homotypic fusion of the outer mitochondrial membranes (Chen et al., 2003).Mutations in Atlastins cause hereditary spastic paraplegia (HSP), a disease that leads to axonal degradation of motor neurons,

emphasizing the correct maintenance of ER morphologyfor human health (Park et al., 2010; Zhao et al., 2001).

3.4.2 ER-organelle contacts

Through its wide spread architecture, ER contacts several sub-cellular organelles including Golgi, mitochondria, plasma membrane, lipid droplets and peroxisomes (English and Voeltz, 2013). ER-mitochondria interaction, which is the main focus of this thesis, is discussed in detailed in the next section (Marchi et al., 2014). ER and Golgi are a part of age-old secretory process involved in anterograde and retrograde transport of proteins (Spang, 2009). Calcium concentration, which is highest in ER at any given time, is set as a gradient in Golgi from trans to cis and this is essential for secretory proteins trafficking. Ceramides are also transported from ER to Golgi where it gets converted to sphingomyelin (Hanada et al., 2009; Lev, 2010). The factors that allow ER-Golgi contact sites are not completely understood.

Peroxisomes, which are essentially derived from ER membrane, are involved in several functions including beta-oxidation of fatty acids (Hoepfner et al., 2005; Tabak et al., 2006). Recent studies have implicated peroxisomes biogenesis with mitochondria through ER-mitochondria contact sites (Mattiazzi Usaj et al., 2015). The interaction between ER and plasma membrane is one of the well-established interactions in inter-organelle crosstalk. The distance between ER and PM has been estimated as ~30nm and is important for calcium regulation, PI metabolism and sterol transfer(English and Voeltz, 2013; Schulz and Prinz, 2007; Stefan et al., 2011). Store operated calcium entry has been studied in various cellular context, when Stim1 on the ER membrane (with its EF domain in the lumen of ER) senses low calcium in ER, oligomerises and interacts with its counterpart, Orai1 on plasma-membrane (Liou et al., 2007;

Liou et al., 2005). Thus the calcium levels are restored in ER, although the structural components that juxtapose the two organelles are not yet completely understood.

3.5 ER-mitochondria connections

This section is covered in a topical review co-authored by me that is here reported as integral part of my thesis work.

Sowmya Lakshminarayanan[1,2] and Luca Scorrano[1,2]

[1]*Department of Biology, University of Padova, Via U. Bassi 58B, 35121 Padova, Italy.*

[2] *Dulbecco-Telethon Institute, Venetian Institute of Molecular Medicine, Via Orus 2, 35129 Padova, Italy.*

Address correspondence to
Luca Scorrano. Email: luca.scorrano@unipd.it

Abstract

Inter-organelle communication amongst the organelles facilitates a dynamic network within the cell to perform different cellular functions. Direct interaction between Endoplasmic reticulum and mitochondria in specialized structures called mitochondrial associated membranes (MAMs) acts a platform for multiple cell functions and have been continuously studied for their implication in human diseases. The advancement in imaging and biochemical methods has led to the rigorous growth of the field in the last few years. In this review, we discuss the molecules identified so far in this compartment emphasizing on their contribution to cell function.

Introduction

Compartmentalization is a key feature of basic cellular functions in eukaryotic cells and it occurs at membrane bound organelles (Bravo-Sagua et al., 2014). The effective spatio-temporal communication amongst the organelles brings out a plethora of cell signaling events. One of the best-characterized inter-organelle cross talk is between Endoplasmic Reticulum (ER) and mitochondria. Also referred to as mitochondria associated ER-membranes (MAMs), their existence was uncovered 50 years ago through electron microscopic studies (Copeland and Dalton, 1959). The biochemical evidence of such contacts came into lime light much later in 1990s when JE Vance observed a “fraction X” which had properties similar to microsomes but sedimented at different density (Rusinol et al., 1994; Vance, 1990). The late 90s saw the first break-through in functional significance of the MAMs when Rizzuto et al., showed that mitochondria are exposed to higher calcium concentration upon its release from ER, suggesting the existence of a proteinaceous link between the two organelles and the existence of calcium hotspots on mitochondria (Mannella et al., 1998; Rizzuto et al., 1998). The exchange of material for phospholipid synthesis in mammals (Shiao et al., 1995; Vance, 2014) and in Yeast (Lang et al., 2015; Michel and Kornmann, 2012; Murley et al., 2015) added to the functional relevance of such tether. Recently, bio-informatics and mass spectrometric analysis has led to discovery of ER-mitochondria extended structure in other non fungi species including *A.castelleni* emphasizing the existence of such complex structures(Wideman et al., 2013).

A distance as low as 10-25 nm between the two organelles explains how proteins located on the membrane of the two organelles interact and tether them. It is fascinating that the juxtaposition of ER on mitochondria is quite dynamic and the two organelles do not fuse thus maintaining distinct structures(Csordas et al., 2006; Lopez-Crisosto et al., 2015).

Since the first electron microscopic observations, the field has progressed rapidly in the recent years, thanks to the availability of various methods to study the structural and functional relevance of such proximities (Elgass et al., 2015; Lopez-Crisosto et al., 2015). Recently, four different proteomics studies of MAM identified approximately 1000 MAM proteins (Horner et al., 2015; Liu et al., 2015; Poston et al., 2013; Zhang et al., 2011). The overlap of proteins amongst these studies was ~ 44%,although this could be attributed to the cell type (Human fibroblast vs mouse brain vs skeletal muscles) or to the pathology (Chronic or acute viral infection) studied, bringing out the complexity in "make and break" of the tether (Lopez-Crisosto et al., 2015). These studies have also raised several interesting questions at the molecular level such as:

(I) Which proteins or protein complexes are involved in tethering the two organelle,

(II) Which proteins are involved in regulation/modulation of the juxtaposition and how do these "regulatory" proteins find their way to the junction,

(III) Which proteins (if any) are involved in keeping the two organelles at a distance,

(IV) What macro-molecular complexes are involved in lipid transfer between the two organelle and at the cellular level which are ubiquitous tether proteins and what kind of tethering differences can one expect amongst different tissue type and the nature of metabolites exchanged between the two organelles, to name a few.

3.6.1 ER-mitochondria connection in lower eukaryotes

ER-mitochondria extended structures (ERMES) were originally discovered in Yeast, *S.cerevesiae* through a genetic screen (Kornmann et al., 2009). This led to the identification of two of the proteins that form a molecular bridge between the two organelles. The ERMES in Yeast is thus made of an ER membrane protein (Mmm1), two OMM proteins (Mdm34 and Mdm10) and a cytosolic protein (Mdm12). Three of the proteins in the ERMES complex contain

synaptotagmin like mitochondria lipid binding domain (SMP). The SMP domain is related to TULIP (Tubular lipid binding) domain, which transports lipids, providing a structural basis for lipid exchange between ER-mitochondria contacts (Kopec et al., 2011). According to one study, the conversion of PS (synthesized in the ER membrane) to PC is impaired in ERMES mutants and an artificial tether complex (which doesn't contain the SMP domain) partially restored this defect (Kornmann et al., 2009).

New studies have also shed light on vacuole-mitochondria contact site called vCLAMP, which might explain the alternate ways mitochondria derive their lipids (Honscher et al., 2014; Ungermann, 2015). Vacuoles and ER maintain a direct contact through nucleus-vacuole junction (NVJ) (Pan et al., 2000). This might explain the complexity as well as the mystery in ERMES transfer of lipids. In fact, cells lacking both ERMES complex and vCLAMP showed strong lipid homeostasis defect, suggesting an underlying compensatory mechanism in this process (Elbaz-Alon et al., 2014). Recently, yet another ER-mitochondria tether called as ER-membrane protein complex (EMC) has been discovered which co-localized with ERMES foci, suggesting possible regulatory function of ERMES on EMC (Lahiri et al., 2014).

ER shaping proteins have also been implicated in ERMES mediated lipid transfer (Voss et al., 2012). These discoveries arise more queries such as what makes ER and mitochondria come together at these specific sites. In addition to the largely explored role of phospho-lipid transfer, ERMES complex has also been implicated in Ca^{2+} exchange, protein import and mitochondrial genome maintenance.

3.6.2 ER-mitochondria connection in mammals

Ever since the isolation of MAMs in 90s and their characterization for Ca^{2+} signaling, the complexity of this signaling junction has seen a colossal growth with already many key and

pathological functions associated(Lopez-Crisosto et al., 2015). Few proteins have been described so far to maintain the structural integrity of the tether (Fig 1). Amongst these, MFN2 stands out as an undisputed molecule for its structural and functional significance in the tether (de Brito and Scorrano, 2008). MFN2, which was originally described as a mitochondrial fusion protein alongside with MFN1 was also shown to be located in ER especially in MAMs where it forms homo/heterotypic association with MFN1/MFN2 thus tethering the two organelles (de Brito and Scorrano, 2008; Rojo et al., 2002). MFN2 activity was shown to be regulated by MITOL and polyubiquitination of MFN2 is necessary for ER-mitochondria tethering (Sugiura et al., 2013).

Another regulator of ER-mitochondria tether is PACS2 wherein depletion of this sorting protein was shown to increase the distance between the two organelles, promoting apoptosis (Simmen et al., 2005). ER-mitochondria tether in mammals also participates in phospholipid synthesis (Vance, 2008; Vance and Tasseva, 2013). Conversion of phosphotidyl-serine (produced in ER) to phosphotidyl-ethanolamine occurs in mitochondria and it is transported back to ER and gets converted to phosphotidyl-choline. Fatty acid-CoA ligase type 4 is also a localized in MAM and plays a key role in lipid synthesis and degradation. For detailed overview of this process, refer (Vance, 2014)

Another protein complex that is found to modulate ER-mitochondria tether is Bap31-FIS1. Upon ER stress, this complex activates procaspase-8, which in turn cleaves Bap31 to form p20Bap31. For detailed review on ER-mitochondria influence on apoptosis, refer (Lang et al., 2015; Naon and Scorrano, 2014).

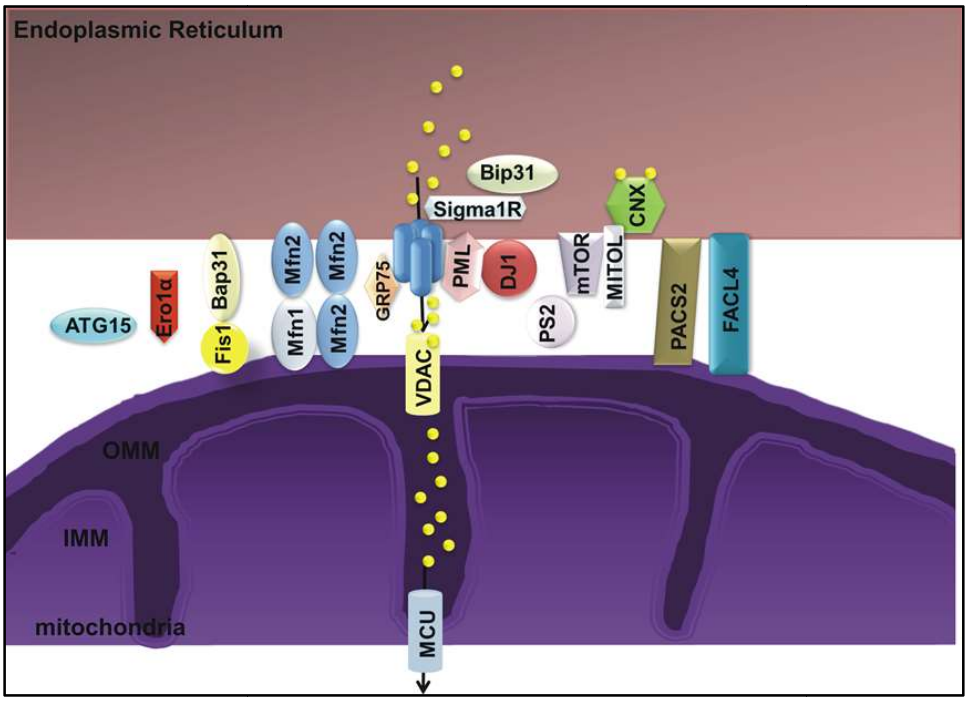

Figure 4: Summary of proteins located at ER-mitochondria junction. OMM – outer mitochondrial membrane; IMM – inner mitochondrial membrane; Ero1α translocates to MAM depending on the redox status of the cell; ATG14 translocates to MAM upon starvation.

3.7.1 ER-mitochondria and organelle dynamics

Mitochondria are dynamic organelle that undergoes constant fusion and fission depending on the tissue type and energy requirements of the cells (Archer, 2013; Mitra, 2013). The molecular mechanism of mitochondrial fission, which is regulated by a dynamin related GTPase, DRP1/Dnm1 is not yet completely understood. DRP1, which is a cytosolic resident protein, (upon de-phosphorylation at Ser637) translocates to mitochondrial outer membrane and forms oligomeric ring that wraps around mitochondria (Cereghetti et al., 2008). The oligomers end in constricting and fragmenting both outer and inner mitochondrial membrane (Smirnova et al., 1998). In lieu with this finding, recently, Freidman et al., with the help of 3D tomography showed that ER tubules mark the sites of mitochondrial division thereby establishing the role for

ER-mitochondria contacts in organelle morphology (Friedman et al., 2011). Interestingly, actin polymerization was thought to be involved in this process and recently, two proteins INF2 (on the ER membrane) and Spire 1C (on the OMM) have been suggested to regulate actin assembly at the ER-mitochondria junctions, thus providing the necessary mechanical force required for constriction and the diameter necessary for DRP1 oligomer formation during mitochondrial division (Chhabra et al., 2009; Korobova et al., 2013; Manor et al., 2015) (refer Fig 2).

These discoveries opens up several exciting queries such as which other proteins involved in tethering ER and mitochondria are involved in regulation of actin polymerization proteins, what are the distribution of these proteins on both the membranes, does actin polymerization and assembly alone or in conjunction with myosin leads to the initial constriction of the mitochondrial tubule. The field has travelled a long way and clearly indicates that modulators of ER-mitochondria tether yet to be identified plays a role in this process.

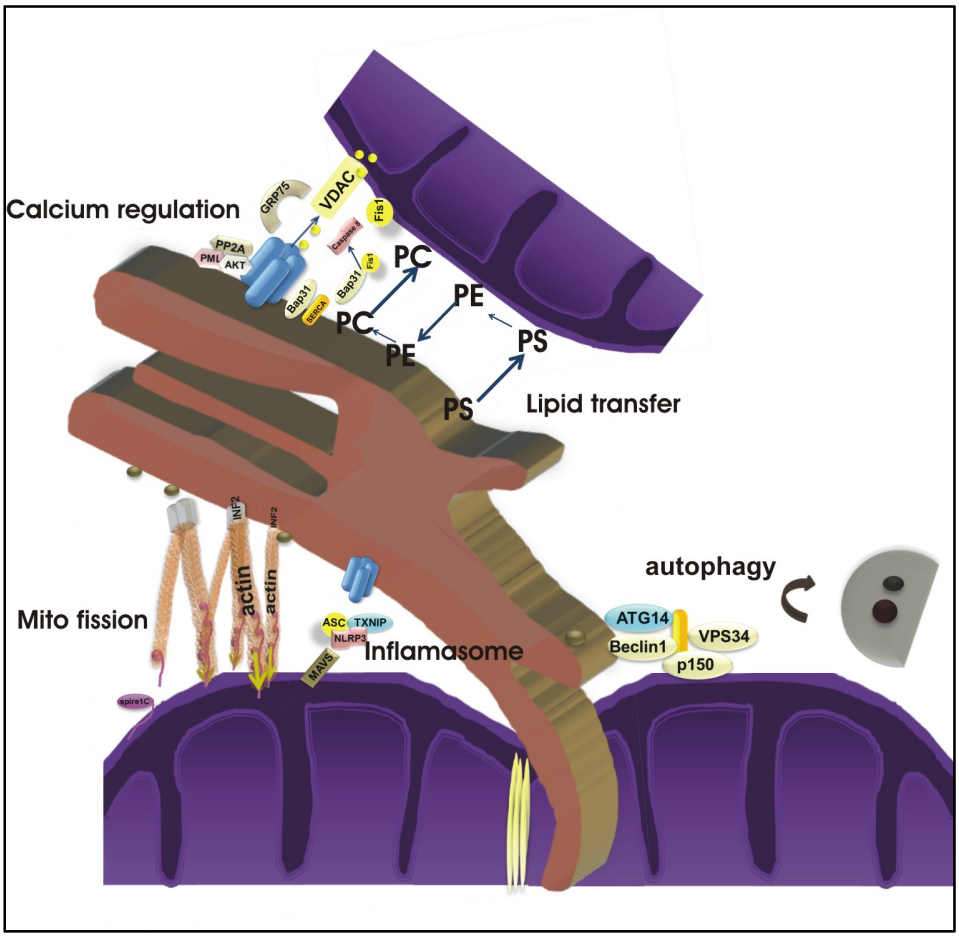

Figure 5: Summary of cellular processes that are modulated by the MAM junction. DRP1 translocation to mitochondria is thought to occur after the initial constriction by actin filaments; Upon starvation, ATG14 along with ATG5 relocates to MAM thus forming the autophagosomes.

3.7.2 ER-mitochondria and calcium connection

Calcium is the key secondary messenger involved in various cellular processes including gene expression, metabolism, muscle contraction and apoptosis. ER is the main storehouse of calcium and the released calcium from ER is directly or indirectly taken up by mitochondria for downstream events (Berridge et al., 2003). Ca^{2+} levels in the interphase of ER and mitochondria have been determined to be greater than 10μM, thus establishing the significance of such organelle interaction (Giacomello et al., 2010; Rizzuto et al., 1998). Mitochondrial calcium

uptake leads to activation of key enzymes involved in TCA cycle including pyruvate dehydrogenase (PD) (indirectly by regulating pyruvate dehydrogenase phosphatase, which increases the enzymatic activity of PD), isocitrate dehydrogenase, oxoglutarate dehydrogenase and glycerol-3-phosphate dehydrogenase (Denton et al., 1972; Denton et al., 1978). It was recently shown that constitutive basal level of Ca^{2+} transfer from ER to mitochondria is essential for cellular bioenergetics while prolonged transfer of Ca^{2+} during stress appears detrimental (Bravo et al., 2011).

On the other hand, ER-mitochondria tether has been extensively studied for its role in Ca^{2+} dependent apoptosis. Increased ER-mitochondria tethering and constitutive activation of IP3R has been observed during apoptosis and several proteins including Trichoplein (TpM) and PML regulate cell survival by either negatively modulating ER-mitochondria tether (TpM) or by modulating activity of IP3R (PML) (Cerqua et al., 2010; Naon and Scorrano, 2014; Pinton et al., 2011) (refer Fig 2). Anti-apoptotic proteins (Bcl2 and BclxL) have been shown to inhibit Ca^{2+} delivery (Ferrari et al., 2002) whereas pro-apoptotic proteins (Bax, Bak, Puma) have been shown to stimulate Ca^{2+} delivery into mitochondria. In fact, reintroduction of ER localized Bak was sufficient to sensitize Bax/Bak DKO cells for calcium mediated cell death (Scorrano et al., 2003).

3.7.3 ER-mitochondria in autophagy and ER stress

Autophagy, which is a highly evolved quality control process in eukaryotes, is a well-studied process that starts with the engulfment of cytoplasmic content including organelles culminating in lysosomal degradation (Singh and Cuervo, 2011). The membrane that contributes to these autophagosomes has always been a matter of debate (Shibutani and Yoshimori, 2014). Recent studies in mammalian cells have demonstrated that starvation

induced autophagosomes derive their membranes from OMM (Hailey et al., 2010). Hailey et al., demonstrated that in Mfn2 KO cells, which has reduced ER-mitochondria contacts has less autophagosomes upon starvation. Phosphoethanolamine (PE), which is the lipid target of LC3, is synthesized in ER through DAG or in mitochondria through PS (which is transferred from ER) also indicates that mitochondria might favour lipid homeostasis via ER-mitochondria contacts under starvation (Hailey et al., 2010).

In recent study, Hamasaki et al., demonstrated that autophagosomes marker ATG14 gets recruited to ER-mitochondria contact sites upon starvation through syntaxin 17 (Hamasaki et al., 2013) (refer fig 2). Since peroxisomal biogenesis protein Pex11 was recently identified in yeast to contact mitochondria through ERMES complex for fatty acid β oxidation (Mattiazzi Usaj et al., 2015). In a study in mammals, it has been shown that lipid droplets are involved in fatty acid trafficking to mitochondria, which are the primary sites of fatty acid oxidation in mammals (Rambold et al., 2015). Whether ER-mitochondria tether is involved in this process needs to be addressed but from the yeast story, it is compelling to speculate the tether involvement in lipid recycling during starvation.

In another study, it was shown that Rab32, which is required by the mTORC2 expressing cells to induce autophagosomes at ER membranes opposing mitochondria (Bui et al., 2010). Indeed, this study showed that Rab32 membrane deficient mutants failed to form autophagic vacuoles. mTOR, which is a nutrient sensing kinase localized to ER-mitochondria in a growth factor dependent manner. mTORC2 was also shown to control Ca^{2+} uptake via PACS2 (Betz et al., 2013). These discoveries regulating growth factors suggest the importance of ER-mitochondria tether in maintaining cellular homeostasis asking us to take a leap about the role of the tether in diseases where metabolic states are altered.

3.7.4 ER-mitochondria and inflamasomes

Since the first observation in 2011 that NOD like receptor 3 protein (NLRP3) inflamasomes are activated by ROS, studies have shown that ROS produced in ER/peroxisomes/mitochondria can alter NLRP3's ER localization to the MAMs (Zhou et al., 2011). Since ROS is a short-lived species, the localization of this inflamasomes complex to ER-mitochondria tether promotes efficient sensing of oxidative stress. Yet another protein, Thioredoxin interacting protein, which interacts with NLRP3 relocates to MAMs upon oxidative stress (Saxena et al., 2010). Breakthrough in the field was identification of mitochondrial antiviral signaling (MAVS) for the formation of NLRP3 inflamasomes (refer fig 2). MAVS was shown to mediate mitochondrial localization of NLRP3 although MAVS $^{-/-}$ did not display any change in ER-mitochondria tether (Subramanian et al., 2013). Ca^{2+} has also been reported to regulate Ilβ1 secretion calling our attention to the activation of NLRP3 by Ca^{2+} sensing receptor (CASR) (Lee et al., 2012). For detailed review, refer (Marchi et al., 2014). The key questions that open up in this avenue of research thus includes the pathway of recruitment of NLRP3 inflamasomes to MAMs and its effect on activation of transcription of Ilβ1 and other genes involved in inflammatory signaling.

3.7.5 Conclusions

During the recent years,the importance of ER-mitochondria communication increased. The field has opened up with several exciting questions, which needs to be addressed, given the importance of the tether in metabolic maintenance and pathologies. More clues on merge of different pathways in ER-mitochondria tether would arise upon identification of exact molecular composition of the tether and how it is modulated under different cellular conditions. Inter-organelle communication has turned the individual organelle field around and has led to progress in the study especially in pathologies. It is of prime importance at this moment to address if such inter-organelle crosstalk is the cause or consequence of the affiliated pathologies such as obesity, Alzheimer's disease, inflammation, cardiac hypertrophy amongst other diseases. In the coming years, with new tools and methods developed to study the contacts, the scientific community will unravel the answered question; the most important of all – composition of ER-mitochondria tether that keeps the two organelles together and how these proteins are recruited to this junction.

Acknowledgments

We thank M.Giacomello for close reading of the manuscript. LS is a Senior Scientist of the Dulbecco-Telethon institute supported by Telethon Italy (GGP12162 and GGP14187A), by the AIRC (the Italian Associationfor Research on Cancer), by the European Research Council (FP7-282280, FP7 CIG PCIG13-GA-2013-618697), and by the Italian Ministry of Research (FIRB RBAP11Z3YA_005).

References

[1] R. Bravo-Sagua, N. Torrealba, F. Paredes, P.E. Morales, C. Pennanen, C. Lopez-Crisosto, R. Troncoso, A. Criollo, M. Chiong, J.A. Hill, T. Simmen, A.F. Quest, S. Lavandero, Organelle communication: signaling crossroads between homeostasis and disease, Int J Biochem Cell Biol, 50 (2014) 55-59.

[2] D.E. Copeland, A.J. Dalton, An association between mitochondria and the endoplasmic reticulum in cells of the pseudobranch gland of a teleost, J Biophys Biochem Cytol, 5 (1959) 393-396.

[3] J.E. Vance, Phospholipid synthesis in a membrane fraction associated with mitochondria, J Biol Chem, 265 (1990) 7248-7256.

[4] A.E. Rusinol, Z. Cui, M.H. Chen, J.E. Vance, A unique mitochondria-associated membrane fraction from rat liver has a high capacity for lipid synthesis and contains pre-Golgi secretory proteins including nascent lipoproteins, J Biol Chem, 269 (1994) 27494-27502.

[5] R. Rizzuto, P. Pinton, W. Carrington, F.S. Fay, K.E. Fogarty, L.M. Lifshitz, R.A. Tuft, T. Pozzan, Close contacts with the endoplasmic reticulum as determinants of mitochondrial Ca2+ responses, Science, 280 (1998) 1763-1766.

[6] Y.J. Shiao, G. Lupo, J.E. Vance, Evidence that phosphatidylserine is imported into mitochondria via a mitochondria-associated membrane and that the majority of mitochondrial phosphatidylethanolamine is derived from decarboxylation of phosphatidylserine, J Biol Chem, 270 (1995) 11190-11198.

[7] J.E. Vance, MAM (mitochondria-associated membranes) in mammalian cells: lipids and beyond, Biochim Biophys Acta, 1841 (2014) 595-609.

[8] A. Lang, A.T. John Peter, B. Kornmann, ER-mitochondria contact sites in yeast: beyond the myths of ERMES, Curr Opin Cell Biol, 35 (2015) 7-12.

[9] A.H. Michel, B. Kornmann, The ERMES complex and ER-mitochondria connections, Biochem Soc Trans, 40 (2012) 445-450.

[10] A. Murley, R.D. Sarsam, A. Toulmay, J. Yamada, W.A. Prinz, J. Nunnari, Ltc1 is an ER-localized sterol transporter and a component of ER-mitochondria and ER-vacuole contacts, J Cell Biol, 209 (2015) 539-548.

[11] J.G. Wideman, R.M. Gawryluk, M.W. Gray, J.B. Dacks, The ancient and widespread nature of the ER-mitochondria encounter structure, Mol Biol Evol, 30 (2013) 2044-2049.

[12] G. Csordas, C. Renken, P. Varnai, L. Walter, D. Weaver, K.F. Buttle, T. Balla, C.A. Mannella, G. Hajnoczky, Structural and functional features and significance of the physical linkage between ER and mitochondria, J Cell Biol, 174 (2006) 915-921.

[13] C. Lopez-Crisosto, R. Bravo-Sagua, M. Rodriguez-Pena, C. Mera, P.F. Castro, A.F. Quest, B.A. Rothermel, M. Cifuentes, S. Lavandero, ER-to-mitochondria miscommunication and metabolic diseases, Biochim Biophys Acta, 1852 (2015) 2096-2105.

[14] K.D. Elgass, E.A. Smith, M.A. LeGros, C.A. Larabell, M.T. Ryan, Analysis of ER-mitochondria contacts using correlative fluorescence microscopy and soft X-ray tomography of mammalian cells, J Cell Sci, 128 (2015) 2795-2804.

[15] S.M. Horner, C. Wilkins, S. Badil, J. Iskarpatyoti, M. Gale, Jr., Proteomic analysis of mitochondrial-associated ER membranes (MAM) during RNA virus infection reveals dynamic changes in protein and organelle trafficking, PLoS One, 10 (2015) e0117963.

[16] Z. Liu, X. Du, J. Deng, M. Gu, H. Hu, M. Gui, C.C. Yin, Z. Chang, The interactions between mitochondria and sarcoplasmic reticulum and the proteome characterization of mitochondrion-associated membrane from rabbit skeletal muscle, Proteomics, 15 (2015) 2701-2704.
[17] C.N. Poston, S.C. Krishnan, C.R. Bazemore-Walker, In-depth proteomic analysis of mammalian mitochondria-associated membranes (MAM), J Proteomics, 79 (2013) 219-230.
[18] A. Zhang, C.D. Williamson, D.S. Wong, M.D. Bullough, K.J. Brown, Y. Hathout, A.M. Colberg-Poley, Quantitative proteomic analyses of human cytomegalovirus-induced restructuring of endoplasmic reticulum-mitochondrial contacts at late times of infection, Mol Cell Proteomics, 10 (2011) M111 009936.
[19] B. Kornmann, E. Currie, S.R. Collins, M. Schuldiner, J. Nunnari, J.S. Weissman, P. Walter, An ER-mitochondria tethering complex revealed by a synthetic biology screen, Science, 325 (2009) 477-481.
[20] K.O. Kopec, V. Alva, A.N. Lupas, Bioinformatics of the TULIP domain superfamily, Biochem Soc Trans, 39 (2011) 1033-1038.
[21] C. Honscher, M. Mari, K. Auffarth, M. Bohnert, J. Griffith, W. Geerts, M. van der Laan, M. Cabrera, F. Reggiori, C. Ungermann, Cellular metabolism regulates contact sites between vacuoles and mitochondria, Dev Cell, 30 (2014) 86-94.
[22] C. Ungermann, vCLAMPs-an intimate link between vacuoles and mitochondria, Curr Opin Cell Biol, 35 (2015) 30-36.
[23] X. Pan, P. Roberts, Y. Chen, E. Kvam, N. Shulga, K. Huang, S. Lemmon, D.S. Goldfarb, Nucleus-vacuole junctions in Saccharomyces cerevisiae are formed through the direct interaction of Vac8p with Nvj1p, Mol Biol Cell, 11 (2000) 2445-2457.
[24] Y. Elbaz-Alon, E. Rosenfeld-Gur, V. Shinder, A.H. Futerman, T. Geiger, M. Schuldiner, A dynamic interface between vacuoles and mitochondria in yeast, Dev Cell, 30 (2014) 95-102.
[25] S. Lahiri, J.T. Chao, S. Tavassoli, A.K. Wong, V. Choudhary, B.P. Young, C.J. Loewen, W.A. Prinz, A conserved endoplasmic reticulum membrane protein complex (EMC) facilitates phospholipid transfer from the ER to mitochondria, PLoS Biol, 12 (2014) e1001969.
[26] C. Voss, S. Lahiri, B.P. Young, C.J. Loewen, W.A. Prinz, ER-shaping proteins facilitate lipid exchange between the ER and mitochondria in S. cerevisiae, J Cell Sci, 125 (2012) 4791-4799.
[27] O.M. de Brito, L. Scorrano, Mitofusin 2 tethers endoplasmic reticulum to mitochondria, Nature, 456 (2008) 605-610.
[28] M. Rojo, F. Legros, D. Chateau, A. Lombes, Membrane topology and mitochondrial targeting of mitofusins, ubiquitous mammalian homologs of the transmembrane GTPase Fzo, J Cell Sci, 115 (2002) 1663-1674.
[29] A. Sugiura, S. Nagashima, T. Tokuyama, T. Amo, Y. Matsuki, S. Ishido, Y. Kudo, H.M. McBride, T. Fukuda, N. Matsushita, R. Inatome, S. Yanagi, MITOL regulates endoplasmic reticulum-mitochondria contacts via Mitofusin2, Mol Cell, 51 (2013) 20-34.
[30] T. Simmen, J.E. Aslan, A.D. Blagoveshchenskaya, L. Thomas, L. Wan, Y. Xiang, S.F. Feliciangeli, C.H. Hung, C.M. Crump, G. Thomas, PACS-2 controls endoplasmic reticulum-mitochondria communication and Bid-mediated apoptosis, EMBO J, 24 (2005) 717-729.
[31] J.E. Vance, Phosphatidylserine and phosphatidylethanolamine in mammalian cells: two metabolically related aminophospholipids, J Lipid Res, 49 (2008) 1377-1387.
[32] J.E. Vance, G. Tasseva, Formation and function of phosphatidylserine and phosphatidylethanolamine in mammalian cells, Biochim Biophys Acta, 1831 (2013) 543-554.

[33] D. Naon, L. Scorrano, At the right distance: ER-mitochondria juxtaposition in cell life and death, Biochim Biophys Acta, 1843 (2014) 2184-2194.
[34] S.L. Archer, Mitochondrial dynamics--mitochondrial fission and fusion in human diseases, N Engl J Med, 369 (2013) 2236-2251.
[35] K. Mitra, Mitochondrial fission-fusion as an emerging key regulator of cell proliferation and differentiation, Bioessays, 35 (2013) 955-964.
[36] G.M. Cereghetti, A. Stangherlin, O. Martins de Brito, C.R. Chang, C. Blackstone, P. Bernardi, L. Scorrano, Dephosphorylation by calcineurin regulates translocation of Drp1 to mitochondria, Proc Natl Acad Sci U S A, 105 (2008) 15803-15808.
[37] E. Smirnova, D.L. Shurland, S.N. Ryazantsev, A.M. van der Bliek, A human dynamin-related protein controls the distribution of mitochondria, J Cell Biol, 143 (1998) 351-358.
[38] J.R. Friedman, L.L. Lackner, M. West, J.R. DiBenedetto, J. Nunnari, G.K. Voeltz, ER tubules mark sites of mitochondrial division, Science, 334 (2011) 358-362.
[39] E.S. Chhabra, V. Ramabhadran, S.A. Gerber, H.N. Higgs, INF2 is an endoplasmic reticulum-associated formin protein, J Cell Sci, 122 (2009) 1430-1440.
[40] F. Korobova, V. Ramabhadran, H.N. Higgs, An actin-dependent step in mitochondrial fission mediated by the ER-associated formin INF2, Science, 339 (2013) 464-467.
[41] U. Manor, S. Bartholomew, G. Golani, E. Christenson, M. Kozlov, H. Higgs, J. Spudich, J. Lippincott-Schwartz, A mitochondria-anchored isoform of the actin-nucleating spire protein regulates mitochondrial division, Elife, 4 (2015).
[42] M.J. Berridge, M.D. Bootman, H.L. Roderick, Calcium signalling: dynamics, homeostasis and remodelling, Nat Rev Mol Cell Biol, 4 (2003) 517-529.
[43] M. Giacomello, I. Drago, M. Bortolozzi, M. Scorzeto, A. Gianelle, P. Pizzo, T. Pozzan, Ca2+ hot spots on the mitochondrial surface are generated by Ca2+ mobilization from stores, but not by activation of store-operated Ca2+ channels, Mol Cell, 38 (2010) 280-290.
[44] R.M. Denton, P.J. Randle, B.R. Martin, Stimulation by calcium ions of pyruvate dehydrogenase phosphate phosphatase, Biochem J, 128 (1972) 161-163.
[45] R.M. Denton, D.A. Richards, J.G. Chin, Calcium ions and the regulation of NAD+-linked isocitrate dehydrogenase from the mitochondria of rat heart and other tissues, Biochem J, 176 (1978) 899-906.
[46] R. Bravo, J.M. Vicencio, V. Parra, R. Troncoso, J.P. Munoz, M. Bui, C. Quiroga, A.E. Rodriguez, H.E. Verdejo, J. Ferreira, M. Iglewski, M. Chiong, T. Simmen, A. Zorzano, J.A. Hill, B.A. Rothermel, G. Szabadkai, S. Lavandero, Increased ER-mitochondrial coupling promotes mitochondrial respiration and bioenergetics during early phases of ER stress, J Cell Sci, 124 (2011) 2143-2152.
[47] C. Cerqua, V. Anesti, A. Pyakurel, D. Liu, D. Naon, G. Wiche, R. Baffa, K.S. Dimmer, L. Scorrano, Trichoplein/mitostatin regulates endoplasmic reticulum-mitochondria juxtaposition, EMBO Rep, 11 (2010) 854-860.
[48] P. Pinton, C. Giorgi, P.P. Pandolfi, The role of PML in the control of apoptotic cell fate: a new key player at ER-mitochondria sites, Cell Death Differ, 18 (2011) 1450-1456.
[49] D. Ferrari, P. Pinton, G. Szabadkai, M. Chami, M. Campanella, T. Pozzan, R. Rizzuto, Endoplasmic reticulum, Bcl-2 and Ca2+ handling in apoptosis, Cell Calcium, 32 (2002) 413-420.

[50] L. Scorrano, S.A. Oakes, J.T. Opferman, E.H. Cheng, M.D. Sorcinelli, T. Pozzan, S.J. Korsmeyer, BAX and BAK regulation of endoplasmic reticulum Ca2+: a control point for apoptosis, Science, 300 (2003) 135-139.
[51] R. Singh, A.M. Cuervo, Autophagy in the cellular energetic balance, Cell Metab, 13 (2011) 495-504.
[52] S.T. Shibutani, T. Yoshimori, A current perspective of autophagosome biogenesis, Cell Res, 24 (2014) 58-68.
[53] D.W. Hailey, A.S. Rambold, P. Satpute-Krishnan, K. Mitra, R. Sougrat, P.K. Kim, J. Lippincott-Schwartz, Mitochondria supply membranes for autophagosome biogenesis during starvation, Cell, 141 (2010) 656-667.
[54] M. Hamasaki, N. Furuta, A. Matsuda, A. Nezu, A. Yamamoto, N. Fujita, H. Oomori, T. Noda, T. Haraguchi, Y. Hiraoka, A. Amano, T. Yoshimori, Autophagosomes form at ER-mitochondria contact sites, Nature, 495 (2013) 389-393.
[55] M. Mattiazzi Usaj, M. Brloznik, P. Kaferle, M. Zitnik, H. Wolinski, F. Leitner, S.D. Kohlwein, B. Zupan, U. Petrovic, Genome-Wide Localization Study of Yeast Pex11 Identifies Peroxisome-Mitochondria Interactions through the ERMES Complex, J Mol Biol, 427 (2015) 2072-2087.
[56] A.S. Rambold, S. Cohen, J. Lippincott-Schwartz, Fatty acid trafficking in starved cells: regulation by lipid droplet lipolysis, autophagy, and mitochondrial fusion dynamics, Dev Cell, 32 (2015) 678-692.
[57] M. Bui, S.Y. Gilady, R.E. Fitzsimmons, M.D. Benson, E.M. Lynes, K. Gesson, N.M. Alto, S. Strack, J.D. Scott, T. Simmen, Rab32 modulates apoptosis onset and mitochondria-associated membrane (MAM) properties, J Biol Chem, 285 (2010) 31590-31602.
[58] C. Betz, D. Stracka, C. Prescianotto-Baschong, M. Frieden, N. Demaurex, M.N. Hall, Feature Article: mTOR complex 2-Akt signaling at mitochondria-associated endoplasmic reticulum membranes (MAM) regulates mitochondrial physiology, Proc Natl Acad Sci U S A, 110 (2013) 12526-12534.
[59] R. Zhou, A.S. Yazdi, P. Menu, J. Tschopp, A role for mitochondria in NLRP3 inflammasome activation, Nature, 469 (2011) 221-225.
[60] G. Saxena, J. Chen, A. Shalev, Intracellular shuttling and mitochondrial function of thioredoxin-interacting protein, J Biol Chem, 285 (2010) 3997-4005.
[61] N. Subramanian, K. Natarajan, M.R. Clatworthy, Z. Wang, R.N. Germain, The adaptor MAVS promotes NLRP3 mitochondrial localization and inflammasome activation, Cell, 153 (2013) 348-361.
[62] G.S. Lee, N. Subramanian, A.I. Kim, I. Aksentijevich, R. Goldbach-Mansky, D.B. Sacks, R.N. Germain, D.L. Kastner, J.J. Chae, The calcium-sensing receptor regulates the NLRP3 inflammasome through Ca2+ and cAMP, Nature, 492 (2012) 123-127.
[63] S. Marchi, S. Patergnani, P. Pinton, The endoplasmic reticulum-mitochondria connection: one touch, multiple functions, Biochim Biophys Acta, 1837 (2014) 461-469.

3.8 How to measure ER-mitochondria connection

The significance of the ER-mitochondria tether has been established in the previous section. With the increasing number of cellular and pathological processes the tether is associated with, it has become of prime importance to evaluate the tools available to quantify the proximity of the two organelles. Since the first electron microscopic observation of the tether, the field has progressed in developing efficient tools, which are used routinely by researchers these days to determine contacts number and extent. This section is dedicated to the current technologies that are available to study the interface between ER and mitochondria.

3.8.1 Light and Electron microscopy to assess the organelle juxtaposition

One of the commonly used techniques to study ER-mitochondria juxtaposition is by fluorescence imaging. In this technique ER and mitochondria are marked with fluorescent proteins and image stacks are acquired in few seconds using a spinning disk confocal microscope(in order to reduce the movement artifacts since both the organelles are dynamic). Image analysis typically involves overlap of the two fluorophores and measurement of the colocalisation coefficient in a 3D space (de Brito and Scorrano, 2008). Quantifying the colocalisation index therefore becomes a rate-limiting step in this process. Amongst the several methods available for colocalisation quantification, Manders' coefficient is most commonly used to analyze colocalisation between ER and mitochondria (Manders et al., 1993).

Manders' coefficient was developed as a successor of Pearson's coefficient (Manders et al., 1993). In Manders' coefficient, original signal intensities occupied in each overlapping pixel is considered. A ratio of such overlapping pixels to the total number of objects in each channel is calculated. Mathematically, Manders' coefficient "r" is calculated

$$r = \frac{\sum mito_i . ER_i}{\sqrt{\sum (mito_i)^2 . \sum (ER_i)^2}}$$

One advantage of this method is that “r” value is not sensitive to difference in signal intensities (which is crucial while measuring ER-mitochondria contacts) caused by differential labeling of the fluorophores or photo bleaching. Since the “r” value considers total number of objects of each fluorophore and this could considerably change while we assess ER and mitochondria (given that the number of individual entities of mitochondria are higher than ER), the coefficient that is often used is the one that measures the extent of ER overlap on mitochondria and is given by

$$M = \frac{\sum ER_{i_{coloc}}}{\sum ER_i}$$

Live cell imaging givesthe biggest advantage whenusing light microscope for measuring ER-mitochondria contacts. The artifacts in the morphology of the organelles causedbyfixation can alter the measured distance(Frigault et al., 2009). Another advantage of this technique is the gain of additional knowledge about the morphology of the individual organelles. One of the limitations of this technique is the resolution limit of the light microscopes, typically being ~200nm while the contacts are typically in magnitudes of 10-50 nm (Csordas et al., 2006; Frigault et al., 2009).

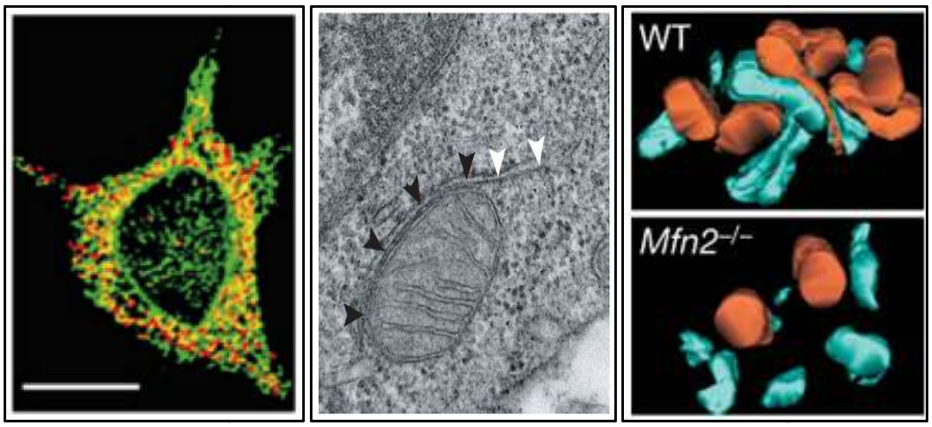

Figure 6: Visualisation of ER-mitochondria tether using various imaging techniques (A) Volume rendered stacks of ER (green) and mitochondria (red) by confocal microscope. (B) Electron microscopic image shows a close juxtaposition of the two organelles (see arrow) (C) Electron tomography image of WT and Mfn2$^{-/-}$ MEFs. (A) and (C) are adapted from (Csordas et al., 2010; de Brito and Scorrano, 2008) (B) is adapted from (Csordas et al., 2010)

Electron microscopy is one of the first developed techniques that allowed visualization of sub-cellular compartments at a resolution of few nano meters. The initial observation of existence of the tether itself in 1950s and 1970s were based on electron microscopic images (Copeland and Dalton, 1959; Morre et al., 1971).Advancement in this technique that has also revolutionized the field of ER-mitochondria contacts is electron tomography. In this technique, a series of electron microscopic images are acquired (tilted aroundone or more axis) and these images are then reconstructed to complete 3D projections (de Brito and Scorrano, 2008).

Electron microscopic images offer a unique advantage of measuring the area and the perimeter of the organelles in contact and helps in delineating between smooth and rough ER (Csordas et al., 2006). Limitations of this technique is the use of fixed samples which might alter the morphology of mitochondria and ER if the sample preparation is not critically followed and hence lead to erroneous distance measurements.

3.8.2 Biochemical fractionation of MAMs

J.E Vance was the first to fractionate MAMs from rat liver in early 90s (Rusinol et al., 1994; Vance, 1990). Today, the field has developedto the extent that MAMs can beextractedfrom several different cell types and to use these preparations to perform proteomics studies to identify the moleculesenriched in this compartment. The protocol for biochemical fractionation of MAMs is summarized in the following figure (Wieckowski et al., 2009).

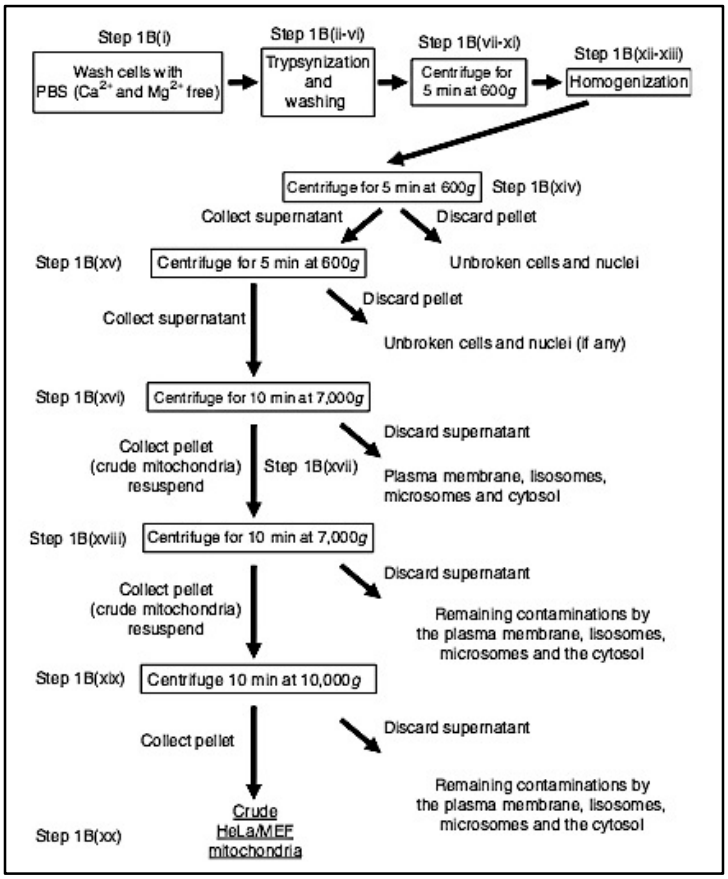

Figure 7: Biochemical fractionation of MAMs. (A) shows the protocol for MAM fractionation from mammalian cells. (Wieckowski et al., 2009)

The main principle in this separation is the use of density gradient to separate heavy mitochondria from light MAMs. The use of percoll and swinging bucket rotor allows the

organelles to undergo isopycnic separation, forcing mitochondria to reach the bottom of the tube while the MAM fraction floats on top.

Several markers have to be used in this technique to determine the purity of the fractions obtained. The commonly used proteins to identify MAM junction include FACL4 and Calnexin; Proteins that are abundant in pure mitochondria are VDAC and cytochrome c; Proteins that are enriched in ER fraction includes Calreticulin and IP3receptors (Wieckowski et al., 2009).

With this elegant technique, the subcellular localization of the protein of interest could be identified. The method has been used to study changes in the protein composition in MAMs following cellular process such as autophagy or viral infection (ref). While the advantage of this technique is that it gives preliminary insight about the localization of the protein in these junctions, it doesn't necessarily address if the protein of interest is a direct tether or not.

3.8.3 In-vitro ER-mitochondria interaction assay

Assessment of the direct tethering role of both the organelles by a protein can also be performed by *in-vitro* ER-mitochondria interaction assay wherein pure fractions of mitochondria and microsomal fractions are incubated for a short duration of time, followed by low speed sedimentation to separate pellet containing mitochondria and ER associated with mitochondria and supernatant containing remaining microsomal fraction(de Brito and Scorrano, 2008). The protocol is summarized in the figure below:

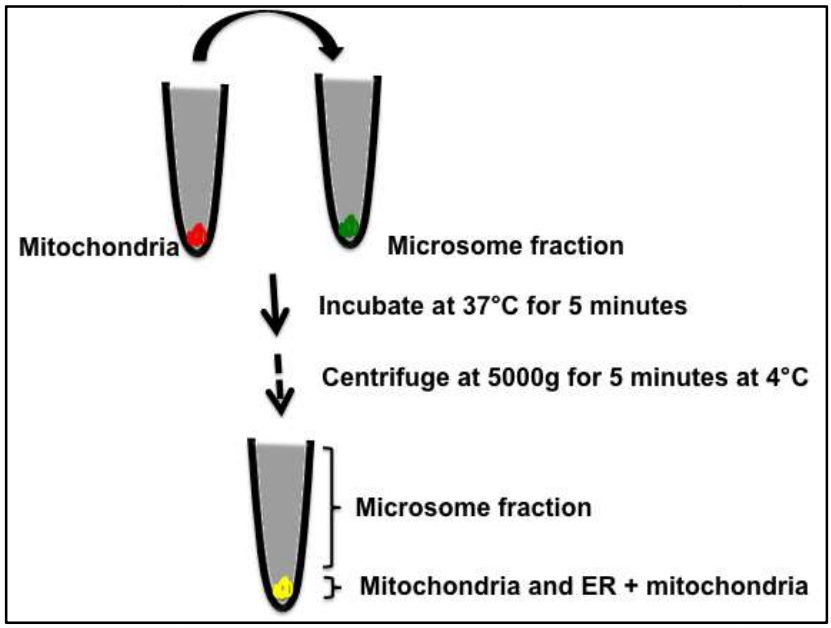

Figure 8: *In-vitro* ER-mitochondria interaction assay. (A) shows the steps followed to assess the interaction between ER and mitochondria *in-vitro*

With this technique, the main advantage is that the proteins that could be classified as tethers (those that structurally integrate the two organelles) can be identified (deBrito and Scorrano, 2008).

3.8.4 Fluorescence resonance energy transfer (FRET) assessment of ER-mitochondria tether

Study of spatial juxtaposition of cellular constituents such as ER and mitochondria has been a challenge since the interface between the two organelles or between any two molecules within the cells occurs at distances that are typically in orders of magnitude lower when compared to the resolution limits of a light microscope (Clegg, 2002) FRET or Forster resonance energy transfer was described in late 1940s. Its implication in protein-protein interaction studies in biological systems has become valuable since it allows measurement of

distance between proteins in live cells at nano meter scale (Truong and Ikura, 2001). FRET is a process in which energy of a molecule in an excited electronic state (called donor D) is transferred to a molecular chromophore called acceptor (A). When there is spectral overlap of the emission peak of D and absorption peak of A and the quantum yield of D is high, there is transfer of energy from D to A. Following the energy transfer, D returns bask to its ground state while A having absorbed this photon, reaches the excited state. When A returns back to the ground state, it can emit a photon, which is typically in its emission range and read as FRET since originally only D had been excited (ref). The concept is summarized in the following figure:

$$D^* + A \Longleftrightarrow D + A^*$$

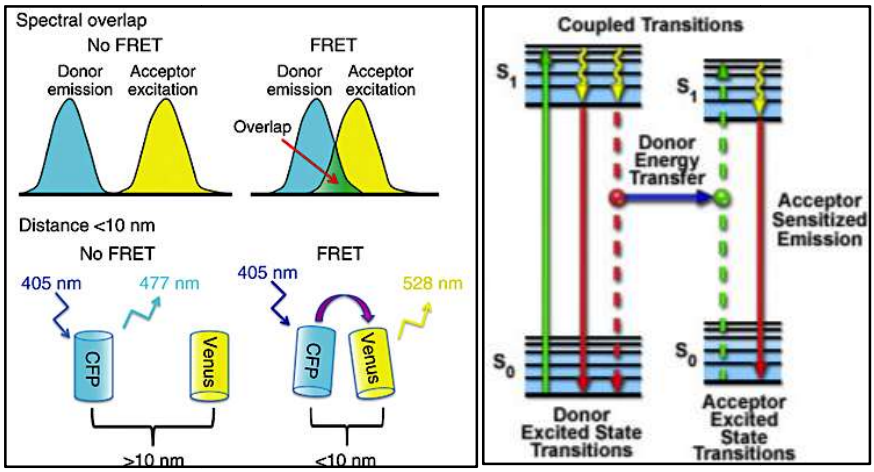

Figure 9: Principle of FRET (A) shows the spectral overlap needed to have efficient FRET and (B) shows the concept of FRET at molecular level. Images are adapted from (Broussard et al., 2013)

FRET is a dipole-dipole interaction and the FRET efficiency E is inversely proportional to the 6^{th} power of the distance between the two fluorophores and occurs effectively when the donor D and acceptor A are typically at a distance less than 10 nm.

Csordas et al. utilized this well-designed energy transfer system, to develop a FRET based biosensor to study ER-mitochondria contacts (Csordas et al., 2010). The biosensor had YFP targeted to mitochondrial outer membrane by Akap sequence and CFP targeted to ER membrane by Sac1 sequence (see figure below). YFP and CFP were fused to FKBP and FRB binding domains respectively, which interact upon addition of Rapamycin. FKBP-12 and its counterpart domain in FRAP (FRB) have Kd value of 2.9 nM (Chen et al., 1995). The fusion of FKBP to mito-YFP and FRB to ER-CFP gives unique advantage of measuring ER-mitochondria contacts proximity at physiological condition (before addition of Rapamycin) and maximum number of contacts possible (after addition of Rapamycin).

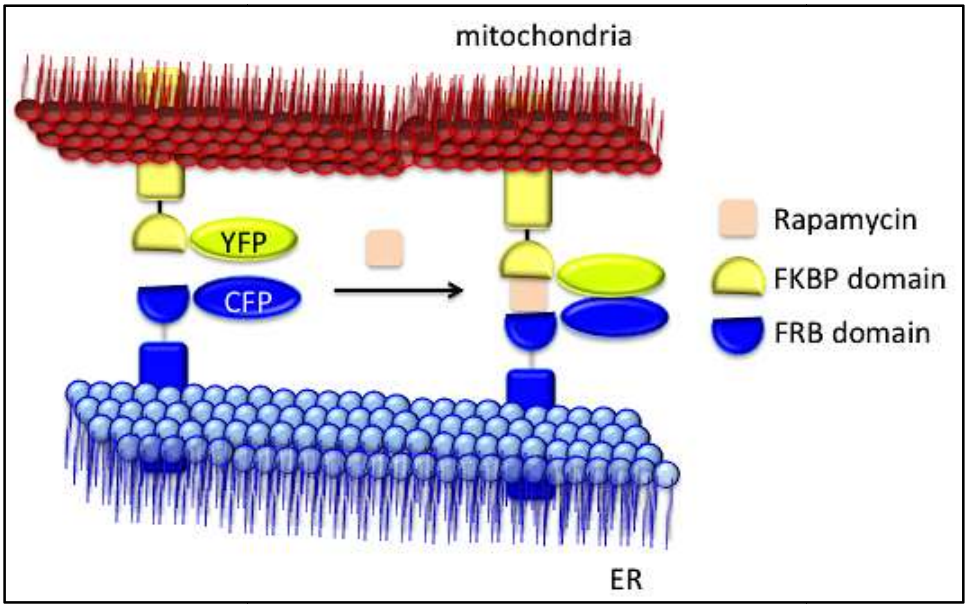

Figure 10: FRET based biosensor to study ER-mitochondria proximity. The cartoon shows the concept of energy transfer between CFP and YFP to measure ER-mitochondria contacts before and after addition of rapamycin. Adapted from (Csordas et al., 2010)

The probe also gives theother advantage of measuring the total number of contacts possible in a short duration since the binding and stabilization of FKBP-FRB is quite rapid (saturation reached at ~ 10 minutes). Third advantage is that mito-YFP is targeted to OMM unlike other

conventional tools used, which are targeted to the lumen and ER-CFP to the ER membrane and hence the biosensor provides us direct evidence in terms of proximities.

In the high content screen described in this thesis, we have used a modified version of theFRET based biosensor to unravel the structural components of the ER-mitochondria tether in mammalian cells.

3.9 High content screening in biology

High content screening has been and continues to be a major contribute in terms of drug discovery. The combination of robotics automation and large data set processing along with miniaturization of the assays have led to vast expansion of the field beyond pharmaceutical industries. Accordingly, the diversity of the screened targets has also grown. At present, assay targets that form large libraries include small molecules, protein libraries, siRNA / shRNA / CRISPR-CAS libraries and cDNA library. Of these, siRNA /shRNA and cDNA libraries are designed for genome wide association studies, which have gained majorimportance since the sequencing of human genome. The goals of such studies (irrespective of the type of library used) are to identify molecular structures that induce a studiedphenotype in the target population.

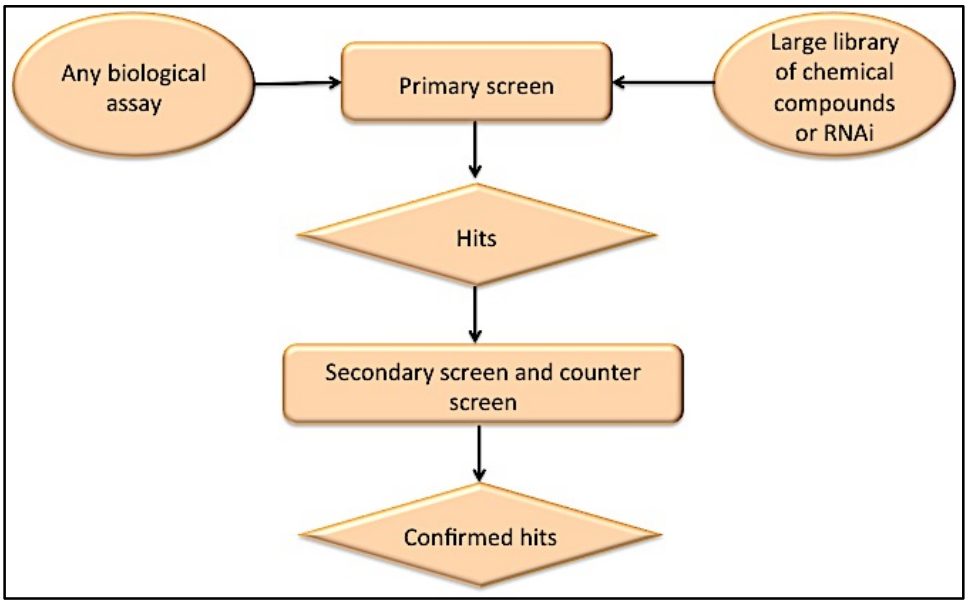

Figure 11: Major steps followed in high content screening. Adapted from (Malo et al., 2006)

With the discovery of RNAi and its first use in *C.elegans* for genome screening, the field quickly evolved to accommodate several cell systems across species. In this respect, the most

commonly used approach for mammalian cells are siRNA or short hairpin RNA (shRNA). Both methods have been recognized as powerful tools in addressing several questions in cell biology, in particular for analysis of signal transduction pathways. Recent years have seen the advancement of RNAi filed in terms of limiting off-target effects and increasing the efficacy of mRNA knock down by means of modifying the basic structure of RNAi. Finally, HTS is a large-scale process testing several thousand genes or molecules. The candidates or the “hits” chosen are then confirmed typically in a confirmatory screen and evaluated for their functional relevance using secondary screen.

In this thesis, we describe a shRNA based genome wide screen we have performed to identify which molecules contribute to the structural integrity of ER-mitochondria tether. Hence, this section will focus on details about high content imaging and the statistical methods available so far to identify candidates/hits from such large data set.

3.9.1 Genome wide screening in mammalian cells using targeted shRNA libraries

The use of RNAi in mammalian cells to study the effect of a particular gene has become a popular technique since the discovery of the technology in *C.elegans (Sonnichsen et al., 2005)*. In mammalian cells, siRNA and shRNA are two most common forms of RNA inhibitors. Amongst them, siRNA has widely been used owing to cost of production and efficacy of knock down. Yet, the transfection efficiency of siRNAs depends on the cell type being used and their transient nature of knock down makes them less appealing for long duration assays. These have been overcome by the use of shRNA based gene knock down (2003).

shRNAs are processed to form siRNAs by Dicer, a dsRNA-specific RNase III. These siRNAs are then loaded into argonaute 2-containing RNA-induced silencing complexes (RISCs). The guide strand of the siRNA is then used by RISC to recognize the mRNA of interest and

cleaves(Bernstein et al., 2001). How the guide strand obtains target specificity is not completely understood. Most focus is on the so-called 'seed region' of bases 2–8, which is defined as the primary targeting region for siRNA action and is the region that is least tolerant of mismatches.

Since the efficiency of knock down is of prime importance in genome wide screens, shRNAs are typically cloned in lenti-viral constructs and the resulting lenti-viral particles are transduced in cells thereby increasing the efficacy of the delivery (Paddison et al., 2002). Another way to circumvent the problem of efficient delivery is to use multiple shRNAs against one particular gene. In a typical RNAi screen, 3-5 shRNAs are provided for every gene to ensure efficient knock down with atleast one shRNA (Moffat and Sabatini, 2006). Another critical factor that needs to be considered while performing RNAi based screen is that of off-target effects, which impose a serious effect on the “hits” considered. The analysis of off-target effects is discussed in the later section.

3.9.2 High content imaging and analysis to perform genome wide screen

A high content screen demands the need for automation of several steps before the output is read. Some of the basic infrastructure required for HTS includes array robots, which can dispense different volumes of liquid in a precise way, a plate reader or a microscope with automated setting for image acquisition and storage and automated image analysis software along with powerful programs to statistically analyze large dataset.

Developed in 1990s, subcellular patterns were recognized by automated analysis algorithms with machine learning capabilities (Shariff et al., 2010). Since spatio-temporal location of proteins/ organelles is of common interest, image analysis softwares have evolved to

include outputs to study several fields including but not limited to apoptosis, stem cell differentiation, tumor biology, neurodegenerative disorders and arterial hypertension. Steps involved in a typical image analysis are summarized in the figure below:

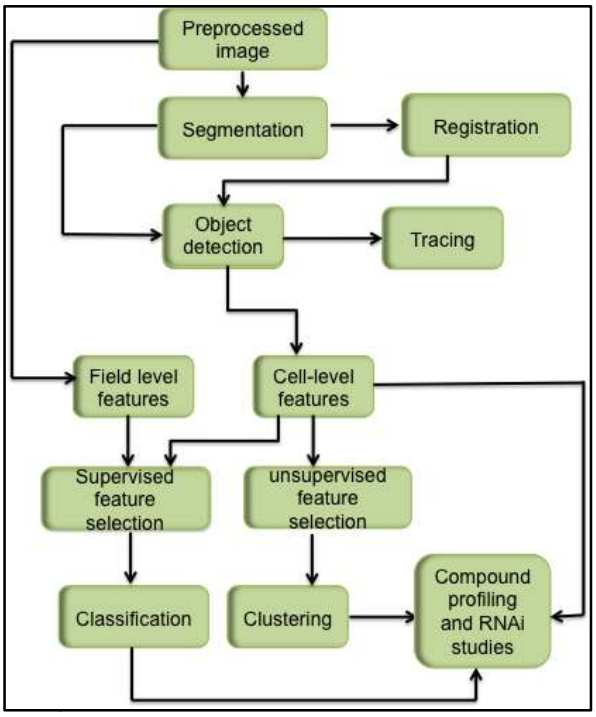

Figure 12: Flow chart of a typical image analysis sequence (adapted from Shariff et al., 2010)

Raw image acquired in a typical screen set up undergo image segmentation to separate cells in a field. This segmentation could either be at the cell level or at the nuclear level. This leads to object detection around which a boundary is drawn to delineate it from surrounding objects and to calculate background. Cell features are then tracked by the algorithm and classified based on learning acquired. Each cell is thus represented in multi-dimensional feature vector by the algorithm and tracked and learnt. Most automated image analysis programs are unsupervised in that the algorithm can be trained manually by the user to include or eliminate objects according to his/her choice i.e. there is no initial assumption by the learning algorithm.

3.9.3 Statistical analysis method for high throughput data

Data analysis to infer the “hits” is one of the major steps in any high throughput screening, which needs careful scrutiny. Statistical data analysis includes four major steps before the candidates are classified as “hits” (Boutros et al., 2006).

(I) Data normalization

(II) Scoring the normalized data

(III) Quality control check of the scored data

(IV) Hit selection and classification

Data normalization is typically done to remove systematic error that occurs from plate to plate thereby making the measurements comparable across plates. The bias caused by systematic error could be equally distributed or could depend on the well position or other external factors including pipetting error. Since large dataset handling needs caution to classify hits, several methods of normalization have been optimized. Control based optimization or non-control based normalization have their unique assumptions that make them a good choice in one assay over the other. In RNAi experiments, non-control based normalization is generally followed (Birmingham et al., 2009; Malo et al., 2006). In a typical RNAi based screen, the number of wells screened per plate is generally large when compared to the number of controls (384 vs. 10 control wells). Hence in this case, the assumption is that most of RNAi don’t have an effect on the cell phenotype studied and hence considered as negative control. One such non-control based method for normalization is Z-score. In this method, normalization is done as follows:

$$Z = \frac{(x_i - \overline{X})}{S_x}$$

X_i → raw measurement on i^{th} compound

$\bar{X}$→ Arithmetic mean of the plate

S_x→ standard deviation with the plate

A modification of this score is robust Z-score where instead of mean and standard deviation, median absolute deviation and median are calculated. This gives a unique advantage to identify the outliers, which are commonly the "hits". MAD is calculated as follows:

$$MAD = median[r_{ijp} - median(r_{ijp})]$$

Where r_{ijp} is the residual of measurement for row_i and $column_j$ on p^{th} plate. Regardless of the method of normalization used, screen data undergoes a rigorous quality control check. One method to assess the quality is reproducibility of the assay in replicate screen. In RNAi based screen, yet another factor is calculated to represent the accuracy and reproducibility of the assay in SSMD (strictly standardized mean difference) takes into account variance amongst the samples and is more consistent for RNAi based screen since each control used can have either a strong/moderate effect (Zhang, 2011; Zhang et al., 2010). SSMD is calculated as follows:

$$\boldsymbol{SSMD} = \frac{\boldsymbol{mean}(\boldsymbol{C_{pos}}) - \boldsymbol{mean}(\boldsymbol{C_{neg}})}{\sqrt{\boldsymbol{std}(\boldsymbol{C_{pos}})^2 + \boldsymbol{std}(\boldsymbol{C_{neg}})^2}}$$

Once the quality control is checked the next critical step is to identifythe "hits". In a typical screen assay, Z-score values lesser or greater than three deviations from the controls are

essentially chosen as “hits”. Replicate assays helps in determining the error rate and % of false positive or false negatives. The need for replicate assay and how it reduces errors is summarized in this figure below:

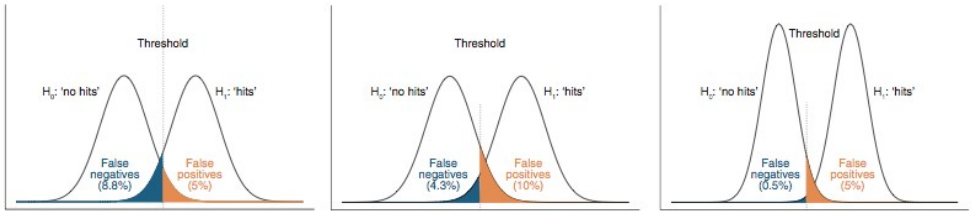

Figure 13: Need for replicate screen in analysis of “hits”. Calculation of false positive and false negative after replicate screen is performed (Malo et al., 2006).

In a typical RNAi based screens, the number of shRNAs / siRNAs screened per gene varies between 2-5. These numbers are chosen to ensure that reproducibility of the assay and also to increase the probability of knock down of the gene to have reliable data (Echeverri and Perrimon, 2006). This method increases the complexity of analysis when it comes to classification of the “hits”. Indeed, new algorithms have been written wherein redundant siRNA activity (RSA) is calculated (after the confirmatory screen) based on the Z-scores for each shRNA of a particular gene (Birmingham et al., 2009; Konig et al., 2007). Implementing *p-values* obtained from the RSA, the “hits” are then ranked based on the number of shRNAs for a particular gene, which have given similar outcome. By this method, the “hits” that have moderate phenotype will also be considered while in the traditional method of classification, they might get eliminated.

Another factor, which needs to be addressed in RNAi based screen, is the probability of off-target effects. To meet this end, algorithms have been created, which analyze the initial seed sequence of each si/shRNA and assigns a probability score based on the frequency of

occurrence of a particular seed sequence amongst different shRNAs (Marine et al., 2012). The “hits”, which have high probability score by this method, are thus eliminated.

In the study to identify ER-mitochondria tethers, we have used the above parameters to critically analyze the candidates and classified them as tethers and spacers.

3.10 Myotonic dystrophy 1 and DMPK

Myotonic dystrophy also known as Steinert's disease is a multisystemic disorder that has been investigated for the past 100 years(Romeo, 2012).. The principal traits of DM1 include myotonic, muscle atrophy (type 1 fibers), early cataract development, insulin insensitivity, cardiac conductiondefects , cognitive impairment, hypogonadism and testicular atrophy(Mateos-Aierdi et al., 2015). Myotonic dystrophy protein kinase (DMPK) is a serine threonine kinase whose discovery in the 90s came close to solving the puzzle for the cause of myotonic dystrophy type 1 (DM1) (Ranum and Day, 2004)

DM1 is an autosomal dominant disorder with 1:8000 individuals affected(Cho and Tapscott, 2007). The discovery that DMPK's 3'UTR had aberrant CTG expansion that lead to the formation of transcript aggregates/foci in the nuclei had led to its recognition as nucleotide repeat mediated disorderssimilarto fragile X syndrome and spinobulbular muscular atrophy (Ranum and Day, 2004). The aberrant expansion could either occur in coding or non-coding region. The aberrant expansion in non-coding region such as the 3' UTR would either attribute to formation of mutated or truncated protein or accumulation of RNA in the nucleus, such as the case in DMPK affecting the processing of nearby genes in the same locus.(Cho and Tapscott, 2007; Kaliman and Llagostera, 2008). In DM1, it has been shown that the aberrant 3' UTR expansion not only results in deregulation of DMPK protein kinase activity, but also the expression of other proteins such as cardiac troponin T when the RNA foci binds to CUG binding proteins and does not allow the transcription to take place. The complexity of the disease severity accounts for anticipation phenomenon i.e. increases with repeat length decrease in age of onset. The severity is attributed to the altered splicing processes (splicopathy) and perturbation of RNA processing for other genes(Kaliman and Llagostera, 2008).

In this thesis, we have analyzed the functional significance of alternate spliced variants of DMPK and their localization to sub-cellular organelles particularly to ER and mitochondria and functional consequences of such interactions. Hence, the introduction will focus on the localization and functional consequence of such localization of DMPK.

3.10.1 Structure and function of DMPK isoforms

DMPK is a tail-anchored kinase and belongs to the AGC group of serine-threonine kinase and has been found to be homologous to MRCK, ROCK/Rho kinase/Rok, NDR1, Warts and Citron kinase (Pearce et al., 2010). These kinases have been implicated in smooth muscle contraction, stress fibre formation, neurite retraction and cytokinesis (Pearce et al., 2010). So far, six isoforms have been shown to be conserved amongst human and mice as a product of alternative splicing event (Wansink et al., 2003). The structure consists of a N-terminal leucine rich domain, kinase domain and a coiled-coil domain (fig. 14). Alternate splicing either includes or excludes VSGGG motif and the composition of amino acid in the C-terminal domain (Wansink et al., 2003). A new human DMPK isoform completely lacking the CUG repeats in the 3' UTR was also reported recently.

The VSGGG motif is thought to modulate the phosphorylation status of the kinase although this data stands from indirect evidence from gel migration assays (Wansink et al., 2003). It was shown that the difference in C-terminal end confers a different substrate specificity and sub-cellular localization. The leucine rich N-terminal domain and coiled-coil domain have been studied for the multimersation of DMPK (van Herpen et al., 2005).

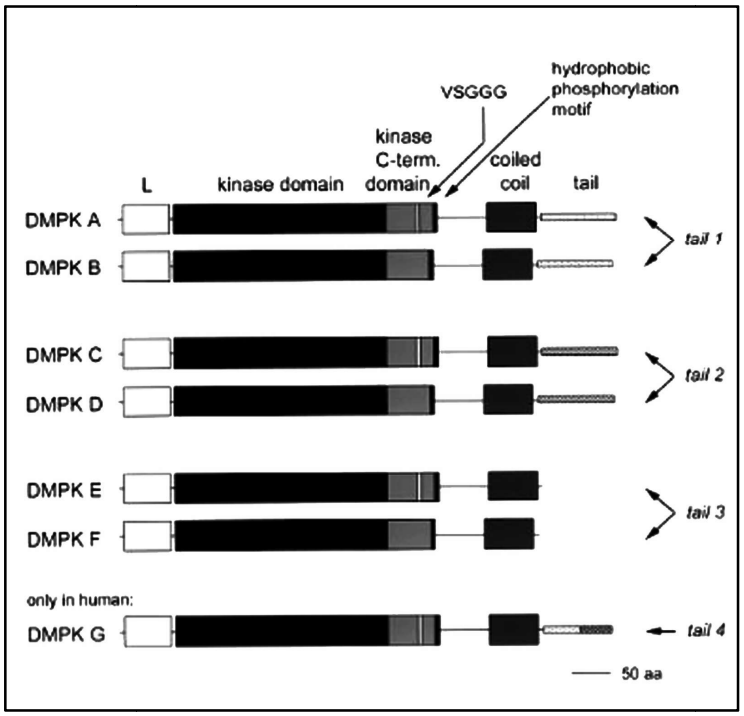

Figure 14: Molecular structure of DMPK isoforms. The cartoon depicts different domains and their modification in alternate spliced isoforms of DMPK. Adapted from (Wansink et al., 2003)

In humans, four isoforms localize to outer mitochondrial membrane (OMM) while mouse isoforms A, B localizes to ER membrane and C, D localizes to OMM, E and F localizes to cytosol (Wansink et al., 2003). The localization difference between ER and mitochondria was found to be attributed by length and hydrophobicity of the trans membrane domain in that strong hydrophobic characteristics of mouse DMPK- A localized it to ER (van Herpen et al., 2005). Mutational analysis of positively charged arginine to alanine in an otherwise hydrophobic stretch of amino acids in human DMPK- A conferred it ER localization, emphasizing the significance of alternate splicing in the C-terminal domain. The coiled-coil domain in different spliced variants of DMPK was shown to mediate homo and hetero multimersation of the protein. Spliced variants exist in homo multimers (440 KDa vs 70 KDa monomer). These interactions were shown to occur independent of kinase activity. Mutations in coiled-coil domain reduced self-association of

DMPK- E and also association with other isoforms. Coiled-coil (CC) domain was also seen to modulate DMPK kinase activity although the exact reason is not deciphered. In addition, Coiled-coil domain modulated isoforms sub-cellular localization; in particular mouse DMPK- C but not mouse DMPK- A relocalised to cytosol upon CC mutation. These studies define the structural capacity of DMPK (van Herpen et al., 2005).

Invitro phosphorylation studies showed DMPK isoforms phosphorylates threonine residues surrounded by arginine and lysine and the consensus sequence for DMPK enzymatic activity was found to be (R/K) XRRX (**T/S**)(L/V) X, where X could be any amino acid (Wansink et al., 2003). It was also shown that depending on the VSGGG motif and C-terminal tail, the preference of trans-phosphorylation was different amongst different DMPK isoforms. The most active form in phosphorylating MYPT1 was the short cytosolic subunits (Wansink et al., 2003). If there was influence from the C-terminal domain or the sub-cellular compartments in the events of phosphorylation, is yet to be studied.

3.10.2 Molecular features of myotonic dystrophy

DM1, which is a multi-systemic disorder, is caused by aberrant expansion of the trinucleotide repeat motif CTG. It has been shown to affect multiple organs and tissues including muscles, eyes, gonads, CNS and to carry an increased risk of developing tumor and aging (Mateos-Aierdi et al., 2015). The following figure describes the molecular mechanism by which the disorder affects several tissues. In recent years, different isoforms discovered for DMPK havebeen found to be associated with different tissues affected in DM1 (Romeo, 2012).

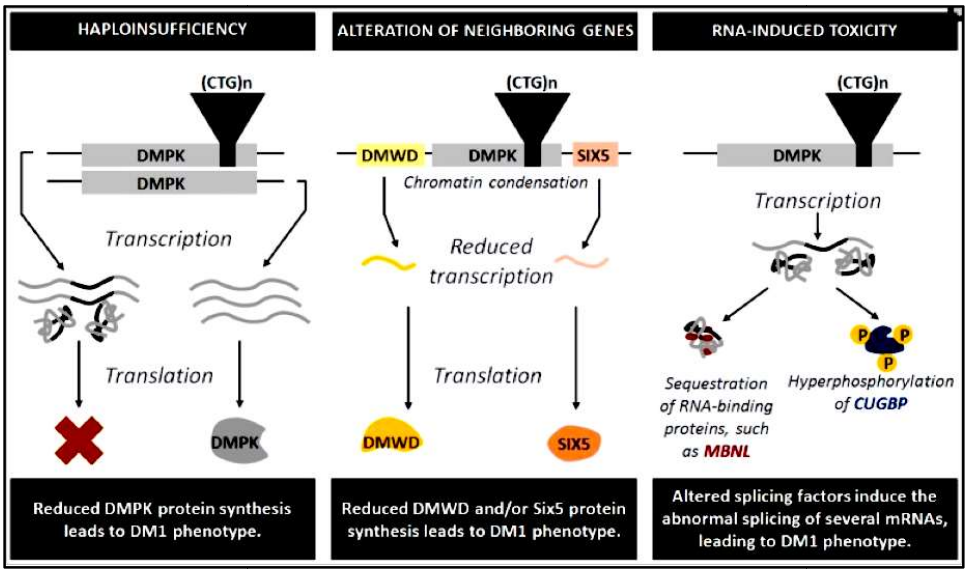

Figure 15: Molecular mechanisms underlying multi systemic effect in DM1 patients. DM1 can be caused either due to reduced amount of DMPK or RNA toxicity in the cell, which doesn't allow RNA transcription factors to bind or aberrant alteration in the splicing of neighboring genes (adapted from Romeo, 2012).

Isoforms A and D (long forms ~ 70KDa) have been implicated in higher levels in skeletal muscle and heart, while the short forms (E and F ~50KDa) are retrievedin smooth muscles (Oude Ophuis et al., 2009). Cardiac defects including arrhythmia and heart block could be a possibility of toxicity of (CUG) expanded mRNAs of both long and short isoforms in ventricles and atrium. Malfunctioning of gastrointestinal tract and vacuolization in the bladder of the patients are also a part of DM1 phenotype associated with smooth muscles (Cho and Tapscott, 2007). The expression of the short DMPK isoforms, specifically in these muscles calls for futher analysis of differential expression of the isoforms and their functional implications.

Long forms of DMPK, found in skeletal muscle of all fibres including Soleus, tibialis, anterior and gastrocnemius muscle connect to the weakness and muscle wasting of distal skeletal muscle (fibre 1 specifically) in DM1 patients. Respiratory distress or speech and swallowing difficulty in DM1 patients could be attributed to the expression of both long and short isoforms in diaphragm and tongue (Ueda et al., 2000). Insulin resistance, due to aberrant

splicing of insulin receptor mRNA (expressed in skeletal muscles) is due to a toxic effect of CUG expanded repeats (Llagostera et al., 2007). In both DM1 patients and DMPK KO mice, it was observed that the concentration of insulin in plasma was higher when compared to wild type conditions. Over-expression of kinase deficient or C-terminal truncated DMPK mutant lead to retention of insulin receptor in the intracellular compartment and in DMPK KO cardiomyocytes, insulin binding to plasma membrane was decreased (Ueda et al., 2000). One possibility suggested for repaired insulin receptor trafficking could be due to impairment of Golgi derived transport carriers through actin mediated cytoskeletal remodeling. It was also observed that in DM1 patients, CTG repeats caused 50% reduction in DMPK protein levels, altered expression of Six 5 gene and nuclear accumulation of DMPK transcripts altered the splicing of other nearby genes by sequestering RNA binding proteins (Cho and Tapscott, 2007).

Thus, although molecular mechanisms observed in DMPK KO mice correspond to certain aspects of DM1, the role of DMPK and its function related to different sub-cellular locations are not completely understood yet.

3.10.3 Molecular interactors of DMPK

Roberts et al.,(Roberts et al., 1997)reported an interaction between DMPK and RNA binding protein termed CUG - BP/hNab50, which is involved in various aspects of RNA processing and binds (CUG) n triplet repeats, However, a detailed mechanistic explanation of the role played by the DMPK – CUG -BP/hNab50 interaction in DM1 pathogenesis is still missing. DMPK has been reported to be involved in ion homeostasis, regulating calcium, sodium and chlorine currents (Mankodi et al., 2002; Mounsey et al., 2000b; Ueda et al., 2000). DHPR (Dihydropyridine receptor), which is located in the T-tubule of skeletal muscle, has been reported to be phosphorylated by DMPK, which in turn allows influx of calcium, thereby

increasing $[Ca^{2+}]_I$ levels in DM cells (Ueda et al., 2000). Calcium homeostasis in DMPK KO derived myotubes was also perturbed (Llagostera et al., 2007). Pall et al., also observed an increase in cytosolic calcium in DMPK KO mice cardiomyocytes, which was attributed to increased phosphorylation of Phospholamban (PLN) (Mounsey et al., 2000a; Pall et al., 2003). PLN upon phosphorylation activates SERCA2 to take calcium into SR. However another group showed a decrease in SR calcium upon phosphorylation of PLN (Ueda et al., 1999). Lack of in vivo interaction between PLM and DMPK, raises the doubt that PLM could be a potential downstream effector of DMPK activity, rather than an interacting partner(Mounsey et al., 2000a). MYPT1, which is involved in rearrangement of actin cytoskeleton, is also thought to interact with DMPK (Muranyi et al., 2001). The molecular mechanism or in-vivo data to support their interaction is missing and hence need to be considered with a pinch of salt.

A critical reappraisal confirms that Mitofusin 2 tethers endoplasmic reticulum to mitochondria.

Deborah Naon[1,2], Marta Zaninello[2,4], Marta Giacomello[1,3], Tatiana Varanita[1,3], Francesca Grespi[1,3], Sowmya Lakshminaranayan[1,4], Annalisa Serafini[1,3], Maria Isabel Hernández-Alvarez[5], Antonio Zorzano[5], Diego de Stefani[2], Gerald W Dorn II[6], Luca Scorrano[1,3]

[1]*Department of Biology, University of Padua, Via U. Bassi 58B, 35121 Padua, Italy*

[2]*Department of Biomedical Sciences, University of Padua, Italy*

[3]*Dulbecco-Telethon Institute, Venetian Institute of Molecular Medicine, Padua, Italy*

[4]*Fondazione S. Lucia IRCCS, Roma, Italy.*

[5]*Institute for Research in Biomedicine (IRB Barcelona). The Barcelona Institute of Science and Technology, Barcelona, Spain; Departament de Bioquímica i Biologia Molecular, Facultat de Biologia, Universitat de Barcelona; CIBER de Diabetes y Enfermedades Metabólicas Asociadas (CIBERDEM), Instituto de Salud Carlos III.*

[6]*Department of Internal Medicine, Center for Pharmacogenomics, Washington University School of Medicine, St Louis MO, USA.*

Running title: Mitofusin 2 tethers mitochondria to ER

Character counts: 19746

Address correspondence to: Luca Scorrano luca.scorrano@unipd.it

Abstract

The discovery of the multiple roles of mitochondria-endoplasmic reticulum (ER) juxtaposition in cell biology often relied on the exploitation of Mitofusin (Mfn) 2 as a ER-mitochondria tether. However, this established Mfn2 function was recently questioned, calling for a critical re-evaluation of Mfn2 role in ER-mitochondria crosstalk. Electron microscopy and fluorescence-based probes of organelle proximity confirmed that ER-mitochondria juxtaposition was reduced by constitutive or acute *Mfn2* deletion. Functionally, mitochondrial uptake of Ca^{2+} released from the ER was reduced following acute *Mfn2* ablation as well as in *Mfn2*$^{-/-}$ cells overexpressing the mitochondrial calcium uniporter (MCU). Mitochondrial Ca^{2+} uptake rate and extent were normal in isolated *Mfn2*$^{-/-}$ liver mitochondria, consistent with the finding that acute or chronic *Mfn2* ablation or overexpression did not alter MCU complex component levels. Hence, *Mfn2* stands as a bona fide ER-mitochondria tether whose ablation decreases interorganellar juxtaposition and communication.

Introduction

Endoplasmic reticulum (ER) and mitochondria are functionally and physically coupled: this juxtaposition has been recognized to be crucial for mitochondrial Ca^{2+} uptake, lipid transfer, autophagosome formation, regulation of ER stress and apoptosis (Cerqua et al., 2010; de Brito and Scorrano, 2010; Hailey et al., 2010; Hamasaki et al., 2013; Munoz et al., 2013; Naon and Scorrano, 2014; Ngoh et al., 2012; Rizzuto et al., 1993; Rizzuto et al., 1998; Schon and Area-Gomez, 2012; Szalai et al., 1999); and is mediated by protein structures that can be visualized in electron microscopy (EM) and electron tomography (ET) studies. These physical tethers span 6-15 nm when connecting smooth ER and 19-30 nm when connecting rough ER to mitochondria (Csordas et al., 2006). Operationally, an ER-mitochondria tether shall fulfill at least these minimal criteria: (i) it is retrieved on the outer mitochondrial membrane (OMM); (ii) it is retrieved in mitochondria associated ER membranes (MAMs), the ER subdomain involved in interaction with mitochondria (Vance, 1990); (iii) it interacts in trans with a homo or heterotypic interactor on the opposing membrane; (iv) its deletion increases the distance between ER and mitochondria; (v) its deletion reduces exchange of Ca^{2+} and/or lipids between ER and mitochondria.

The molecular nature of tethers remained elusive for many years. The scaffold protein PACS2 modulates their extent (Simmen et al., 2005), and they include the heterotypic association between inositol triphosphate (IP3) receptor on the ER and the OMM channel VDAC (Szabadkai et al., 2006). By using a combination of imaging, electron tomography, genetics and biochemical and functional assays we discovered that ablation of the mitochondria-shaping protein Mitofusin 2 (Mfn2) increases the distance between ER and mitochondria; that a fraction of Mfn2 is retrieved in MAMs; and that ER Mfn2 *interacts in trans* with Mfn1 or Mfn2 on the mitochondria to physically tether the organelles. Importantly, *Mfn2* ablation decreases agonist-evoked Ca^{2+} transfer from ER to mitochondria (de Brito and Scorrano, 2008), a process known to depend on the close association between the two organelles and the generation of high Ca^{2+} microdomains at their interface (Csordas et al., 2010; Giacomello et al., 2010). Our earlier findings were confirmed independently in the heart (Chen et al., 2012), in pro-opiomelanocortin neurons (Schneeberger et al., 2013) and in the liver (Sebastian et al., 2012). Mfn2 dependent tethering is regulated by posttranslational modifications: non degradative Mfn2 ubiquitination by the E3 ligase MITOL reduces ER-mitochondria tethering and Ca^{2+} transfer without affecting mitochondrial or ER morphology (Sugiura et al., 2013). Furthermore, Mfn2 deletion impacts other facets of ER-

mitochondria communication like phosphatidylcholine (Hailey et al., 2010), cholesterol (Area-Gomez et al., 2012; Duarte et al., 2012; Wasilewski et al., 2012) and perhaps ubiquinone precursors (Mourier et al., 2015) transfer to mitochondria. Finally, Mfn2 participates in other types of heterotypic mitochondria tethering with melanosomes and lipid droplets (Daniele et al., 2014; Sandoval et al., 2014). Structurally, homo or heterotypic *in trans* interaction between ER-Mfn2 and mitochondrial Mfn2 or Mfn1 are supported by Mfn2 role in mitochondrial tethering and fusion (Rojo et al., 2002; Santel and Fuller, 2001). Two Mfn2 coiled coil (CC) 2 domains can fold into a dimeric antiparallel coiled coil and that Mfn2 CC2 can interact with Mfn1 CC1, supporting the notion that trans Mfns complexes between opposing mitochondrial membranes depend on Mfns CC domains (Koshiba et al., 2004). ER-Mfn2 harboring only the CC1 domain engages in homo- or heterotypic interactions with mitochondrial Mfns (de Brito and Scorrano, 2008), indicating that also CC1 can participate in Mfn2 oligomers formation. Biochemically, Mfn2 participates in homo and heterotypic tethering of mitochondria in trans, whereas the fusion reaction depends on the higher GTPase activity of Mfn1 (Chen et al., 2003; Eura et al., 2003; Pyakurel et al., 2015). Mfn2 tethering function is not conserved among all eukaryotes. In the yeast *S. cerevisiae* the ER-mitochondria tether complexes ERMES (Kornmann et al., 2009) and EMC (Lahiri et al., 2014) function independently of the ancestral single yeast mitofusin and are formed by proteins located on the ER and on the outer mitochondrial membrane. Conversely in higher non mammalian eukaryotes Mfn2 does mediate ER-mitochondria crosstalk. For example, ER stress is a major causative component of the pathology caused by the deletion of the single *D. melanogaster* mitofusin (Marf) (Bhandari et al., 2015; Debattisti et al., 2014), and Marf ablation is complemented by mammalian *Mfn2* (but not Mfn1) (Debattisti et al., 2014; Sandoval et al., 2014)

Despite evidence by multiple laboratories, Mfn2 ER-mitochondria tether function was recently challenged in two studies grounded on EM inspection of *Mfn2* deficient cells (Cosson et al., 2012; Filadi et al., 2015). Morphometric analyses and functional assays in *Mfn2*$^{-/-}$ fibroblasts as well as in cells where *Mfn2* was acutely silenced indicated an increase in the mitochondrial surface closely juxtaposed to the ER. Accordingly, when *Mfn2* was acutely ablated, Ca^{2+} transfer between the two organelles was increased; in cells where *Mfn2* was chronically deleted, the decreased mitochondrial Ca^{2+} uptake upon agonist mediated ER Ca^{2+} release was deemed to be a consequence of reduced mitochondrial Ca^{2+} uniporter (MCU) levels. Since these studies challenge two criteria fulfilled by Mfn2 to be considered as an ER-mitochondria tether, we decided to critically re-evaluate if chronic or acute *Mfn2* ablation impacts on ER-mitochondria proximity and

Ca^{2+} transfer. Morphometric analysis of mitochondrial surface juxtaposition to ER, unbiased fluorescent probes of ER-mitochondrial proximity, novel cellular models of acute *Mfn2* genetic ablation, biochemical and genetic analyses of MCU complex components and Ca^{2+} uptake measurement in purified mitochondria corroborate the wealth of evidence indicating that Mfn2 tethers ER to mitochondria.

Results and Discussion

In order to compare our previous observation that Mfn2 tethers ER to mitochondria with recent EM data questioning this result, we analyzed by EM the effect of *Mfn2* ablation in mouse embryonic fibroblasts (MEFs). Visual inspection of EM images acquired by facility personnel blinded to sample identity revealed that *Mfn2* ablation increased the distance between ER cisternae and mitochondria. The defect was specific because reintroduction of *Mfn2* recovered the close juxtaposition between the two organelles (Fig. 1A). Arbitrary definition of tethering distance can be a confounding parameter in interpretation of organelle proximity. Tethers identified in electron tomography span from a minimum of 9 to a maximum of 30 nm (Csordas et al., 2006). We therefore measured the average distance between mitochondria and ER located within 30nm from the former. Morphometric analysis of 200 interactions per condition revealed that *Mfn2* ablation resulted in a ~20% increase in the distance between the organelles (Fig 1B). This increase was confirmed also when we analyzed ER membranes located <20nm from mitochondria (Fig. S1A). Previous morphometric analyses (Cosson et al., 2012; Filadi et al., 2015) did not measure distance between the ER and mitochondria within a range known to be spanned by physical tethers, whereas our initial analysis does not take into account the possibility that number of contacts and their overall length increases and did not correct for changes in mitochondrial surface and perimeter. Mitochondrial surface increase were indeed deemed to artificially decrease Pearson's and Manders' indexes of colocalization based on individual pixel channel overlap (Manders et al., 1993) and therefore to account for the tethering reduction measured in *Mfn2*$^{-/-}$ cells by confocal microscopy. As a proof of this concept, in a simulation experiment a ~10% decrease in the Manders' coefficient was achieved by a computational ~70% increase in the surface of the mitochondrial object. Conversely, mitochondrial surface-ER juxtaposition measured by confocal microscopy was reduced by ~10-15% in MEFs upon *Mfn2*-mediated changes in mitochondrial morphology (Filadi et al., 2015). It shall be mentioned that this mitochondrial surface increase was (Filadi et al., 2015) or was not found (Cosson et al., 2012) in EMs of *Mfn2*$^{-/-}$ MEFs, questioning its importance in ER-mitochondria interaction. We nevertheless decide to take this parameter into account and devised an ER-MItochondria Contact Coefficient (ERMICC) that computes not only the distance between ER and mitochondria but also the interaction length and the perimeter of the mitochondria involved in the interaction, i.e. the overall surface of the organelle (Fig. 1C). ERMICC was reduced more than 70% upon *Mfn2* ablation, irrespectively of whether we considered ER cisternae positioned within a 30 (Fig. 1D) or 20 (Fig. S1B) nm radius

from mitochondria. This extent of ERMICC decrease cannot be explained even if we consider the 30% increase in mitochondrial perimeter measured in *Mfn2*$^{-/-}$ cells (Filadi et al., 2015). Indeed, fitting the formula with data from (Cosson et al., 2012) and with the measured increase in ER-mitochondria distance (Fig. 1B), ERMICC *decreases* by approx. 30% in *Mfn2*$^{-/-}$ cells, indicating that the observed ERMICC reduction is the compound effect of reduced mitochondrial surface in contact with ER and ER-mitochondria distance increase. Finally, since tethering measurements based on EM or confocal image analysis can be prone to operator bias, we turned to assays of ER-mitochondria proximity based on a dimerization-dependent GFP (ddGFP) fluorescent probe. This ddGFP sensor of ER-mitochondria juxtaposition is formed by two monomeric non fluorescent GFPs, one targeted to the ER surface, the other to the OMM: when the two GFPs are closer than 20 nm a fluorescent dimer is formed (Alford et al., 2012). Flow cytometry revealed a ~73% decrease in ddGFP fluorescence in *Mfn2*$^{-/-}$ MEFs compared to their WT counterparts (Fig. 1E,F). We also measured ER-mitochondria tethering using a modified a fluorescence resonance energy transfer (FRET)-based indicator of ER-Mitochondria Proximity (FEMP). This sensor contains a dimerization domain that allows maximal juxtaposition and FRET by brief rapamycin treatment (Csordas et al., 2010). FRET intensity is inversely proportional to the sixth power of the distance between the two fluorophores and it occurs when the two FEMP fluorophores are closer than 15 nm (Majoul et al., 2002). The modified sensor is expressed from a single mRNA that allows equimolar levels of the ER and mitochondria anchored fluorescent proteins, thanks to the introduction of a self-cleavable viral Tav2A sequence between the two mRNAs (Luke and Ryan, 2013) (Fig. S2A). The two fluorescent proteins are appropriately targeted and measure basal as well as maximal (rapamycin induced levels) organelle proximity in MEFs (Fig. S2B, C). FRET ratios measured using the FEMP probe were significantly reduced in *Mfn2*$^{-/-}$ MEFs as compared to their WT counterparts. In conclusion, multiple methods confirm decreased ER-mitochondria juxtaposition upon chronic *Mfn2* ablation.

The morphometric, ddGFP and FEMP results complement our previous analyses of ER-mitochondria juxtaposition based on electron tomography, confocal microscopy, and in vitro isolated organelle interaction assays (de Brito and Scorrano, 2008) and are in accordance with other EM studies that revealed decreased juxtaposition in *Mfn2* deficient neurons (Schneeberger et al., 2013) and cardiomyocytes (Chen et al., 2012). These data are difficult to reconcile with the reported tethering increase upon *Mfn2* ablation (Cosson et al., 2012; Filadi et al., 2015), but a potential explanation for the latter resides in the nutritional status of the cells. Stress (Bravo et al.,

2011) and starvation tightens ER-mitochondria contacts (Csordas et al., 2006; Sood et al., 2014) and cell proliferation increases upon *Mfn2* downregulation (Bucha et al., 2015): indeed, ddGFP signal was increased in cells from overgrown cultures (not shown), suggesting that culture conditions and nutrient availability could explain the discrepancy and calling for multiple approaches to measure interorganellar juxtaposition.

Clonal differences in established *Mfn2*$^{-/-}$ cell lines might also explain the discrepancies on Mfn2 role as a tether. We therefore decided to turn to models of *Mfn2* acute ablation. Earlier observations indicated that *MFN2* gene silencing in human cells increases the distance and reduces the crosstalk between ER and mitochondria (Cerqua et al., 2010; de Brito and Scorrano, 2008; Hamasaki et al., 2013), yet these results required to be validated by unbiased fluorescent probes of ER-mitochondria proximity located only on organelle surface and in models of *Mfn2* gene ablation rather than silencing (where off-target RNAi effects might confound the interpretation of the results). We therefore measured the effect of two different shRNAs targeting *Mfn2* on FRET ratios in FEMP-expressing MEFs. Normalized FRET values were comparably and significantly reduced upon silencing of Mfn2 or of the other known ER-mitochondria tether regulator PACS2 (Fig. 2A), indicating that ER-mitochondria tethering decreases irrespective of whether *Mfn2* is acutely or constitutively ablated. In order to circumvent the issue of potential shRNAs off-target effects, we then generated MEFs from conditional *Mfn2* knockout (*Mfn2*$^{flx/flx}$) mice (Chen et al., 2010) and induced acute *Mfn2* deletion by means of adenoviral delivery of CRE recombinase. MFN2 was reduced at 24hrs post infection and almost completely lost at 48hrs (not shown and Fig. 4A). In 3D reconstructions of z-confocal stacks of mtYFP and ER targeted dsRED (ER-RFP) mitochondria and ER appeared grossly fragmented 48 hrs post infection (Fig. 2B) and ER-mitochondria pseudocolocalization was reduced like in *Mfn2*$^{-/-}$ cells (de Brito and Scorrano, 2008) (Fig. 2B,C). Flow cytometry analysis of ddGFP fluorescence confirmed the increased ER-mitochondria distance, revealing a 5 fold decrease in ddGFP positive events upon Cre mediated *Mfn2* ablation (Fig. 2 D, E). Finally, EM revealed that acute *Mfn2* ablation increased ER-mitochondria distance (Fig. 2F,G) and decreased the contact coefficient ERMICC (Fig. 2H). Like for *Mfn2*$^{-/-}$ cells, these morphometric parameters were independent from the maximum distance of the tethers considered, i.e lower than 20 or 30nm (Fig. S3). In conclusion, ER-mitochondria tethering measured by fluorescence and EM morphometry is decreased irrespective of the mean used to acutely ablate *Mfn2*.

If *Mfn2* ablation decreases ER-mitochondria tethering, crosstalk between the two organelles shall be altered, as reported by many (Cerqua et al., 2010; Chen et al., 2012; de Brito and Scorrano, 2008; Schneeberger et al., 2013; Sood et al., 2014; Sugiura et al., 2013). However, the key feature of reduced mitochondrial Ca^{2+} uptake following agonist induced ER Ca^{2+} release in *Mfn2*$^{-/-}$ MEFs was explained not as a consequence of lower tethering, but of lower mitochondrial Ca^{2+} uniporter (MCU) levels (Filadi et al., 2015). MCU is the channel forming subunit of the MCU holocomplex that contains other essential regulatory components including MICU1, MICU2 and EMRE (Kamer and Mootha, 2015; Rizzuto et al., 2012). In cells where *Mfn2* was silenced, MCU as well as ER Ca^{2+} levels appeared normal, but mitochondrial Ca^{2+} transients were approx. 40% higher, a phenotype compatible with increased ER-mitochondria juxtaposition (Filadi et al., 2015). To circumvent potential issues of off-target siRNA effects, we turned to our model of acute *Mfn2* deletion. In the absence of extracellular Ca^{2+}, agonist induced ER Ca^{2+} release was however increased in *Mfn2*$^{flx/flx}$ infected with Cre adenoviruses (Fig. 3A), indicating an increase in ER Ca^{2+} stores similar to that recorded in *Mfn2*$^{-/-}$ MEFs (de Brito and Scorrano, 2008). This greater availability of cytosolic Ca^{2+} resulted in increased mitochondrial Ca^{2+} uptake which was maximized upon reintroduction of extracellular Ca^{2+} (Fig. 3B,C), when mitochondria are exposed to capacitative Ca^{2+} entry (CCE). These data are in accordance with previous reports of increased CCE upon *Mfn2* reduction (Kasahara et al., 2013; Singaravelu et al., 2011) and require that mitochondrial Ca^{2+} uptake is measured (i) excluding CCE by chelating extracellular Ca^{2+}; (ii) and exposing mitochondria to comparable Ca^{2+} levels, by titrating the IP3-coupled agonist ATP to generate the same $[Ca^{2+}]_i$ peak (Fig. 3D,E). In these conditions, mitochondrial Ca^{2+} uptake was significantly lower (Fig. 3F,G) and slower (Fig. 3H) in *Mfn2*$^{flx/flx}$ infected with Cre adenoviruses. These data are consistent with previous reports of chronic (de Brito and Scorrano, 2008) and tissue specific (Chen et al., 2012) *Mfn2* ablation and can be explained by reduced ER-mitochondria juxtaposition upon acute *Mfn2* deletion (see above) or by reduced intrinsic Ca^{2+} uptake ability of *Mfn2* deficient mitochondria, as suggested by (Filadi et al., 2015). We therefore turned to purified liver mitochondria, where Ca^{2+} uptake measurements can be carried out without the confounding effects of contaminating ER (with its high Ca^{2+} affinity SERCA pumps), by monitoring extramitochondrial Ca^{2+} insensitive to the equilibrium between the intramitochondrial stores and the targeted dye, and in the presence of the permeability transition pore inhibitor cyclosporine A to avoid confusion from simultaneous Ca^{2+} efflux through this Ca^{2+} sensitive non selective inner membrane channel (Bernardi, 1999). Recordings of Ca^{2+} uptake and release upon pulses of Ca^{2+} were superimposable in control (wt)

and *Mfn2* deficient (*Mfn2*^{LKO}) liver mitochondria (Fig. 3I-K), whose respiratory efficiency (and hence driving force for Ca^{2+} uptake) and Ca^{2+} retaining capacity were equivalent (Fig. S4). As expected from these functional results, MCU, MICU1 and MICU2 levels were not affected upon *Mfn2* ablation (Fig. 4A-C). Quantitative transcriptional analysis by RNA-sequencing of mouse hearts with cardiomyocyte-directed *Mfn2* ablation (Chen and Dorn, 2013) or overexpression (Gong et al., 2015) confirmed that uniporter holoplex component mRNAs do not change when Mfn2 is genetically manipulated (Fig. 4D). Concordantly, MCU, MICU1 and MICU2 levels as judged by immunoblotting were indistinguishable in *Mfn2*$^{-/-}$ and WT MEFs (Fig. 5A-D). Thus, genetic modulation of *Mfn2* levels does not affect the intrinsic mitochondrial Ca^{2+} uptake machinery or process, whereas in cells acute *Mfn2* deletion decreases interorganellar tethering and mitochondrial uptake of Ca^{2+} released from the ER. Several potential explanations exist for the differences between our results and those of (Filadi et al., 2015): first, the cell permeabilization procedure or the concomitant presence of the ER (with active SERCA that is upregulated in *Mfn2*$^{-/-}$ cells (de Brito and Scorrano, 2008)) in the (Filadi et al., 2015) permeabilized cell preparation might affect mitochondrial Ca^{2+} uptake; second, since acute, like chronic *Mfn2* deletion, increases ER Ca^{2+} content (and hence release), ER Ca^{2+} release might not have been comparable; third, the *Mfn2* siRNA used might have had potential off target effects, as highlighted by the need to pre-deplete ER Ca^{2+} stores in experiments of *Mfn2* re-expression in order to obtain similar ER Ca^{2+} release (Filadi et al., 2015).

In order to definitively test the relationship between *Mfn2* ablation, MCU levels and mitochondrial Ca^{2+} uptake, we went back to wt and *Mfn2*$^{-/-}$ MEFs where we adenovirally delivered high and comparable MCU levels (Fig. 5D). When agonist-induced $[Ca^{2+}]_i$ peaks were comparable (Fig. 5E,F), mitochondrial Ca^{2+} uptake was still lower and slower in MCU overexpressing *Mfn2*$^{-/-}$ MEFs (Fig. 5G,H). Given that no differences in mitochondrial membrane potential were observed basally (Filadi et al., 2015) as well as upon MCU overexpression (not shown), decreased ER-mitochondria tethering stands as the most probable explanation for the reduced mitochondrial Ca^{2+} uptake observed in this experiment.

The critical reappraisal of the role of Mfn2 in ER-mitochondria juxtaposition supports previous results identifying this molecule as the a physical tether between the two organelles in multiple tissues and call to critically reconsider the conclusions of the two recent papers confuting Mfn2 ER-mitochondria tethering function based on limited experimental approaches (Cosson et al.,

2012; Filadi et al., 2015). It is difficult to rationalize the proposed role for Mfn2 as a negative regulator of tethering (Filadi et al., 2015) with previous knowledge on the function of this dynamin related protein in membrane biology. Mfn2 was indeed originally identified as the mitochondrial fusion factor (Santel and Fuller, 2001) whose overexpression induces clusters of closely apposed, yet individual mitochondria, indicating that it likely mediates mitochondrial adhesion (Eura et al., 2003; Rojo et al., 2002). In a similar scenario, Mfn2 on the ER engages in homo- or hetero-typic interactions with mitochondrial Mfn2 or Mfn1 to tether the two organelles. Not surprisingly, its acute or chronic ablation decreases juxtaposition measured by EM, pseudocolocalization, FRET or GFP based probes, and by in vitro assays of purified ER-mitochondria cosedimentation. Functionally, transfer of Ca^{2+} from ER to mitochondria is blunted in *Mfn2* deficient cells, without any intrinsic defect in mitochondrial Ca^{2+} uptake machinery. Conversely, Mfn2 shall not be considered the only mammalian tether: multiple other factors have been identified to grant mitochondria-ER juxtaposition independently of Mfn2. Indeed, the two organelles are still (albeit to a lower extent) tethered in cells lacking both Mfns and our own FEMP data confirm the validity of other identified tethers such as PACS2. Irrespectively of the complexity of the anatomy of the ER-mitochondria interface, Mfn2 fulfills the basic criteria to stand as a bona fide tether and the discoveries on the biology of this interface based on Mfn2 stand solid.

Acknowledgements

We thank Drs. F. Caicci and F. Boldrin (EM Facility, Dept. of Biology, University of Padova) for performing EM. LS is a Senior Scientist of the Dulbecco-Telethon Institute. Supported by Telethon-Italy GGP12162, GGP14187A, AIRC Italy, ERC FP7-282280, FP7 CIG PCIG13-GA-2013-618697, Italian Ministry of Research FIRB RBAP11Z3YA_005 to LS, by NHLBI R01s HL59888, 108943, and 128071 from the USA National Institutes of Health to GWD and by MINECO SAF2013-40987R, Generalitat de Catalunya Grant 2014SGR48, ICREA Academia, CIBERDEM and PIE14/00045 from Instituto de Salud Carlos III to AZ.

Materials and methods

Molecular Biology

mtYFP, ERYFP, mtRFP, MFN2 plasmids were previously described (de Brito and Scorrano, 2008). ddGFP was a kind gift from D. Campbell . For the generation of the modified FRET ER-mitochondria sensor, cDNAs encoding for the two moieties of the FRET based Mito-ER Linker probe (FEMP) were kindly provided by prof. G.Hajnoczky (Csordas et al 2010, plasmids provided: pEGFP-N1 AKAP1 (34-63)-FKBP-YFP and pEGFP-C3 CFP-HA-FRB-Helix-ER (Sac1)). The cDNA coding for AKAP1 (34-63)-FKBP-YFP was subcloned into pcDNA4/TO (Invitrogen) with EcoRV and KpnI before the Tav2a peptide sequence (derived from GFP-2A-CherryFP in pJC3, kindly provided by Prof. M Ryan, University of St Andrews). CFP-HA-FRB-Helix-ER (Sac1) was introduced after the Tav2a sequence between ClaI and XbaI restriction sites. MCU-Flag adenoviruses were generated as described (Raffaello et al., 2013). Deep RNA sequencing of mouse hearts was performed and analyzed as described (Matkovich and Dorn, 2015) on Illumina HiSeq systems.

Cell culture

SV40-transformed wt, and *Mfn2*$^{-/-}$ mouse embryonic fibroblasts (MEFs) were cultured and transfected as described (de Brito and Scorrano, 2008).

Mfn2 $^{flx/flx}$ MEFs were generated from *Mfn2*$^{loxp/loxp}$ 11.5 days embryos as described (Song et al., 2015) and SV40 immortalized by transfection with pMS-SV-LT and selection by cultivation in DMEM supplemented with 250 µM Neomycin until resistant clones emerged. SV40 transformed MEFs were cultured as described (de Brito and Scorrano, 2008). Where indicated, cells were infected with AAV-CMV-mtYFP (mtYFP) and AAV-CMV-CRE-2A mtYFP (CRE) adenoviruses at a multiplicity of infection (MOI) of 50pfu/cell for 16 hrs or with pLV-CMV-NLSCRE lentiviruses (LVP339, Gentarget) at a MOI of 100pfu/cell for 96hrs.

Confocal and FRET Imaging

For confocal microscopy imaging of live cells, 2×10^5 cells seeded onto 24-mm round glass coverslips, treated as indicated were placed on the stage of a Nikon Eclipse TE300 inverted microscope equipped with a PerkinElmer Ultraview LCI confocal system, a piezoelectric z-axis

motorized stage (Pifoc, Physik Instrumente) and an Orca ER 12-bit CCD camera (Hamamatsu Photonics). Acquisition, deconvolution, 3D reconstruction, volume rendering of the stacks as well as analysis of the mitochondria to ER interaction was performed as described (de Brito and Scorrano, 2008).

For FRET experiments, 9000 cells/ml were seeded on Cell carrier 384 well plate (Perkin Elmer) and were transduced with *Mission* lentiviral viral particles (~10^6 TU), (Sigma). After 24 hours, cells were transfected with FEMP cDNA using Genjet (SignaGen laboratories) according to manufacturer's instruction and after a further 24 hours cells were imaged using a Perkin Elmer Operetta High Content imaging system. To obtain basal level FRET ($FRET_{basal}$), images were collected using the following filters: CFP (ex 410-430, em 460-500), YFP (ex 490-510, em 520-560) and YFP_{FRET} (ex 410-430, em 520-560). To image the maximum FRET intensity ($FRET_{max}$), the cells were treated with 100 nM Rapamycin for 15 minutes and then fixed with 1% Formaldehyde for 10 minutes. Acquisition of $FRET_{max}$ was performed as before in 1X PBS. Images were analyzed using Perkin Elmer Harmony 3.5 image analysis software. YFP channel was chosen to mark the ROI and around each ROI, a second boundary was drawn to measure the background intensity. $FRET_{basal}$ and $FRET_{max}$ were calculated as: $(F_{YFPFRETcell}-F_{YFPFRETbg})/(F_{CFPcell}-F_{CFPbg})$; FRET Ratio was calculated as $(FRET_{max}–FRET_{basal})/FRET_{basal}$.

Flow cytometry and cell sorting

For evaluation of dimerization depend GFP (ddGFP) formation cells were co-transfected with a cytosolic marker (cyto-dsRED) and non-fluorescent GFP monomers targeted to ER and mitochondria. Flow cytometric analyses of cell size (forward scatter, FSC), cytosolic dsRED level (red signal intensity detected by FL2 channel) and ddGFP fluorescence (GFP signal intensity detected by 15 mW argon ion laser tuned at 488 nm; CellQuest software, Becton 10 Dickinson Biosciences) were performed on a FacsCalibur Flow Cytometer (Becton Dickinson, San Jose, CA). Acquisition was stopped when 50000 FL2+ events were reached. Data are shown as dot plot of FL1 versus side scatter derived from FL2+ gated events.

For sorting, 1x10^6 MEFs were transfected with pEGFP and 16 hrs later were analyzed through a 530 nm band pass filter as they traversed the beam of an argon ion laser (488 nm, 100 mW) of an FACSAria (BD). 3 x10^5 GFP positive sorted cells were cultured in DMEM supplemented with 2 mM

glutamine, 1 mM penicillin/streptomycin, 20% fetal bovine serum and incubated 24 hrs at 37°C in a fully humidified atmosphere of 95% air and 5% CO2. On the following day, medium was replaced to remove dead cells. Growing cells were fixed after 8 hrs and prepared for EM images.

Electron microscopy

MEFs of indicated background were fixed with 1.25% (v/v) glutaraldehyde in 0.1 M sodium cacodylate at pH 7.4 for 1 h at room temperature. Electron microscopy was performed as described (de Brito and Scorrano, 2008). Thin sections were imaged on a Tecnai-20 electron microscope (Philips-FEI). Morphometric measurements were carried out using ImageJ (National Institutes of Health, Bethesda)).

Immunoblotting

Cells ($1.8x10^6$) at 80% of confluence were harvested 48 or 96 h after transfection and disrupted in 150 mM NaCl, 1% Nonidet P-40/0, 0.25% deoxycholate, 1 mM EDTA, and 50 mM Tris, pH 7.4 in the presence of complete protease inhibitor mixture (Sigma-Aldrich). 40 μg of extracted proteins were separated by 4‑12% Bis-Tris SDS-PAGE (NuPAGE; Invitrogen), transferred onto polyvinylidene difluoride (Bio-Rad Laboratories) membranes, and probed using the following antibodies: anti-Actin (1:2,000; EMD Millipore), anti-*Mfn2* (1:1000; Abcam: ab 50838 or Abnova: H00009927-M3), anti-Tom20 (1:5000; Santa Cruz Biotechnology), Anti MCU (1.1000, Sigma-Aldrich: HPA016480), MICU 1 (1:1000; Sigma-Aldrich: HPA037480), MICU 2 (1:1000, Sigma-Aldrich: HPA 045511). Densitometry was performed using ImageJ (National Institutes of Health, Besthesda).

In Vitro Mitochondrial Assays

Mitochondria from liver-specific *Mfn2* knockout mice (*Mfn2*$^{loxP/loxP}$::Alb-Cre$^{+/-}$) and control littermates (*Mfn2*$^{loxP/loxP}$::Alb-Cre$^{-/-}$) (Sebastian et al., 2012) were isolated as described (Frezza et al., 2007). Mitochondrial oxygen consumption was measured with a Clark type oxygen electrode (Hansatech Instruments) (Frezza et al., 2007). Mitochondrial Ca^{2+} uptake and retaining capacity were measured fluorimetrically using a Perkin Elmer LS50B fluorimeter (λ_{ex} 505 nm; λ_{em}: 535 nm,

slit 2.5 nm). Freshly isolated mitochondria were resuspended in experimental buffer (EB) (Frezza et al., 2007) supplemented with 5mM glutamate/2.5mM malate and 1µM Calcium Green-5N (Invitrogen). Pulses of 50 µM Ca^{2+} were added until PTP induction. For measurements of Ca^{2+} uptake EB was also supplemented with 2 µM cyclosporine A.

Aequorin measurements of Ca^{2+} concentration.

Cells grown on 13 mm round glass coverslips at 50% confluence were cotransfected with cytosolic (cyt) or mitochondrial (mt) AEQ and the plasmids indicated. Cyt and mtAEQ reconstitution, measurement and calibration were performed as described (Pinton et al, 2000). AEQ reconstruction were performed with in Krebs Buffers (KRB, 125 mM NaCl, 5 mM KCl, 1 mM Na3PO4, 1 mM MgSO4, 5.5 mM glucose, 20 mM HEPES, pH 7.4) containing 1 mM Ca^{2+}. AEQ measurements were carried out without Ca^{2+} in KRB in presence of 100 mM EGTA. When indicated, KRB was supplemented with 1mM Ca^{2+}.

Statistics

Data are presented as means±SEM of n independent experiments. Statistical significance was determined using unpaired Student's t tests with p set at 0.05 unless differently specified.

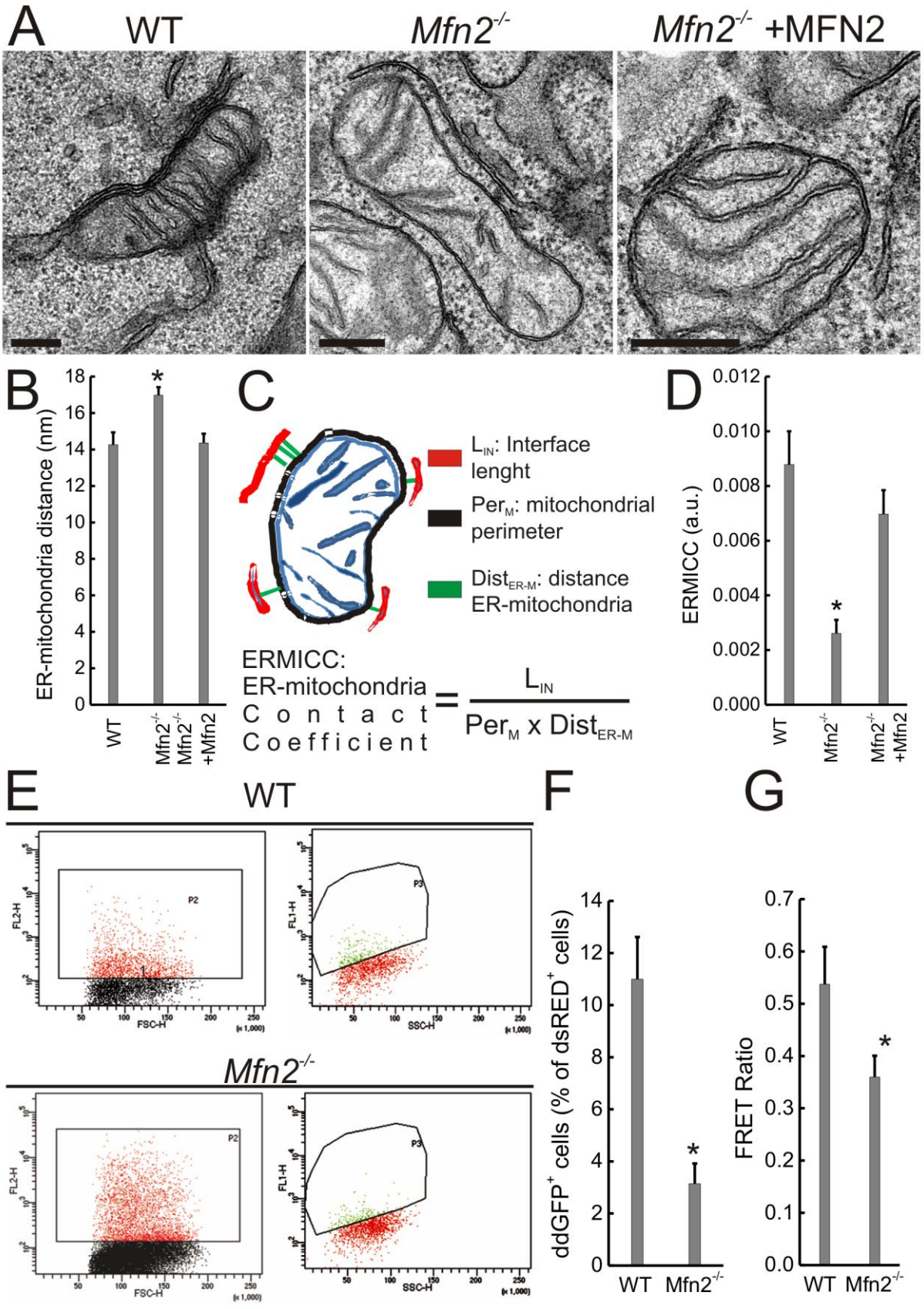

Figure 1. *Mfn2* ablation increases ER-mitochondria distance.

A) Representative EM images of MEFs of the indicated genotype. Where indicated, *Mfn2*$^{-/-}$ MEFs were cotransfected with MFN2 and GFP, sorted and processed for EM Scale bars, 500 nm.
B) Morphometric analysis of ER located at less than 30 nm from mitochondria calculated from 70 images per condition with >5 mitochondria per image. Data represent mean±SEM of 3 independent experiments. *, P<0.05 vs. WT.
C) A cartoon of the ERMICC contact index.
D) Data represent mean±SEM of ERMICC calculated from 3 independent experiments performed as in A. *, P<0.05 vs. WT
E) Flow cytometry analysis of ddGFP fluorescence in cells of the indicated genotype. Cells were cotransfected with ddGFP monomers and cytosolic dsRED. Left, scatterplots of the gated RPF dsRED expressing cells. Right, GFP+ dsRED+ population.
F) Quantitative analysis of ddGFP positive events in MEFs of the indicated genotype. Experiments were as in E. Data represent Mean±SEM of 3 independent experiments. *, P<0.05 vs. WT
G) FEMP measurement of ER-mitochondria contacts in MEFs of the indicated genotype transfected with FEMP and imaged as described. Data represent mean±SEM of 4 independent experiments in which FRET Ratio was calculated as described. *, P<0.05 vs. WT

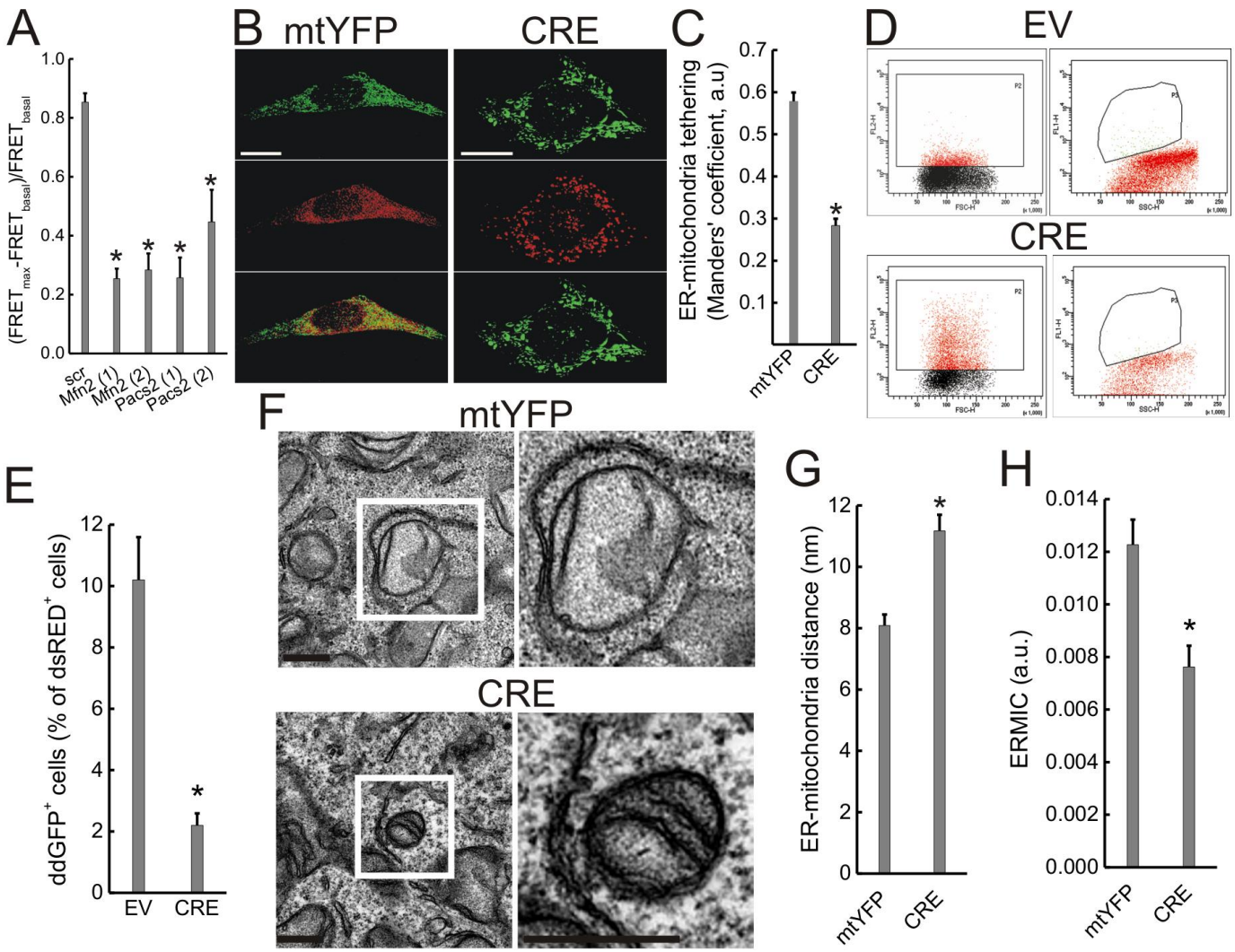

Figure 2. Acute *Mfn2* ablation increases ER-mitochondria distance.

A) FEMP measurement of ER-mitochondria contacts in WT MEFs transduced with the indicated shRNA lentiviral particles for 24 hours (note that two different shRNAs were used for Mfn2 and PACS2). Cells were then transfected with FEMP and after further 24 hrs imaged and FRET Ratio calculated as described. Data represent mean±SEM of 9 independent experiments. *, P<0.05 vs. scr

B) Volume rendered 3D reconstructions of confocal z-stacks of mitochondria (green), ER (red) and merged images (bottom panels) in *Mfn2*$^{flx/flx}$ MEFs infected with AAV-CMV-mtYFP or AAV-CMV-CRE-2A-mtYFP (CRE) adenoviruses. 24 hrs after infection cells were transfected ER-dsRED (pseudocolored in green) and after further 24hrs imaged. Scale bar, 30 µm.

C) Morphometric analysis of experiments performed as in B. Data represent mean±SEM of 10 independent experiments (n=10 cells per experiment). *, P<0.05 vs. mtYFP

D) Flow cytometry analysis of ddGFP fluorescence in *Mfn2*$^{flx/flx}$ MEFs. Cells were infected pLV-CMV (EV) or with pLV-CMV-NLSCRE (CRE) lentiviruses, cotransfected after 48 hrs with ddGFP monomers and cytosolic dsRED and 24 hrs later analyzed by flow cytometry. Left, scatterplots of the gated dsRED expressing cells. Right, GFP^{+}, dsRED^{+} population.

E) Quantitative analysis of ddGFP positive events in *Mfn2*$^{flx/flx}$ MEFs infected as indicated. Experiments were as in D. Data represent mean±SEM of 3 independent experiments. *, P<0.05 vs. EV

F) Representative EM images of *Mfn2*$^{flx/flx}$ MEFs infected with AAV-CMV-mtYFP (mtYFP) or AAV-CMV-CRE-2A mtYFP (CRE) adenoviruses. After 48 hrs cells were fixed and processed for EM. The boxed areas are magnified in the right panels. Scale bars, 500 nm.

G) Morphometric analysis of ER located at less than 30 nm from mitochondria calculated from 70 images per condition with >5 mitochondria per image. Data represent mean±SEM of 3 independent experiments performed as in F. *, P<0.05 vs. mtYFP

H) Data represent mean±SEM of ERMICC calculated from 3 independent experiments performed as in G. *, P<0.05 vs. mtYFP

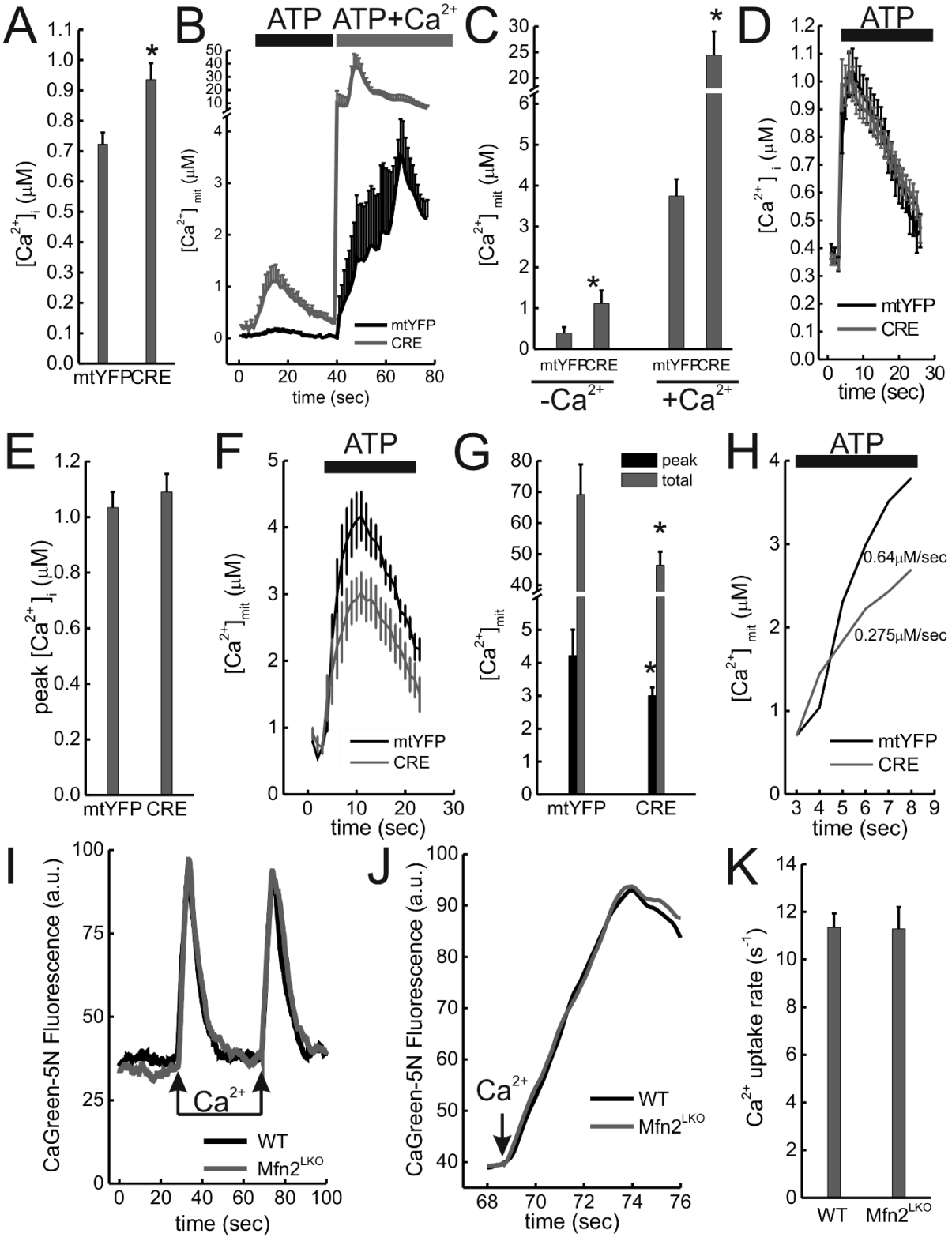

Figure 3. *Mfn2* ablation decreases mitochondrial Ca^{2+} uptake in situ but not in vitro.

A) Peak cytosolic Ca^{2+} concentrations recorded in response to ATP (0.2mM) in *Mfn2*$^{flx/flx}$ MEFs infected AAV-CMV-mtYFP (mtYFP) AAV-CMV-CRE-2A-mtYFP (CRE) adenoviruses and after 48hrs

transfected with cytAEQ. Experiments were performed in cells incubated in extracellular Ca^{2+} free media. Data represent mean ±SEM of 3 independent experiments (n=10 recording per experiment). *, P<0.05 vs. mtYFP

B) Recordings of mitochondrial Ca^{2+} in *Mfn2*$^{flx/flx}$ MEFs infected with AAV-CMV-mtYFP (mtYFP) AAV-CMV-CRE-2A-mtYFP (CRE) adenoviruses and after 48hrs transfected with mtAEQ. Experiments were performed in cells incubated in extracellular Ca^{2+} free media. Where indicated cells were perfused with 0.2 mM ATP and with 0.2 mM ATP and 2 mM extracellular Ca^{2+}. Data represent mean ±SEM of 3 independent experiments (n=10 recording per experiment).

C) Average ± SEM of 3 independent peak mitochondrial Ca^{2+} uptake in 3 experiments performed as in B. *, P<0.05 vs. mtYFP

D) Cytosolic Ca^{2+} recordings in *Mfn2*$^{flx/flx}$ MEFs infected AAV-CMV-mtYFP (mtYFP) AAV-CMV-CRE-2A mtYFP (CRE) adenoviruses and after 48hrs transfected with cytAEQ. . Cre infected cells were incubated for 30 min in Ca2+ free media to predeplete ER Ca^{2+} stores to levels comparable to mtYFP infected MEFs. Where indicated cells were perfused with 0.2 mM ATP.

E) Average ± SEM of peak cytosolic Ca^{2+} transients in 3 independent experiments performed as in D.

F) Recordings of mitochondrial Ca^{2+} in *Mfn2*$^{flx/flx}$ MEFs infected AAV-CMV-mtYFP (mtYFP) AAV-CMV-CRE-2A mtYFP (CRE) adenoviruses and after 48hrs transfected with mtAEQ. Experiments were performed as in D. Where indicated cells were perfused with 0.2 mM ATP. Data represent mean ±SEM of 3 independent experiments (n=10 recording per experiment).

G) Average±SEM of 3 independent peak mitochondrial Ca^{2+} transients in experiments performed as in F. *, P<0.05 vs. the corresponding mtYFP bar.

H) Expanded scale of G. The Ca^{2+} uptake rate is indicated.

I) Purified mitochondria (0.5 mg/ml) from control (WT) and liver specific *Mfn2* knockout mice (*Mfn2*^{LKO}) were incubated in experimental buffer supplemented with 1µM CaGreen5N and 2 µM cyclosporine A. Where indicated, 50 µM Ca^{2+} pulses were added.

J) Expanded scale of I.

K) Average±SEM of mitochondrial Ca^{2+} uptake rate recorded from 3 couples of littermates in experiments performed as in I.

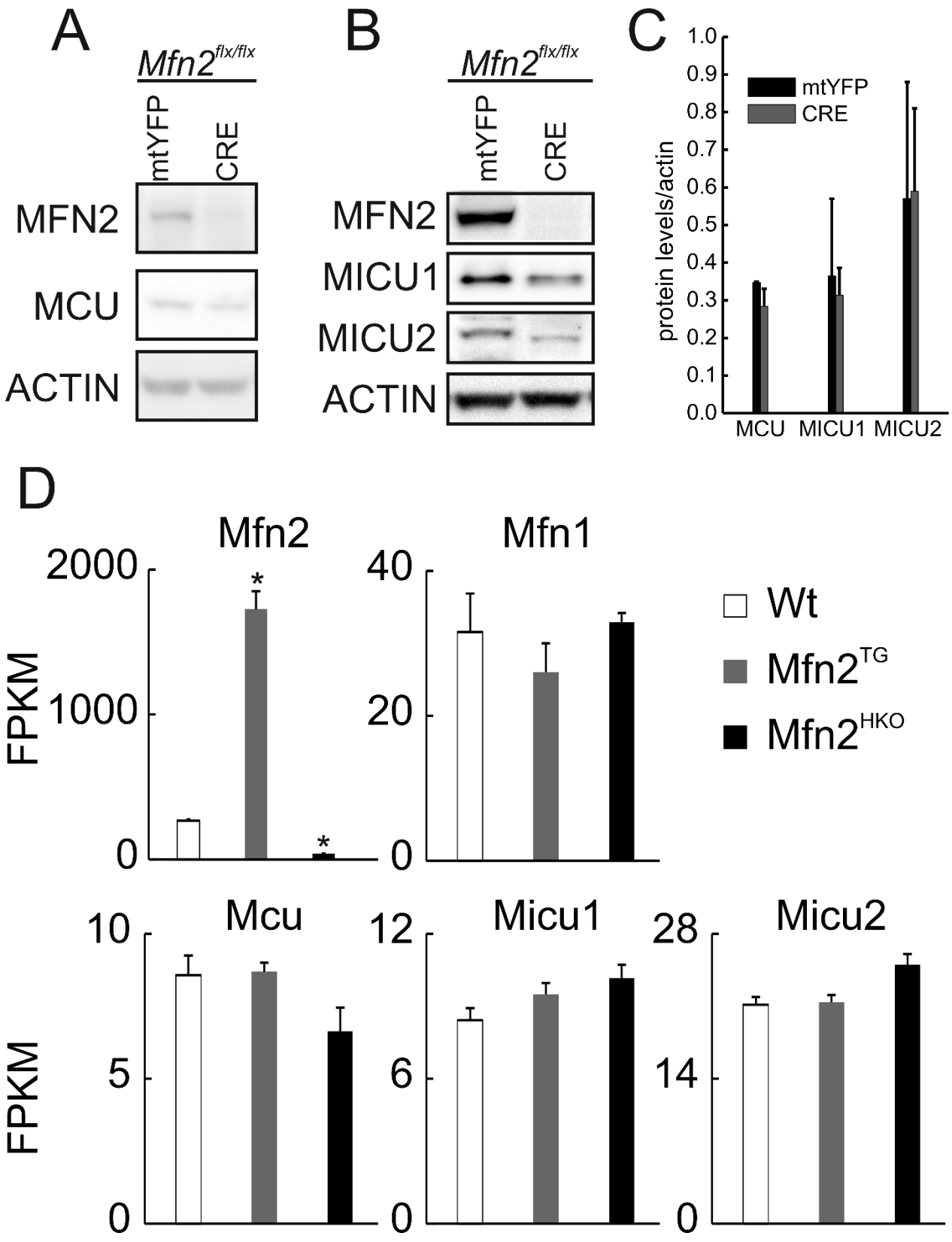

Figure 4. *Mfn2* levels do not affect components of the mitochondrial Ca^{2+} uptake machinery. A,B) *Mfn2*$^{flx/flx}$ MEFs were infected with AAV-CMV-mtYFP (mtYFP) AAV-CMV-CRE-2A mtYFP (CRE) adenoviruses and after 48 hrs equal amounts (40 µg) of protein were separated by SDS PAGE and immunoblotted using the indicated antibodies.

C) Densitometric quantification of MCU, MICU1 and MICU2 protein levels in *Mfn2*$^{flx/flx}$ MEFs infected as indicated. Experiments were as in A. Data represent mean±SEM of 3 independent experiments.
D) RNA seq results for wild-type (Wt), cardiomyocyte-specific Mfn2 transgenic (Mfn2^{tg}), and cardiomyocyte-directed Mfn2 knockout (Mfn2^{HKO}) mouse hearts, expressed as read fragments per kilobase of exon per million reads mapped (FPKM). *,P<0.02 vs Wt (ANOVA).

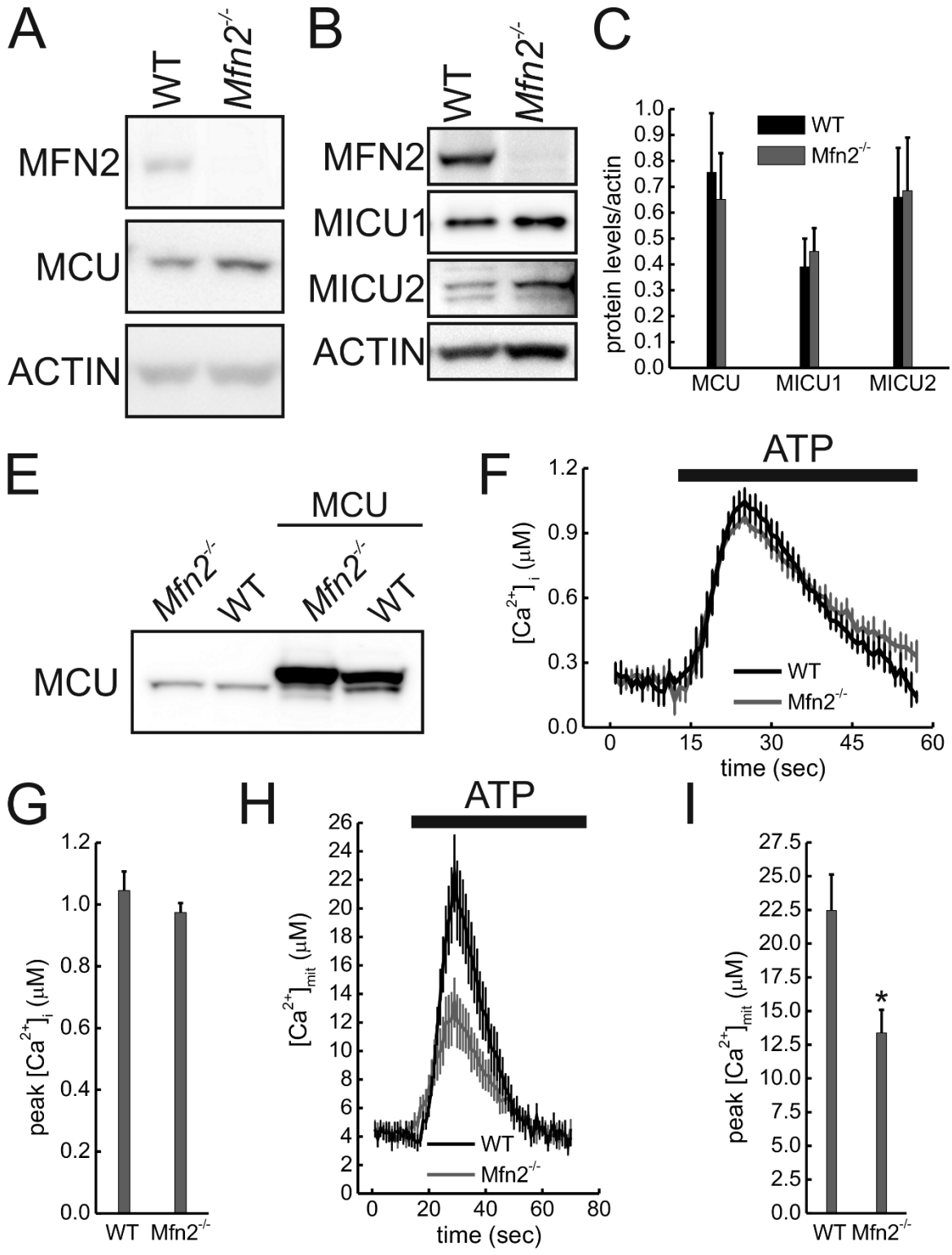

Figure 5. *Mfn2* ablation impairs mitochondrial Ca^{2+} uptake in an MCU-independent manner.
A, B) Equal amounts (40 μg) of total lysates from cells of the indicated genotypes were separated by SDS PAGE and immunoblotted using the indicated antibodies.
C) Densitometric quantification of levels of the indicated MCU holoplex components. Experiments were as in A, B. Data represent mean±SEM of 3 (MICU1,2) or 10 (MCU) independent experiments.

D) *Mfn2*$^{-/-}$ and WT MEFs were infected with the MCU expressing adenoviruses where indicated and after 48h lysed and equal amount of proteins (40 μg) separated by SDS-PAGE and immunoblotted with the indicated antibodies.
E) Recordings of $[Ca^{2+}]_i$ in cells of the indicated genotypes overexpressing MCU. Where indicated, MEFs were perfused with 0.2 mM (wt) or 10 μM (*Mfn2*$^{-/-}$) ATP.
F) Peak of $[Ca^{2+}]_i$ from experiments performed as in E. Data represent mean±SEM of 3 independent experiments.
G) Recordings of $[Ca^{2+}]_{mit}$ in experiments performed as in E.
H) Mean±SEM of peak of $[Ca^{2+}]_{mit}$ from 3 independent experiments performed as in G. *, $P<0.05$ vs. WT

References

Alford, S.C., Y. Ding, T. Simmen, and R.E. Campbell. 2012. Dimerization-dependent green and yellow fluorescent proteins. *ACS Synth.Biol*. 1:569-575.

Area-Gomez, E., C.M. Del Carmen Lara, M.D. Tambini, C. Guardia-Laguarta, A.J. de Groof, M. Madra, J. Ikenouchi, M. Umeda, T.D. Bird, S.L. Sturley, and E.A. Schon. 2012. Upregulated function of mitochondria-associated ER membranes in Alzheimer disease. *EMBO J.*

Bernardi, P. 1999. Mitochondrial transport of cations: channels, exchangers, and permeability transition. *Physiol.Rev.* 79:1127-1155.

Bhandari, P., M. Song, and G.W. Dorn, 2nd. 2015. Dissociation of mitochondrial from sarcoplasmic reticular stress in Drosophila cardiomyopathy induced by molecularly distinct mitochondrial fusion defects. *Journal of molecular and cellular cardiology*. 80:71-80.

Bucha, S., D. Mukhopadhyay, and N.P. Bhattacharyya. 2015. Regulation of mitochondrial morphology and cell cycle by microRNA-214 targeting Mitofusin2. *Biochem Biophys Res Commun*. 465:797-802.

Cerqua, C., V. Anesti, A. Pyakurel, D. Liu, D. Naon, G. Wiche, R. Baffa, K.S. Dimmer, and L. Scorrano. 2010. Trichoplein/mitostatin regulates endoplasmic reticulum-mitochondria juxtaposition. *EMBO Rep.* 11:854-860.

Chen, H., S.A. Detmer, A.J. Ewald, E.E. Griffin, S.E. Fraser, and D.C. Chan. 2003. Mitofusins Mfn1 and Mfn2 coordinately regulate mitochondrial fusion and are essential for embryonic development. *J.Cell Biol.* 160:189-200.

Chen, H., M. Vermulst, Y.E. Wang, A. Chomyn, T.A. Prolla, J.M. McCaffery, and D.C. Chan. 2010. Mitochondrial fusion is required for mtDNA stability in skeletal muscle and tolerance of mtDNA mutations. *Cell*. 141:280-289.

Chen, Y., G. Csordas, C. Jowdy, T.G. Schneider, N. Csordas, W. Wang, Y. Liu, M. Kohlhaas, M. Meiser, S. Bergem, J.M. Nerbonne, G.W. Dorn, 2nd, and C. Maack. 2012. Mitofusin 2-containing mitochondrial-reticular microdomains direct rapid cardiomyocyte bioenergetic responses via interorganelle Ca(2+) crosstalk. *Circ Res*. 111:863-875.

Chen, Y., and G.W. Dorn, 2nd. 2013. PINK1-phosphorylated mitofusin 2 is a Parkin receptor for culling damaged mitochondria. *Science*. 340:471-475.

Cosson, P., A. Marchetti, M. Ravazzola, and L. Orci. 2012. Mitofusin-2 independent juxtaposition of endoplasmic reticulum and mitochondria: an ultrastructural study. *Plos One*. 7:e46293.

Csordas, G., C. Renken, P. Varnai, L. Walter, D. Weaver, K.F. Buttle, T. Balla, C.A. Mannella, and G. Hajnoczky. 2006. Structural and functional features and significance of the physical linkage between ER and mitochondria. *J.Cell Biol.* 174:915-921.

Csordas, G., P. Varnai, T. Golenar, S. Roy, G. Purkins, T.G. Schneider, T. Balla, and G. Hajnoczky. 2010. Imaging interorganelle contacts and local calcium dynamics at the ER-mitochondrial interface. *Mol Cell*. 39:121-132.

Daniele, T., I. Hurbain, R. Vago, G. Casari, G. Raposo, C. Tacchetti, and M.V. Schiaffino. 2014. Mitochondria and melanosomes establish physical contacts modulated by Mfn2 and involved in organelle biogenesis. *Curr Biol*. 24:393-403.

de Brito, O.M., and L. Scorrano. 2008. Mitofusin 2 tethers endoplasmic reticulum to mitochondria. *Nature.* 456:605-610.

de Brito, O.M., and L. Scorrano. 2010. An intimate liaison: spatial organization of the endoplasmic reticulum-mitochondria relationship. *EMBO J*. 29:2715-2723.

Debattisti, V., D. Pendin, E. Ziviani, A. Daga, and L. Scorrano. 2014. Reduction of endoplasmic reticulum stress attenuates the defects caused by Drosophila mitofusin depletion. *J Cell Biol*. 204:303-312.

Duarte, A., C. Poderoso, M. Cooke, G. Soria, F. Cornejo Maciel, V. Gottifredi, and E.J. Podesta. 2012. Mitochondrial fusion is essential for steroid biosynthesis. *PLoS One*. 7:e45829.

Eura, Y., N. Ishihara, S. Yokota, and K. Mihara. 2003. Two mitofusin proteins, mammalian homologues of FZO, with distinct functions are both required for mitochondrial fusion. *J.Biochem.(Tokyo)*. 134:333-344.

Filadi, R., E. Greotti, G. Turacchio, A. Luini, T. Pozzan, and P. Pizzo. 2015. Mitofusin 2 ablation increases endoplasmic reticulum-mitochondria coupling. *Proc Natl Acad Sci U S A*. 112:E2174-2181.

Frezza, C., S. Cipolat, and L. Scorrano. 2007. Organelle isolation: functional mitochondria from mouse liver, muscle and cultured fibroblasts. *Nat.Protoc.* 2:287-295.

Giacomello, M., I. Drago, M. Bortolozzi, M. Scorzeto, A. Gianelle, P. Pizzo, and T. Pozzan. 2010. Ca2+ hot spots on the mitochondrial surface are generated by Ca2+ mobilization from stores, but not by activation of store-operated Ca2+ channels. *Mol Cell*. 38:280-290.

Gong, G., M. Song, G. Csordas, D.P. Kelly, S.J. Matkovich, and G.W. Dorn Ii. 2015. Parkin-mediated mitophagy directs perinatal cardiac metabolic maturation in mice. *Science*. in press.

Hailey, D.W., A.S. Rambold, P. Satpute-Krishnan, K. Mitra, R. Sougrat, P.K. Kim, and J. Lippincott-Schwartz. 2010. Mitochondria supply membranes for autophagosome biogenesis during starvation. *Cell*. 141:656-667.

Hamasaki, M., N. Furuta, A. Matsuda, A. Nezu, A. Yamamoto, N. Fujita, H. Oomori, T. Noda, T. Haraguchi, Y. Hiraoka, A. Amano, and T. Yoshimori. 2013. Autophagosomes form at ER-mitochondria contact sites. *Nature*. 495:389-393.

Kamer, K.J., and V.K. Mootha. 2015. The molecular era of the mitochondrial calcium uniporter. *Nat Rev Mol Cell Biol*. 16:545-553.

Kasahara, A., S. Cipolat, Y. Chen, G.W. Dorn, and L. Scorrano. 2013. Mitochondrial fusion directs cardiomyocyte differentiation via calcineurin and Notch signaling. *Science*. 342:734-737.

Kornmann, B., E. Currie, S.R. Collins, M. Schuldiner, J. Nunnari, J.S. Weissman, and P. Walter. 2009. An ER-mitochondria tethering complex revealed by a synthetic biology screen. *Science*. 325:477-481.

Koshiba, T., S.A. Detmer, J.T. Kaiser, H. Chen, J.M. McCaffery, and D.C. Chan. 2004. Structural basis of mitochondrial tethering by mitofusin complexes. *Science*. 305:858-862.

Lahiri, S., J.T. Chao, S. Tavassoli, A.K. Wong, V. Choudhary, B.P. Young, C.J. Loewen, and W.A. Prinz. 2014. A conserved endoplasmic reticulum membrane protein complex (EMC) facilitates phospholipid transfer from the ER to mitochondria. *PLoS Biol*. 12:e1001969.

Majoul, I., M. Straub, R. Duden, S.W. Hell, and H.D. Soling. 2002. Fluorescence resonance energy transfer analysis of protein-protein interactions in single living cells by multifocal multiphoton microscopy. *J.Biotechnol.* 82:267-277.

Manders, E.M., F.J. Verbeek, and J.A. Aten. 1993. Measurement of co-localisation of objects in dual-colour confocal images. *J.Microsc.* 169:375-382.

Matkovich, S.J., and G.W. Dorn, 2nd. 2015. Deep sequencing of cardiac microRNA-mRNA interactomes in clinical and experimental cardiomyopathy. *Methods Mol Biol*. 1299:27-49.

Mourier, A., E. Motori, T. Brandt, M. Lagouge, I. Atanassov, A. Galinier, G. Rappl, S. Brodesser, K. Hultenby, C. Dieterich, and N.G. Larsson. 2015. Mitofusin 2 is required to maintain mitochondrial coenzyme Q levels. *J Cell Biol*. 208:429-442.

Munoz, J.P., S. Ivanova, J. Sanchez-Wandelmer, P. Martinez-Cristobal, E. Noguera, A. Sancho, A. Diaz-Ramos, M.I. Hernandez-Alvarez, D. Sebastian, C. Mauvezin, M. Palacin, and A. Zorzano. 2013. Mfn2 modulates the UPR and mitochondrial function via repression of PERK. *EMBO J*. 32:2348-2361.

Naon, D., and L. Scorrano. 2014. At the right distance: ER-mitochondria juxtaposition in cell life and death. *Biochim.Biophys.Acta*. 1843:2184-2194.

Ngoh, G.A., K.N. Papanicolaou, and K. Walsh. 2012. Loss of mitofusin 2 promotes endoplasmic reticulum stress. *J.Biol.Chem.* 287:20321-20332.

Pyakurel, A., C. Savoia, D. Hess, and L. Scorrano. 2015. Extracellular Regulated Kinase Phosphorylates Mitofusin 1 to Control Mitochondrial Morphology and Apoptosis. *Mol Cell*.

Raffaello, A., S.D. De, D. Sabbadin, E. Teardo, G. Merli, A. Picard, V. Checchetto, S. Moro, I. Szabo, and R. Rizzuto. 2013. The mitochondrial calcium uniporter is a multimer that can include a dominant-negative pore-forming subunit. *EMBO J.* 32:2362-2376.

Rizzuto, R., M. Brini, M. Murgia, and T. Pozzan. 1993. Microdomains with high Ca2+ close to IP3-sensitive channels that are sensed by neighboring mitochondria. *Science*. 262:744-747.

Rizzuto, R., S.D. De, A. Raffaello, and C. Mammucari. 2012. Mitochondria as sensors and regulators of calcium signalling. *Nat.Rev.Mol.Cell Biol*. 13:566-578.

Rizzuto, R., P. Pinton, W. Carrington, F.S. Fay, K.E. Fogarty, L.M. Lifshitz, R.A. Tuft, and T. Pozzan. 1998. Close contacts with the endoplasmic reticulum as determinants of mitochondrial Ca2+ responses. *Science*. 280:1763-1766.

Rojo, M., F. Legros, D. Chateau, and A. Lombes. 2002. Membrane topology and mitochondrial targeting of mitofusins, ubiquitous mammalian homologs of the transmembrane GTPase Fzo. *J.Cell Sci.* 115:1663-1674.

Sandoval, H., C.K. Yao, K. Chen, M. Jaiswal, T. Donti, Y.Q. Lin, V. Bayat, B. Xiong, K. Zhang, G. David, W.L. Charng, S. Yamamoto, L. Duraine, B.H. Graham, and H.J. Bellen. 2014. Mitochondrial fusion but not fission regulates larval growth and synaptic development through steroid hormone production. *eLife*. 3.

Santel, A., and M.T. Fuller. 2001. Control of mitochondrial morphology by a human mitofusin. *J.Cell Sci.* 114:867-874.

Schneeberger, M., M.-á. Dietrich, D. Sebasti+ín, M. Imbern+¦n, C. Casta+¦o, A. Garcia, Y. Esteban, A. Gonzalez-Franquesa, I.-á.n. Rodr+¡guez, A.a. Bortolozzi, P.-á. Garcia-Roves, R. Gomis, R. Nogueiras, T.-á. Horvath, A. Zorzano, and M. Claret. 2013. Mitofusin 2 in POMC Neurons Connects ER Stress with Leptin Resistance and Energy Imbalance. *Cell*. 155:172-187.

Schon, E.A., and E. Area-Gomez. 2012. Mitochondria-associated ER membranes in Alzheimer disease. *Mol.Cell Neurosci.*

Sebastian, D., M.I. Hernandez-Alvarez, J. Segales, E. Sorianello, J.P. Munoz, D. Sala, A. Waget, M. Liesa, J.C. Paz, P. Gopalacharyulu, M. Oresic, S. Pich, R. Burcelin, M. Palacin, and A. Zorzano. 2012. Mitofusin 2 (Mfn2) links mitochondrial and endoplasmic reticulum function with insulin signaling and is essential for normal glucose homeostasis. *Proc.Natl.Acad.Sci.U.S.A*. 109:5523-5528.

Simmen, T., J.E. Aslan, A.D. Blagoveshchenskaya, L. Thomas, L. Wan, Y. Xiang, S.F. Feliciangeli, C.H. Hung, C.M. Crump, and G. Thomas. 2005. PACS-2 controls endoplasmic reticulum-mitochondria communication and Bid-mediated apoptosis. *EMBO J*. 24:717-729.

Singaravelu, K., C. Nelson, D. Bakowski, O.M. de Brito, S.W. Ng, C.J. Di, T. Powell, L. Scorrano, and A.B. Parekh. 2011. Mitofusin 2 Regulates STIM1 Migration from the Ca2+ Store to the Plasma Membrane in Cells with Depolarized Mitochondria. *J Biol Chem.* 286:12189-12201.

Song, M., K. Mihara, Y. Chen, L. Scorrano, and G.W. Dorn, 2nd. 2015. Mitochondrial fission and fusion factors reciprocally orchestrate mitophagic culling in mouse hearts and cultured fibroblasts. *Cell Metab*. 21:273-285.

Sood, A., D.V. Jeyaraju, J. Prudent, A. Caron, P. Lemieux, H.M. McBride, M. Laplante, K. Toth, and L. Pellegrini. 2014. A Mitofusin-2-dependent inactivating cleavage of Opa1 links changes in

mitochondria cristae and ER contacts in the postprandial liver. *Proc Natl Acad Sci U S A*. 111:16017-16022.

Sugiura, A., S. Nagashima, T. Tokuyama, T. Amo, Y. Matsuki, S. Ishido, Y. Kudo, H.M. McBride, T. Fukuda, N. Matsushita, R. Inatome, and S. Yanagi. 2013. MITOL regulates endoplasmic reticulum-mitochondria contacts via Mitofusin2. *Mol.Cell*. 51:20-34.

Szabadkai, G., K. Bianchi, P. Varnai, S.D. De, M.R. Wieckowski, D. Cavagna, A.I. Nagy, T. Balla, and R. Rizzuto. 2006. Chaperone-mediated coupling of endoplasmic reticulum and mitochondrial Ca2+ channels. *J.Cell Biol.* 175:901-911.

Szalai, G., R. Krishnamurthy, and G. Hajnoczky. 1999. Apoptosis driven by IP(3)-linked mitochondrial calcium signals. *EMBO J.* 18:6349-6361.

Vance, J.E. 1990. Phospholipid synthesis in a membrane fraction associated with mitochondria. *J Biol Chem.* 265:7248-7256.

Wasilewski, M., M. Semenzato, S.M. Rafelski, J. Robbins, A.I. Bakardjiev, and L. Scorrano. 2012. Optic atrophy 1-dependent mitochondrial remodeling controls steroidogenesis in trophoblasts. *Curr.Biol.* 22:1228-1234.

A critical reappraisal confirms that Mitofusin 2 tethers endoplasmic reticulum to mitochondria.

Deborah Naon et al.

Supplementary online material

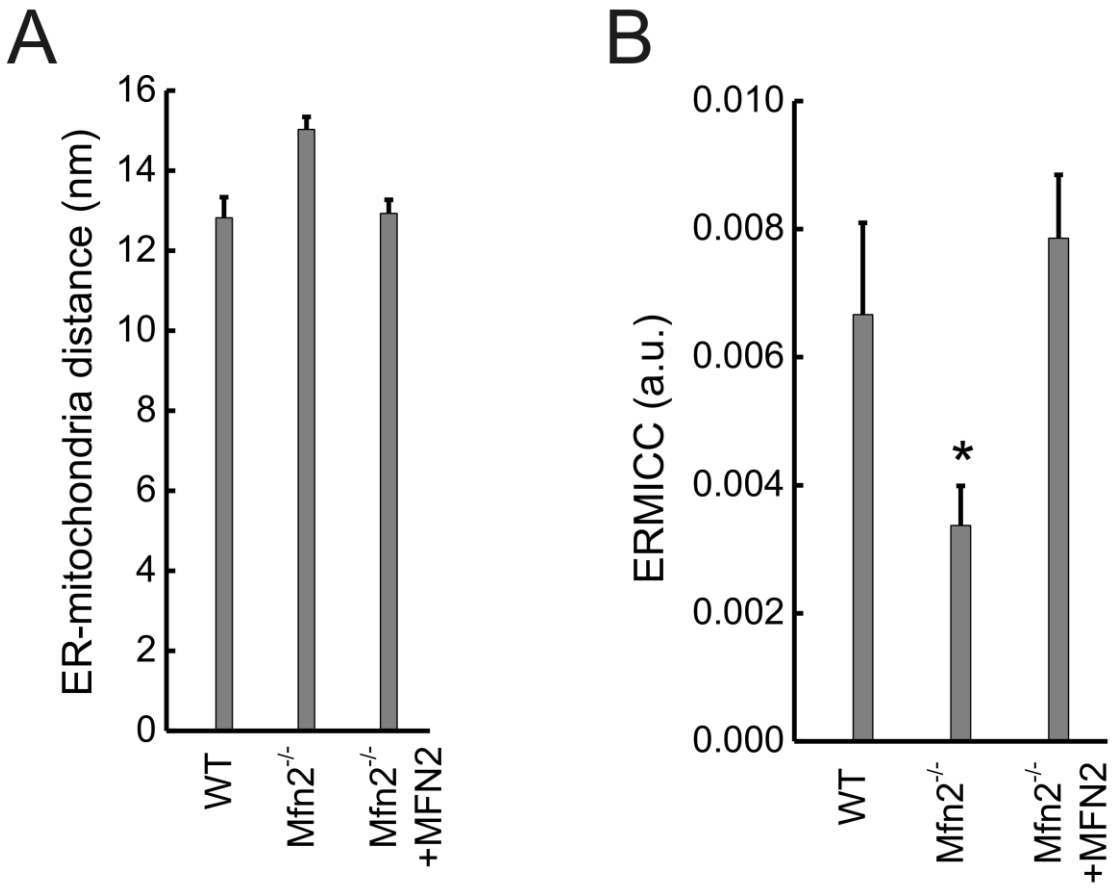

Supplementary Figure 1. *Mfn2* ablation increases ER-mitochondria distance.

A) Morphometric analysis of ER located at less than 20 nm from mitochondria calculated from 70 images per condition with >5 mitochondria per image. Data represent mean±SEM of 3 independent experiments. *, P<0.05 vs. WT.

B) Quantification of ER-mitochondria contact coefficient (ERMICC) of ER located at 20nm maximum distance from mitochondria. Data represent mean ±SEM of 3 independent experiments (n=350 mitochondria per experiment).

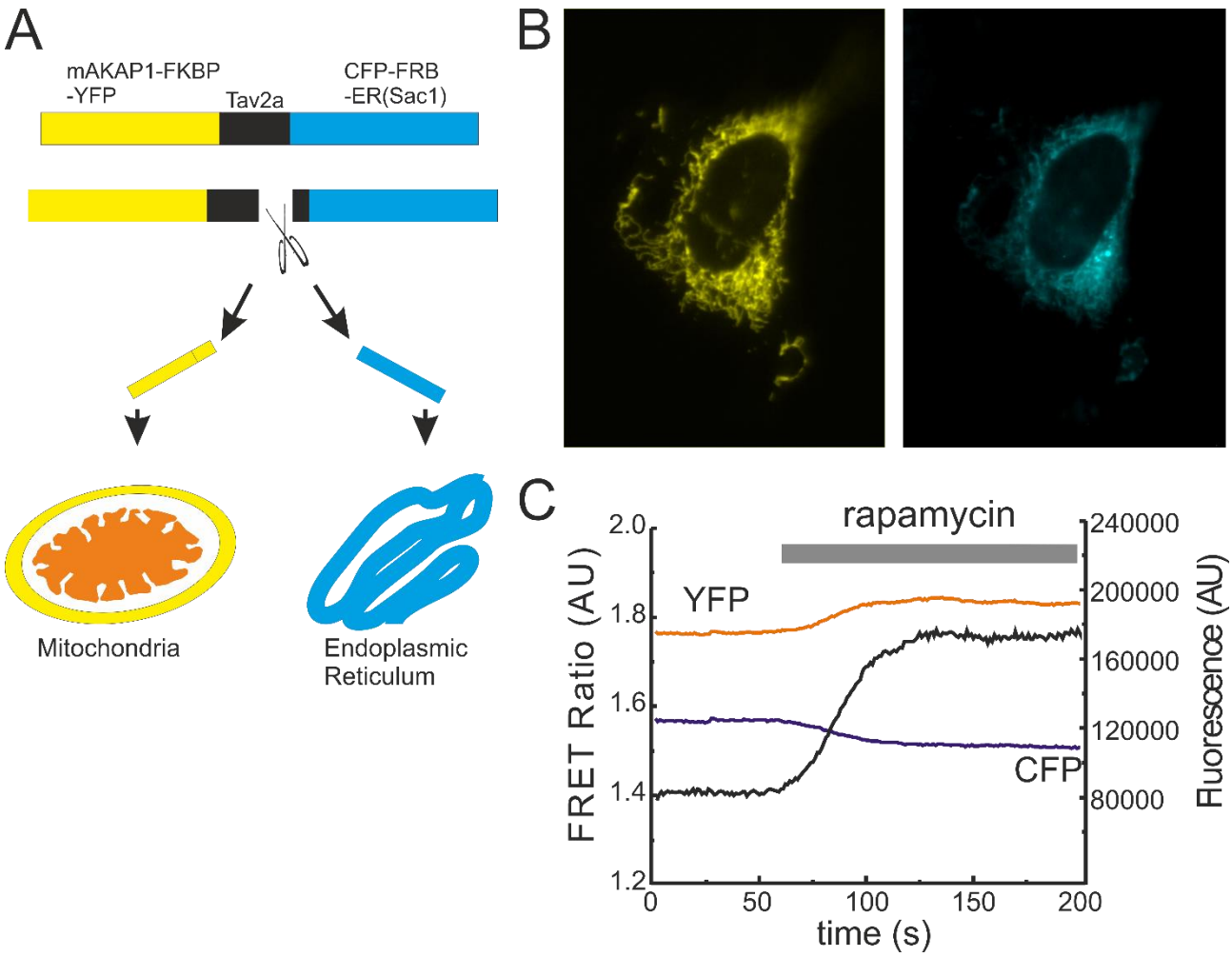

Supplementary Figure 2. FEMP probe measures proximity between ER and mitochondria.

A) Schematic of the modified FEMP probe targeted to mitochondrial outer membrane and ER. A self-cleaving Tav2A peptide was inserted following YFP sequence. Following translation, the peptide undergoes autocleavage and releases YFP and CFP, which are targeted to mitochondria and ER by Akap1 and Sac1 targeting sequences, respectively.

B) Representative confocal images of the FEMP probe localized to mitochondria (yellow panel) and ER (cyan panel).

C) Time lapse imaging of WT MEFs expressing FEMP probe. Where indicated, cells were treated with 100nM Rapamycin. Black trace, calculated YFP/CFP FRET intensity.

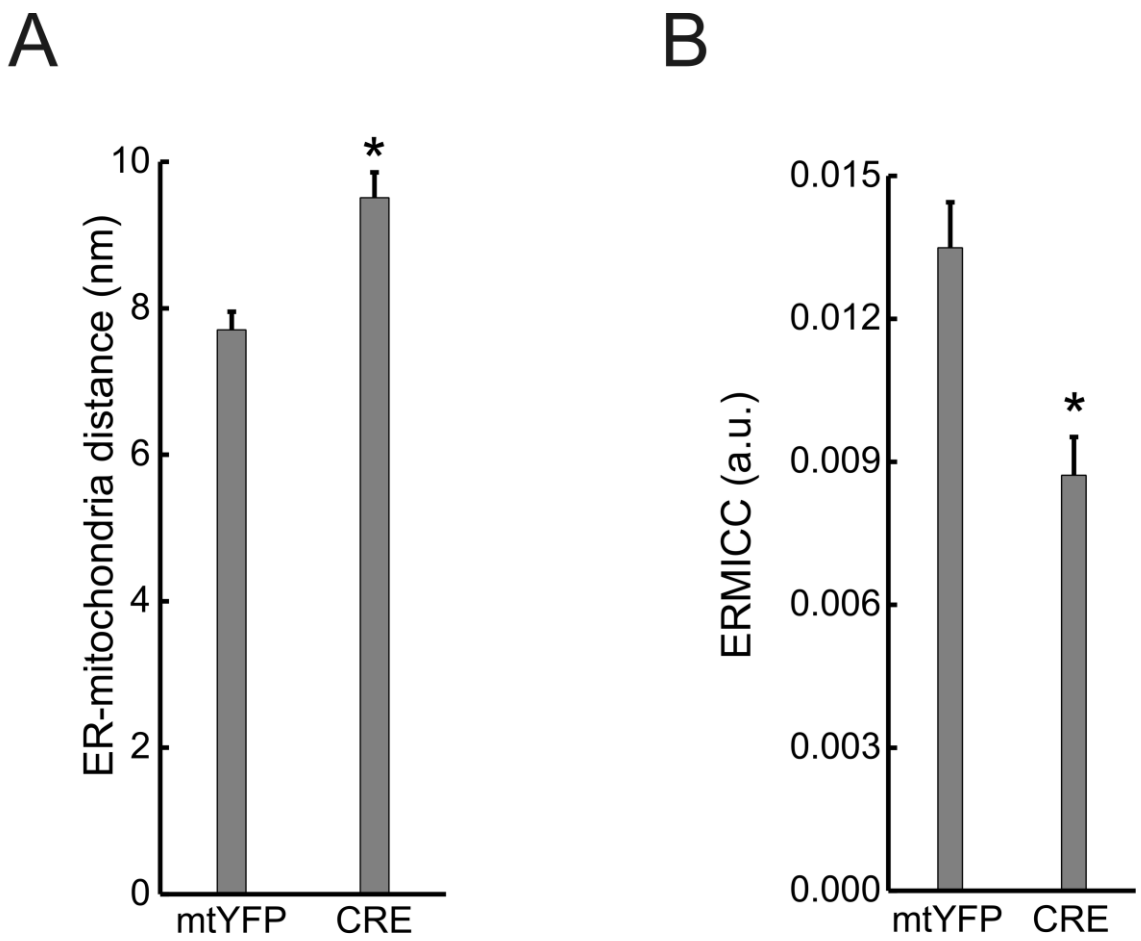

Supplementary Figure 3. Acute *Mfn2* ablation increases ER-mitochondria distance and decreases ER-mitochondria contacts.

A) Morphometric analysis of ER located at less than 30 nm from mitochondria calculated from 70 images per condition with >5 mitochondria per image in *Mfn2*$^{flx/flx}$ MEFs infected with AAV-CMV-mtYFP (mtYFP) or AAV-CMV-CRE-2A mtYFP (CRE) adenoviruses. Data represent mean±SEM of 3 independent experiments performed as in F. *, P<0.05 vs. mtYFP

B) Data represent mean±SEM of ERMICC calculated from 3 independent experiments performed as in A. *, P<0.05 vs. mtYFP

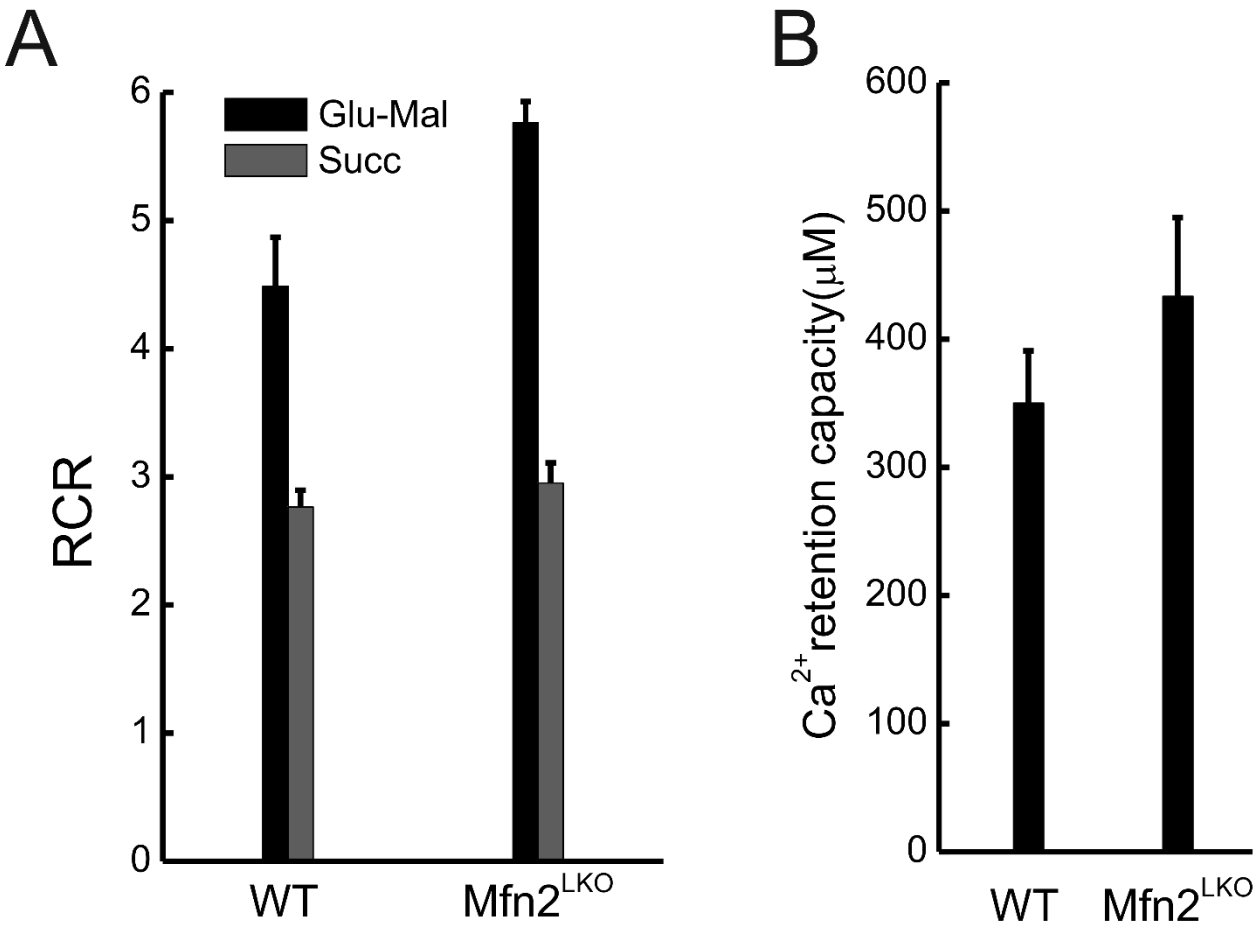

Supplementary Figure 4. *Mfn2* ablation in liver does not alter mitochondrial function and Ca^{2+} retaining capacity.

A) Respiratory control ratio (RCR) in isolated mitochondria from control (WT) and Mfn2 liver specific knockout ($Mfn2^{LKO}$) mice energized using glutamate/malate (Glu-Mal) or Succinate (Succ).

B) Ca^{2+} retention capacity in isolated mitochondria of the indicated genotypes measured using 1μM CaGreen-5N. Pulses of 50μM Ca^{2+} were added until PTP induction.

4 Results

A FRET based high content screen identifies DMPK as a novel tether of ER and mitochondria

Sowmya Lakshminarayanan[1,2], Annalisa Serafini[1,2] and Marta Giacomello[1,2], Luca Scorrano[1, 2]

1 Dept. of Biology, University of Padova, CIS-Vallisneri. 3, 35121 Padova, Italy;

2 Dulbecco Telethon Institute, Venetian Institute of Molecular Medicine, Via Orus 2, 35129 Padova, Italy;

Address correspondence to

Marta Giacomello or Luca Scorrano. Email: luca.scorrano@unipd.it

Summary

Communication between endoplasmic reticulum (ER) and mitochondria participates in several key signalling processes, including autophagy, Ca^{2+} and lipid transfer, and is fulfilled by proteinaceous interorganellar tethers whose nature is yet to be clarified. Here we provide a compendium of the ER-mitochondria tethers and spacers, identified by means of a FRET based genome-wide high content imaging screen (HCS). Screening of ~10000 genes yielded a list of 2840 proteins involved in diverse cellular processes that directly or indirectly affect ER-mitochondria proximity. Only 8 candidates from this list are annotated to be localized both on the mitochondrial and ER surface and are therefore likely structural links between the two. While low-throughput assays are ongoing for some candidates, confirmatory experiments allowed the characterization of the hit Dystrophia myotonica protein kinase (DMPK) as a novel ER-mitochondria tether. Our results have implications for understanding DMPK function and pathogenesis of myotonic dystrophy and, more generally, provide a compendium of the ER-mitochondria interface molecular anatomy.

Introduction

Mitochondria are fundamental organelles that regulate a plethora of cell processes. They fulfil the cell energy requirements by producing ATP, participate in pathways involving secondary messengers such as Ca^{2+}, amplify signalling events eventually leading to apoptosis (Ferri and Kroemer, 2001; Rizzuto and Pozzan, 2006). The spatial positioning of mitochondria in proximity with other organelles is crucial for these complex tasks (Bravo-Sagua et al., 2014).One of the most studied organelles crosstalk in which mitochondria are involved is the mitochondria-Endoplasmic reticulum (ER)interaction (Lopez-Crisosto et al., 2015).

ER-mitochondria contacts (ER-mito contacts) were originally implied in the regulation of lipid biosynthesis. Indeed, the Mitochondria Associated Membranes (MAMs) patches of ER membranes associated to the outer mitochondrial membrane (OMM) that represent the biochemical counterpart of ER-mito contacts, mediate the direct exchange of fatty acid precursors between the two organelles (Vance, 1990, 2014). ER-mito contacts also regulate transfer of Ca^{2+} from ER to mitochondria, upon its release from the ER Inositol trisphosphate receptors (Rizzuto et al., 1993; Rizzuto et al., 1998; Rizzuto et al., 1992). Recently, the field has expanded and highlighted the role of ER-mito crosstalk in other important processes including autophagosome biogenesis, organelle dynamics, inflamasome formation, peroxisomes biogenesis and response to stress and metabolic

adaptations(Bui et al., 2010; Friedman et al., 2011; Lang et al., 2015; Lopez-Crisosto et al., 2015; Naon and Scorrano, 2014).

The juxtaposition between ER and mitochondria appears dynamic, like the two organelles themselves. EM images reveal that their membranes run in parallel, at a distance ranging from 10 to 50 nm, for several nm in length (Csordas et al, 2006) without fusing together, thus maintaining their distinct lipid architecture. These evidences, together with the observation of electron dense structures that can be visualized in EM images, suggest the existence of proteinaceous links that bridge together the two organelles (Csordas et al., 2006; Lopez-Crisosto et al., 2015). Little is known about the molecular identity of the proteins and/or protein complexes that tether ER and mitochondria. Early evidence indicated that depletion of PACS-2, a multifunctional sorting protein mainly localised at ER induced BAP31 cleavage yielding a product which ultimately caused mitochondria to fragment and uncouple from ER (Simmen et al., 2005). Similarly, Drp1 has also been shown to increase the tethering by causing peri-nuclear clustering of mitochondria (Pitts et al., 1999, Ritcher et al., 2014). From a structural perspective, the first evidence for the existence of a direct proteinaceous bridge between ER and mitochondria relies on Mitofusin 2 (Mfn2), a protein originally known for its role on mitochondrial fusion along with Mfn1 (de Brito and Scorrano, 2008). This dynamin related GTPase regulates also the shape of the ER and it tethers ER to mitochondria by engaging in homotypic and/or heterotypic interactions with Mfn1 (de Brito and Scorrano, 2008). Loss of Mfn2 increases the distance between the two

organelles and affects Ca^{2+} transfer from ER to mitochondria(de Brito and Scorrano, 2008). As ablation of Mfn2 results in a 40% decrease of ER-mito contacts, tethers others than Mfn2 must exist(de Brito and Scorrano, 2008). To fill this gap on the knowledge of the biology of ER-mito contacts, we have conducted a genome wide high content imaging screen (HCS), in mouse embryonic fibroblasts (MEFs), based on a modified version of a FRET based probe (Csordas 2010; Naon et al, submitted).Panther database analysis of the data (Mi et al., 2013; Thomas et al., 2006) indicate that several pathways modulate the ER-mitochondria tether. Most importantly, we have identified 8 proteins, reported to locate at both ER an OMM, that potentially link the two organelles together either by homotypic or heterotypic interactions, as reported for the first identified tether Mfn2 (de Brito and Scorrano, 2008). Indeed, the hit Dystrophia myotonica protein kinase (DMPK), mutated in myotonic dystrophy, is enriched in MAMs and its down-regulation increases ER and mitochondria distance. Our list, although not complete, represents the most extensive to date compendium of the modulators of ER-mitochondria interface and illustrates its usefulness to investigate the role of the ER-mitochondria interface in biology and pathology.

Results

A high-content screening assay for regulators of ER-mitochondria contacts

To identify the proteins involved in the crosstalk between mitochondria and ER, we conducted a genome-wide shRNA screen based on a FRET probe of ER-mitochondria proximity (FEMP) recently developed in our laboratory. In this probe, two appropriate fluorescent proteins are targeted to the surface of the ER and mitochondria and equimolarly expressed by means of weighted promoters from the same plasmid backbone. FRET occurs only at the points of closest juxtaposition between the two organelles and can be maximized by brief rapamycin treatment that brings CFP and YFP in closest proximity thanks to the existence of a split Rapamycin binding motif in the two FEMP halves (Naon et al, submitted). Changes in the FRET ratio values would mirror alterations in ER-mitochondria proximity and knockdown of proteins that regulate the extent of this juxtaposition would decrease or increase the FRET Ratio value according to their role as positive (tethers) or negative (Spacers) regulators (Figure1A).

Wild type MEFs seeded in 384 well plates and transduced with lenti-viral particles carrying gene-specific shRNA were transfected with plasmids encoding FEMP (Figure 1B). 24 hours post transfection, cells were imaged to record basal and maximal (Rapamycin-induced) FRET values (Figure 2A). The raw HCS data were analysed by means of high content image analysis that allowed automatic identification of cellular boundaries and regions of

interest (Extended Figure 2). Normalization of FRET Ratio values (as detailed in materials and methods) obtained upon addition of Rapamycin to the basal levels has been considered as representative (proportional) of the maximum number of contacts possible. To compare different wells of the plate, we imaged samples upon fixation at a time point in which the FRET Ratio had reached a plateau and was stable (that is, fixation after 15 minutes of treatment with rapamycin, a condition that does not affect the basal and maximum FRET Ratio; Extended figure 1A). Eventual positional effect across the 384 well plate was also monitored in wild type MEFs expressing FEMP (Figure 2B), and the conditions for efficient transduction of MEFs were established by using Turbo GFP lenti-viral particles: we observed over 70% transduction efficiency with a MOI of ~1 (Extended Figure 1B). As a control for efficiency of knockdown and reliability of the established assay, we measured FRET Ratio changes before and after addition of Rapamycin in cells treated with lenti-viral particles targeting the well-known ER-mito proteins PACS-2, Mfn2 and MITOL (Extended figure1C and D).

Statistical analysis of active shRNAs identifies novel ER-mito contacts components

High Content images obtained from the primary screen were processed through a rigorous statistical analysis with the cell HTS2 package in R program (Boutros et al., 2006)Raw data were filtered for outliers and negative values, which were eliminated before proceeding with using

robust Z score normalization at single plate and experiment level. Each gene was targeted by 4-5 unique shRNAs in the library (Figure 3). To classify genes as tethers, we took advantage of the Z score calculated for PACS-2 and Mfn2 shRNA and set them as cut-off values to identify target genes (Figure 4A). The hits that passed the threshold were further classified according to their number of active shRNAs into high confidence (3-4-5 shRNAs per gene), moderate confidence (2 shRNAs per gene) or discarded (1 or 0 shRNAs per gene) (figure 4B). To identify spacers, we chose as cut off the Z score +2MAD value of Non target control (scramble) (Figure 4A). Again, we sub classified spacers into high confidence (3-4-5 shRNAs active per gene), moderate confidence (2 shRNAs active) and discarded (1 or 0 shRNAs) genes (Figure 4C). Overall, this classification yielded 14.4% high confidence tethers and 5.34% high confidence spacers.

The full list of identified hits from the primary screen was analysed though the web interface of Mitominer(Smith and Robinson, 2016) with the aim to identify proteins located in the OMM and ER, likely structural components of the ER-mitochondria contacts. Of the135 genes predicted to be localized at either of the two organelles, 127 were localised in ER and 8 were localised in mitochondria. Eight proteins (0.5%) were predicted to be localised in both ER and mitochondria (Figure 4D and E, Extended table 5 and 6).

Bioinformatics analysis of the candidate list reveals gene clusters and cell signalling pathways controlling ER-mitochondria proximity

To get further insights on the subcellular processes that control the ER-mitochondria contacts, we undertook a system biology approach and performed pathway enrichment analysis. The whole list of candidates (that is, all the genes listed in Extended tables 1-4) was submitted to the Panther database. Using over-representation analysis in Panther database, which highlights cellular pathways that are significantly represented amongst the genes, both the tethers and spacers genes were classified for the respective protein classes, which they belong to (Figure 5Aand B). While most of protein classes were common to both Tethers and Spacers, some protein classes were differentially represented (Figure 5C). The overlap amongst the pathways between the two classifications provides us new clues to how ER and mitochondria communicate in various signalling pathways.

DMPK is a ER-mitochondria tether

One of the eight proteins that were predicted to be localised in both outer mitochondrial membrane and ER was myotonic dystrophy protein Kinase (DMPK), a serine threonine protein kinase involved in myotonic dystrophy (DM). Ablation of DMPK in WT MEFs decreased the maximum number of contact possible (FRET intensity) when compared to Scrambled (Figure 6A and B). Biochemical fractionation of WT MEFs also indicated that DMPK localizes to MAMs, thus confirming the primary screen data (Figure 6C).These results provide us preliminary evidence for DMPK as a novel tether of ER and mitochondria.

Discussion

The molecular complexity of ER-mitochondria interface could be inferred by its implication in several key signalling processes. Although few proteins have been identified as responsible for ER-mitochondria crosstalk, the overall nature of the tether has yet not been completely understood. Aim of this study was to identify proteins that tether (or modulate tethering) and space (or modulate the distance) ER and mitochondria.

Through rigorous statistical analysis of the first replicate of data from a FRET probe based HCS we classified 14.4% genes as tethers and 5.34% genes as spacers from a list of 10,000 genes screened. Confidence in our approach and in the chosen cut-off limits is reinforced by the retrieval of previously reported tethers/regulators of tethers among the list, including PML, Akt2, mTOR, SERAC1, Soat1, ACSL4 and Grp78(Betz et al., 2013; Giorgi et al., 2010; Joyce et al., 2000; Lewin et al., 2001; Vance, 1990; Wortmann et al., 2012). The contexts in which these proteins were found to be regulate ER-mitochondria tethering were different - while PML has been found to regulate apoptosis at ER-mitochondria interface by modulating calcium release, Akt2 and mTOR were identified in MAMs upon metabolic stress, SERAC1, Soat1 and ACSL4 are associated with lipid trafficking between the two organelles. The fact that we found these proteins as "hits" indicates high degree of robustness of our screen.

The genes identified as spacers and tethers often belong to the same pathways as indicated by Panther database analysis, although certain pathways were enriched individually in the Tethers or in the Spacers pools

(Figure 5C). An interesting cellular component that is involved in the modulation of ER-mitochondria contacts is the class of cytoskeletal proteins that can modulate mitochondrial dynamics (Anesti et al., 2006). Mitochondrial motility occurs along the microtubule network through Kinesin, Miro and Milton (Reynolds et al., 2004, Boldogh et al., 2007, Glater et al., 2006). This movement seems essential to maintain differential distribution of mitochondria within the cell to exploit the diverse energy requirements of cellular compartments (Hollenbeck et al., 2005). For instance, in neurons, mitochondria are accumulated in active regions of growth cones and branches and pre-synaptic terminals, where energy demand is high (Hollenbeck et al., 2005). In this regards mitochondrial localisation and movement restriction is due to the local ATP levels and recently through calcium levels (Brough et al., 2005). ER on the other hand, is a complex organelle spreading widely across the cell undergoing constant remodelling in formation of tubules (Waterman-Storer et al., 1998). The movement of ER depends on both microtubule dynamics and actin filaments and is calcium dependent (Borgese et al., 2006). It is tempting to speculate that the actin/microtubule motor binding proteins found in this screen modulate tethering by altering reciprocal ER-mitochondrial distribution. Moreover actin and myosin mediated constriction gives Drp1 the right diameter to form helical ring around mitochondria (Korobova et al., 2014; Manor et al., 2015) at sites where ER tubules mark mitochondria for division (Friedman et al., 2011).

Another protein class enriched in the Spacers list is that of oxidoreductases (figure 5C). In early phases of ER stress cells respond by increasing the number of ER-mitochondria contacts, thereby facilitating direct exchange of Ca^{2+} between ER and mitochondria and increasing mitochondrial respiration (Bravo et al., 2012 ;Bravo-Sagua et al., 2014). In type 2 Diabetes mellitus and cardiovascular disorders the oxidoreductases ERp44, ERp57 and Ero1α regulate ER calcium pumps and hence calcium flux from the ER, thereby modulating ER-mitochondria calcium exchange and the cellular metabolic output (Lopez-Crisosto et al., 2015). Given that oxidoreductases are enriched in the spacers vs the tethers list (5.8% vs. 2.4%), we can speculate that reductases normally impinge on structural tethers to keep the organelles at the right distance: when they are activated, they force ER and mitochondria to separate in an attempt to reduce the spread of damage from the ER to the mitochondria.

One protein of particular interest that showed up as a tether of ER and mitochondria is myotonic dystrophy protein kinase (DMPK). DMPK is implicated in myotonic dystrophy (DM) because of aberrant CUG expansion in the 3’ UTR of the gene. The protein exists in 6 isoforms in humans and mouse and is known to localise to ER or to mitochondria owing to difference in the C-terminal domain (Wansink et al., 2003). In addition to its known function as a modulator of endo(sarco)plasmic reticulum and cellular Ca2+ homeostasis, DMPK possesses coiled coil domains that are known to participate in protein multimerization and are suggestive of the possibility for in trans organelle interaction (van Herpen et al., 2005). While

multiple mechanisms have been proposed to link 3'UTR DMPK changes and DM, in most patients levels of DMPK are reduced suggesting haploinsufficiency as a crucial component of DM pathogenesis (Romeo, 2012). Interestingly, some of the features of a DMPK knockout mouse model might be explained as a consequence of altered ER-mitochondria tethering, such as the changes in cellular Ca2+ homeostasis, the alterations in action potential of the heart conducting system, the myopathy (Cho and Tapscott, 2007, Ueda et al., 2000). Our biochemical analysis indicates that in MEFs DMPK is highly enriched in MAMs and that its reduction increases the distance between mitochondria and ER, suggesting new function for DMPK as a tether of ER and mitochondria. Further characterisation of DMPK, particularly whether it interacts with other known tethers (Mfn2) to bring the two organelles together will provide us further insight into how these higher order structures are formed and maintained.

Acknowledgments

LS is a Senior Scientist of the Dulbecco-Telethon institute supported by Telethon Italy (GGP12162 and GGP14187A), by the AIRC (the Italian Association for Research on Cancer), by the European Research Council (FP7-282280, FP7 CIG PCIG13-GA-2013-618697), and by the Italian Ministry of Research (FIRB RBAP11Z3YA_005).

Materials and methods

Molecular biology

pEGFP-N1 YFP-Akap1 (34-63)-FKBP and pEGFP-C3 CFP-HA-FRB-Sac1 (ER)-CFP were kindly provided by G. Hajnoczky(Csordas et al., 2010). The cloning of the modified FEMP is described in (Naon D et al., submitted).

Cell culture

SV40 transformed WT MEFs were cultured as described before (de Brito and Scorrano, 2008). Media used for the screen was purchased from life technologies and is as follows:

Complete DMEM (DMEM high glucose; *Life technologies* #12800-082) with 10% FBS, 1X Pencillin/Streptamycin 100µM and 1X NEAA. Transfection mix was prepared in the same medium, lacking FBS.

High content genome wide shRNA library pool

A murine shRNA ready to use lentiviral library was procured from Sigma (MISSION^{TM} shRNA lentiviral particles) and stored at -80ºC until used. The total screen covered ~10,000 genes and each gene consisted of 4-5 unique shRNAs in different wells and arranges in 384 well plates format.

Automated shRNA screening

WT MEFs were thawed from frozen stocks and cultured for 2-3 days before being used in HCS. On day 1, upon harvesting with Trypsin 0,25% EGTA, cells were plated at a density of 900 cells per well in 384 well plates in a final volume of 90µl using BiotekprecisionXS micro plate sample processor

using natural sterile tip. Plating was performed by means of an automated system (BiotekprecisionXS) with dedicated plastic ware (*starlab natural tips, #E1079-2410)*. 24 hours post plating, cells were incubated with 8µg/ml polybrene for 30'. Subsequently transduction was performed with 5µl of shRNA lentiviral particles (BiotekprecisionXS microplate sample processor, *starlab* sterile filter tips, # E1079-2418). Empty wells randomly distributed within the library plates were filled with control shRNAs: non targeting controls (scrambled, Scr) and positive controls (shRNAs targeting PACS2, Mfn2and MITOL). In order to eliminate the positional effects, controls were placed in different parts of each plate. The plates were spun at 500g for 15minutes. 24 hours post transduction, 80µl of medium was removed and 50µl of fresh complete DMEM was added per each well (all steps performed with the Precision XS-system). Transfection complex was prepared in FBS free DMEM with a 1:3 mixture of FEMP cDNA: Genjet lipid Transfection reagent (Signagen, #SL100488). The transfection mixture was incubated for 10', and then dispensed at a concentration of 100ng/well with a multichannel pipette 16 channels (Integra electronics). Cells were further incubated for 24 hours at 37 degrees before imaging. Before imaging each plate was equilibrated at room temperature. After imaging in resting conditions, plates were incubated in media containing Rapamycin at a final concentration of 100nM for 15 minutes. Post incubation, cells were fixed with 70µl of 1% Formaldehyde without methanol (diluted from a stock of 37% formaldehyde using PBS, pH 7.4) and subsequently rinsed with PBS. Image acquisition upon Rapamycin addition was performed in the presence of PBS.

Image acquisition and processing

Image acquisition was carried out in the Operetta High content imaging system (Perkin Elmer) and image acquisition settings were established with the Harmony 3.5 software. Images were acquired with 20X objective (high working distance,) and the following filters: CFP (ex 410-430, em 460-500), YFP (ex 490-510, em 520-560) and YFP_{FRET} (ex 410-430, em 520-560). Acquisition of $FRET_{max}$was performed as before in 1X PBS. Images were analysed using Perkin Elmer Harmony 3.5 image analysis software.

Technical details of image analysis

High throughput image analysis was performed with the Harmony image analysis software 3.5.2 (Perkin Elmer). A custom workflow was set to execute analysis of the screen images (see Extended figure 2). YFP channel images were chosen to set image segmentation and draw Regions of Interest (ROIs) corresponding to single cell. The following parameters were chosen to identify cell boundaries:

Area>150 μm^2;

Splitting coefficient: 0.30;

Common threshold: 0.20.

A background ROI was drawn around every cell boundary to estimate the background intensity of each channel. CFP intensity was estimated for each ROIs and used to select a CFP-positive subpopulation. Based on this procedure, only cells expressing both CFP and YFP were considered for the

final HCS analysis. For each ROIs, YFP, CFP and FRET intensities were measured and background corrected. Finally, the FRET Ratio was calculated as follows:

$$\text{Raw FRET intensity} = \frac{F_{YFPFRETcell} - F_{YFPFRETbg}}{F_{CFPcell} - F_{CFPbg}}$$

$$\text{Max number of contacts possible} = \frac{FRET_{Max} - FRET_{basal}}{FRET_{basal}}$$

Screen quality control, data processing and candidate selection

After the first round of the HCS, data from all the plates were pooled together and normalised to the overall experiment using MAD value. This allowed direct comparison of all the data by means of the cellHTS2 package R program (Boutros et al., 2006). We utilised Robust Z-score method (as calculated below) for normalisation since it is non-control based and is insensitive to outliers, which are essentially the candidate genes of interest (Birmingham et al., 2009; Malo et al., 2006).

$$\acute{Z} = \frac{(x_i - \widetilde{X})}{MAD_x}$$

X_i → raw measurement on i^{th} well

$\tilde{X}$ → Median of the plate

MAD_x → median absolute deviation within the plate, where MAD is calculated as

$$MAD_x = median[r_{ijp} - median(r_{ijp})]$$

The Robust Z-score obtained were then used to identify candidate genes, which have been classified as tethers and spacers in case of higher or lower Robust Z- score (Figure 3). The identified spacers and tethers were then further sub-categorised into groups according to the number of active shRNAs (Figure 3).The genes were then classified using the Panther database with a 95% confidence. Clusters of enriched genes were further analysed for interactions or associations using the STRING functional protein association tool. The cut-off for interactions was set as “medium”.

Biochemical fractionation of MAMs and western blotting

Biochemical fractionation of MAMs and western blots were done as reported in (de Brito and Scorrano, 2008). Antibodies concentration is as follows: DMPK (1:250, Santa cruz), ACSL4 (1:1000, Santa cruz) and Mfn2 (1:1000, Abnova).

References

Birmingham, A., Selfors, L.M., Forster, T., Wrobel, D., Kennedy, C.J., Shanks, E., Santoyo-Lopez, J., Dunican, D.J., Long, A., Kelleher, D.*, et al.* (2009). Statistical methods for analysis of high-throughput RNA interference screens. Nat Methods *6*, 569-575.

Boutros, M., Bras, L.P., and Huber, W. (2006). Analysis of cell-based RNAi screens. Genome Biol *7*, R66.

Bravo-Sagua, R., Torrealba, N., Paredes, F., Morales, P.E., Pennanen, C., Lopez-Crisosto, C., Troncoso, R., Criollo, A., Chiong, M., Hill, J.A.*, et al.*(2014). Organelle communication: signaling crossroads between homeostasis and disease. Int J Biochem Cell Biol *50*, 55-59.

Bui, M., Gilady, S.Y., Fitzsimmons, R.E., Benson, M.D., Lynes, E.M., Gesson, K., Alto, N.M., Strack, S., Scott, J.D., and Simmen, T. (2010). Rab32 modulates apoptosis onset and mitochondria-associated membrane (MAM) properties. J Biol Chem *285*, 31590-31602.

Csordas, G., Renken, C., Varnai, P., Walter, L., Weaver, D., Buttle, K.F., Balla, T., Mannella, C.A., and Hajnoczky, G. (2006). Structural and functional features and significance of the physical linkage between ER and mitochondria. J Cell Biol *174*, 915-921.

Csordas, G., Varnai, P., Golenar, T., Roy, S., Purkins, G., Schneider, T.G., Balla, T., and Hajnoczky, G. (2010). Imaging interorganelle contacts and local calcium dynamics at the ER-mitochondrial interface. Mol Cell *39*, 121-132.

de Brito, O.M., and Scorrano, L. (2008). Mitofusin 2 tethers endoplasmic reticulum to mitochondria. Nature *456*, 605-610.

Ferri, K.F., and Kroemer, G. (2001). Organelle-specific initiation of cell death pathways. Nat Cell Biol *3*, E255-263.

Friedman, J.R., Lackner, L.L., West, M., DiBenedetto, J.R., Nunnari, J., and Voeltz, G.K. (2011). ER tubules mark sites of mitochondrial division. Science *334*, 358-362.

Korobova, F., Gauvin, T.J., and Higgs, H.N. (2014). A role for myosin II in mammalian mitochondrial fission. Curr Biol *24*, 409-414.

Lang, A., John Peter, A.T., and Kornmann, B. (2015). ER-mitochondria contact sites in yeast: beyond the myths of ERMES. Curr Opin Cell Biol *35*, 7-12.

Lopez-Crisosto, C., Bravo-Sagua, R., Rodriguez-Pena, M., Mera, C., Castro, P.F., Quest, A.F., Rothermel, B.A., Cifuentes, M., and Lavandero, S. (2015). ER-to-mitochondria miscommunication and metabolic diseases. Biochim Biophys Acta *1852*, 2096-2105.

Malo, N., Hanley, J.A., Cerquozzi, S., Pelletier, J., and Nadon, R. (2006). Statistical practice in high-throughput screening data analysis. Nat Biotechnol *24*, 167-175.

Manor, U., Bartholomew, S., Golani, G., Christenson, E., Kozlov, M., Higgs, H., Spudich, J., and Lippincott-Schwartz, J. (2015). A mitochondria-anchored isoform of the actin-nucleating spire protein regulates mitochondrial division. Elife *4*.

Mi, H., Muruganujan, A., and Thomas, P.D. (2013). PANTHER in 2013: modeling the evolution of gene function, and other gene attributes, in the context of phylogenetic trees. Nucleic Acids Res *41*, D377-386.

Naon, D., and Scorrano, L. (2014). At the right distance: ER-mitochondria juxtaposition in cell life and death. Biochim Biophys Acta *1843*, 2184-2194.

Pitts, K.R., Yoon, Y., Krueger, E.W., and McNiven, M.A. (1999). The dynamin-like protein DLP1 is essential for normal distribution and morphology of the endoplasmic reticulum and mitochondria in mammalian cells. Mol Biol Cell *10*, 4403-4417.

Rizzuto, R., Brini, M., and Pozzan, T. (1993). Intracellular targeting of the photoprotein aequorin: a new approach for measuring, in living cells, Ca2+ concentrations in defined cellular compartments. Cytotechnology *11 Suppl 1*, S44-46.

Rizzuto, R., Pinton, P., Carrington, W., Fay, F.S., Fogarty, K.E., Lifshitz, L.M., Tuft, R.A., and Pozzan, T. (1998). Close contacts with the endoplasmic reticulum as determinants of mitochondrial Ca2+ responses. Science *280*, 1763-1766.

Rizzuto, R., and Pozzan, T. (2006). Microdomains of intracellular Ca2+: molecular determinants and functional consequences. Physiol Rev *86*, 369-408.

Rizzuto, R., Simpson, A.W., Brini, M., and Pozzan, T. (1992). Rapid changes of mitochondrial Ca2+ revealed by specifically targeted recombinant aequorin. Nature *358*, 325-327.

Simmen, T., Aslan, J.E., Blagoveshchenskaya, A.D., Thomas, L., Wan, L., Xiang, Y., Feliciangeli, S.F., Hung, C.H., Crump, C.M., and Thomas, G. (2005).

PACS-2 controls endoplasmic reticulum-mitochondria communication and Bid-mediated apoptosis. EMBO J *24*, 717-729.

Smith, A.C., and Robinson, A.J. (2016). MitoMiner v3.1, an update on the mitochondrial proteomics database. Nucleic Acids Res *44*, D1258-1261.

Snel, B., Lehmann, G., Bork, P., and Huynen, M.A. (2000). STRING: a web-server to retrieve and display the repeatedly occurring neighbourhood of a gene. Nucleic Acids Res *28*, 3442-3444.

Szklarczyk, D., Franceschini, A., Wyder, S., Forslund, K., Heller, D., Huerta-Cepas, J., Simonovic, M., Roth, A., Santos, A., Tsafou, K.P.*, et al.* (2015). STRING v10: protein-protein interaction networks, integrated over the tree of life. Nucleic Acids Res *43*, D447-452.

Thomas, P.D., Kejariwal, A., Guo, N., Mi, H., Campbell, M.J., Muruganujan, A., and Lazareva-Ulitsky, B. (2006). Applications for protein sequence-function evolution data: mRNA/protein expression analysis and coding SNP scoring tools. Nucleic Acids Res *34*, W645-650.

Vance, J.E. (1990). Phospholipid synthesis in a membrane fraction associated with mitochondria. J Biol Chem *265*, 7248-7256.

Vance, J.E. (2014). MAM (mitochondria-associated membranes) in mammalian cells: lipids and beyond. Biochim Biophys Acta *1841*, 595-609.

Figure legends

Figure 1.Workflow of the FEMP based HCS.

(A) Strategy for identification of genes essential for ER-mito contacts formation/regulation. In resting state, cells expressing FEMP are characterized by a basal FRET Ratio and addition of Rapamycin would allow determining the maximum FRET Ratio value obtainable per each cell. Down regulation of a protein involved in the maintenance of ER-mito contacts would affect the FRET Ratio either by decreasing or increasing it. Accordingly, changes in the FRET Ratio could be used to classify the identified hits as a tether (if ablation of the candidate decreases the FRET Ratio, due to an enhanced distance among the two organelles) or spacer (in case of an increased FRET Ratio).

(B) Schematic of the workflow of the FEMP based HCS.A general workflow of the screen and the timelines for every plate. See materials and methods for detailed description

Figure2. A high-content screening assay to investigate the molecular nature of ER-mitochondria contacts.

(A) **Representative images of mito-ER contacts assay**. These are typical images from one experiment before and after rapamycin addition/fixation).

(B) **Time lapse high content imaging and automated image analysis of FEMP probe**. WT MEFs transfected with FEMP probe was imaged for every 1 minute for 35 minutes. After the first minute, 100nM Rapamycin was added to the cells. Data represents average ± S.E.M from 3 independent experiments (N=1894 objects).

(C, D) **Basal and maximum FRET intensity measurements across a 384 well plate**. Data represents average ± S.E.M from 3 independent experiments (N= ~3000 objects per experiment analysed using automated image analysis).

Figure 3.Workflow of image and statistical analysis of the genome wide HCS data.

Overview of data analysis workflow. Raw numerical data from high content genome wide screen was first normalised amongst different experimental plates. Data points were excluded for negative or raw FRET value >5. The genes were then categorised as tethers and spacers according to their Z scores. See materials and methods for complete details.

Figure 4. Statistical and bioinformatics analysis predicts mitochondria and ER localised tethers and spacers

(A) **Z–score distribution of the candidate genes**. Robust Z-score was calculated for each raw value and cut-off limits were chosen as described in main text. The data followed normal distribution curve.

(B, C) **Classification of candidates as high and low confidence hits**. The genes that passed the threshold value was classified as high, moderate and low confidence depending on the number of shRNAs that have responded.

(D) **Mitominer analysis of the gene candidates to identify ER and mitochondria localised hits.** The candidates that were classified as high confidence hits from both tethers and spacers were analysed using Mitominer.

Figure 5. GO term classification of the candidate list

(A-C) **Bioinformatics analysis using Panther database of the candidate hits.** The high confidence candidate genes were classified using Panther cellular pathway analysis for both spacers and tethers. The protein classes between tether and spacers were then compared to identify pathways that show enrichment either in spacer or in tether. Refer materials and methods for complete details.

Figure 6. DMPK is a novel tether of ER and mitochondria

(A) **DMPK ablation reduces ER-mitochondria tethering.** WT MEFs transduced with Scr or DMPK shRNAs were transfected with FEMP and imaged before and after addition of rapamycin.

(B) **DMPK ablation decreases FRET intensity in WT MEFs.** Data represents average ± S.E.M from 2 independent experiments (N= ~100 objects per experiment analysed using automated image analysis).

(C) **DMPK is enriched in MAM fraction**. Subcellular fractionation performed in WT MEFs to enrich for MAMs. DMPK was enriched in the fractions enriched for Mfn2 and FACL4.

Figure 1

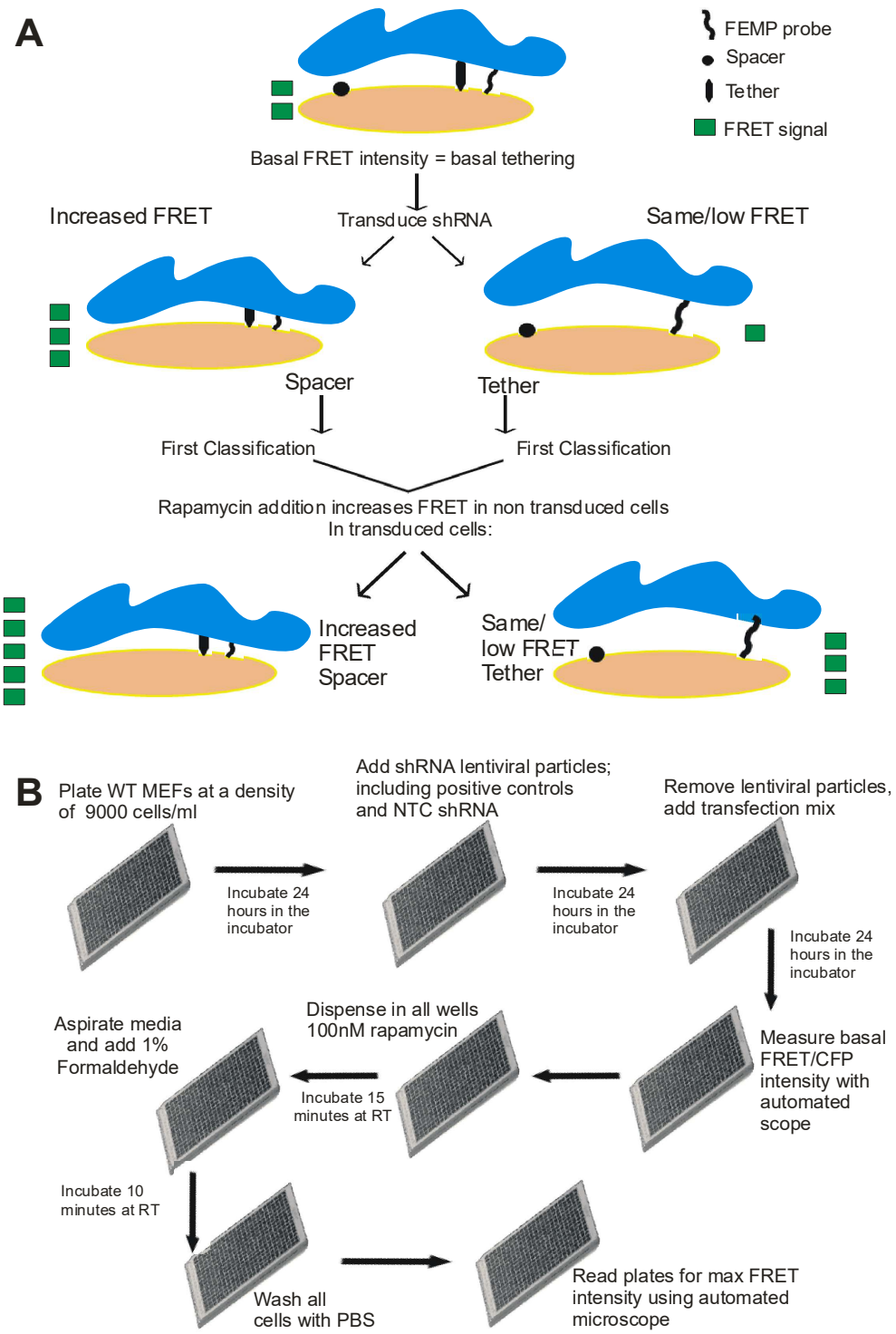
A
FEMP probe
Spacer
Tether
FRET signal
Basal FRET intensity = basal tethering
Transduce shRNA
Increased FRET
Same/low FRET
Spacer
Tether
First Classification
First Classification
Rapamycin addition increases FRET in non transduced cells
In transduced cells:
Increased FRET Spacer
Same/ low FRET Tether
B
Plate WT MEFs at a density of 9000 cells/ml
Incubate 24 hours in the incubator
Add shRNA lentiviral particles; including positive controls and NTC shRNA
Incubate 24 hours in the incubator
Remove lentiviral particles, add transfection mix
Incubate 24 hours in the incubator
Measure basal FRET/CFP intensity with automated scope
Dispense in all wells 100nM rapamycin
Incubate 15 minutes at RT
Aspirate media and add 1% Formaldehyde
Incubate 10 minutes at RT
Wash all cells with PBS
Read plates for max FRET intensity using automated microscope

Figure 2

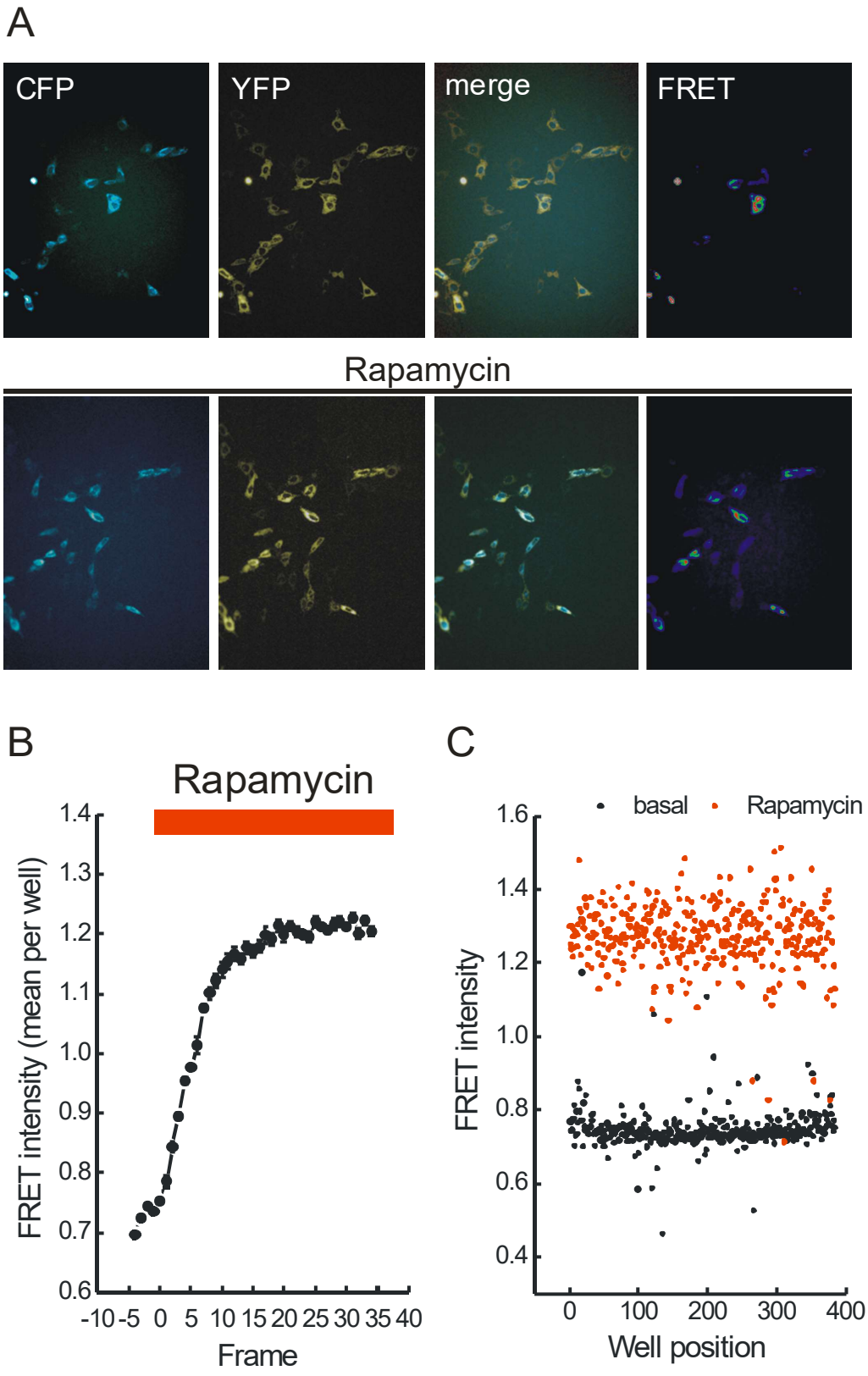
A
CFP
YFP
merge
FRET
Rapamycin
B
Rapamycin
FRET intensity (mean per well)
1.4
1.3
1.2
1.1
1.0
0.9
0.8
0.7
0.6
-10 -5 0 5 10 15 20 25 30 35 40
Frame
C
basal
Rapamycin
FRET intensity
1.6
1.4
1.2
1.0
0.8
0.6
0.4
0 100 200 300 400
Well position

Figure 3

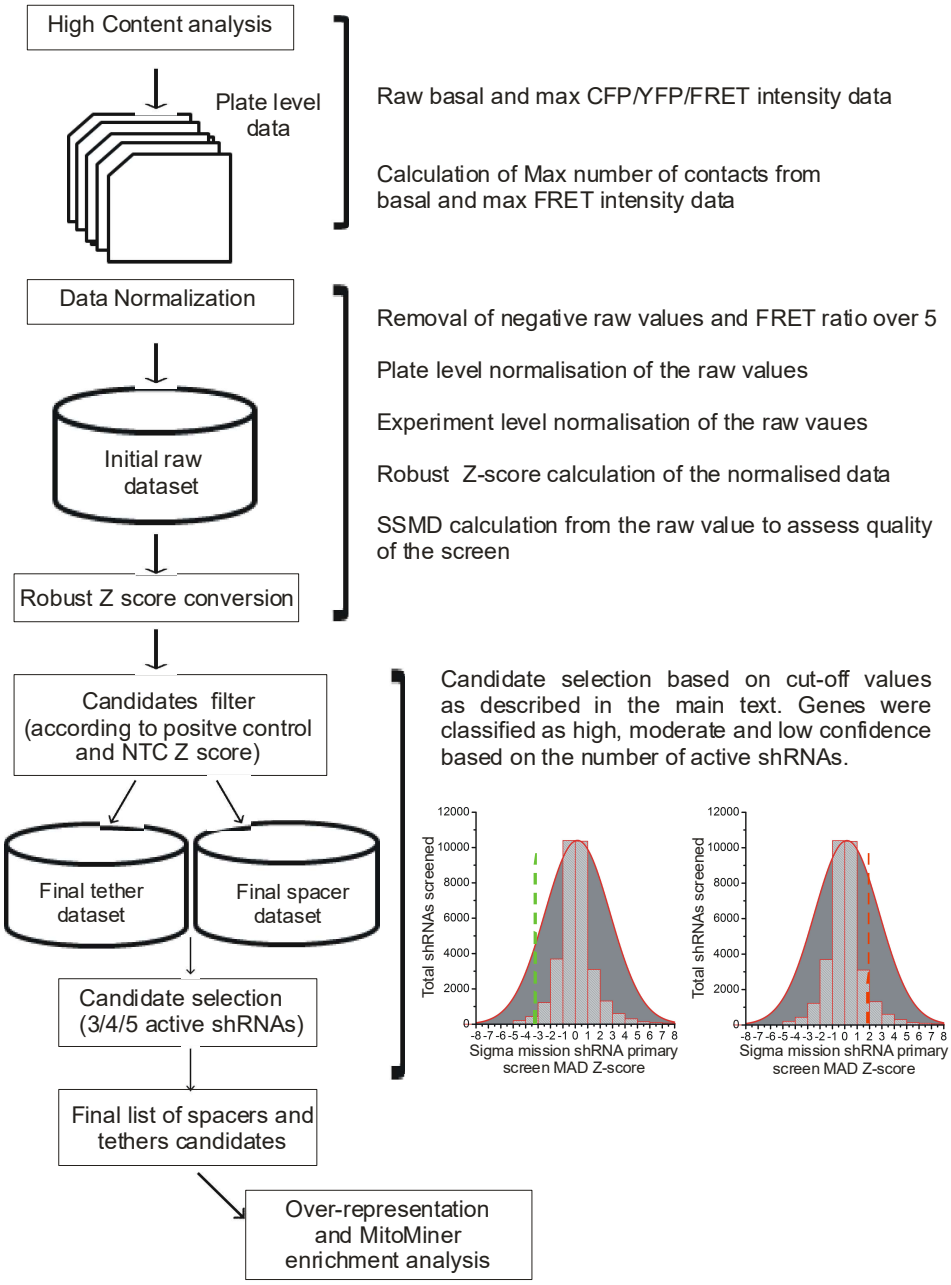
High Content analysis
Plate level data
Raw basal and max CFP/YFP/FRET intensity data
Calculation of Max number of contacts from basal and max FRET intensity data
Data Normalization
Initial raw dataset
Robust Z score conversion
Removal of negative raw values and FRET ratio over 5
Plate level normalisation of the raw values
Experiment level normalisation of the raw vaues
Robust Z-score calculation of the normalised data
SSMD calculation from the raw value to assess quality of the screen
Candidates filter (according to positve control and NTC Z score)
Final tether dataset
Final spacer dataset
Candidate selection (3/4/5 active shRNAs)
Final list of spacers and tethers candidates
Over-representation and MitoMiner enrichment analysis
Candidate selection based on cut-off values as described in the main text. Genes were classified as high, moderate and low confidence based on the number of active shRNAs.
Total shRNAs screened
Sigma mission shRNA primary screen MAD Z-score
Total shRNAs screened
Sigma mission shRNA primary screen MAD Z-score

Figure 4

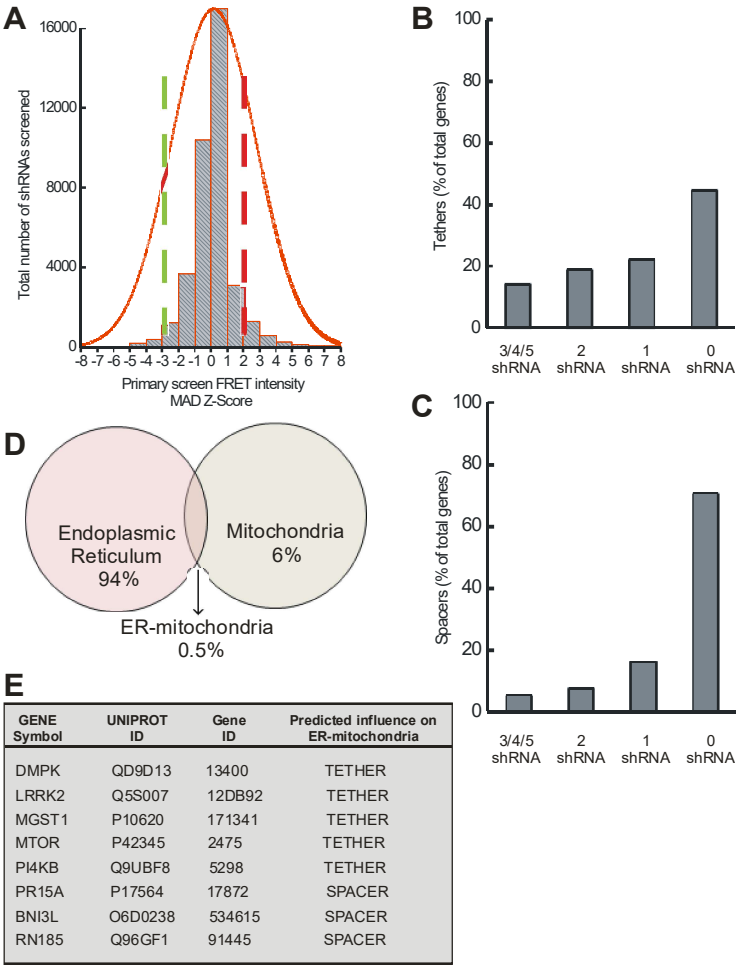

E

GENE Symbol	UNIPROT ID	Gene ID	Predicted influence on ER-mitochondria
DMPK	QD9D13	13400	TETHER
LRRK2	Q5S007	12DB92	TETHER
MGST1	P10620	171341	TETHER
MTOR	P42345	2475	TETHER
PI4KB	Q9UBF8	5298	TETHER
PR15A	P17564	17872	SPACER
BNI3L	O6D0238	534615	SPACER
RN185	Q96GF1	91445	SPACER

Figure 5

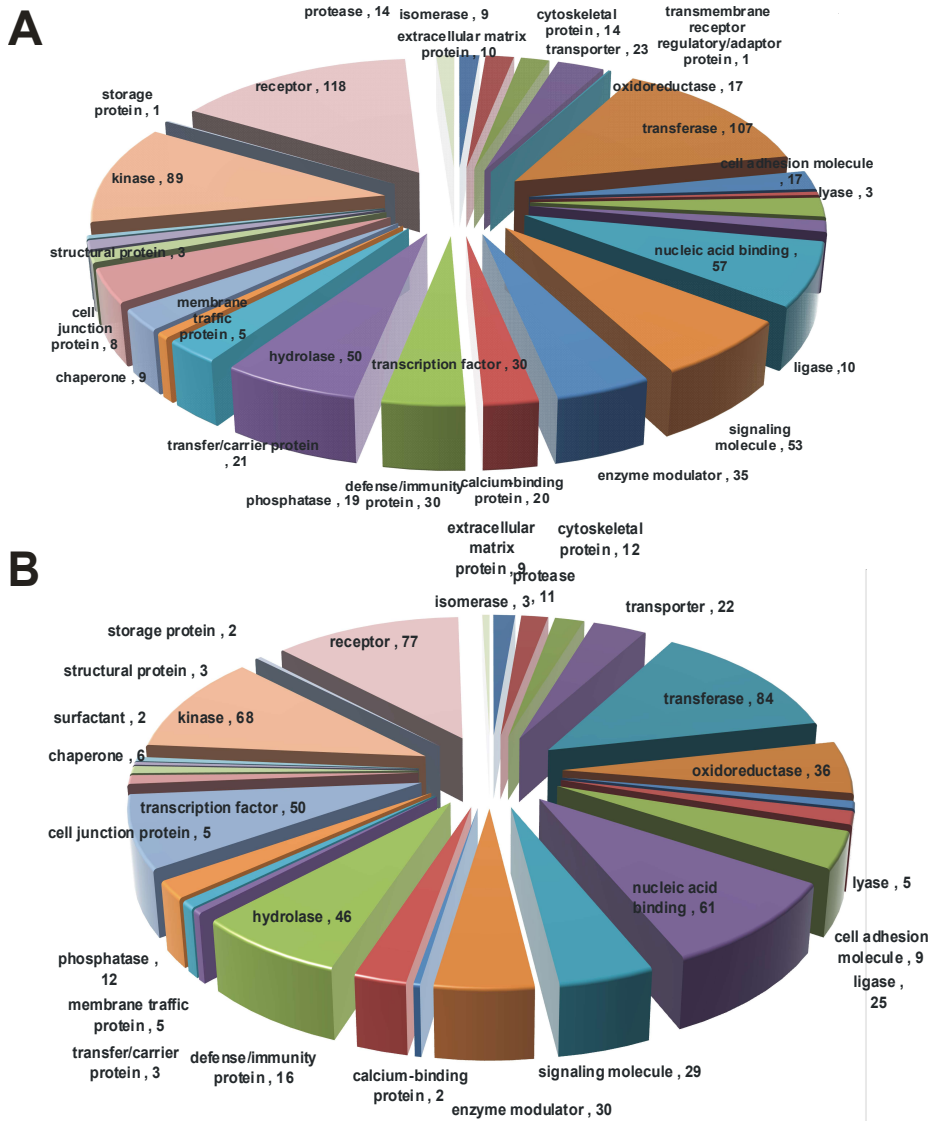
A
protease , 14
isomerase , 9
extracellular matrix protein , 10
cytoskeletal protein , 14
transporter , 23
transmembrane receptor regulatory/adaptor protein , 1
oxidoreductase , 17
transferase , 107
cell adhesion molecule , 17
lyase , 3
nucleic acid binding , 57
ligase ,10
signaling molecule , 53
enzyme modulator , 35
calcium-binding protein , 20
defense/immunity protein , 30
phosphatase , 19
transfer/carrier protein , 21
hydrolase , 50
transcription factor , 30
membrane traffic protein , 5
cell junction protein , 8
chaperone , 9
kinase , 89
structural protein , 3
storage protein , 1
receptor , 118
B
extracellular matrix protein , 9
cytoskeletal protein , 12
protease , 11
isomerase , 3
transporter , 22
transferase , 84
oxidoreductase , 36
lyase , 5
cell adhesion molecule , 9
ligase , 25
nucleic acid binding , 61
signaling molecule , 29
enzyme modulator , 30
calcium-binding protein , 2
defense/immunity protein , 16
transfer/carrier protein , 3
hydrolase , 46
phosphatase , 12
membrane traffic protein , 5
transcription factor , 50
cell junction protein , 5
chaperone , 6
surfactant , 2
kinase , 68
structural protein , 3
storage protein , 2
receptor , 77
C
Percentage of genes classified using Panther database
5.0
4.5
4.0
3.5
3.0
2.5
2.0
1.5
1.0
0.5
0.0
Tether
Spacer
Oxidoreductase
Ligase
Ca2+ binding protein
Isomerase

Figure 6

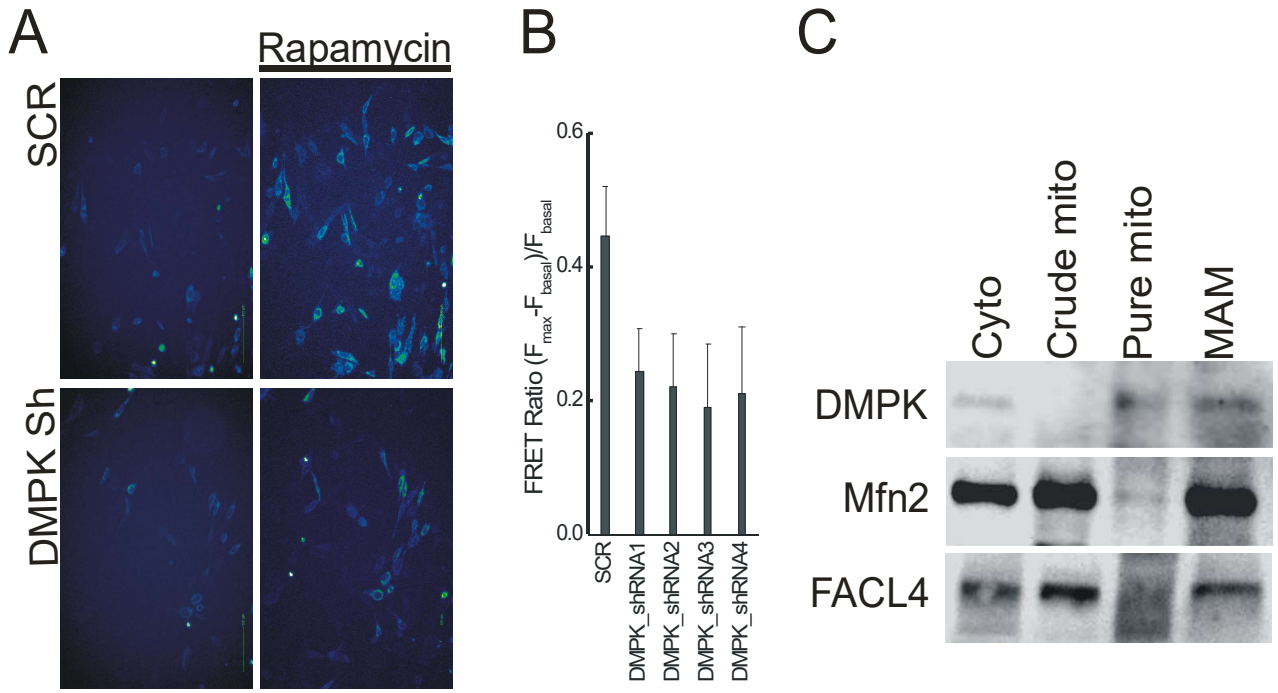
A
Rapamycin
SCR
DMPK Sh
B
FRET Ratio (F_max -F_basal)/F_basal
0.6
0.4
0.2
0.0
SCR
DMPK_shRNA1
DMPK_shRNA2
DMPK_shRNA3
DMPK_shRNA4
C
Cyto
Crude mito
Pure mito
MAM
DMPK
Mfn2
FACL4

A FRET based high content screen identifies DMPK as a novel tether of ER and mitochondria

Sowmya Lakshminarayanan, Annalisa Serafini and Marta Giacomello, Luca Scorrano

Supplementary online material

Extended figures legend

Extended Figure1.

Work flow of the automated image analysis

Overview of the image analysis for the genome wide screen. Cells from the raw images were segmented using YFP channel and intensity measures of CFP, YFP and FRET along with corresponding background intensities were measured. Mean FRET intensity was then calculated by subtracting the background and normalising to CFP intensity. See materials and methods for complete details of the image analysis.

Extended figure2.

Validation of the HCS assay procedure.

(A) **Formaldehyde Fixation does not affect FRET Ratio in MEFs expressing FEMP.** Basal and maximum FRET intensity pre and post fixation analysis. Data represents average ± S.E.M from 3 independent experiments. (N= 1453 objects).

(B) **Verification of transduction efficiency in wild type MEFs**. WT MEFs were transduced with GFP lenti-viral particles at 5 MOI. 48 hours post transduction, they were imaged in Operetta high content microscope (Perkin Elmer). Scale bar: 100 µm

(C) **Efficiency of gene silencing of the first identified ER-mitochondria tether**. WT MEFs were either transduced with Scr or Mfn2 shRNA lentiviral particles and 48 hours post transduction imaged at the Operetta high

content microscope (Perkin Elmer). As expected, Mfn2 down regulation yielded a disrupted mitochondrial morphology. Scale bar: 100 µm

(D**) Effect of FRET intensity after shRNA treatment against known tethers.** WT MEFs were transduced with Scr or Mfn2/PACS2 shRNA and 24 hours post transduction, transfected with FEMP probe. Data represents average ± S.E.M from 10 independent experiments.

Extended figure 1

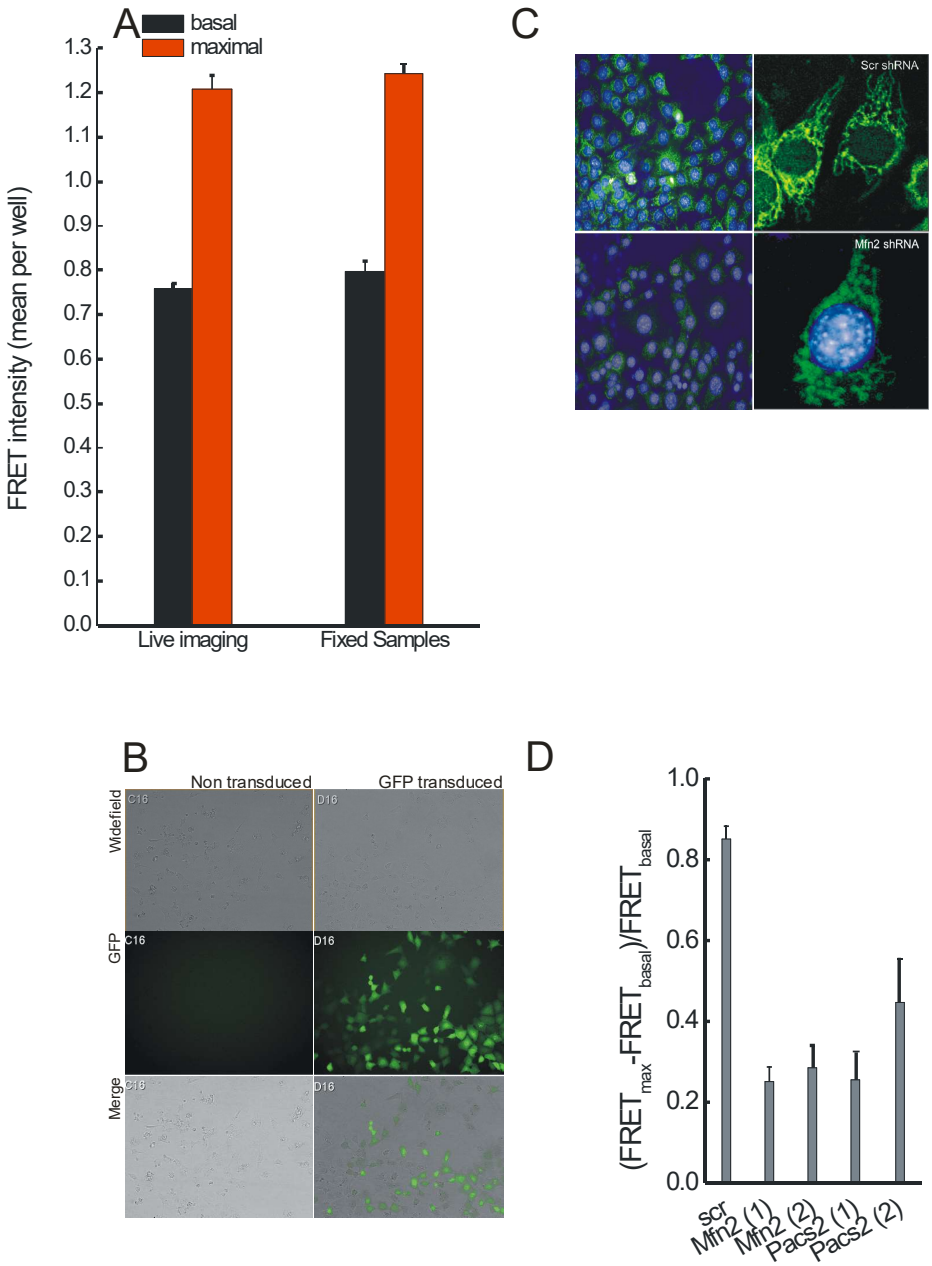

Extended figure 2

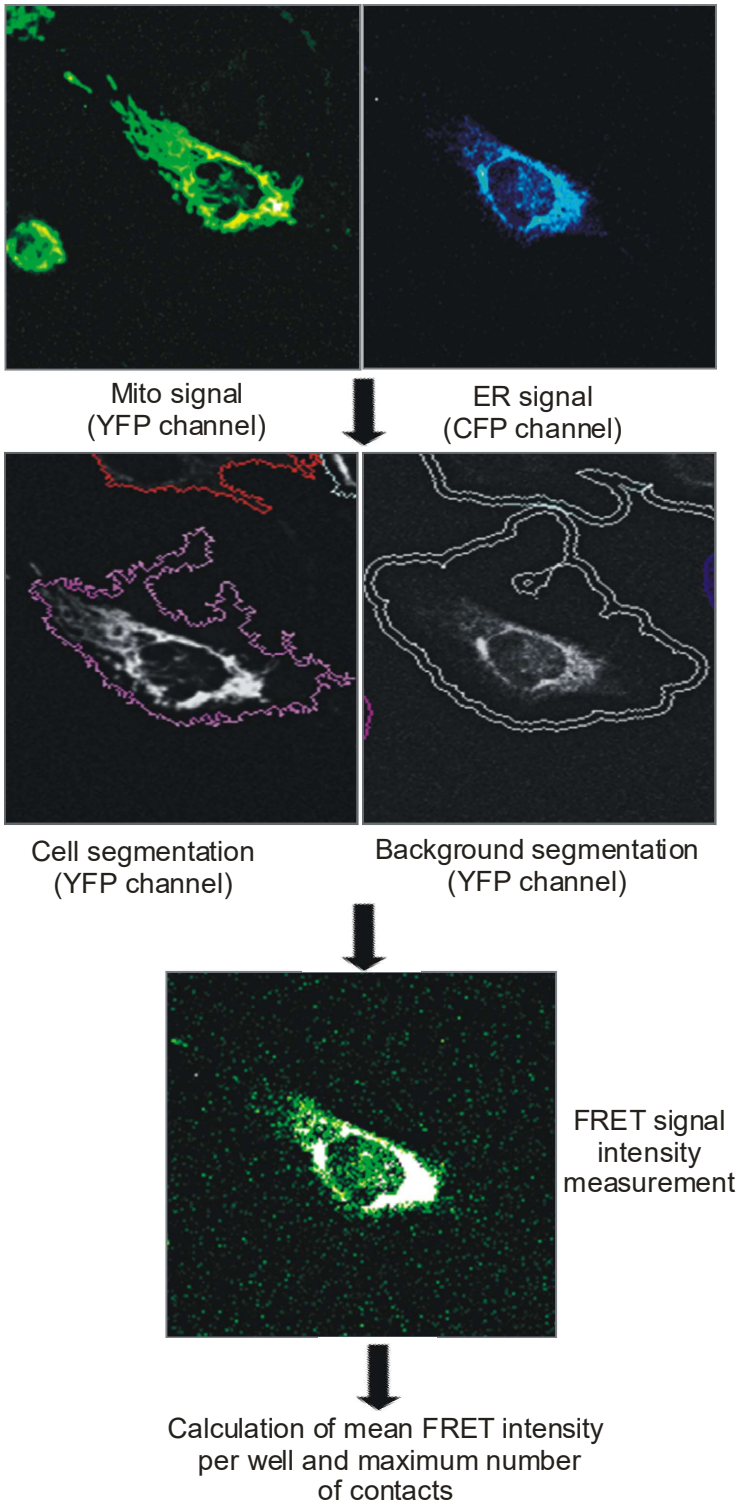

Extended Table legends

Extended table 1

Gene annotation of data on screen-specific ER-mitochondria tethers (genes that kept the two organelles together) in which 3 out of 5 shRNAs per gene has the phenotype – low FRET intensity compared to Scr shRNA.

Extended table 2

Gene annotation of data on screen-specific ER-mitochondria tethers (genes that kept the two organelles together) in which 4 out of 5 shRNAs per gene has the phenotype – low FRET intensity compared to SCR shRNA.

Extended table 3

Gene annotation of data on screen-specific ER-mitochondria Spacers (genes that kept the two organelles at a distance) in which 3 out of 5 shRNAs per gene has the phenotype – increased FRET intensity compared to SCR shRNA.

Extended table 4

Gene annotation of data on screen-specific ER-mitochondria Spacers (genes that kept the two organelles at a distance) in which 4 out of 5 shRNAs per gene has the phenotype – increased FRET intensity compared to SCR shRNA.

Extended Table 5

List of candidate tether genes with GO annotation match to "mitochondria" or to “Endoplasmic reticulum”, a member of Mitominer database.

Extended Table 6

List of candidate Spacer genes with GO annotation match to "mitochondria" or to “Endoplasmic reticulum”, a member of Mitominer database.

Extended Table1

S.No	Genesymbol	GeneID	Z-score
1	0610009A07Rik	70337	-0.53
2	0610010K06Rik	71678	0.13
3	1110006G06Rik	73833	-2.21
4	1110008B24Rik	73736	-0.33
5	1110012L19Rik	68618	-0.35
6	1110018G07Rik	68497	-0.41
7	1110020C03Rik	68625	-0.41
8	1110029E03Rik	242406	-1.85
9	1110034O07Rik	68744	-1.09
10	1190005I06Rik	68918	-0.13
11	1300007F04Rik	67477	-2.16
12	1500010J02Rik	68964	-0.28
13	1600029D21Rik	76509	-1.14
14	1700001C02Rik	75434	-2.53
15	1700001J03Rik	69282	-0.71
16	1700012H17Rik	242297	-2.21
17	1700027J05Rik	69440	-1.06
18	1700029P11Rik	66346	-1.57
19	1700049E17Rik	73415	-0.73
20	1700108M19Rik	71156	-0.66
21	1700112C13Rik	74306	-0.63
22	1810011O16Rik	66266	0.29
23	1810036H07Rik	66284	-1.4
24	1810049H19Rik	435889	-1.04
25	2010100O12Rik	67067	0.47
26	2010305A19Rik	69893	0.45
27	2210018M11Rik	233545	-0.64
28	2310008M10Rik	66357	-0.63
29	2310065K24Rik	102122	-2.11
30	2410015N17Rik	66422	-1.28
31	2410116G06Rik	68236	0.82
32	2410127E18Rik	76788	-1.35
33	2410127L17Rik	67383	-0.44
34	2600011C06Rik	67039	-2.56
35	2810003C17Rik	108897	-0.59
36	2810403A07Rik	74200	-0.25
37	2810417M05Rik	68027	-1.42
38	2810428I15Rik	66462	-3
39	2810443J12Rik	67228	-0.99
40	2900042E01Rik	72927	-0.64

S.No	Genesymbol	GeneID	Z-score
41	3300001M20Rik	66926	-1.11
42	4632404H12Rik	74034	-0.74
43	4921507A12	330513	-0.51
44	4922504M18Rik	244179	-0.68
45	4930408F14Rik	74851	-0.57
46	4930417G10Rik	74855	-1.21
47	4930430A15Rik	67575	-1.08
48	4930455C21Rik	76916	-1.05
49	4930506L13Rik	78802	-1.88
50	4930511M11Rik	75010	-0.8
51	4930523C11Rik	238405	-0.53
52	4930527D15Rik	67736	-0.75
53	4930533C12Rik	211430	-0.84
54	4931428F04Rik	74356	-1.7
55	4932411K12Rik	328325	-2.38
56	4932422E22Rik	319695	-0.23
57	4933409G03Rik	227998	0.08
58	4933425O20Rik	66766	-2.81
59	4933440M02Rik	71208	-0.36
60	5330410G16Rik	67937	-0.49
61	5730407K14Rik	101113	0.01
62	5830457H20Rik	217708	-1.77
63	5930422O12Rik	319688	-0.97
64	6330403K07Rik	103712	-0.36
65	6330409N04Rik	66674	-1.45
66	6330577E15Rik	67788	-0.49
67	6430502M16Rik	218440	-2.65
68	6430601A21Rik	228491	-0.55
69	8030411F24Rik	78609	-0.78
70	9030224M15Rik	327747	-2.15
71	9130011J15Rik	66818	-0.48
72	9230002F21Rik	442835	-1.91
73	9230112E08Rik	320800	-0.6
74	9230119C12Rik	77909	-0.46
75	9330182L06Rik	231014	0.22
76	9430071P14Rik	320590	-4.43
77	9530085L02Rik	442822	-0.49
78	9530098N22Rik	320640	-2.06
79	9930038B18Rik	319503	-0.67
80	A030004J04Rik	109314	-3.14

81	A030008J09	328231	-1.21
82	A130066N16Rik	442804	-0.25
83	A230051G13Rik	216792	-1.11

121	Angel2	52477	-1.16
122	Ankfy1	11736	-2.45
123	Ankra2	68558	-0.35

84	A430090L17Rik	319803	-0.9
85	A530099J19Rik	319293	-0.59
86	A630098G03Rik	230623	-1.48
87	A730020M07Rik	319738	-1.54
88	A830031A19Rik	268391	-2.06
89	A930024E05Rik	109202	-3.5
90	AA415398	433752	-3.81
91	AA467197	433470	-1.29
92	Abhd11	68758	-0.57
93	Abi1	11308	0.52
94	Acd	497652	-1.94
95	Acot11	329910	-1.75
96	Acp6	66659	-0.63
97	Acvr2b	11481	-0.2
98	Adam15	11490	-0.96
99	Adam33	110751	-0.62
100	Adam39	546055	-0.96
101	Adamts1	11504	-1.41
102	Adcyap1r1	11517	-2.81
103	Add3	27360	-0.35
104	Adora1	11539	-1.77
105	Adora3	11542	-3.34
106	Adra1d	11550	-0.45
107	Agtr1b	11608	-0.36
108	AI661453	224833	0.02
109	AI839735	104885	-0.82
110	AI842396	103844	-1.47
111	Akap7	432442	-0.47
112	Akt3	23797	-0.77
113	Alkbh5	268420	-1.14
114	Alox12	11684	-2.02
115	Amacr	17117	-0.12
116	Amdhd2	245847	-0.61
117	Amdhd2	245847	-1.51
118	Amhr2	110542	-1.53
119	Amigo3	320844	-1.99
120	Amot	27494	-1.06
124	Ankrd1	107765	-0.65
125	Ankrd10	102334	-1.11
126	Ankrd15	107351	-0.34
127	Ankrd49	56503	-0.45
128	Ankrd5	319196	-1.41
129	Anks3	72615	-1.03
130	Apoa1bp	246703	0.92
131	Arhgap19	71085	-0.61
132	Arhgap5	11855	-4.01
133	Arhgef15	442801	-3.99
134	Arhgef15	442801	-0.59
135	Arid1a	93760	-0.8
136	Art1	11870	-4.17
137	Asb15	78910	-0.95
138	Asb8	78541	-1.45
139	Asphd2	72898	-2.59
140	Atf4	11911	-2.25
141	Atf7	223922	-0.8
142	Atrx	22589	-1.61
143	AW549877	106064	-1.5
144	B130055D15Rik	78658	-0.83
145	B230120H23Rik	65964	-0.53
146	B230342M21Rik	100637	-1.14
147	B530045E10Rik	320966	-0.38
148	B930018B01	232599	-0.89
149	B930041G04	245643	-2.62
150	Baz2b	407823	0.02
151	BC003324	80291	-0.49
152	BC003331	226499	0.44
153	BC005764	216152	-0.66
154	BC006662	223267	-1.53
155	BC020535	228788	-0.83
156	BC022224	192970	-0.59
157	BC024139	271278	-1.71
158	BC024479	235184	-2.78
159	BC025575	217219	0.19
160	BC025816	234796	-0.61
161	BC030477	216881	-0.79
162	BC037703	242125	-0.83
163	BC048502	223927	-0.24
164	BC050092	235048	-2.94
165	BC052040	399568	-1.39
166	BC052046	240063	-0.88
167	BC057593	240067	-0.54
168	Bcor	71458	-3.25
169	Bdkrb2	12062	-1.06
170	Bmpr1a	12166	-1.27
201	Ccl21b	18829	-1.41
202	Ccl5	20304	-0.6
203	Ccl9	20308	-0.84
204	Ccnb1	268697	-1.12
205	Ccnb3	209091	-1.91
206	Ccng2	12452	-1.95
207	Ccnh	66671	-0.32
208	Ccnt1	12455	-2.05
209	Ccr1l1	12770	-0.72
210	Cd14	12475	-0.61

171	Bmpr2	12168	0.56
172	Brms1	107392	-1.76
173	Brp44l	55951	-1.96
174	Brs3	12209	-2.17
175	C130026L21Rik	330164	-3.7
176	C130086A10	208820	-0.53
177	C1s	50908	-0.43
178	C230013L11Rik	319712	-2.26
179	C230096C10Rik	230866	0.04
180	C330011K17Rik	238692	-2.5
181	C3ar1	12267	-1.5
182	Cacna1i	239556	-1.54
183	Cacna2d1	12293	-2.98
184	Cacnb1	12295	-4.3
185	Calca	12310	-0.95
186	Calm2	12314	-1.6
187	Camk1	52163	-1.25
188	Camkk1	55984	-0.65
189	Card12	268973	-2.04
190	Carhsp1	52502	-0.82
191	Carkl	74637	-4.1
192	Cart1	216285	-0.24
193	Casp4	12363	-2.25
194	Cast	12380	-1.57
195	Catsper2	212670	-1.11
196	Cbfb	12400	-0.42
197	Ccdc102a	234582	-2.12
198	Ccdc54	69339	-0.26
199	Ccdc60	269693	-1.53
200	Ccdc7	74703	-0.65

211	Cd19	12478	-2.45
212	Cd3eap	70333	0.61
213	Cd46	17221	-1.86
214	Cd59b	333883	-0.7
215	Cd72	12517	-2.61
216	Cd79b	15985	-0.08
217	Cd81	12520	-0.15
218	Cd86	12524	-2
219	Cdc42bpa	226751	-0.65
220	Cdca7	66953	-0.45
221	Cdkn2a	12578	-3.22
222	Cdyl	12593	-1.71
223	Cecr6	94047	-0.76
224	Celsr1	12614	-0.83
225	Cenpj	219103	-0.86
226	Cenpp	66336	-1.37
227	Ces5	234673	-0.6
228	Chchd5	66170	-0.78
229	Chic1	12212	-1.5
230	Cidea	12683	-1.82
231	Clcn6	26372	-0.59
232	Clec2e	232409	-3.38
233	Clic3	69454	-0.59
234	Clic5	224796	-1.33
235	Cln3	12752	-1.02
236	Cnnm1	83674	-0.22
237	Cnnm3	94218	-2.12
238	Cnot4	53621	-0.81
239	Commd10	69456	-1.12
240	Comp	12845	-0.59

241	Cox6a1	12861	-3.89
242	Cpeb4	67579	-0.27
243	Cpn2	71756	-2.14
244	Cpne4	74020	-1.43
245	Cpsf6	432508	-3.81
246	Creb3	12913	-0.88
247	Crebl1	12915	-1.11
248	Crem	12916	-1.01
249	Crhr2	12922	-1.25
250	Crispld2	78892	-3.27
251	Csrp2	13008	-0.35
252	Ctbs	74245	-2.25
253	Ctf1	13019	-3.47
254	Ctps	51797	-0.52
255	Cutc	66388	-2.11
256	Cxcr4	12767	-2.78
257	Cyp2c66	69888	-1.59

281	Dnase2b	56629	-0.86
282	Dok5	76829	-0.98
283	Dpep2	319446	-0.58
284	Drd1a	13488	-1.05
285	Drd1ip	68566	-0.45
286	Drd3	13490	-0.29
287	Dtnb	13528	-0.34
288	Dtx2	74198	-3.12
289	Dusp11	72102	-0.8
290	Dyrk1a	13548	-1.26
291	E030049G20Rik	210356	0.12
292	E230015B07Rik	320001	0.35
293	E2f2	242705	-0.78
294	E330013P04Rik	107376	-0.31
295	E4f1	13560	-1.67
296	Ect2	13605	-0.48
297	Eda	13607	-0.71

258	Cyp2s1	74134	-0.92
259	Cyp4f14	64385	-0.42
260	D0H4S114	27528	-2.36
261	D130059P03Rik	320538	-3.79
262	D14Ertd449e	66039	0.66
263	D17Ertd441e	52009	-1.83
264	D830046C22Rik	320197	-0.62
265	D930016N04Rik	245368	-1.96
266	Dab1	13131	0.18
267	Dbndd2	52840	-3.1
268	Dcamkl2	70762	-2.67
269	Dcun1d1	114893	-1.55
270	Ddit4l	73284	-1.96
271	Ddx4	13206	-1.12
272	Ddx52	78394	-3.1
273	Depdc1a	76131	-1.26
274	Depdc1b	218581	-0.84
275	Dgkd	227333	-0.65
276	Dgkg	110197	-3.46
277	Dgkq	110524	-1.15
278	Diras2	68203	-1
279	Dlgh2	23859	-2.3
280	Dmrt2	226049	-1.68

298	Eda2r	245527	-1.17
299	Edf1	59022	-1.44
300	Efna2	13637	-0.65
301	Egfl7	353156	-0.72
302	Eif2b2	217715	-0.79
303	Elf5	13711	-3.6
304	Eprs	107508	-1.2
305	Ercc6l	236930	-1.05
306	Erf	13875	-0.95
307	Ergic2	67456	-3.5
308	Ets2	23872	-0.74
309	Etv3	27049	-0.17
310	Etv6	14011	-0.28
311	Exoc8	102058	-1.02
312	F2r	14062	-1.8
313	Fbxl14	101358	-1.1
314	Fbxl3	50789	-4
315	Fbxo15	50764	-0.06
316	Fbxo2	230904	-0.37
317	Fbxo22	71999	-0.62
318	Fbxo36	66153	-1.34
319	Fbxo43	78803	-1.44
320	Fbxo6b	50762	-0.6

321	Fbxw2	30050	-1.38
322	Fbxw4	30838	-2.35
323	Fbxw5	30839	-2.03
324	Fbxw7	50754	-1.09
325	Fcgrt	14132	-1.11
326	Fdx1	14148	-2.18
327	Fgf3	14174	-1.05
328	Fgf6	14177	-0.27
329	Fgfr2	14183	-2.72
330	Figf	14205	-4
331	Fin15	14210	-4.34
332	Fosb	14282	-3.48
333	Fosl2	14284	-0.76
334	Foxa3	15377	-1.38
335	Foxb1	64290	-2.31
336	Foxd2	17301	-0.65
337	Foxd2	17301	-1.13
338	Foxf1a	15227	-0.63
339	Foxl1	14241	-0.47
340	Fpr-rs3	14290	-0.75
341	Fpr-rs4	14291	-0.42
342	Frap1	56717	-4.64
343	Frem2	242022	-0.28
344	Fshr	14309	-3.84

361	Gnb3	14695	-1.7
362	Gne	50798	-1.49
363	Gpam	14732	-1.48
364	Gpatc3	242691	-0.58
365	Gpbar1	227289	-1.4
366	Gpd1l	333433	-2
367	Gpr115	78249	-0.6
368	Gpr135	238252	-0.37
369	Gpr146	80290	-3.73
370	Gpr153	100129	-1.36
371	Gpr158	241263	-0.39
372	Gpr20	239530	-0.63
373	Gpr31c	436440	-0.41
374	Gpr75	237716	-1.25
375	Gpr77	319430	-4.28
376	Gpr77	319430	-0.33
377	Gpr84	80910	-1.45
378	Gprc5a	232431	-0.73
379	Gprc5b	64297	-0.46
380	Gprk6	26385	-1.49
381	Grm6	108072	-0.33
382	Gsdmdc1	69146	-1.24
383	Gt4-1	107459	-1.65
384	Gtf2a1lf	71828	-0.6

345	Fxyd2	11936	-1.06
346	Fzd3	14365	-1.11
347	Fzd6	14368	-0.73
348	G630049C14Rik	234700	-1.5
349	Galr3	14429	-2.15
350	Gata2	14461	-2.63
351	Gata3	14462	-1.25
352	Ggps1	14593	-0.95
353	Gja1	14609	-2.28
354	Gja8	14616	-3.59
355	Glipr1	73690	-0.63
356	Glt25d2	269132	-1.3
357	Glt25d2	269132	-0.61
358	Gm360	245335	-1.84
359	Gm489	244049	-0.02
360	Gm93	225497	-1.06

385	Gtf2h2	23894	-1.44
386	Gtf3a	66596	-1.85
387	Gtf3c1	233863	-0.6
388	Gucy2g	73707	-1.44
389	Gykl1	14625	-0.91
390	Gzmb	14939	-0.78
391	Gzmc	14940	-1.98
392	H2-Ea	14968	-0.81
393	H2-Ea	14968	-0.5
394	H6pd	100198	-0.76
395	Hace1	209462	-0.91
396	Hao1	15112	-0.81
397	Hccs	15159	-4.51
398	Hecw1	94253	-1.47
399	Hemt1	15202	-1.22
400	Hey1	15213	-0.72

401	Hey2	15214	-0.29
402	Hif3a	53417	-0.58
403	Hist3h2bb	382522	-0.92
404	Hkr3	100090	-0.93
405	Hlcs	110948	-3.3
406	Hmga2	15364	-2.09
407	Hmgb3	15354	-1.25
408	Hnrpd	11991	-1.38
409	Hnrpf	98758	-1.21
410	Hnrph3	432467	-0.97
411	Homez	239099	-2.47
412	Hoxc4	15423	-3.87
413	Hoxc5	15424	-0.59
414	Hoxc9	15427	-1.19
415	Hps5	246694	-3.07
416	Hsf2	15500	-0.75
417	Hsf4	26386	-0.81
418	Hspb3	56534	-0.4
419	Htr5a	15563	-0.35
420	Hus1b	210554	-1.5
421	Ifna12	242519	-3.79
422	Ifna13	230396	-0.62
423	Ifna9	15972	-1.82
424	Ifnb1	15977	-1.17
425	Igsf4b	94332	-0.75
426	Igsf6	80719	-0.61
427	Ihpk3	271424	-2.17
428	Ikbkb	16150	-0.08
429	Il28ra	242700	-2.61
430	Il2rb	16185	-1.04

441	Irak4	266632	0.33
442	Isgf3g	16391	-0.8
443	Isl1	16392	-3.24
444	Itch	16396	-1.49
445	Itga5	16402	-1.2
446	Itga7	16404	-0.28
447	Itgb4	192897	-0.71
448	Itpkb	320404	-1.97
449	Jub	16475	-0.55
450	Junb	16477	-1.53
451	Kcng4	66733	-3.15
452	Kcnh1	16510	-2.42
453	Kcnh5	238271	-1.17
454	Kcnj15	16516	-1.86
455	Kcnj4	16520	-0.53
456	Kcnk3	16527	-0.42
457	Kcnk7	16530	-1.05
458	Kcnq3	110862	-0.98
459	Kctd16	383348	-0.38
460	Kctd6	71393	-1.28
461	Kctd8	243043	-1.95
462	Klf15	66277	-1.21
463	Klf6	23849	-0.16
464	Klf8	245671	-3.68
465	Klhl13	67455	-1.19
466	Klk1b4	18048	-0.57
467	Klrd1	16643	-1.04
468	Krt1-15	16665	-0.86
469	Krtap6-2	16701	-1.71
470	Lasp1	16796	-1.91

431	Il6ra	16194	-1.95
432	Il7	16196	-2.09
433	Ildr1	106347	-0.57
434	Ilk	16202	-0.93
435	Iltifb	116849	-0.16
436	Impact	16210	-1.22
437	Inhbe	16326	-2.08
438	Insl6	27356	-4.47
439	Insm1	53626	-1.51
440	Irak2	108960	0.05

471	Lcn3	16820	-0.88
472	Lep	16846	-1.17
473	Lgals3bp	19039	-1.17
474	Lig3	16882	-1.3
475	Lipc	15450	-1.17
476	LOC218963	218963	-0.71
477	LOC224582	224582	-2.64
478	LOC225594	225594	-1.35
479	LOC382243	382243	-2.13
480	LOC382395	382395	-0.86

481	LOC386042	386042	-1.28
482	LOC433180	433180	-0.9
483	LOC433406	433406	-0.84
484	LOC433481	433481	-1.12
485	LOC433886	433886	-0.55
486	LOC434405	434405	-0.57
487	LOC434459	434459	-0.56
488	LOC435637	435637	-0.75
489	LOC435940	435940	-1.96
490	LOC436147	436147	-1.09
491	LOC544988	544988	0.05
492	LOC545013	545013	-0.68
493	LOC545471	545471	-0.6
494	LOC546723	546723	0.06
495	LOC547343	547343	-0.59
496	LOC623195	623195	-4.26
497	LOC623215	623215	-1.85
498	Loh11cr2a	67776	-0.89
499	Loxl4	67573	-1.05
500	Lrfn4	225875	-1.66
501	Lrrc29	234684	-1.93
502	Lrrc4	192198	-0.57
503	Lrrc54	244152	-2.02
504	Lrrc8b	433926	-0.65
505	Lrrc9	78257	-2.04
506	Lrrn6d	320747	-0.34
507	Lrrtm1	74342	-1.85
508	Lsm7	66094	-0.86
509	Lta	16992	-0.79
510	Ltb	16994	-0.92
511	Ly6k	76486	-0.79
512	Ly96	17087	-0.15
513	Lztfl1	93730	-0.11
514	Lzts1	211134	-1.13
515	Madcam1	17123	-0.72
516	Man2a2	140481	-0.49
517	Man2b1	17159	-0.27

521	Mare	17168	-1.63
522	Marveld3	73608	-0.38
523	Mctp1	78771	-0.51
524	Mea1	17256	-1.54
525	Med28	66999	-0.65
526	Meig1	104362	0.34
527	Mgat1	17308	-0.53
528	Mgat3	17309	0.82
529	Mgat4a	269181	-0.25
530	Mgmt	17314	-0.87
531	Mgst1	56615	-2.14
532	Mink1	50932	-1.51
533	Mpp3	13384	-0.34
534	Mre11a	17535	-0.66
535	Mreg	381269	-2.15
536	Mrfap1	67568	-0.34
537	Mrg2	17537	-0.32
538	Mrgprf	211577	-0.29
539	Mrpl9	78523	-0.15
540	Mrps27	218506	-0.15
541	Mta3	116871	-0.24
542	Mtfmt	69606	-1.08
543	Mtmr12	268783	-0.76
544	Mtmr3	74302	-1.45
545	Myd116	17872	-1.63
546	Myd88	17874	-1.54
547	Myf5	17877	-0.32
548	Myf6	17878	-0.85
549	Myo3a	214682	-0.69
550	Nbn	27354	-2.22
551	Ndufb10	68342	-0.19
552	Ndufc2	68197	-1.73
553	Ndufs6	407785	-1.34
554	Necap1	67602	0.39
555	Nedd8	18002	-1.32
556	Nek2	18005	-0.52
557	Nek6	59126	-3.09

518	Map3k11	26403	0.13
519	Map4k3	225028	-0.85
520	Marcksl1	17357	0.48
558	Neurog2	11924	-0.46
559	Neurog3	11925	-1.65
560	Nfat5	54446	-2.27

561	Nfe2	18022	-2.17
562	Nfe2l1	18023	-0.91
563	Nfil3	18030	-0.57
564	Nkx2-9	18094	-1.3
565	Nme1	18102	-2.33
566	Nme5	75533	-3.24
567	Nme6	54369	-0.41
568	Nme7	171567	-4.16
569	Nmur2	216749	-2.05
570	Nnt	18115	-1.7
571	Nos2	18126	-1.42
572	Notch3	18131	-1.83
573	Npsr1	319239	-1.38
574	Npy2r	18167	-3.68
575	Nrg1	211323	-0.78
576	Nthl1	18207	-2.08
577	Ntsr1	18216	-2.21
578	Ntsr2	18217	-0.23
579	Obox2	246792	-1.91
580	Obox5	252829	-3.26
581	Obox6	252830	-2.27
582	Ocrl	320634	-1.14
583	Olfr102	258218	-0.77
584	Olfr1111	258586	-0.5
585	Olfr1276	258390	-0.78
586	Olfr1302	258891	-1.74
587	Olfr1415	258228	-0.81
588	Olfr145	258310	-1.19
589	Olfr1489	258628	-1.04
590	Olfr152	258640	-0.69
591	Olfr202	258997	-2.33
592	Olfr215	258438	-0.58
593	Olfr23	18321	-0.57
594	Olfr259	258766	-0.51
595	Olfr32	18331	-1.86
596	Olfr33	18332	-1.49
597	Olfr419	258710	-1.81
598	Olfr478	258729	-0.49
599	Olfr513	258718	-1.01
600	Olfr541	258964	-1.59
601	Olfr549	259105	-0.67
602	Olfr553	233578	-0.56
603	Olfr605	258156	-0.49
604	Olfr608	258751	-1.14
605	Olfr617	258838	-0.85
606	Olfr657	258309	-1.43
607	Olfr672	258755	-0.51
608	Olfr693	258445	-0.64
609	Olfr711	259037	-3.38
610	Olfr777	258537	-0.82
611	Olfr782	257985	-0.66
612	Olfr900	258874	-0.56
613	Olfr904	258797	-1.43
614	Onecut1	15379	-0.25
615	Oprl1	18389	-1.01
616	Oprm1	18390	-1.02
617	ORF34	207375	-0.37
618	Otx1	18423	-0.76
619	Ovol1	18426	-0.81
620	P2rx5	94045	-8.73
621	P2ry12	70839	-0.27
622	Pax1	18503	-1.59
623	Pax6	18508	-0.49
624	Pax8	18510	-1.56
625	Pax9	18511	-3.79
626	Pbxip1	229534	-1.67
627	Pcbp4	59092	-2.15
628	Pcp4	18546	-0.68
629	Pdgfrb	18596	-2.53
630	Pdpk1	18607	-3.12
631	Pdxp	57028	-0.61
632	Penk1	18619	-0.86
633	Pgk1	18655	-0.72
634	Phf7	71838	-3.83
635	Phlpp	98432	-0.89
636	Phpt1	75454	-1.48
637	Pik3cb	74769	-3.38
638	Pik3r1	18708	-1.95
639	Pip5k1c	18717	-2.23
640	Pip5k2c	117150	-3.97

641	Pit1	18736	-0.26
642	Pkd1l2	76645	-1.56
643	Pla2g6	53357	-1.03
681	Ptpn9	56294	-0.91
682	Ptprc	19264	-0.65
683	Ptprcap	19265	-1.88

644	Plaa	18786	-0.96
645	Pld3	18807	-0.92
646	Plekha6	240753	-0.3
647	Plk2	20620	-1.52
648	Plxdc2	67448	-0.76
649	Plxna3	18846	-1
650	Plxnb1	235611	-1.97
651	Plxnd1	67784	-3.56
652	Pnpla7	241274	-1.7
653	Podn	242608	-1.03
654	Podxl2	319655	-0.43
655	Pou2af1	18985	-0.15
656	Pou3f2	18992	-2.39
657	Pou3f3	18993	-0.82
658	Pou6f2	218030	-0.39
659	Ppm1k	243382	-0.73
660	Ppm1l	242083	-1.89
661	Ppm2c	381511	-0.65
662	Ppox	19044	-0.77
663	Ppp1r12c	232807	-0.53
664	Pramel5	347710	-2.64
665	Prb1	381833	-0.83
666	Prickle2	243548	-1.2
667	Prkacb	18749	-2.52
668	Prkar2a	19087	-2.54
669	Prkcn	75292	-1.55
670	Prkd2	101540	-0.07
671	Prokr1	58182	-3.46
672	Pros1	19128	-1
673	Psma8	73677	-1.23
674	Psmd8	57296	0.08
675	Psmf1	228769	-0.96
676	Ptch2	19207	-0.91
677	Ptgir	19222	-2.13
678	Ptgis	19223	-1.67
679	Ptn	19242	-0.54
680	Ptpn21	24000	-1.95
684	Ptprf	19268	-2.8
685	Ptprt	19281	-1.08
686	Pycard	66824	-0.51
687	Qscn6	104009	-1.61
688	Qtrt1	60507	-3.16
689	Rai14	75646	-2.61
690	Ranbp3	71810	-2.04
691	Rarsl	109093	-1.38
692	Rbbp5	213464	-0.63
693	Rel	19696	-0.49
694	Rem1	19700	-2.01
695	Rfxdc1	320995	-1.41
696	Rg9mtd2	108943	-1.08
697	Rhbdf2	217344	-0.67
698	Rhox5	18617	-0.93
699	Rin3	217835	-0.22
700	Ripk1	19766	0.07
701	Rnasel	24014	-0.24
702	Rnd3	74194	-1.29
703	Rnf123	84585	-2.56
704	Rnf139	75841	-1.07
705	Rnf25	57751	-4.54
706	Rnf43	207742	-2.62
707	Rpp25	102614	-1.37
708	Rps6ka1	20111	-0.71
709	Rsnl2	78785	-0.43
710	Runx3	12399	-0.69
711	Rxfp3	239336	-0.69
712	Rxrg	20183	-2.52
713	Rybp	56353	-1.25
714	Sbf1	77980	-0.92
715	Scarb1	20778	-1
716	Scn10a	20264	-0.95
717	Scn7a	20272	-1.15
718	Scyl1	78891	-1.46
719	Sele	20339	-1.12
720	Senp8	71599	-1.41

721	Serpina1b	20701	-4.53
722	Serpina3f	238393	-0.74
723	Serpinb2	18788	-2.63
724	Serpinb6b	20708	-1.9
725	Serpine1	18787	-1.73
726	Sestd1	228071	-1.95
727	Sgcb	24051	-1.52
728	Sgk3	170755	-1.58
729	Sgol1	72415	-1.79
730	Skp1a	21402	-1.13
761	Slc39a4	72027	-1.24
762	Slc3a2	17254	-0.8
763	Slc5a11	233836	-0.35
764	Slc5a4b	64454	-1.26
765	Slc6a13	14412	-0.28
766	Slc6a3	13162	-0.28
767	Slc7a10	53896	-1.21
768	Slc7a4	224022	-0.89
769	Slc7a6os	66432	-1.51
770	Slc7a7	20540	-2.25

731	Sla	20491	-1.64
732	Slc12a9	83704	-1.77
733	Slc13a4	243755	-1.55
734	Slc15a1	56643	-1.11
735	Slc16a11	216867	-0.95
736	Slc16a2	20502	-0.55
737	Slc16a6	104681	-2.24
738	Slc16a9	66859	-0.66
739	Slc17a2	218103	-0.35
740	Slc18a2	214084	-0.72
741	Slc1a5	20514	-1.25
742	Slc20a2	20516	-2.8
743	Slc22a4	30805	-2.66
744	Slc22a5	20520	-0.34
745	Slc24a1	214111	-0.38
746	Slc25a14	20523	-1.28
747	Slc25a16	73132	-4.9
748	Slc26a3	13487	-1.07
749	Slc28a3	114304	-1.23
750	Slc2a12	353169	-0.94
751	Slc2a13	239606	-1.66
752	Slc2a6	227659	-1.87
753	Slc2a9	117591	-1.6
754	Slc30a5	69048	-1.3
755	Slc31a1	20529	-3.92
756	Slc35a2	22232	-2.34
757	Slc35c2	228875	-0.64
758	Slc37a3	72144	-1.76
759	Slc39a10	227059	-0.31
760	Slc39a3	106947	-2.34
771	Slc7a8	50934	-2.44
772	Slc7a9	30962	-0.32
773	Slc9a8	77031	-3.5
774	Slco4a1	108115	-0.99
775	Slfn3	20557	-0.6
776	Slitrk2	245450	-0.5
777	Slitrk5	75409	-0.2
778	Slitrk6	239250	-1.29
779	Slk	20874	-0.63
780	Smarca5	93762	-0.77
781	Smarcb1	20587	-0.56
782	Smarcc2	68094	-0.34
783	Smarce1	57376	-2.4
784	Snf8	27681	-2.46
785	Snrpn	20646	-1.78
786	Sox13	20668	-2.25
787	Sox13	20668	-1.08
788	Sox13	20668	-0.81
789	Sox15	20670	-0.15
790	Sox18	20672	-0.64
791	Sp8	320145	-1.89
792	Spata4	69281	-0.53
793	Spdyb	74673	-0.41
794	Speer2	224318	-0.65
795	Spin2	278240	-0.43
796	Spinlw1	75526	-3.13
797	Spred2	114716	-0.33
798	Sprr2g	20761	-2.4
799	Ssbp3	72475	-0.89
800	Stk32a	269019	-1.97

801	Stk32c	57740	-0.91
802	Stk38	106504	-1.29
803	Stk38l	232533	-1.2
804	Strbp	20744	-0.25
805	Styx	56291	-2.12
806	Supt3h	109115	-2.09
807	Sval1	71578	-1.17
808	Syce2	71846	-0.4
809	Syt15	319508	-0.7
810	Taar7d	435206	-1.31
811	Taf1b	21340	-3.73
812	Tagln3	56370	-0.79
813	Tal1	21349	-0.98
814	Taok1	216965	-1.37
815	Tas2r120	387348	-0.48
816	Tas2r131	387356	-2.86
817	Tbrg1	21376	-1.08
841	Tm7sf3	67623	-1.96
842	Tm9sf2	68059	-0.75
843	Tmc7	209760	-1.16
844	Tmc8	217356	-0.43
845	Tmem132d	243274	-0.19
846	Tmem157	67698	-1.13
847	Tmprss11f	243083	-1.2
848	Tnfrsf8	21941	-1.3
849	Tnfsf10	22035	0.26
850	Tnfsf11	21943	-0.44
851	Tnfsf18	240873	-1.26
852	Tnni3k	435766	-1.79
853	Tnrc9	244579	-1.61
854	Tns3	319939	-0.94
855	Tollip	54473	-1.94
856	Top2b	21974	-1.6
857	Top3b	21976	-1.68

818	Tbx18	76365	-2.2
819	Tbx19	83993	-0.35
820	Tcerg1l	70571	-1.17
821	Tcf1	21405	-1.91
822	Tcf7l2	21416	-1.76
823	Tcfap2d	226896	-0.75
824	Tcfap4	83383	-1.5
825	Tcfeb	21425	-0.96
826	Tcp11	21463	-1.25
827	Tdo2	56720	-1.86
828	Tead1	21676	-0.55
829	Tgfb1i1	21804	-0.62
830	Tgfb2	21808	-1.56
831	Tgfb2	21808	-4.24
832	Tgfbrap1	73122	-1
833	Thsd4	207596	-2.21
834	Thtpa	105663	-1.71
835	Timm8b	30057	-1.54
836	Titf1	21869	-0.21
837	Tk1	21877	-3.06
838	Tloc1	69276	-1.26
839	Tlr9	81897	-2.8
840	Tm4sf4	229302	-1.28

858	Tpcn2	233979	-1.15
859	Traf1	22029	-3.91
860	Trafd1	231712	-1.68
861	Traip	22036	-0.05
862	Trhr	22045	-0.8
863	Trhr2	170732	-0.5
864	Trp63	22061	-1.55
865	Trp73	22062	-1.56
866	Trpc1	22063	-2.59
867	Tsga2	22092	-3.84
868	Tslp	53603	-1.54
869	Tspyl1	22110	-0.77
870	Tssc4	56844	-1.07
871	Tusc2	80385	-0.73
872	Twist2	13345	-0.72
873	Txndc3	73412	-3.36
874	Tyms	22171	-2.99
875	Uba52	22186	-0.61
876	Ube1x	22201	-1.57
877	Ube2m	22192	-1.95
878	Ubp1	22221	-0.54
879	Ubqln3	244178	-1.11
880	Ugdh	22235	-0.66

881	Ugt2a2	552899	-0.27
882	Ugt3a2	223337	-1.94
883	Uhmk1	16589	-0.35
884	Unc13d	70450	-1.3
885	Unc93a	381058	-0.6
886	UNK	238119	-3.07
887	UNK	329248	-1.98
888	UNK	218456	-1.3
889	UNK	384361	-2.23
890	UNK	384054	-0.81
891	UNK	381815	-1.61
892	UNK	436432	-1.06
893	UNK	381861	-2.43
894	UNK	385828	-2.25
895	UNK	433718	-2.54
896	UNK	436127	-0.2
897	UNK	436178	-3.43
898	UNK	385186	-1.58
899	UNK	433112	-0.95
900	UNK	435347	-1.69
901	UNK	435625	-2.25
902	UNK	433880	-1.42
903	UNK	626662	-0.54
904	UNK	435386	-0.55

921	V1rd8	404283	0.65
922	V1re10	171263	-1.02
923	V1re5	171228	-1.14
924	V1re6	171229	-1.56
925	Vipr1	22354	-0.47
926	Vmd2l1	212989	-1.7
927	Wdr39	26371	-0.28
928	Wdr8	59002	-0.67
929	Wfdc13	408190	-1.61
930	Wnk1	232341	-2.51
931	Xkr4	497097	-0.53
932	Ybx1	22608	-1.27
933	Zc3hc1	232679	-0.9
934	Zcchc12	72693	-1.71
935	Zdhhc13	243983	-2.46
936	Zfp108	54678	-3.14
937	Zfp109	56869	-1.02
938	Zfp11	22648	-0.34
939	Zfp119	104349	-1.63
940	Zfp131	72465	-0.16
941	Zfp146	26465	-0.16
942	Zfp207	22680	-1.14
943	Zfp275	27081	-0.67
944	Zfp316	54201	-1.47

905	UNK	435262	-0.44
906	UNK	433915	-0.71
907	UNK	433915	-0.82
908	UNK	435635	-1.34
909	UNK	433391	-1.58
910	UNK	432816	-0.29
911	UNK	436273	-0.45
912	UNK	245589	-1.22
913	UNK	436110	-1.37
914	UNK	435630	-0.33
915	UNK	385028	-0.5
916	Uqcr	66594	-1.27
917	Usp44	327799	-0.72
918	Usp50	75083	-0.64
919	Usp7	252870	-1.22
920	V1ra8	113850	-1.74

945	Zfp322a	218100	-3.01
946	Zfp334	228876	-0.36
947	Zfp352	236537	-2.43
948	Zfp354b	27274	-0.28
949	Zfp354c	30944	-2.18
950	Zfp358	140482	-0.43
951	Zfp367	238673	-0.17
952	Zfp418	232854	-0.45
953	Zfp449	78619	-0.87
954	Zfp496	268417	-1.19
955	Zfp513	101023	-0.62
956	Zfp52	22710	-1.96
957	Zfp535	52712	-1.6
958	Zfp606	67370	-1.16
959	Zfp612	234725	-1.02
960	Zfp628	232816	-0.9

961	Zfp689	71131	-0.53
962	Zfp84	74352	-0.4
963	Zfp90	22751	-0.44
964	Zfp99	67235	-1.45
965	Zfpm1	22761	-1.48
966	Zfpn1a1	22778	-0.35
967	Zfpn1a5	67143	-0.97
968	Zfr	22763	-0.49
969	Zim1	22776	-0.71

Extended Table 2

S.No	Genesymbol	GeneID	Z-score
1	42071	71779	-0.52
2	1190002A17Rik	68870	-3
3	1200002N14Rik	71712	-1.06
4	1700007G11Rik	75784	-1.12
5	1700008P20Rik	69301	-0.53
6	1700010A17Rik	75495	-3.6
7	1700010A17Rik	75495	-4.57
8	1700016D06Rik	76413	-1.05
9	1700025E21Rik	75647	-0.73
10	1700034I23Rik	73297	-1.08
11	1700034I23Rik	73297	-1.49
12	1810030N24Rik	66291	-1.28
13	2310003H01Rik	71885	-0.72
14	2310057D15Rik	67870	-0.53
15	2410004N11Rik	66989	-0.44
16	2410018C17Rik	74504	0.41

S.No	Genesymbol	GeneID	Z-score
41	Acad8	66948	-1.46
42	Acp2	11432	-1.74
43	Acpl2	235534	-1.38
44	Actr8	56249	-1.43
45	Acvr1b	11479	-1.26
46	Acvr1c	269275	-1.9
47	Acvr2a	11480	-0.65
48	Adam23	23792	-1.17
49	Adam32	353188	-0.45
50	Adamts8	30806	-0.82
51	Adipoq	11450	-0.95
52	Admr	11536	-2.01
53	Adnp	11538	-0.75
54	Adora2b	11541	-3.85
55	Adra1b	11548	-0.53
56	Adrb2	11555	-1.24

17	2410039E07Rik	68239	-1.17
18	2610028H24Rik	76964	-1.59
19	2810021J22Rik	69944	-0.68
20	2810401C16Rik	72168	-2.02
21	2810452K22Rik	67236	-0.73
22	3110001D03Rik	66928	-0.3
23	4833424O15Rik	75769	-1.14
24	4921523A10Rik	110332	-1.2
25	4921528H16Rik	74354	-2.67
26	4930429M06Rik	252876	-1.38
27	4930432E11Rik	243900	-4.23
28	4930481M05	331529	-0.27
29	4931428L18Rik	70988	-0.53
30	4933417A18Rik	66761	-0.68
31	5730403M16Rik	232853	-0.51
32	5730536A07Rik	68250	0
33	6030452D12Rik	330837	-0.38
34	6530403A03Rik	67797	-0.48
35	9030612M13Rik	208292	-0.55
36	9430023L20Rik	68118	-0.3
37	9430071P14Rik	320590	-0.43
38	A030007L22	328264	-1.18
39	A630052C17Rik	320757	-0.51
40	A930002I21Rik	109226	-3.17
57	AI591476	231986	-1.05
58	AK162044	211147	-1.51
59	Akt2	11652	0.41
60	Alpk2	225638	-1.55
61	Amica1	270152	-1.4
62	Ankk1	244859	-0.29
63	Ankrd22	52024	-0.29
64	Aof2	99982	-0.41
65	Arhgap23	58996	-0.98
66	Armcx1	78248	-1.49
67	Asb10	117590	-2.99
68	Asb5	76294	-0.6
69	Asb6	72323	-1.02
70	Asb8	78541	-2.17
71	Ash1l	192195	-1.49
72	Atf7	223922	-1.78
73	Atf7ip	54343	-0.99
74	Atm	11920	-1.85
75	Atp6v0e2	76252	-1.96
76	Atpbd1c	68080	-1.5
77	AU022252	230696	-0.98
78	Aurkc	20871	-1.13
79	Avpr2	12000	-1.33
80	AY702102	446211	0.06

81	B2m	12010	-1.01
82	B4galt1	14595	-1.44
83	Baz2a	116848	-0.47
84	BC021891	234878	0.83
85	BC043934	270185	-0.61
86	BC049816	232313	-0.76
87	BC063749	414801	-1.16
88	Bcdin3	231803	-2.59
89	Bhlhb2	20893	-0.36
90	Bin1	30948	-0.83
91	Blr1	12145	-3.7
92	Bmpr1b	12167	-0.5
93	Braf	109880	0
94	C130032F08Rik	243372	-0.8
95	C330002I19Rik	77480	-0.16
96	C330018K18Rik	235533	-1.98
97	C920005C14Rik	338368	-0.44
98	Camk1g	215303	-1.24
99	Camk2g	12325	-1.68
100	Camkv	235604	-2.63
101	Capns1	12336	-0.76
102	Cask	12361	-3.38
103	Ccl20	20297	-0.51
121	Cova1	209224	0.27
122	Creb3l1	26427	-2.34
123	Ctf1	13019	-0.92
124	Cutl2	13048	-0.76
125	Cxcl7	57349	-0.4
126	Cyp17a1	13074	-2.2
127	Cyp2b19	13090	-0.59
128	Cyp2c70	226105	-0.05
129	Dbpht1	20749	-0.66
130	Dcamkl3	245038	-1.9
131	Ddx3x	13205	-3.96
132	Diap2	54004	-1.89
133	Dlgh4	13385	-1.92
134	Dmpk	13400	-1.44
135	Dmrt1	50796	-1.99
136	Dnase1l1	69537	-0.65
137	Dtx4	207521	-0.78
138	Dtymk	21915	-3.68
139	Dusp10	63953	-0.66
140	E130304F04Rik	245269	-2.9
141	Ecd	70601	-0.45
142	Ecgf1	72962	-2.41
143	Edem1	192193	-1.3

104	Ccna2	12428	-1.55
105	Ccpg1	72278	-1.11
106	Ccr1	12768	-0.25
107	Ccr3	12771	-0.73
108	Ccr5	12774	-0.29
109	Ccrl2	54199	-1.04
110	Cd1d1	12479	-0.83
111	Cd40	21939	-0.35
112	Cd84	12523	-0.19
113	Chd9	109151	-0.32
114	Chek1	12649	-1.31
115	Clca3	23844	-0.67
116	Clca5	229933	-2.11
117	Clcnkb	56365	-1.04
118	Clec9a	232414	-1.63
119	Clic6	209195	-0.65
120	Col7a1	12836	-2.47

144	Edg1	13609	-0.96
145	Edg3	13610	-2.58
146	Efhc1	71877	-1.5
147	Ei24	13663	-0.27
148	Elk4	13714	-0.66
149	Epas1	13819	-0.24
150	Ercc6	319955	-1.23
151	Ets1	23871	-0.61
152	Fbp1	14121	-2.16
153	Fer1l4	74562	-1.21
154	Ferd3l	114712	-0.43
155	Fgf17	14171	-0.49
156	Foxj3	230700	-4.46
157	Foxk1	17425	-0.27
158	Fxyd5	18301	-1.37
159	Fxyd6	59095	-2.06
160	Fxyd7	57780	-1.3

161	Gak	231580	-2.29
162	Galk2	69976	-1.11
163	Gdf11	14561	-1.79
164	Gfer	11692	-0.36
165	Gfi1b	14582	-1.54
166	Ghsr	208188	-1.49
167	Gm1078	381835	-2.26
168	Gm1389	384283	-1.82
169	Gm1553	432480	-1.65
170	Gm1757	385727	-1.41
171	Gm1860	276756	-1.76
172	Gm1872	380676	-0.81
173	Gm555	215415	-1.17
174	Gpr156	239845	-2.15
175	Gpr18	110168	-2.79
176	Gpr21	338346	-1.11
177	Gpr37	14763	-2.79
178	Gpr37l1	171469	-0.48
179	Gpr82	319200	-1.82
180	Gpr84	80910	-0.35
181	Gpr98	110789	-1.28
182	Gtf2f1	98053	-2.59
183	Gtf2f2	68705	-1.29
184	Gucy1b2	239134	-0.67
185	Hcrtr2	387285	-2.41
186	Hint1	15254	-1.05
187	Hmgb2l1	70823	-0.54
188	Hrh1	15465	-0.91
189	Hsp110	15505	-0.3
190	Htr5a	15563	-0.38

201	Irf4	16364	-1.31
202	Itga4	16401	0.18
203	Itga6	16403	-1.35
204	Itga8	241226	-0.23
205	Jmjd4	194952	-0.45
206	Kcne2	246133	-1.58
207	Kcnf1	382571	-1.64
208	Kcnh5	238271	-2.24
209	Kcnip2	80906	-3.28
210	Kcnj10	16513	-0.96
211	Kcnj16	16517	-3.89
212	Kcnj2	16518	-1.99
213	Kcnj8	16523	-2.18
214	Kcnj9	16524	-1.41
215	Kcnrg	328424	-0.52
216	Kcnv2	240595	-3.41
217	Klf17	75753	-0.42
218	Klra18	93970	-1.86
219	Klra20	93967	-2.23
220	Klra22	93969	-1.44
221	Klra5	16636	-3.23
222	Klrd1	16643	-0.41
223	Klrg1	50928	-1.04
224	Ksr1	16706	-0.03
225	Ksr2	333050	-0.49
226	Lgals2	107753	-0.89
227	Lgi4	243914	-2.44
228	Limk1	16885	-0.27
229	Limk2	16886	-0.8
230	Lims1	110829	-1.84

191	Icam2	15896	-1.69
192	Icosl	50723	-1.84
193	Ighmbp2	20589	-0.59
194	Il17ra	16172	-2.11
195	Il1a	16175	-0.86
196	Il28ra	242700	-1.37
197	Ipp	16351	-0.64
198	Iqsec1	232227	-0.65
199	Irak3	73914	0.84
200	Irf3	54131	-0.96

231	LOC216394	216394	-0.91
232	LOC224763	224763	-0.66
233	LOC239502	239502	-0.67
234	LOC242517	242517	-0.65
235	LOC382133	382133	-2.24
236	LOC383956	383956	-1.18
237	LOC385049	385049	-1.84
238	LOC432436	432436	-1.2
239	LOC433158	433158	-0.51
240	LOC433743	433743	-0.37

241	LOC434960	434960	-2.02
242	LOC436217	436217	-1.44
243	Lrrk2	66725	-1.26
244	Mad2l1	56150	-2.67
245	Magmas	66449	-1.28
246	Man1a	17155	-0.5
247	Man1c1	230815	-2.37
248	Mansc1	67729	-1.42
249	Map3k10	269881	-0.28
250	Map3k12	26404	-0.94
251	Map3k7	26409	-0.3
252	Map3k9	338372	0.26
253	Mapkapk3	102626	-1.56
254	Mapkapk5	17165	-2.07
255	Mark1	226778	-2.63
256	Mark4	232944	-0.99
257	Mgat2	217664	-0.06
258	Mgat4b	103534	0.48
259	Mgll	23945	-0.96
260	Mkx	210719	-1.38
261	Mlxipl	58805	-0.58
262	Mmachc	67096	-0.86
263	Mmp16	17389	-0.79
264	Mogat2	233549	-0.52
265	Morn2	378462	-0.8
266	Mpp2	50997	-1.89
267	Mpp4	227157	-2.4
268	Mrgpra4	235854	-1.88
269	Myog	17928	-1.42
270	Ndufa12	66414	-1.34
271	Nek5	330721	-0.68
272	Nek9	217718	0.01
273	Neurod2	18013	-0.78
274	Ngrn	83485	-0.7
275	Npy6r	18169	-1.67
276	Ntn1	18208	-0.78
277	Nuak2	74137	-1.51

281	Olfr151	406176	-1.66
282	Olfr554	258322	-0.9
283	Olfr821	258772	-0.56
284	Orc5l	26429	0.47
285	Oxtr	18430	-2.21
286	Pak1	18479	-1.46
287	Paqr3	231474	-3
288	Parp16	214424	-1.19
289	Pax3	18505	-0.46
290	Pdik1l	230809	-1.26
291	Pdlim1	54132	-1.16
292	Pebp1	23980	-3.67
293	Perq1	57330	-1.84
294	Pex11c	69129	-0.08
295	Pex3	56535	-0.41
296	Pfkfb2	18640	-2.71
297	Pfn2	18645	-1.75
298	Phkg2	68961	-1.63
299	Phtf2	68770	-1.09
300	Pi4k2b	67073	-2.6
301	Pias1	56469	-2.28
302	Pigb	55981	-0.15
303	Pigq	14755	0.34
304	Pira1	18722	-0.31
305	Pkn3	263803	0.62
306	Pla2g4f	271844	-2.08
307	Plag1	56711	0.13
308	Plcl2	224860	-0.29
309	Plekhj1	78670	-2.29
310	Plk1	18817	-1.01
311	Pou3f1	18991	-1.54
312	Ppan	235036	-0.64
313	Ppap2c	50784	-0.84
314	Ppp2r5a	226849	-1.06
315	Prkca	18750	-1.6
316	Prpsap1	67763	-1.16
317	Psmb2	26445	-0.71

278	Olfm2	244723	-0.06
279	Olfr1444	258697	-0.35
280	Olfr1477	258691	-1.74

318	Psmd12	66997	0.26
319	Psmd13	23997	-0.44
320	Psmd2	21762	-1.31

321	Psmd3	22123	-2.91
322	Psmd5	66998	-1.89
323	Psme4	103554	-1.86
324	Ptges	64292	-2.1
325	Ptpmt1	66461	-0.68
326	R3hdm1	226412	-0.9
327	Ranbp17	66011	-0.99
328	Rbm13	67920	-2.41
329	Rbm35a	207920	-0.13
330	Resp18	19711	-0.41
331	Rfx4	71137	-1.08
332	Rg9mtd1	52575	-0.8
333	Rhog	56212	-1.16
334	Rhox11	194738	-0.29
335	Ribc1	66611	-0.84
336	Ripk2	192656	-3.28
337	Ripk4	72388	-0.97
338	Rnut1	66069	-0.18
339	Rpia	19895	-0.6
340	Rps6ka3	110651	-3.4
341	Rps6ka5	73086	-3.45
342	Rps6kb1	72508	-3.02
343	Rrbp1	81910	0.48
344	Rspo1	192199	-0.82
345	Rtel1	269400	-2.24
346	Rxfp4	242093	-0.36
347	Satb2	212712	-0.61
348	Scarf1	380713	-1.19
349	Sec11l1	56529	-0.23
350	Serpina3g	20715	-0.87
351	Sip1	66603	-0.9
352	Slc13a1	55961	-1.2
353	Slc13a3	114644	-1.4
354	Slc16a13	69309	-0.33
355	Slc22a12	20521	-0.58
356	Slc22a7	108114	-0.78
357	Slc22a8	19879	-0.38
358	Slc23a2	54338	-0.47
359	Slc25a1	13358	-0.9
360	Slc30a4	22785	-1.96

361	Slc34a3	142681	-1.85
362	Slc39a6	106957	-0.85
363	Slc39a7	14977	-0.55
364	Slc4a3	20536	-0.45
365	Slc6a4	15567	-0.36
366	Slc7a2	11988	-1.87
367	Slco5a1	240726	-0.61
368	Slfn5	327978	-2.01
369	Slitrk1	76965	-0.81
370	Smarca3	20585	-0.59
371	Smarca4	20586	-0.37
372	Snai3	30927	-0.29
373	Snf1lk2	235344	-1.56
374	Snrk	20623	-4.71
375	Soat1	20652	-1.94
376	Sorl1	20660	-0.65
377	Sp6	83395	-0.58
378	Spata16	70862	-2.48
379	Spcs1	69019	-0.02
380	Sphk1	20698	-0.86
381	Spred1	114715	-0.41
382	Sprn	212518	-1.29
383	Sprr2j	20764	-1.15
384	Spz1	79401	-1.92
385	Srcrb4d	109267	-1.7
386	Stat4	20849	-0.89
387	Stk17b	98267	-4.71
388	Supt4h2	20923	-0.77
389	Surf5	20933	-1.06
390	Svop	68666	-0.42
391	Synpo2	118449	-2.52
392	Syt3	20981	0.11
393	T	20997	-0.67
394	Taar1	111174	-0.76
395	Taar8a	215859	0.05
396	Taf1c	21341	-1.55
397	Tbx1	21380	-1.34
398	Tbx15	21384	-0.53
399	Tbx22	245572	-3.16
400	Tceal5	331532	-1.9

401	Tceb3	27224	-0.55
402	Tesk1	21754	-0.93
403	Tesk2	230661	0.08

441	UNK	380953	-0.77
442	UNK	433358	-1.52
443	UNK	327891	-0.76

404	Tex14	83560	-1.25
405	Tex15	104271	-0.86
406	Tgfb1	21803	-0.38
407	Tgfbr1	21812	-1.97
408	Timp4	110595	-3.35
409	Tlr7	170743	-0.42
410	Tlr8	170744	-0.92
411	Tlr9	81897	-2.69
412	Tm2d1	94043	-0.53
413	Tmem130	243339	-0.43
414	Tmem132a	98170	-0.39
415	Tmem16k	102566	-0.37
416	Tnfsf15	326623	-2.37
417	Tor1b	30934	-1.3
418	Traf2	22030	-0.77
419	Trem1	58217	-2.98
420	Trib2	217410	-2.9
421	Trpc4	22066	-1.68
422	Trps1	83925	-0.37
423	Tsga13	116732	-1.1
424	Tssk3	58864	-2.56
425	Tssk6	83984	-2.67
426	Ttl	69737	-0.56
427	Ufc1	66155	-0.52
428	Unc13c	208898	-0.98
429	UNK	433325	-1.7
430	UNK	382814	-1.05
431	UNK	233024	-0.92
432	UNK	216178	-0.96
433	UNK	381082	-2.35
434	UNK	386422	-2.85
435	UNK	383458	-1.87
436	UNK	383535	-2.74
437	UNK	629990	-1.44
438	UNK	216790	-0.24
439	UNK	383507	-3.32
440	UNK	435233	-1.34
444	UNK	433669	-1.62
445	UNK	432728	-1.36
446	Upk3b	100647	-0.17
447	Usp39	28035	-0.59
448	V1re13	252910	-0.41
449	V1rg11	171267	-1.53
450	V1rh11	171270	-0.46
451	V1rh9	171252	-2.81
452	Vezt	215008	-0.35
453	Vipr2	22355	-2.23
454	Waspip	215280	-1.52
455	Wdr26	226757	0.35
456	Wdr55	67936	0.29
457	Wipi2	74781	-0.54
458	Wrb	71446	0.62
459	Xkr8	381560	-1.03
460	Zbtb20	56490	-0.51
461	Zc3h6	78751	-0.92
462	Zcchc10	67966	-1.5
463	Zcd1	52637	-0.38
464	Zfp191	59057	-2.85
465	Zfp467	68910	-2.52
466	Zfp533	241494	-1.84
467	Zfp647	239546	-2.99
468	Zfp672	319475	-0.57
469	Zfp96	22758	-0.75
470	Zfp97	22759	-1.67
471	Zfy1	22767	-1.57
472	Zswim4	212168	-1.14

Extended Table 3

S.No	Genesymbol	GeneID	Z-score
1	42070	57438	0.23
2	0610040J01Rik	76261	-0.08
3	0710001B24Rik	67446	-0.19
4	1110007F12Rik	68487	0.32
5	1110034O07Rik	68744	-1.09
6	1110049F12Rik		1.82
7	1600021P15Rik	239796	1.59
8	1700012B09Rik	69325	2.25
9	1700017G21Rik	71847	0.12
10	1700029M20Rik	73937	1.48
11	1700040L02Rik	73287	1.3
12	1700111I05Rik	76629	0.19
13	1810014F10Rik	69064	0.66
14	1810015A11Rik	69101	-0.1
15	1810031K17Rik	69171	-0.17
16	2010011I20Rik	67017	1.65
17	2010208K18Rik	72096	-0.36
18	2310002B06Rik	53951	0.34
19	2310005E10Rik	67861	1.5
20	2310061C15Rik	66531	0.48
21	2410005H09Rik	232969	1.39
22	2410129H14Rik	76789	0.77
23	2610019F03Rik	72148	1.22
24	2810437L13Rik	68033	6.64
25	3110001I22Rik	66598	0.51
26	3110003A22Rik	68053	2.66
27	4833427G06Rik	235345	1.13
28	4921509C19Rik	381393	1.78
29	4921511I16Rik	70925	2.85
30	4930432E11Rik	243900	0.26
31	4930506M07Rik	71653	0.66
32	4930539E08Rik	207819	0.6
33	4930549O06	233164	0.94
34	4930595M18Rik	245492	0.66
35	4931406C07Rik	70984	0.31
36	4933411G11Rik	330228	1.06
37	5330437I02Rik	319888	0.05
38	5730509K17Rik	231214	0.15
39	5930416I19Rik	72440	2.7
40	6030446N20Rik	338363	0.22
41	6330527O06Rik	76161	1.86
42	6430601A21Rik	228491	-0.55
43	6720487G11Rik	319231	1.44
44	8430410K20Rik	78100	1.11
45	9130014G24Rik	215772	4.67
46	9130401M01Rik	75758	0.89
47	9230112K01Rik	433181	0.42
48	9430076C15Rik	320189	0.28
49	9530053A07Rik	319482	0.43
50	A530088I07Rik	212167	5.84
51	A630008I04	329541	1.44
52	A830020B06Rik	271711	0.34
53	A830058L05Rik	210503	3.03
54	A930034L06Rik	319317	0.12
55	A930037G23Rik	320678	0.65
56	Aacs	78894	NA
57	Abhd5	67469	1.09
58	Abp1	76507	1.49
59	Abt1	30946	2.7
60	Accn1	11418	NA
61	Acot3	171281	0.63
62	Acp5	11433	0.48
63	Acrv1	11451	0.33
64	Adamts14	237360	0.21
65	Adamts7	108153	0.24
66	Adarb1	110532	0.31
67	Adck1	72113	-0.14
68	Adck5	268822	2.69
69	Adrb3	11556	2.31
70	Adrm1	56436	0.94
71	Aff1	17355	1.19
72	Agt	11606	0.18
73	Ahcy	269378	0.92
74	AI451617	209387	4.66
75	AI662250	106639	0.4
76	AK122525	331623	0.12
77	Akp2	11647	0.5
78	Akr1b8	14187	2.13
79	Akr1c13	27384	0.95
80	Akr1c18	105349	1.23
81	Akr1e1	56043	0.71
82	Aldh7a1	110695	0.24
83	Angpt1	11600	1.73
121	Bid	12122	0.29
122	Blvrb	233016	0.39
123	Bmx	12169	-0.71

84	Ankrd13c	433667	3.04
85	Ankrd52	237615	0.38
86	Apbb1	11785	0.81
87	Apc	11789	-2.2
88	Aplp2	11804	0.37
89	Arhgap15	76117	2.52
90	Arhgap22	239027	0.62
91	Armcx5	494468	1.07
92	Ash2l	23808	0.67
93	Ass1	11898	0.16
94	Asz1	74068	0.34
95	Atad4	217138	2.1
96	Atf2	11909	23.48
97	Atf5	107503	0.16
98	Atf5	107503	2.65
99	Atp5g2	67942	0.49
100	Atp5g3	228033	1.48
101	Atp5h	71679	3.89
102	Atp8a1	11980	0.55
103	Attp	54122	0.92
104	B130052G07Rik	226841	0.82
105	B230317F23Rik	320383	2.21
106	B3gnt2	53625	0.69
107	Bat4	81845	0.31
108	BC017643	217370	0.26
109	BC022623	224093	2.27
110	BC027057	212937	0.67
111	BC027344	233057	0.56
112	BC033915	70661	1.12
113	BC038822	239647	0.66
114	BC061494	381832	0.57
115	BC107364	329716	-0.15
116	Bcl6b	12029	1.02
117	Bclaf1	72567	1.41
118	Bcmo1	63857	1.67
119	Bet1	12068	0.68
120	Bet1l	54399	0.45

124	Bnip3	12176	1.07
125	Bnip3l	12177	1.33
126	Brd2	14312	1.48
127	Bxdc5	70285	0.74
128	C030004A17Rik	109229	0.21
129	C030048B08Rik	269623	1.99
130	C130060K24Rik	243407	2.39
131	C1d	57316	17.75
132	C1galt1	94192	1.03
133	C1qa	12259	6
134	C1qbp	12261	7.05
135	C630041L24Rik	78709	2.85
136	C79127	232941	2.03
137	Cacna1a	12286	5.09
138	Cacng4	54377	0.22
139	Cacng6	54378	2.26
140	Cant1	76025	0.74
141	Capza2	12343	1.37
142	Car13	71934	0.95
143	Casp14	12365	4.42
144	Casp3	12367	1.1
145	Casp6	12368	0.72
146	Casr	12374	7.47
147	Cbl	12402	1.08
148	Ccl12	20293	7.16
149	Ccnb2	12442	0.1
150	Ccnc	51813	2.69
151	Ccne1	12447	0.48
152	Ccne2	12448	2.03
153	Ccnf	12449	1.1
154	Ccng1	12450	2.13
155	Ccrl1	252837	1.73
156	Cd302	66205	0.08
157	Cd52	23833	0.92
158	Cd8a	12525	1.79
159	Cd96	84544	0.41
160	Cdadc1	71891	0.19

161	Cdc42	12540	4.61
162	Cdk2ap1	13445	0.27
163	Ceacam19	319930	4.24
164	Ceacam19	319930	2.67
165	Cep55	74107	1.24
166	Cerk	223753	3.33
167	Cfl1	12631	0.95
168	Ches1	71375	0.67
169	Chkb	12651	0.4
170	Chmp5	76959	0.27

201	Cul4b	72584	3.6
202	Cxcr3	12766	5.98
203	Cyb5	109672	1.11
204	Cyb5r4	266690	1.15
205	Cyp27a1	104086	2.14
206	Cyp3a44	337924	0.61
207	Cyp7b1	13123	0.45
208	D030051N19Rik	228361	0.79
209	D13Wsu50e	28077	9.68
210	D16Ertd472e	67102	4.5

171	Chrm3	12671	2.89
172	Chst11	58250	2.89
173	Ckm	12715	10.39
174	Clca4	229927	2.35
175	Clcc1	229725	4.14
176	Clcn2	12724	1.17
177	Clcn3	12725	2.52
178	Clec4b1	69810	0.27
179	Clns1a	12729	1.6
180	Clpb	20480	2.78
181	Clstn3	232370	0.27
182	Col17a1	12821	0.82
183	Col4a3bp	68018	0.4
184	Coq4	227683	11.7
185	Cox5a	12858	1.42
186	Cox5b	12859	0.46
187	Cpa1	109697	0.24
188	Cpne8	66871	1.01
189	Cpox	12892	8.27
190	Creb3	12913	0.9
191	Creb3l4	78284	0.92
192	Crp	12944	3.66
193	Crsp3	70208	10.7
194	Csnk1e	27373	0.65
195	Csnk2b	13001	3.16
196	Cstb	13014	2.04
197	Ctnnb1	12387	5.16
198	Ctrc	76701	0.36
199	Cul1	26965	2.7
200	Cul4a	99375	2.67

211	D4Wsu114e	28010	1.29
212	D5Ertd585e	71782	2.59
213	D7Wsu128e	28018	2.25
214	D830039M14Rik	320949	3.68
215	D930010J01Rik	107227	0.56
216	Dach1	13134	0.74
217	Dapk2	13143	5.97
218	Dbp	13170	0.4
219	Dcc	13176	0.8
220	Dclre1b	140917	5.15
221	Dclre1c	227525	0.5
222	Dcxr	67880	0.24
223	Ddi2	68817	2.06
224	Ddit3	13198	1.77
225	Defb4	56519	0.43
226	Defb4	56519	0.34
227	Derl1	67819	0.57
228	Dhdds	67422	2.59
229	Dhfr	13361	0.97
230	Dhrs1	52585	0.41
231	Dhrs4	28200	0.23
232	Diap3	56419	1.26
233	Dmtf1	23857	1.68
234	Dpf3	70127	0.67
235	Dph1	116905	4.61
236	Dppa4	73693	1.1
237	Dppa5	434423	0.39
238	Drap1	66556	0.48
239	Duoxa1	213696	1.48
240	Dus3l	224907	1.71

241	Dusp12	80915	2.17
242	Dusp22	105352	0.54
243	E2f1	13555	0.36
244	E2f4	104394	0.59
245	E2f6	50496	0.53
246	Ear3	53876	0.71
247	Ebna1bp2	69072	3.03
248	Edaradd	171211	3.6
249	Edg5	14739	0.39
250	Edn1	13614	2.3
251	Efcab5	319634	2.66
252	Efna4	13639	3.94
253	Egln1	112405	0.28
254	Ehf	13661	1.95
255	Eif4e	13684	1.3
256	Ela2a	13706	0.84
257	Elf1	13709	1.32

281	Foxf2	14238	1.27
282	Foxg1	15228	1.91
283	Foxi1	14233	0.75
284	Foxj2	60611	15.11
285	Foxl2	26927	0.72
286	Foxn2	14236	0.53
287	Foxo3a	56484	2.07
288	Foxp4	74123	3.6
289	Foxq1	15220	0.51
290	Frmd3	242506	0.4
291	Fstl3	83554	3.11
292	Fxyd4	108017	0.2
293	Fzd1	14362	1.06
294	Fzd4	14366	1.72
295	G6pc2	14378	0.28
296	Gad2	14417	1.21
297	Garnl1	56784	0.37

258	Elovl2	54326	1.27
259	En2	13799	0.23
260	Endogl1	208194	0.79
261	Eomes	13813	0.33
262	Ep400	75560	1.4
263	Epha7	13841	0.64
264	Eras	353283	2.08
265	Etv2	14008	0.23
266	Evc2	68525	1.7
267	Exoc2	66482	-0.12
268	F8a	14070	0.95
269	Fancl	67030	0.4
270	Fastk	66587	-0.16
271	Fbxl16	214931	0.27
272	Fbxl7	448987	0.46
273	Fbxo4	106052	0.86
274	Fbxw15	382105	2.34
275	Fem1c	240263	0.46
276	Fgr	14191	0.34
277	Fmo3	14262	1.19
278	Foxa2	15376	0.63
279	Foxb2	14240	0.62
280	Foxc1	17300	1.52

298	Gata1	14460	2.71
299	Gata6	14465	1.75
300	Gcm1	14531	0.88
301	Gdpd4	233537	3.22
302	Gja4	14612	2.49
303	Gja5	14613	2.73
304	Gm1079	381836	27.19
305	Gm131	229697	1.18
306	Gm1805	241950	-0.08
307	Gm234	215946	0.08
308	Gm514	208080	1.03
309	Gm962	381201	2.55
310	Gmeb1	56809	0.85
311	Gnb2	14693	1.85
312	Golph4	73124	2.04
313	Gorasp2	70231	0.58
314	Gpr68	238377	3.42
315	Gpr89	67549	16.85
316	Gpx2	14776	1.24
317	Gpx4	625249	3.21
318	Grhl2	252973	0.42
319	Gss	14854	0.58
320	Gtf2a1	83602	0.16

321	Gtf2e2	68153	0.71
322	Gtf2ird1	57080	2.1
323	Gtf3c4	269252	2
324	Gucy1a3	60596	1.84
325	Gys2	232493	0.47
326	Hbp1	73389	0.9
327	Hcfc1	15161	0.83
328	Hcfc1r1	353502	0.04
329	Hcfc2	67933	0.43
330	Hdac4	208727	0.68
331	Hes3	15207	0.89
332	Hes5	15208	0.33
333	Hira	15260	9.59
334	Hivep1	110521	2.6
335	Hk3	212032	1.03
336	Hkr2	232878	1.08
337	Hmmr	15366	1.71
338	Hnf4g	30942	0.41
339	Hoxc6	15425	21.62
340	Hsd17b9	27400	0.08
341	Htr5b	15564	0.72
342	Id1	15901	0.34
343	Ier3ip1	66191	1.61
344	Ifi202b	26388	0.62

361	Kcne1	16509	2.08
362	Kcnh2	16511	1.7
363	Kcnip1	70357	0.3
364	Kcnj12	16515	0.43
365	Kcnj5	16521	1.52
366	Kcnk5	16529	0.36
367	Kcnq5	226922	0.83
368	Kcns3	238076	2.3
369	Kctd1	106931	3.17
370	Kctd15	233107	2.04
371	Kirrel1	170643	1.39
372	Klf17	75753	1.26
373	Klf2	16598	1.51
374	Klhl17	231003	1.25
375	Klhl23	277396	0.85
376	Kng1	16644	8.53
377	Kntc2	67052	0.65
378	Krtap16-3	170653	2.45
379	Ktn1	16709	2.04
380	Lancl3	236285	1.13
381	Lass2	76893	1.15
382	Lass6	241447	1.15
383	Lck	16818	-0.44
384	Lcn10	332578	2.11

345	Ifitm1	68713	3.01
346	Ift172	67661	0.16
347	Igf1r	16001	0.57
348	Il12b	16160	2.32
349	Il19	329244	2.13
350	Iqcg	69707	1.15
351	Irf5	27056	2.06
352	Isl2	104360	0.21
353	Isyna1	71780	0.45
354	Itga9	104099	4.55
355	Itih4	16427	0.52
356	Itsn1	16443	2.75
357	Jak3	16453	0.59
358	Kcna10	242151	0.31
359	Kcnab1	16497	0.5
360	Kcnc1	16502	0.46

385	Lcp1	18826	0.7
386	Ldhal6b	106557	1.77
387	Ldoc1	434784	1.19
388	Ldoc1l	223732	0.14
389	Lefty2	320202	3.66
390	Llgl2	217325	0.42
391	Lmo4	16911	1.34
392	LOC208256	208256	0.5
393	LOC224508	224508	0.89
394	LOC227506	227506	1.29
395	LOC232077	232077	0.59
396	LOC238678	238678	0.52
397	LOC245128	245128	1.67
398	LOC245576	245576	5.2
399	LOC268650	268650	0.82
400	LOC280487	280487	0.26

401	LOC384144	384144	0.27
402	LOC432676	432676	0.2
403	LOC432823	432823	0.37
404	LOC433844	433844	0.27
405	LOC434849	434849	0.39
406	LOC436523	436523	2.2
407	Lrfn3	233067	0.18
408	Lrrc40	67144	1.92
409	Lrrc50	68270	0.56
410	Lrrc59	98238	1.91
411	Lrtm1	319476	0.88
412	Lss	16987	0.2
413	Lxn	17035	0.36
414	Lyl1	17095	0.63
415	Lyn	17096	0.05
416	Malt1	240354	0.44
417	Manba	110173	0.55
418	Map2k1	26395	1.27
419	Map2k2	26396	2.52
420	Map3k1	26401	-0.38
421	Map3k13	71751	0.55
422	Map4k4	26921	1.98
423	Marco	17167	0.46
424	Mark3	17169	0.21
425	Mccc2	78038	2.06
426	Mchr1	207911	0.65
427	Mea1	17256	2.14
428	Mertk	17289	0.81
429	Mfsd2	76574	0.61
430	Mid1	17318	0.43
431	Mizf	102423	1.63

441	Msrb3	320183	0.41
442	Mthfd1	108156	1.2
443	Mtmr1	53332	1.03
444	Mx1	17857	0.65
445	Mxd1	17119	0.53
446	Myh4	17884	1.77
447	Myh6	17888	0.92
448	Myh9	17886	0.28
449	Mylip	218203	0.74
450	Mylk	107589	-0.21
451	Myocd	214384	0.45
452	Myod1	17927	1.04
453	Myt1	17932	3.76
454	Mzf1	109889	0.47
455	Naaladl1	381204	0.68
456	Ndor1	78797	0.07
457	Nebl	74103	0.9
458	Neurod1	18012	0.61
459	Neurod4	11923	0.42
460	Nfix	18032	0.84
461	Nfyc	18046	1.57
462	Nkx2-2	18088	0.26
463	Nme2	18103	-0.42
464	Nmur2	216749	1.05
465	Nol3	78688	1.18
466	Nox4	50490	1.34
467	Nphp4	260305	-0.07
468	Npy5r	18168	4.49
469	Nr0b2	23957	0.34
470	Nr1h5	381463	2.02
471	Nr2c2	22026	0.51

432	Mkl1	223701	0.86
433	Mkrn2	67027	0.63
434	Mllt6	246198	0.8
435	Mnat1	17420	0.47
436	Mpped1	223726	5.96
437	Mras	17532	0.13
438	Mrpl32	75398	0.78
439	Msh2	17685	1.01
440	Msra	110265	0.43

472	Nr6a1	14536	0.06
473	Nrbp2	223649	0.03
474	Nrip2	60345	0.58
475	Nrl	18185	1.17
476	Nt5c2	76952	0.44
477	Ntng1	80883	2.01
478	Ntrk3	18213	2.56
479	Nudt1	17766	0.97
480	Numa1	101706	2.9

481	Nupr1	56312	0.77
482	Nutf2	68051	0.3
483	Oas1g	23960	1.19
484	Obfc1	108689	0.44
485	Odf2l	52184	0.92
486	Olfr110	258325	0.45
487	Olfr1110		5.98
488	Olfr114	258284	0.84
489	Olfr1166	258644	0.63
490	Olfr118	404308	2.46
491	Olfr1188	258921	0.47
492	Olfr1206	258896	0.83
493	Olfr1299	258886	4.02
494	Olfr1469	258690	1.59
495	Olfr159	29849	0.47
496	Olfr160	80706	0.62
497	Olfr177		1.51
498	Olfr19	18316	0.73
499	Olfr228	258400	1.31
500	Olfr284		12.66
501	Olfr313	258529	1.1
502	Olfr516	258720	0.71
503	Olfr550	259108	0.36
504	Olfr611	258722	0.54
505	Olfr683	259047	1.34
506	Olfr705	259034	0.65
507	Olfr866	258551	0.88
508	Olfr872	258553	3.11
509	Olfr905	258800	0.46
510	Olfr910		2.43
511	Olfr912	258806	1.33
512	Olfr914	258782	0.24
513	Olfr92	258448	1.39
514	Olfr921	258778	1.08
515	Olfr924	404322	2.73
516	Olfr993	258427	1.35
517	Oprd1	18386	1.8
518	Ormdl3	66612	-0.02

521	Ott	18422	0.63
522	Oxa1l	69089	0.37
523	Oxnad1	218885	0.05
524	Oxsm	71147	-0.23
525	P2ry4	57385	0.44
526	P42pop	232934	3.71
527	Pank1	75735	0.48
528	Pax5	18507	0.92
529	Pax6	18508	0.61
530	Pcdhgb2	93700	1.29
531	Pcsk9	100102	0.57
532	Pcyox1	66881	4.97
533	Pdgfb	18591	0.76
534	Pdhx	27402	2.18
535	Pecr	111175	0.38
536	Pet2	18630	2.17
537	Pfkfb1	18639	0.68
538	Pfkfb4	270198	0.99
539	Phf6	70998	0.57
540	Pi15	94227	1.15
541	Pi16	74116	1.53
542	Pias2	17344	0.56
543	Pik3c2a	18704	0.14
544	Pik3c2b	240752	0.72
545	Pik3cg	30955	3.06
546	Pik4cb	107650	4.1
547	Pip5k2b	108083	1.94
548	Pip5k3	18711	0.32
549	Pja2	224938	1
550	Pklr	18770	-0.34
551	Pla2r1	18779	1.13
552	Plcb3	18797	0.74
553	Plod1	18822	1.72
554	Plxnb2	140570	2.64
555	Pmaip1	58801	0.15
556	Pnpla8	67452	9.99
557	Pou3f4	18994	2.9
558	Pou4f2	18997	0.2

519	Ostf1	20409	0.64	559	Pou4f3	18998	0.18
520	Otc	18416	0.9	560	Pou6f1	19009	1.28

561	Ppm1j	71887	1.09	601	Rnf113a2	66381	0.17
562	Ppm1m	67905	2.62	602	Rnf130	59044	1.65
563	Ppp1cc	19047	2.94	603	Rnf185	193670	4.33
564	Ppp1r12b	329251	1.46	604	Rogdi	66049	0.98
565	Ppp1r13b	21981	0.98	605	Rora	19883	2.55
566	Ppp1r16a	73062	0.36	606	Ros1	19886	-0.21
567	Ppp4r1	70351	0.89	607	Rph3a		1.47
568	Pptc7	320717	1.25	608	Rpl41	67945	0.75
569	Prdm16	70673	1.96	609	Rragc	54170	0.09
570	Prdx5	54683	2.3	610	Rtn4r	65079	1.01
571	Prkaa2	108079	-0.29	611	Rufy2	70432	0.04
572	Prkab1	19079	4.56	612	Rxra	20181	0.67
573	Prop1	19127	0.57	613	Sav1	64010	0.09
574	Prps1	19139	0.25	614	Sc5d	235293	2.1
575	Prss15	74142	0.67	615	Scap	235623	-0.13
576	Prss7	19146	1.77	616	Sdc2	15529	0.86
577	Psme2b-ps	19191	2.57	617	Sdha	66945	0.59
578	Ptk9l	23999	1.39	618	Senp6	215351	0.48
579	Ptpn13	19249	3.05	619	Serpina3k	20714	0.94
580	Ptpn4	19258	1.94	620	Serpina3n	20716	1.81
581	Pts	19286	2.09	621	Serpina5	268591	0.23
582	Pwp1	103136	2.62	622	Serpinb11	66957	5.53
583	Pxk	218699	0.28	623	Serpinb9c	20707	2.37
584	Pxt1	69307	0.28	624	Serping1	12258	0.69
585	Pycr1	209027	0.81	625	Serpini1	20713	4.37
586	Rab11fip5	52055	2.26	626	Sesn1	140742	0.27
587	Rad17	19356	0.83	627	Sesn2	230784	0.9
588	Rai14	75646	1.56	628	Sfrs3	20383	1.03
589	Rarsl	109093	0.16	629	Sfrs8	231769	1.86
590	Rbak	57782	3.39	630	Sgol2	68549	0.55
591	Rbbp6	19647	0.61	631	Sgpp1	81535	1.28
592	Reck	53614	2.14	632	Sin3a	20466	0.49
593	Ret	19713	-0.25	633	Sin3b	20467	0.78
594	Rfx3	19726	0.96	634	Slc10a2	20494	0.63
595	Rhoa	11848	3.29	635	Slc11a2	18174	3.89
596	Rhox2	75199	1.72	636	Slc12a1	20495	0.56
597	Rhox3	382209	1.4	637	Slc12a3	20497	0.71
598	Ric8	101489	0.46	638	Slc12a4	20498	1.73
599	Riok1	71340	0.88	639	Slc12a6	107723	0.55
600	Riok2	67045	1.71	640	Slc12a7	20499	2.03

641	Slc16a1	20501	0.87	681	Slfn1	20555	0.67
642	Slc16a14	71781	2.41	682	Slitrk4	245446	2.33
643	Slc16a4	229699	0.63	683	Slmap		2.13
644	Slc16a7	20503	0.46	684	Smarcc2	68094	1.94

645	Slc17a5	235504	1.12
646	Slc17a8	216227	0.29
647	Slc18a3	20508	0.81
648	Slc19a2	116914	0.21
649	Slc22a19	207151	0.69
650	Slc22a3	20519	2.5
651	Slc24a2	76376	0.51
652	Slc25a12	78830	0.92
653	Slc25a15	18408	4.15
654	Slc25a25	227731	1.48
655	Slc25a32	69906	0.85
656	Slc26a6	171429	0.24
657	Slc26a7	208890	0.24
658	Slc27a2	26458	3.21
659	Slc28a1	434203	2.88
660	Slc30a3	22784	0.85
661	Slc30a6	210148	7.41
662	Slc33a1	11416	0.44
663	Slc34a1	20505	2.51
664	Slc36a2	246049	1.71
665	Slc36a3	215332	6.57
666	Slc37a1	224674	0.39
667	Slc38a1	105727	0.2
668	Slc39a1	30791	0.35
669	Slc43a1	72401	4.99
670	Slc45a2	22293	2.19
671	Slc4a9	240215	1.17
672	Slc5a7	63993	1.86
673	Slc6a17	229706	0.18
674	Slc6a7	240332	1.99
675	Slc7a13	74087	0.89
676	Slc8a1	20541	2.11
677	Slc9a7	236727	3.48
678	Slco1a5	108096	1.31
679	Slco1c1	58807	0.35
680	Slco6c1	74441	0.54

685	Sox17	20671	0.33
686	Sox2	20674	1.72
687	Sox8	20681	0.89
688	Sp1	20683	2.51
689	Sp4	20688	1
690	Sp7	170574	0.62
691	Sp8	320145	0.21
692	Spag4	245865	1.04
693	Spcs2	66624	0.37
694	Spp1	20750	1.69
695	Sprr2h	20762	0.39
696	Srd5a1	78925	1.09
697	Srd5a2l2	243078	0.19
698	Sstr1	20605	4.09
699	Sstr3	20607	6.11
700	St3gal4	20443	3.31
701	St6gal2	240119	2.49
702	Stat3	20848	4.15
703	Stfa1	20861	0.92
704	Stk19	54402	0.82
705	Stk33	117229	1.79
706	Sumo1	22218	2.11
707	Sva	20939	-0.14
708	Syap1	67043	0.09
709	Syt15	319508	0.68
710	Tac4	93670	0.41
711	Tacc3	21335	2.16
712	Taf10	24075	0.3
713	Taf11	68776	0.11
714	Taf6	21343	0.19
715	Tap2	21355	3.95
716	Tas2r116	112408	-0.48
717	Tas2r129	387354	-0.28
718	Tatdn2	381801	1.04
719	Tbc1d8	54610	1.3
720	Tbk1	56480	0.3

721	Tbrg4	21379	1.4
722	Tbx20	57246	1.21
723	Tbx4	21387	8.48
724	Tbxa2r	21390	5.08
725	Tcerg1	56070	0.3
726	Tcf15	21407	0.34
727	Tcf19	106795	1.71
728	Tcf20	21411	0.33
729	Tcf7	21414	2.65
730	Tcfap2a	21418	1.38
731	Tcfcp2	21422	0.92

761	Tpcn1	252972	1.73
762	Tpm3	59069	1.59
763	Tpr	108989	6.11
764	Treh	58866	-0.5
765	Trhr	22045	2.54
766	Trim27	19720	0.5
767	Trim56	384309	1.5
768	Trim66	330627	0.61
769	Trim68	101700	0.19
770	Trim7	94089	0.59
771	Trip10	106628	0.79

732	Tcfec	21426	1.82
733	Tcp11	21463	1.1
734	Tdg	21665	0.73
735	Tdpoz2	399673	1.36
736	Tfb2m	15278	4.89
737	Tfg	21787	0.89
738	Thop1	50492	0.52
739	Tia1	21841	0.49
740	Tiam1	21844	0.69
741	Tinf2	28113	4.02
742	Tktl1	83553	2.12
743	Tlk1	228012	5.86
744	Tlr12	384059	2.33
745	Tm7sf4	75766	0.67
746	Tmc5	74424	1.86
747	Tmc6	217353	2.81
748	Tmeff2	56363	0.39
749	Tmem12	212070	-0.3
750	Tmem127	69470	0.81
751	Tmem25	71687	0.24
752	Tmem40	94346	1.95
753	Tmtc4	70551	0.72
754	Tnfaip3	21929	0.72
755	Tnfrsf1a	21937	2.33
756	Tnk2	51789	2.82
757	Tnni3k	435766	14.06
758	Top3a	21975	8.3
759	Tor2a	30933	1.86
760	Tox	252838	1.16

772	Trip12	14897	0.17
773	Trp53bp2	209456	1.3
774	Trp53rk	76367	0.04
775	Trpc7	26946	4.01
776	Tslp	53603	0.29
777	Txnrd2	26462	0.42
778	Tyki	22169	0.02
779	Ube1dc1	66663	0.92
780	Ube1l	74153	0.49
781	Ube2n	93765	0.12
782	Ube2v1	66589	0.48
783	Uble1a	56459	0.89
784	Ugt1a10	394430	0.97
785	Ulbp1	77777	0.59
786	Ulk1	22241	0.76
787	UNK	218171	0.75
788	UNK	385092	2.67
789	UNK	269282	3.02
790	UNK	381971	1.29
791	UNK	384046	2.72
792	UNK	435820	1.04
793	UNK	240711	1.09
794	UNK	244555	1.55
795	UNK	435230	1.71
796	UNK	435267	6.94
797	UNK	433336	0.85
798	UNK	19257	1.41
799	UNK	433453	0.64
800	UNK	634306	0.35

801	UNK	217503	0.27
802	UNK	432510	2.12
803	UNK	433139	1.49
804	UNK	434886	0.34
805	UNK	381751	1.6
806	UNK	383101	0.63
807	UNK	434190	1.19
808	UNK	236223	0.43
809	UNK	236223	2.57
810	UNK	433285	0.24
811	UNK	435722	0.48
812	UNK	436104	0.23
813	UNK	435406	0.62
814	UNK	436530	0.42
815	UNK	433641	0.26
816	UNK	433869	0.92
817	Upp2	76654	0.92
818	Uqcrb	67530	0.58

841	Zfp13	22654	1.54
842	Zfp189	230162	6.76
843	Zfp212	232784	0.84
844	Zfp235	56525	0.48
845	Zfp263	74120	0.8
846	Zfp27	22689	0.38
847	Zfp31	269585	0.5
848	Zfp313	81018	0.84
849	Zfp322a	218100	1.35
850	Zfp341	228807	0.75
851	Zfp354a	21408	0.95
852	Zfp36l2	12193	1.95
853	Zfp37	22696	1.42
854	Zfp39	22698	0.73
855	Zfp406	380993	0.34
856	Zfp449	78619	1.77
857	Zfp455	218311	1.71
858	Zfp60	22718	0.8

819	Usp37	319651	0.47
820	Usp49	224836	3.81
821	V1rc10	171183	3.19
822	V1rc16	171189	0.96
823	V1rc28	171201	0.93
824	V1rd7	81012	-0.44
825	V1rl1	171262	0.6
826	Wdhd1	218973	0.73
827	Wfikkn2	278507	0.88
828	Wt1	22431	0.45
829	Xab1	74254	0.76
830	Xcr1	23832	2.57
831	Xtrp3s1	102680	2.16
832	Ythdf3	229096	2.53
833	Zbp1	58203	0.37
834	Zbtb10	229055	4.37
835	Zbtb3	75291	1.83
836	Zbtb39	320080	2.75
837	Zbtb8	215627	5.33
838	Zdhhc24	70605	0.31
839	Zfp1	22640	0.58
840	Zfp111	56707	1.32
859	Zfp61	22719	1.37
860	Zfp94	22756	1.27
861	Zfpn1a2	22779	1.59
862	Zik1	22775	0.24
863	Znrf2	387524	0.67
864	Zscan2	22691	1.7

Extended Table 4

S.No	Genesymbol	GeneID	Z-score
1	42065	224703	-0.55
2	1110018M03Rik	67606	1.16
3	1110020G09Rik	68646	-0.06
4	1500001M20Rik	68971	0.84
5	1500003O22Rik		1.47
6	1500026B10Rik	66104	-1.77
7	1500026B10Rik	66104	2.18
8	1700010I14Rik	66931	0.22
9	1700011K15Rik	75456	3.02
10	1700029I01Rik	70005	2.64
11	1700065D16Rik	73410	-0.02
12	2010001J22Rik	70113	2.6
13	2010005H15Rik	76770	1.6
14	2010321M09Rik	69882	0.82
15	2610020C11Rik	72154	0.62
16	2610024A01Rik	72160	0.44
17	2810408M09Rik	381406	0.12
18	4631402N15Rik	70793	0.3
19	4631426E05Rik	66696	2.29
41	A630047E20Rik	271981	1.35
42	Abi3	66610	0.82
43	Abtb1	80283	1.7
44	Acyp1	66204	0.99
45	Adck2	57869	1.04
46	Adh7	11529	1.29
47	AI413782	104799	0.59
48	Ak1	11636	1.86
49	Akr1a4	58810	1.22
50	Akr1b3	11677	0.98
51	Alpk1	71481	1.19
52	Ankrd33	208258	0.75
53	Ankrd48	76389	1.81
54	Anks4b	72074	0.72
55	Ar	11835	1.56
56	Ascl1	17172	-1.62
57	Atp1b4	67821	0.28
58	AU045404	380959	-2.05
59	Aurka	20878	14.02

20	4632428N05Rik	74048	1.51
21	4921501E09Rik	74042	0.03
22	4921504I05Rik	66707	1.59
23	4930432K21Rik	74666	0.55
24	4930444A02Rik	74653	1
25	4930548G07Rik	75339	0.92
26	4930558O21Rik	68307	2.64
27	4930563M21Rik	75258	0.62
28	4933405K07Rik	74400	2.05
29	4933434E20Rik	99650	2.09
30	5430413K10Rik	71425	0.23
31	5730467H21Rik	78088	4.19
32	5730508B09Rik	70617	0
33	5830417C01Rik	78825	0.49
34	6230410P16Rik	235582	0.98
35	6330416L07Rik	319615	0.22
36	6330514A18Rik	216166	0.95
37	6430514L14Rik	76886	0.66
38	6430573F11Rik	319582	0.53
39	6720467C03Rik	68099	-0.02
40	9130011E15Rik	71617	0.49

60	AW209491	105351	1.38
61	AW548124	106522	-0.57
62	B4galnt3	330406	0.53
63	Bard1	12021	1.05
64	BC013529	215751	0.26
65	BC031901	231296	1.1
66	BC052883	381759	1.09
67	Bcan	12032	-0.02
68	Bcl3	12051	0.58
69	Becn1	56208	0.2
70	Bhlhb8	17341	1.71
71	Blnk	17060	1.33
72	Blvra	109778	0.64
73	Bmp2k	140780	0.06
74	Bmyc	107771	0.44
75	Bpnt1	23827	0.7
76	Btf3l4	70533	0.51
77	Btk	12229	2.45
78	C80638	97086	0.94
79	Cacna1f	54652	0.8
80	Cacng3	54376	0.59

81	Cacng5	140723	0.2
82	Cacng8	81905	0.67
83	Camkk1	55984	2.63
84	Catsper1	225865	1.75
85	Catsper3	76856	0.68
86	Ccdc106	232821	2.23
87	Ccdc92	215707	0.57
88	Ccin	442829	2.71
89	Ccm2	216527	-0.17
90	Cd200r3	74603	4.08
91	Cdkn2d	12581	0.37
92	Cdkn3	72391	1.13
93	Cebpz	12607	2.55
94	Cenpo	52504	-0.02
95	Cfl2	12632	0.95
96	Chchd8	68185	0.51
97	Chga	12652	0.85
98	Chrac1	93696	1.1
99	Chrm1	12669	2.26
100	Cic	71722	0.7
101	Cks2	66197	0.72
102	Clca2	80797	0.38
103	Clcn1	12723	0.16
104	Clcn7	26373	0.83
105	Clic1	114584	2.07
106	Cnksr2	245684	1.71

121	Ctrl	109660	0.48
122	Cul2	71745	1.61
123	Cxcl13	55985	3.4
124	Cybb	13058	1.01
125	Cyp3a16	13114	0.67
126	Cyp4a10	13117	2.87
127	Cyp4x1	81906	1.78
128	D11Ertd18e	52466	0.53
129	D3Ertd300e	56790	1
130	D4st1	72136	2.32
131	Daxx	13163	0.36
132	Dcamkl1	13175	3.24
133	Ddit4	74747	2.69
134	Deaf1	54006	1.21
135	Dhcr24	74754	0.17
136	Dmrtc2	71241	1.96
137	Dpf2	19708	1.77
138	Dppa2	73703	0.56
139	Dusp16	70686	0.62
140	Ebf3	13593	1.8
141	Edg2	14745	0.79
142	Egfr	13649	2.37
143	Egln3	112407	0.8
144	Egr1	13653	1.92
145	Eif2ak1	15467	0.83
146	Eif4g2	13690	2.99

107	Cog7	233824	-0.18
108	Cops4	26891	0.5
109	Creb3l3	208677	1.26
110	Crlf3	54394	0.87
111	Csf1r	12978	4.69
112	Csnk1a1	93687	4.61
113	Csnk1d	104318	0.09
114	Csnk1g1	214897	1.77
115	Csnk1g2	103236	2.07
116	Csnk1g3	70425	-0.58
117	Csnk2a2	13000	2.71
118	Cst12	69362	2.57
119	Ctbp1	13016	0.18
120	Ctbp2	13017	1.63

147	Enpp6	320981	0.53
148	Entpd1	12495	1.52
149	Entpd2	12496	0.02
150	Epha10	230735	1.94
151	Epha2	13836	-0.44
152	Epha8	13842	1.86
153	Ephb4	13846	1.76
154	Epm2aip1	77781	-0.07
155	Ercc5	22592	0.1
156	Ercc5	22592	2.02
157	Esrra	26379	0.92
158	Esrrg	26381	3.29
159	Exosc3	66362	1.83
160	Faf1		2.89

161	Fank1	66930	0.74
162	Fbxo33	70611	2.22
163	Fes	14159	2.96
164	Fetub	59083	0.71
165	Fgf4	14175	0.47
166	Flt4	14257	0.72
167	Foxn4	116810	2.41
168	Fpr-rs1	14288	3.16
169	Ftmt	67634	0.35
170	Galp	232836	1.58
171	Gata5	14464	0.22
172	Gfra2	14586	0.79
173	Glb1	12091	0.59
174	Glis1	230587	2.33
175	Gm1247	383107	3.1
176	Gm1872	380676	-0.08
177	Gm270	218241	-0.14
178	Gm272	218244	1.53
179	Gmfb	63985	1.45
180	Golt1b	66964	0.11
181	Gpr22	73010	2.9
182	Gpr61	229714	4.02
183	Gpr83	14608	2.71
184	Gprc6a	210198	5.78
185	Grhl1	195733	0.42
186	Grpr	14829	4.53
187	Gsc	14836	0.58
188	Gtf2e1	74197	0.5
189	Gtf2i	14886	0.37
190	Gtf3c5	70239	0.43
191	Gucy1b3	54195	0.75
192	Guk1	14923	0.55
193	Hand2	15111	1.32

201	Il3	16187	0.33
202	Il4ra	16190	2.6
203	Il9	16198	3.7
204	Inpp1	16329	3.49
205	Insm2	56856	1.78
206	Insrr	23920	-0.28
207	Itgb3	16416	0.36
208	Itih3	16426	4.58
209	Kcna6	16494	1.2
210	Kcnd2	16508	0.12
211	Kcnip4	80334	0.82
212	Kcnj3	16519	1.45
213	Kcnj6	16522	1.53
214	Kcnk1	16525	1.1
215	Kcnk2	16526	-0.3
216	Kcnn4	16534	2.74
217	Kcnt1	227632	0.93
218	Kctd10	330171	2.36
219	Kctd13	233877	1.49
220	Kirrel2	243911	1.23
221	Kit	16590	0.93
222	Klf7	93691	3.1
223	Klk1b3	18050	2.21
224	Klra17	170733	1.85
225	Klrc3	58179	0.4
226	Kremen2	73016	0.41
227	Lactb2	212442	0.87
228	Lancl1	14768	-0.25
229	Leprel2	14789	0.61
230	Lgals1	16852	1.46
231	Lilrb4	14728	0.82
232	Lmbr1l	74775	0.43
233	LOC229005	229005	-0.02

194	Hand2	15111	0.34
195	Has1	15116	2.15
196	Higd1a	56295	1.37
197	Hlf	217082	0.56
198	Hmgb2	97165	1.83
199	Hmox1	15368	0.38
200	Il3	16187	0.2

234	LOC236413	236413	0.37
235	LOC241051	241051	0.34
236	LOC245350	245350	0.4
237	LOC381390	381390	4.83
238	LOC381936	381936	1.59
239	LOC433762	433762	0.52
240	LOC545925	545925	1.95

241	Lrpap1	16976	0.4
242	Mafb	16658	0.59
243	Map2k5	23938	1.76
244	Map3k15	270672	6.88
245	Map3k2	26405	1.1
246	Map3k6	53608	0.87
247	Map4k5	399510	1.64
248	Mas1	17171	0.56
249	Mecp2	17257	0.53
250	Mef2b	17259	0.17
251	Mef2d	17261	0.42
252	Melk	17279	0.44
253	Met	17295	1.34
254	Mipep	70478	1.14
255	Mllt1	64144	0.5
256	Mnt	17428	0.55
257	Morf4l1	21761	0.48
258	Mrgprx1	404242	0.19
259	Ms4a4c	64380	1.1
260	Msmb	17695	1.17
261	Mtmr9	210376	0.48
262	Mug2	17837	1.23
263	Musk	18198	2.62
264	Myc	17869	1.04
265	Mylk2	228785	4.86
266	Mynn	80732	3.29
267	Myst4	54169	0.89
268	Nck1	17973	11.71
269	Ndufa9	66108	0.94
270	Nek4	23955	-0.04
271	Nek6	59126	1.01
272	Nek7	59125	0.43
273	Nek8	140859	1.15
274	Neurod4	11923	2.27
275	Nfam1	74039	-0.39
276	Nfe2l3	18025	18.04
277	Nfic	18029	0.59
278	Nfrkb	235134	0.63
279	Nifun	66383	0.63
280	Nkx2-4	228731	1.76

281	Nkx2-6	18092	0.67
282	Nnat	18111	0.27
283	Npdc1	18146	0.37
284	Npr3	18162	-0.22
285	Nr0b1	11614	1.21
286	Nr1d1	217166	2.37
287	Nr1h4	20186	0.61
288	Nr2c1	22025	2.12
289	Nr2e1	21907	4.38
290	Nr2f1	13865	1.87
291	Nr2f6	13864	-0.34
292	Nr4a1	15370	-0.24
293	Nr4a2	18227	1.44
294	Nr4a3	18124	0.6
295	Nr5a2	26424	12.86
296	Ntrk2	18212	-0.06
297	Nudc	18221	0.85
298	Nudt16l1	66911	0.82
299	Nxt2	237082	0.33
300	Olfr345	258947	0.46
301	Olfr574	258357	2.89
302	Olfr700	258593	2.21
303	Olfr801	258282	0.77
304	Olfr808	258930	0.6
305	Olfr987	257951	1.48
306	Omg	18377	1.22
307	ORF63	224419	4.99
308	Otp	18420	0.71
309	Pak2	224105	0.08
310	Pak4	70584	2.29
311	Pak6	214230	-0.58
312	Pak7	241656	-0.63
313	Papss2	23972	4.77
314	Pax2	18504	0.29
315	Pax4	18506	1.44
316	Pbk	52033	2.4
317	Pbp2	76400	1.09
318	Pbx3	18516	1.89
319	Pcdhga3	93711	0.27
320	Pde6g	18588	2.2

321	Peg3	18616	1.58
322	Pelp1	75273	0.16
323	Per1	18626	2.86
324	Phf11	219131	1.47
325	Phka1	18679	3.39
326	Phkb	102093	0.09
327	Phtf1	18685	2.3
328	Pim2	18715	1.34
329	Pip5kl1	227733	-0.18
330	Plekha1	101476	2.25
331	Plk4	20873	1.68
332	Plxna1	18844	0.45
333	Pnliprp2	18947	0.43
334	Ppap2a	19012	0.55
335	Ppef1	237178	0.87
336	Ppm1f	68606	0.37
337	Ppp1r7	66385	0.33
338	Ppp2r2c	269643	0.49
339	Ppp3ca	19055	1.83
340	Ppy	19064	0.12
341	Prdm9	213389	0.78
342	Prf1	18646	0.46
343	Prh1	19131	-0.04
344	Prkdc	19090	3.7
345	Pth	19226	0.56
346	Ptk6	20459	1.46
347	Ptk7	71461	0.36
348	Ptpn1	19246	1.92
349	Ptprz1	19283	2.12
350	Pycr2	69051	0.58
351	Rab11fip2	74998	0.83
352	Racgap1	26934	0.91
353	Ralb	64143	10.57
354	Rarg	19411	0.91
355	Rcor2	104383	1.4
356	Rhox3	382209	0.49
357	Riok3	66878	0.03
358	Rnuxa	56698	1.06
359	Ror2	26564	2.16
360	Rorb	225998	2.75

361	Rorc	19885	-0.34
362	Rrm2b	382985	0.09
363	Sass6	72776	1.33
364	Scyl2	213326	11.43
365	Scyl3	240880	4.27
366	Sepw1	20364	-0.06
367	Serpina1a	20700	1.66
368	Serpina1e	20704	1.14
369	Serpinb10	241197	0.3
370	Serpinb9b	20706	0.29
371	Serpinb9g	93806	4.01
372	Serpinf1	20317	1.96
373	Serpinf2	18816	2.14
374	Serpinf2	18816	0.62
375	Sesn3	75747	0.76
376	Sh2d1b1	26904	0.94
377	Shank3	58234	12.28
378	Siglece	83382	2.17
379	Slc15a2	57738	4.03
380	Slc17a3	105355	0.29
381	Slc1a1	20510	1.24
382	Slc22a2	20518	1.05
383	Slc22a6	18399	2.8
384	Slc24a6	170756	1.62
385	Slc25a11	67863	7.19
386	Slc26a11	268512	1.02
387	Slc26a2	13521	0.79
388	Slc27a1	26457	0.52
389	Slc29a1	63959	3.04
390	Slc29a2	13340	2.86
391	Slc2a1	20525	0.35
392	Slc2a2	20526	0.25
393	Slc2a4	20528	1.9
394	Slc30a7	66500	3.9
395	Slc35c1	228368	0.56
396	Slc35f1	215085	1.64
397	Slc35f3	210027	0.23
398	Slc39a8	67547	0.23
399	Slc4a1	20533	1.54
400	Slc4a2	20535	1.2

401	Slc4a2	20535	0.98
402	Slc4a8	59033	0.63
403	Slc5a9	230612	0.83
404	Slc6a12	14411	5.23
405	Slc6a18	22598	0.3
406	Slc6a19	74338	1.84

441	Taf6l	225895	0.58
442	Taok2	381921	2.04
443	Tas1r3	83771	1.71
444	Tas2r110	387344	0.77
445	Tas2r134	387511	-0.08
446	Tbl1xr1	81004	2.64

407	Slc6a2	20538	0.17	447	Tbn	63856	0.83
408	Slc6a20	22599	2.06	448	Tbx5	21388	1.32
409	Slc7a1	11987	0.93	449	Tcfeb	21425	1.45
410	Slco2b1	101488	97.31	450	Tec	21682	0.64
411	Slco3a1	108116	0.96	451	Tgif2	228839	0.69
412	Smarca2	67155	0.38	452	Thap1	73754	2.83
413	Smarcc2	68094	0.09	453	Timp1	21857	0.19
414	Smoc1	64075	1.34	454	Tlk2	24086	0.19
415	Sncaip	67847	1.26	455	Tm9sf4	99237	0.73
416	Sox1	20664	0.91	456	Tmem117	320709	0.07
417	Sox7	20680	0.57	457	Tmem19	67226	2.54
418	Sp4	20688	1.63	458	Tmem30a	69981	0.26
419	Spa17	20686	2.11	459	Tmem46	219134	0.64
420	Spag9	70834	3.53	460	Tmem67	329795	2.03
421	Spint4	78239	10	461	Tmsb4x	19241	1.04
422	Src	20779	1.32	462	Tnik	69014	0
423	Ssh2	237860	0.34	463	Tnk1	83813	1.76
424	Sstr2	20606	1.88	464	Top2a	21973	5.03
425	St8sia2	20450	0.55	465	Trim33	94093	0.81
426	Stambpl1	76630	1.44	466	Trim59	66949	0.15
427	Stat6	20852	10.51	467	Trim8	93679	0.55
428	Stk10	20868	1.12	468	Trip13	69716	-0.04
429	Stk11	20869	13.55	469	Trpc2	22064	1.07
430	Stk24	223255	0.07	470	Trpm1	17364	1.86
431	Stk31	77485	1.67	471	Trpm6	225997	0.47
432	Stk39	53416	20.74	472	Trpm7	58800	1.41
433	Stk40	74178	0.31	473	Trpv4	63873	9.77
434	Stmn1	16765	0.32	474	Tshz3	243931	0.72
435	Supt4h1	20922	1.35	475	Tssk2	22115	-0.39
436	Susd2	71733	1.29	476	Ttbk2	140810	1.68
437	Syk	20963	3.19	477	Txk	22165	3.15
438	Sync		1.44	478	Txndc14	66958	0.03
439	Taf1	270627	0.21	479	Tyro3	22174	-0.48
440	Taf1a	21339	1.99	480	Ugt2b34	100727	0.92

481	Ulk2	29869	0.36	521	Zfp277	246196	0.82
482	UNK	245074	0.02	522	Zfp286	192651	1.83
483	UNK	333716	1.6	523	Zfp324	243834	0.25
484	UNK	241864	-0.37	524	Zfp398	272347	0.81
485	UNK	272680	2.99	525	Zfp454	237758	0.82
486	UNK	384538	0.07	526	Zfp521	225207	0.37
487	UNK	333667	0.47	527	Zfp641	239652	2.34
488	UNK	382590	1.49	528	Zfp661	72180	1.3
489	UNK	383133	0.49	529	Zfp709	236193	0.91
490	UNK	385054	3.73	530	Zfp748	212276	0.84
491	UNK	383073	3.53	531	Zfp75	244713	1.15
492	UNK	269990	1.91	532	Zfpn1a1	22778	2.15
493	UNK	381252	0.15	533	Zfyve20	78287	1.45

494	UNK	433649	0.54
495	UNK	435891	1.62
496	UNK	433793	1.69
497	UNK	382264	0.92
498	UNK	433890	0.28
499	UNK	434313	0.52
500	UNK	433830	2.16
501	UNK	381556	0.24
502	UNK	385018	1.25
503	UNK	328752	0.7
504	Upf1	19704	0.61
505	Usp38	74841	0.68
506	V1rd4	81014	0.57
507	V1ri6	171257	0.99
508	Vdr	22337	1.24
509	Vmo1	327956	0.6
510	Vrk1	22367	2.13
511	Vrk2	69922	1.42
512	Vrk3	101568	2.23
513	Wee1	22390	1.67
514	Wnk1	232341	1.46
515	Wnk3	279561	1.47
516	Wrnip1	78903	1.24
517	Yes1	22612	1.13
518	Yipf5	67180	-0.43
519	Zbtb33	56805	0.28
520	Zfhx4	80892	2.61
534	Zic4	22774	1.13
535	Zmpste24	230709	0.41

Extended Table 5

S.No	Gene symbol	Gene ID	Predicted localization
1	ATF6B		Endoplasmic reticulum
2	ccr1	2541038	Endoplasmic reticulum
3	Cisd1	52637	Mitochondrion outer membrane
4	Creb3l1	26427	Endoplasmic reticulum
5	Dmpk	13400	Endoplasmic reticulum
	Dmpk	13400	Mitochondrion outer membrane
6	Drd1a	13488	Endoplasmic reticulum
7	Edem1	192193	Endoplasmic reticulum
8	Ei24	13663	Endoplasmic reticulum
9	Ergic2	67456	Endoplasmic reticulum
10	Gpam	14732	Mitochondrion outer membrane
11	Gpr37	117549	Endoplasmic reticulum
12	Grm6	108072	Endoplasmic reticulum
13	Mgst1	171341	Endoplasmic reticulum
	Mgst1	171341	Mitochondrion outer membrane
14	Mogat2	233549	Endoplasmic reticulum

15	Nfe2l1	18023	Endoplasmic reticulum
16	Parp16	214424	Endoplasmic reticulum
17	Pigb	55981	Endoplasmic reticulum
18	Pld3	18807	Endoplasmic reticulum
19	Pnpla7	241274	Endoplasmic reticulum
20	Ptgis	19223	Endoplasmic reticulum
21	Rhbdf2	217344	Endoplasmic reticulum
22	Rnf139	75841	Endoplasmic reticulum
23	Rnf43	207742	Endoplasmic reticulum
24	Rrbp1	81910	Endoplasmic reticulum
25	Sec11a	56529	Endoplasmic reticulum
26	Sec62	69276	Endoplasmic reticulum
27	Slc16a11	216867	Endoplasmic reticulum
28	SLC28A3	64078	Endoplasmic reticulum
29	Slc39a7	14977	Endoplasmic reticulum
30	Soat1	20652	Endoplasmic reticulum
31	Spcs1	69019	Endoplasmic reticulum
32	Tmc8	217356	Endoplasmic reticulum
33	Tmem132a	98170	Endoplasmic reticulum
34	Wrb	288233	Endoplasmic reticulum

Extended Table 6

S.No	Gene symbol	Gene ID	Predicted localisation
1	ABP1	828120	Endoplasmic reticulum
2	Ankle2	71782	Endoplasmic reticulum
3	Ankrd13c	433667	Endoplasmic reticulum
4	Atf2	102641666	Mitochondrion outer membrane
5	Atp8a1	11980	Endoplasmic reticulum
6	bet1	2542068	Endoplasmic reticulum
7	Bnip3	12176	Mitochondrion outer membrane
8	Bnip3l	12177	Endoplasmic reticulum
	Bnip3l	12177	Mitochondrion outer membrane
9	Cant1	246272	Endoplasmic reticulum
10	Cers2	76893	Endoplasmic reticulum
11	Cers6	241447	Endoplasmic reticulum
12	Clcc1	170927	Endoplasmic reticulum
13	Clstn3	232370	Endoplasmic reticulum
14	Col4a3bp	68018	Endoplasmic reticulum
15	Creb3l3	208677	Endoplasmic reticulum
16	CYB5	855612	Endoplasmic reticulum
17	Cyb5r4	171015	Endoplasmic reticulum
18	Cyp3a16	13114	Endoplasmic reticulum
19	Cyp4a10	13117	Endoplasmic reticulum
20	Cyp4x1	246767	Endoplasmic reticulum
21	Cyp7b1	13123	Endoplasmic reticulum

22	Dcstamp	75766	Endoplasmic reticulum
23	Derl1	67819	Endoplasmic reticulum
24	Dhcr24	74754	Endoplasmic reticulum
25	Dhdds	67422	Endoplasmic reticulum
26	Elovl2	498728	Endoplasmic reticulum
27	ENTPD2	954	Endoplasmic reticulum
28	Epm2aip1	77781	Endoplasmic reticulum
29	Fmo3	14262	Endoplasmic reticulum
30	G6pc2	14378	Endoplasmic reticulum
31	Hsd17b6	27400	Endoplasmic reticulum
32	Ier3ip1	66191	Endoplasmic reticulum
33	Kcnk2	170899	Endoplasmic reticulum
34	KTN1	3895	Endoplasmic reticulum
35	Leprel2	14789	Endoplasmic reticulum
36	Lrpap1	116565	Endoplasmic reticulum
37	Lrrc59	287633	Endoplasmic reticulum
38	Lss	16987	Endoplasmic reticulum
39	MID1	855425	Endoplasmic reticulum
40	Msrb3	320183	Endoplasmic reticulum
41	MX1	280872	Endoplasmic reticulum
42	Nck1	17973	Endoplasmic reticulum
43	Nox4	50490	Endoplasmic reticulum
44	Ormdl3	360618	Endoplasmic reticulum
45	Pcsk9	100102	Endoplasmic reticulum
46	Pi4kb	107650	Endoplasmic reticulum
	Pi4kb	107650	Mitochondrion outer membrane
47	PIK3C2B	5287	Endoplasmic reticulum
48	Pja2	192256	Endoplasmic reticulum
49	Plod1	18822	Endoplasmic reticulum
50	Pnpla8	67452	Endoplasmic reticulum
51	Ptpn1	19246	Endoplasmic reticulum
52	Rnf185	193670	Endoplasmic reticulum
	Rnf185	193670	Mitochondrion outer membrane
53	Sc5d	235293	Endoplasmic reticulum
54	Sgpp1	81535	Endoplasmic reticulum
55	Shisa2	219134	Endoplasmic reticulum
56	Slc11a2	18174	Mitochondrion outer membrane
57	SLC17A3	10786	Endoplasmic reticulum
58	SLC26A6	65010	Endoplasmic reticulum
59	Slc27a2	26458	Endoplasmic reticulum
60	Slc33a1	11416	Endoplasmic reticulum
61	SLC39A1	27173	Endoplasmic reticulum
62	Spcs2	66624	Endoplasmic reticulum
63	Srd5a1	78925	Endoplasmic reticulum
64	Tmc6	217353	Endoplasmic reticulum
65	TMEM67	91147	Endoplasmic reticulum
66	Tor2a	30933	Endoplasmic reticulum
67	UGT1A10	54575	Endoplasmic reticulum

68	ULBP1	80329	Endoplasmic reticulum
69	Vrk2	69922	Endoplasmic reticulum
70	Yipf5	361315	Endoplasmic reticulum
71	Zmpste24	230709	Endoplasmic reticulum

5 Conclusions and perspective

In this thesis, we had set to identify the molecular players of ER-mitochondria junction (MAMs) through a high content screen. We have utilized a modified FRET based biosensor to measure the proximity of ER and mitochondria. Our high-throughput data suggested eight novel proteins that are either involved in tethering or spacing the two organelles. Our low through-put data has confirmed Myotonic dystrophy protein kinase (DMPK) to be localised in MAMs.

FRET based biosensor (FEMP) provided us with a distinct advantage of measuring both basal FRET that corresponded to the proximity of ER-mitochondria contacts at any time point but also maximum FRET that corresponded to the maximum number of contacts possible. The distances measured using this probe is typically in orders of magnitude of ER-mitochondria contacts and we thus established the robustness of the assay.

High content screening of ~10,000 genes and rigorous statistical analysis yielded 14.4% high confidence tethers or modulators of tethers and 5.34% high confidences spacers or modulators of spacers. Bioinformatics analysis of these high confidence tethers and spacers by Mitominer yielded eight proteins that were predicted to be localised in ER and outer mitochondrial membrane. Panther database classification also yielded high confidence protein classes that the “hits” belong to.

Myotonic dystrophy protein kinase (DMPK) was identified as a tether of ER and mitochondria in the high-throughput screen. Biochemical fractionation data also confirmed the localisation of DMPK to MAMs, thus confirming the high content screen analysis. DMPK’s role in myotonic dystrophy (DM) is

not yet completely understood. One of the causes of myotonic dystrophy being decreased protein levels of DMPK opens new areas of research with respect to ER-mitochondria tethering implications in DM.

The genes identified as spacers and tethers often belong to the same pathways as indicated by Panther database analysis, although certain pathways were enriched individually in the Tethers or in the Spacers pools. One tempting possibility for this difference could be inherent nature of the cell to maintain balance during resting or in response to pathological conditions such as cellular stress. Since pathways where ER-mitochondria tethering have already been implicated have also turned up in high throughput analysis, our data could provide the missing blocks to solve the already existing puzzles.

Our study on ER-mitochondria tether has opened new avenues of research owing to the fact that the genes, which we have identified spans cellular pathways that are already known to be involved in ER-mitochondria tether and others that are yet to be described.

6 References

Clegg, R.M. (2002). FRET tells us about proximities, distances, orientations and dynamic properties. Reviews in Molecular Biotechnology *82*, 177-179.

(2003). Whither RNAi? Nat Cell Biol *5*, 489-490.

Alexander, C., Votruba, M., Pesch, U.E., Thiselton, D.L., Mayer, S., Moore, A., Rodriguez, M., Kellner, U., Leo-Kottler, B., Auburger, G.*, et al.* (2000). OPA1, encoding a dynamin-related GTPase, is mutated in autosomal dominant optic atrophy linked to chromosome 3q28. Nat Genet *26*, 211-215.

Archer, S.L. (2013). Mitochondrial dynamics--mitochondrial fission and fusion in human diseases. N Engl J Med *369*, 2236-2251.

Bereiter-Hahn, J., and Voth, M. (1994). Dynamics of mitochondria in living cells: shape changes, dislocations, fusion, and fission of mitochondria. Microsc Res Tech *27*, 198-219.

Bernstein, E., Denli, A.M., and Hannon, G.J. (2001). The rest is silence. RNA *7*, 1509-1521.

Berridge, M.J., Bootman, M.D., and Roderick, H.L. (2003). Calcium signalling: dynamics, homeostasis and remodelling. Nat Rev Mol Cell Biol *4*, 517-529.

Betz, C., Stracka, D., Prescianotto-Baschong, C., Frieden, M., Demaurex, N., and Hall, M.N. (2013). Feature Article: mTOR complex 2-Akt signaling at mitochondria-associated endoplasmic reticulum membranes (MAM) regulates mitochondrial physiology. Proc Natl Acad Sci U S A *110*, 12526-12534.

Bian, X., Klemm, R.W., Liu, T.Y., Zhang, M., Sun, S., Sui, X., Liu, X., Rapoport, T.A., and Hu, J. (2011). Structures of the atlastin GTPase provide insight into homotypic fusion of endoplasmic reticulum membranes. Proc Natl Acad Sci U S A *108*, 3976-3981.

Birmingham, A., Selfors, L.M., Forster, T., Wrobel, D., Kennedy, C.J., Shanks, E., Santoyo-Lopez, J., Dunican, D.J., Long, A., Kelleher, D.*, et al.* (2009). Statistical methods for analysis of high-throughput RNA interference screens. Nat Methods *6*, 569-575.

Boutros, M., Bras, L.P., and Huber, W. (2006). Analysis of cell-based RNAi screens. Genome Biol *7*, R66.

Bravo-Sagua, R., Torrealba, N., Paredes, F., Morales, P.E., Pennanen, C., Lopez-Crisosto, C., Troncoso, R., Criollo, A., Chiong, M., Hill, J.A.*, et al.* (2014). Organelle communication: signaling crossroads between homeostasis and disease. Int J Biochem Cell Biol *50*, 55-59.

Bravo, R., Vicencio, J.M., Parra, V., Troncoso, R., Munoz, J.P., Bui, M., Quiroga, C., Rodriguez, A.E., Verdejo, H.E., Ferreira, J.*, et al.* (2011). Increased ER-mitochondrial coupling promotes mitochondrial respiration and bioenergetics during early phases of ER stress. J Cell Sci *124*, 2143-2152.

Broussard, J.A., Rappaz, B., Webb, D.J., and Brown, C.M. (2013). Fluorescence resonance energy transfer microscopy as demonstrated by measuring the activation of the serine/threonine kinase Akt. Nat Protoc *8*, 265-281.

Bui, M., Gilady, S.Y., Fitzsimmons, R.E., Benson, M.D., Lynes, E.M., Gesson, K., Alto, N.M., Strack, S., Scott, J.D., and Simmen, T. (2010). Rab32 modulates apoptosis onset and mitochondria-associated membrane (MAM) properties. J Biol Chem *285*, 31590-31602.

Byrnes, L.J., and Sondermann, H. (2011). Structural basis for the nucleotide-dependent dimerization of the large G protein atlastin-1/SPG3A. Proc Natl Acad Sci U S A *108*, 2216-2221.

Cali, T., Ottolini, D., and Brini, M. (2013). Calcium and endoplasmic reticulum-mitochondria tethering in neurodegeneration. DNA Cell Biol *32*, 140-146.

Cereghetti, G.M., Stangherlin, A., Martins de Brito, O., Chang, C.R., Blackstone, C., Bernardi, P., and Scorrano, L. (2008). Dephosphorylation by calcineurin regulates translocation of Drp1 to mitochondria. Proc Natl Acad Sci U S A *105*, 15803-15808.

Cerqua, C., Anesti, V., Pyakurel, A., Liu, D., Naon, D., Wiche, G., Baffa, R., Dimmer, K.S., and Scorrano, L. (2010). Trichoplein/mitostatin regulates endoplasmic reticulum-mitochondria juxtaposition. EMBO Rep *11*, 854-860.

Chen, H., Detmer, S.A., Ewald, A.J., Griffin, E.E., Fraser, S.E., and Chan, D.C. (2003). Mitofusins Mfn1 and Mfn2 coordinately regulate mitochondrial fusion and are essential for embryonic development. J Cell Biol *160*, 189-200.

Chen, J., Zheng, X.F., Brown, E.J., and Schreiber, S.L. (1995). Identification of an 11-kDa FKBP12-rapamycin-binding domain within the 289-kDa FKBP12-rapamycin-associated protein and characterization of a critical serine residue. Proc Natl Acad Sci U S A *92*, 4947-4951.

Chen, S., Desai, T., McNew, J.A., Gerard, P., Novick, P.J., and Ferro-Novick, S. (2015). Lunapark stabilizes nascent three-way junctions in the endoplasmic reticulum. Proc Natl Acad Sci U S A *112*, 418-423.

Chen, S., Novick, P., and Ferro-Novick, S. (2013). ER structure and function. Curr Opin Cell Biol *25*, 428-433.

Chhabra, E.S., Ramabhadran, V., Gerber, S.A., and Higgs, H.N. (2009). INF2 is an endoplasmic reticulum-associated formin protein. J Cell Sci *122*, 1430-1440.

Cho, D.H., Nakamura, T., Fang, J., Cieplak, P., Godzik, A., Gu, Z., and Lipton, S.A. (2009). S-nitrosylation of Drp1 mediates beta-amyloid-related mitochondrial fission and neuronal injury. Science *324*, 102-105.

Cho, D.H., and Tapscott, S.J. (2007). Myotonic dystrophy: emerging mechanisms for DM1 and DM2. Biochim Biophys Acta *1772*, 195-204.

Cipolat, S., Martins de Brito, O., Dal Zilio, B., and Scorrano, L. (2004). OPA1 requires mitofusin 1 to promote mitochondrial fusion. Proc Natl Acad Sci U S A *101*, 15927-15932.

Copeland, D.E., and Dalton, A.J. (1959). An association between mitochondria and the endoplasmic reticulum in cells of the pseudobranch gland of a teleost. J Biophys Biochem Cytol *5*, 393-396.

Cribbs, J.T., and Strack, S. (2007). Reversible phosphorylation of Drp1 by cyclic AMP-dependent protein kinase and calcineurin regulates mitochondrial fission and cell death. EMBO Rep *8*, 939-944.

Csordas, G., Renken, C., Varnai, P., Walter, L., Weaver, D., Buttle, K.F., Balla, T., Mannella, C.A., and Hajnoczky, G. (2006). Structural and functional features and significance of the physical linkage between ER and mitochondria. J Cell Biol *174*, 915-921.

Csordas, G., Varnai, P., Golenar, T., Roy, S., Purkins, G., Schneider, T.G., Balla, T., and Hajnoczky, G. (2010). Imaging interorganelle contacts and local calcium dynamics at the ER-mitochondrial interface. Mol Cell *39*, 121-132.

de Brito, O.M., and Scorrano, L. (2008). Mitofusin 2 tethers endoplasmic reticulum to mitochondria. Nature *456*, 605-610.

de Brito, O.M., and Scorrano, L. (2009). Mitofusin-2 regulates mitochondrial and endoplasmic reticulum morphology and tethering: the role of Ras. Mitochondrion *9*, 222-226.

Delettre, C., Lenaers, G., Griffoin, J.M., Gigarel, N., Lorenzo, C., Belenguer, P., Pelloquin, L., Grosgeorge, J., Turc-Carel, C., Perret, E*., et al.* (2000). Nuclear gene OPA1, encoding a mitochondrial dynamin-related protein, is mutated in dominant optic atrophy. Nat Genet *26*, 207-210.

Denton, R.M., Randle, P.J., and Martin, B.R. (1972). Stimulation by calcium ions of pyruvate dehydrogenase phosphate phosphatase. Biochem J *128*, 161-163.

Denton, R.M., Richards, D.A., and Chin, J.G. (1978). Calcium ions and the regulation of NAD+-linked isocitrate dehydrogenase from the mitochondria of rat heart and other tissues. Biochem J *176*, 899-906.

Dohm, J.A., Lee, S.J., Hardwick, J.M., Hill, R.B., and Gittis, A.G. (2004). Cytosolic domain of the human mitochondrial fission protein fis1 adopts a TPR fold. Proteins *54*, 153-156.

Duvezin-Caubet, S., Koppen, M., Wagener, J., Zick, M., Israel, L., Bernacchia, A., Jagasia, R., Rugarli, E.I., Imhof, A., Neupert, W*., et al.* (2007). OPA1 processing reconstituted in yeast depends on the subunit composition of the m-AAA protease in mitochondria. Mol Biol Cell *18*, 3582-3590.

Echeverri, C.J., and Perrimon, N. (2006). High-throughput RNAi screening in cultured cells: a user's guide. Nat Rev Genet *7*, 373-384.

Elbaz-Alon, Y., Rosenfeld-Gur, E., Shinder, V., Futerman, A.H., Geiger, T., and Schuldiner, M. (2014). A dynamic interface between vacuoles and mitochondria in yeast. Dev Cell *30*, 95-102.

Elgass, K.D., Smith, E.A., LeGros, M.A., Larabell, C.A., and Ryan, M.T. (2015). Analysis of ER-mitochondria contacts using correlative fluorescence microscopy and soft X-ray tomography of mammalian cells. J Cell Sci *128*, 2795-2804.

English, A.R., and Voeltz, G.K. (2013). Endoplasmic reticulum structure and interconnections with other organelles. Cold Spring Harb Perspect Biol *5*, a013227.

Ferrari, D., Pinton, P., Szabadkai, G., Chami, M., Campanella, M., Pozzan, T., and Rizzuto, R. (2002). Endoplasmic reticulum, Bcl-2 and Ca2+ handling in apoptosis. Cell Calcium *32*, 413-420.

Friedman, J.R., Lackner, L.L., West, M., DiBenedetto, J.R., Nunnari, J., and Voeltz, G.K. (2011). ER tubules mark sites of mitochondrial division. Science *334*, 358-362.

Friedman, J.R., and Voeltz, G.K. (2011). The ER in 3D: a multifunctional dynamic membrane network. Trends Cell Biol *21*, 709-717.

Friedman, J.R., Webster, B.M., Mastronarde, D.N., Verhey, K.J., and Voeltz, G.K. (2010). ER sliding dynamics and ER-mitochondrial contacts occur on acetylated microtubules. J Cell Biol *190*, 363-375.

Frigault, M.M., Lacoste, J., Swift, J.L., and Brown, C.M. (2009). Live-cell microscopy - tips and tools. J Cell Sci *122*, 753-767.

Giacomello, M., Drago, I., Bortolozzi, M., Scorzeto, M., Gianelle, A., Pizzo, P., and Pozzan, T. (2010). Ca2+ hot spots on the mitochondrial surface are generated by Ca2+ mobilization from stores, but not by activation of store-operated Ca2+ channels. Mol Cell *38*, 280-290.

Giorgi, C., Missiroli, S., Patergnani, S., Duszynski, J., Wieckowski, M.R., and Pinton, P. (2015). Mitochondria-associated membranes: composition, molecular mechanisms, and physiopathological implications. Antioxid Redox Signal *22*, 995-1019.

Goyal, U., and Blackstone, C. (2013). Untangling the web: mechanisms underlying ER network formation. Biochim Biophys Acta *1833*, 2492-2498.

Grigoriev, I., Gouveia, S.M., van der Vaart, B., Demmers, J., Smyth, J.T., Honnappa, S., Splinter, D., Steinmetz, M.O., Putney, J.W., Jr., Hoogenraad, C.C*., et al.* (2008). STIM1 is a MT-plus-end-tracking protein involved in remodeling of the ER. Curr Biol *18*, 177-182.

Hailey, D.W., Rambold, A.S., Satpute-Krishnan, P., Mitra, K., Sougrat, R., Kim, P.K., and Lippincott-Schwartz, J. (2010). Mitochondria supply membranes for autophagosome biogenesis during starvation. Cell *141*, 656-667.

Hamasaki, M., Furuta, N., Matsuda, A., Nezu, A., Yamamoto, A., Fujita, N., Oomori, H., Noda, T., Haraguchi, T., Hiraoka, Y*., et al.* (2013). Autophagosomes form at ER-mitochondria contact sites. Nature *495*, 389-393.

Hanada, K., Kumagai, K., Tomishige, N., and Yamaji, T. (2009). CERT-mediated trafficking of ceramide. Biochim Biophys Acta *1791*, 684-691.

Harder, Z., Zunino, R., and McBride, H. (2004). Sumo1 conjugates mitochondrial substrates and participates in mitochondrial fission. Curr Biol *14*, 340-345.

Hermann, G.J., Thatcher, J.W., Mills, J.P., Hales, K.G., Fuller, M.T., Nunnari, J., and Shaw, J.M. (1998). Mitochondrial fusion in yeast requires the transmembrane GTPase Fzo1p. J Cell Biol *143*, 359-373.

Hetzer, M.W., Walther, T.C., and Mattaj, I.W. (2005). Pushing the envelope: structure, function, and dynamics of the nuclear periphery. Annu Rev Cell Dev Biol *21*, 347-380.

Hoepfner, D., Schildknegt, D., Braakman, I., Philippsen, P., and Tabak, H.F. (2005). Contribution of the endoplasmic reticulum to peroxisome formation. Cell *122*, 85-95.

Honscher, C., Mari, M., Auffarth, K., Bohnert, M., Griffith, J., Geerts, W., van der Laan, M., Cabrera, M., Reggiori, F., and Ungermann, C. (2014). Cellular metabolism regulates contact sites between vacuoles and mitochondria. Dev Cell *30*, 86-94.

Horner, S.M., Wilkins, C., Badil, S., Iskarpatyoti, J., and Gale, M., Jr. (2015). Proteomic analysis of mitochondrial-associated ER membranes (MAM) during RNA virus infection reveals dynamic changes in protein and organelle trafficking. PLoS One *10*, e0117963.

Hu, J., Prinz, W.A., and Rapoport, T.A. (2011). Weaving the web of ER tubules. Cell *147*, 1226-1231.

Hu, J., Shibata, Y., Zhu, P.P., Voss, C., Rismanchi, N., Prinz, W.A., Rapoport, T.A., and Blackstone, C. (2009). A class of dynamin-like GTPases involved in the generation of the tubular ER network. Cell *138*, 549-561.

Ishihara, N., Eura, Y., and Mihara, K. (2004). Mitofusin 1 and 2 play distinct roles in mitochondrial fusion reactions via GTPase activity. J Cell Sci *117*, 6535-6546.

Ishihara, N., Fujita, Y., Oka, T., and Mihara, K. (2006). Regulation of mitochondrial morphology through proteolytic cleavage of OPA1. EMBO J *25*, 2966-2977.

James, D.I., Parone, P.A., Mattenberger, Y., and Martinou, J.C. (2003). hFis1, a novel component of the mammalian mitochondrial fission machinery. J Biol Chem *278*, 36373-36379.

Kaliman, P., and Llagostera, E. (2008). Myotonic dystrophy protein kinase (DMPK) and its role in the pathogenesis of myotonic dystrophy 1. Cell Signal *20*, 1935-1941.

Klopfenstein, D.R., Kappeler, F., and Hauri, H.P. (1998). A novel direct interaction of endoplasmic reticulum with microtubules. EMBO J *17*, 6168-6177.

Konig, R., Chiang, C.Y., Tu, B.P., Yan, S.F., DeJesus, P.D., Romero, A., Bergauer, T., Orth, A., Krueger, U., Zhou, Y.*, et al.* (2007). A probability-based approach for the analysis of large-scale RNAi screens. Nat Methods *4*, 847-849.

Kopec, K.O., Alva, V., and Lupas, A.N. (2011). Bioinformatics of the TULIP domain superfamily. Biochem Soc Trans *39*, 1033-1038.

Kornmann, B., Currie, E., Collins, S.R., Schuldiner, M., Nunnari, J., Weissman, J.S., and Walter, P. (2009). An ER-mitochondria tethering complex revealed by a synthetic biology screen. Science *325*, 477-481.

Korobova, F., Ramabhadran, V., and Higgs, H.N. (2013). An actin-dependent step in mitochondrial fission mediated by the ER-associated formin INF2. Science *339*, 464-467.

Lahiri, S., Chao, J.T., Tavassoli, S., Wong, A.K., Choudhary, V., Young, B.P., Loewen, C.J., and Prinz, W.A. (2014). A conserved endoplasmic reticulum membrane protein complex (EMC) facilitates phospholipid transfer from the ER to mitochondria. PLoS Biol *12*, e1001969.

Lang, A., John Peter, A.T., and Kornmann, B. (2015). ER-mitochondria contact sites in yeast: beyond the myths of ERMES. Curr Opin Cell Biol *35*, 7-12.

Lee, G.S., Subramanian, N., Kim, A.I., Aksentijevich, I., Goldbach-Mansky, R., Sacks, D.B., Germain, R.N., Kastner, D.L., and Chae, J.J. (2012). The calcium-sensing receptor regulates the NLRP3 inflammasome through Ca2+ and cAMP. Nature *492*, 123-127.

Lee, Y.J., Jeong, S.Y., Karbowski, M., Smith, C.L., and Youle, R.J. (2004). Roles of the mammalian mitochondrial fission and fusion mediators Fis1, Drp1, and Opa1 in apoptosis. Mol Biol Cell *15*, 5001-5011.

Lev, S. (2010). Non-vesicular lipid transport by lipid-transfer proteins and beyond. Nat Rev Mol Cell Biol *11*, 739-750.

Liou, J., Fivaz, M., Inoue, T., and Meyer, T. (2007). Live-cell imaging reveals sequential oligomerization and local plasma membrane targeting of stromal interaction molecule 1 after Ca2+ store depletion. Proc Natl Acad Sci U S A *104*, 9301-9306.

Liou, J., Kim, M.L., Heo, W.D., Jones, J.T., Myers, J.W., Ferrell, J.E., Jr., and Meyer, T. (2005). STIM is a Ca2+ sensor essential for Ca2+-store-depletion-triggered Ca2+ influx. Curr Biol *15*, 1235-1241.

Liu, Z., Du, X., Deng, J., Gu, M., Hu, H., Gui, M., Yin, C.C., and Chang, Z. (2015). The interactions between mitochondria and sarcoplasmic reticulum and the proteome characterization of mitochondrion-associated membrane from rabbit skeletal muscle. Proteomics *15*, 2701-2704.

Llagostera, E., Catalucci, D., Marti, L., Liesa, M., Camps, M., Ciaraldi, T.P., Kondo, R., Reddy, S., Dillmann, W.H., Palacin, M.*, et al.* (2007). Role of myotonic dystrophy protein kinase (DMPK) in glucose homeostasis and muscle insulin action. PLoS One *2*, e1134.

Lopez-Crisosto, C., Bravo-Sagua, R., Rodriguez-Pena, M., Mera, C., Castro, P.F., Quest, A.F., Rothermel, B.A., Cifuentes, M., and Lavandero, S. (2015). ER-to-mitochondria miscommunication and metabolic diseases. Biochim Biophys Acta *1852*, 2096-2105.

Luke, G.A., de Felipe, P., Lukashev, A., Kallioinen, S.E., Bruno, E.A., and Ryan, M.D. (2008). Occurrence, function and evolutionary origins of '2A-like' sequences in virus genomes. J Gen Virol *89*, 1036-1042.

Malo, N., Hanley, J.A., Cerquozzi, S., Pelletier, J., and Nadon, R. (2006). Statistical practice in high-throughput screening data analysis. Nat Biotechnol *24*, 167-175.

Manders, E.M.M., Verbeek, F.J., and Aten, J.A. (1993). Measurement of co-localization of objects in dual-colour confocal images. Journal of Microscopy *169*, 375-382.

Mankodi, A., Takahashi, M.P., Jiang, H., Beck, C.L., Bowers, W.J., Moxley, R.T., Cannon, S.C., and Thornton, C.A. (2002). Expanded CUG repeats trigger aberrant splicing of ClC-1 chloride channel pre-mRNA and hyperexcitability of skeletal muscle in myotonic dystrophy. Mol Cell *10*, 35-44.

Mannella, C.A., Buttle, K., Rath, B.K., and Marko, M. (1998). Electron microscopic tomography of rat-liver mitochondria and their interaction with the endoplasmic reticulum. Biofactors *8*, 225-228.

Manor, U., Bartholomew, S., Golani, G., Christenson, E., Kozlov, M., Higgs, H., Spudich, J., and Lippincott-Schwartz, J. (2015). A mitochondria-anchored isoform of the actin-nucleating spire protein regulates mitochondrial division. Elife *4*.

Marchi, S., Patergnani, S., and Pinton, P. (2014). The endoplasmic reticulum-mitochondria connection: one touch, multiple functions. Biochim Biophys Acta *1837*, 461-469.

Margulis, L. (1971). Symbiosis and evolution. Sci Am *225*, 48-57.

Marine, S., Bahl, A., Ferrer, M., and Buehler, E. (2012). Common seed analysis to identify off-target effects in siRNA screens. J Biomol Screen *17*, 370-378.

Mateos-Aierdi, A.J., Goicoechea, M., Aiastui, A., Fernandez-Torron, R., Garcia-Puga, M., Matheu, A., and Lopez de Munain, A. (2015). Muscle wasting in myotonic dystrophies: a model of premature aging. Front Aging Neurosci *7*, 125.

Mattiazzi Usaj, M., Brloznik, M., Kaferle, P., Zitnik, M., Wolinski, H., Leitner, F., Kohlwein, S.D., Zupan, B., and Petrovic, U. (2015). Genome-Wide Localization Study of Yeast Pex11 Identifies Peroxisome-Mitochondria Interactions through the ERMES Complex. J Mol Biol *427*, 2072-2087.

Michel, A.H., and Kornmann, B. (2012). The ERMES complex and ER-mitochondria connections. Biochem Soc Trans *40*, 445-450.

Misaka, T., Miyashita, T., and Kubo, Y. (2002). Primary structure of a dynamin-related mouse mitochondrial GTPase and its distribution in brain, subcellular localization, and effect on mitochondrial morphology. J Biol Chem *277*, 15834-15842.

Mitra, K. (2013). Mitochondrial fission-fusion as an emerging key regulator of cell proliferation and differentiation. Bioessays *35*, 955-964.

Moffat, J., and Sabatini, D.M. (2006). Building mammalian signalling pathways with RNAi screens. Nat Rev Mol Cell Biol *7*, 177-187.

Morre, D.J., Merritt, W.D., and Lembi, C.A. (1971). Connections between mitochondria and endoplasmic reticulum in rat liver and onion stem. Protoplasma *73*, 43-49.

Mounsey, J.P., John, J.E., 3rd, Helmke, S.M., Bush, E.W., Gilbert, J., Roses, A.D., Perryman, M.B., Jones, L.R., and Moorman, J.R. (2000a).

Phospholemman is a substrate for myotonic dystrophy protein kinase. J Biol Chem *275*, 23362-23367.

Mounsey, J.P., Mistry, D.J., Ai, C.W., Reddy, S., and Moorman, J.R. (2000b). Skeletal muscle sodium channel gating in mice deficient in myotonic dystrophy protein kinase. Hum Mol Genet *9*, 2313-2320.

Muranyi, A., Zhang, R., Liu, F., Hirano, K., Ito, M., Epstein, H.F., and Hartshorne, D.J. (2001). Myotonic dystrophy protein kinase phosphorylates the myosin phosphatase targeting subunit and inhibits myosin phosphatase activity. FEBS Lett *493*, 80-84.

Murley, A., Sarsam, R.D., Toulmay, A., Yamada, J., Prinz, W.A., and Nunnari, J. (2015). Ltc1 is an ER-localized sterol transporter and a component of ER-mitochondria and ER-vacuole contacts. J Cell Biol *209*, 539-548.

Naon, D., and Scorrano, L. (2014). At the right distance: ER-mitochondria juxtaposition in cell life and death. Biochim Biophys Acta *1843*, 2184-2194.

Olichon, A., Baricault, L., Gas, N., Guillou, E., Valette, A., Belenguer, P., and Lenaers, G. (2003). Loss of OPA1 perturbates the mitochondrial inner membrane structure and integrity, leading to cytochrome c release and apoptosis. J Biol Chem *278*, 7743-7746.

Ong, S.B., and Hausenloy, D.J. (2010). Mitochondrial morphology and cardiovascular disease. Cardiovasc Res *88*, 16-29.

Orso, G., Pendin, D., Liu, S., Tosetto, J., Moss, T.J., Faust, J.E., Micaroni, M., Egorova, A., Martinuzzi, A., McNew, J.A.*, et al.* (2009). Homotypic fusion of ER membranes requires the dynamin-like GTPase atlastin. Nature *460*, 978-983.

Oude Ophuis, R.J., Mulders, S.A., van Herpen, R.E., van de Vorstenbosch, R., Wieringa, B., and Wansink, D.G. (2009). DMPK protein isoforms are differentially expressed in myogenic and neural cell lineages. Muscle Nerve *40*, 545-555.

Paddison, P.J., Caudy, A.A., Bernstein, E., Hannon, G.J., and Conklin, D.S. (2002). Short hairpin RNAs (shRNAs) induce sequence-specific silencing in mammalian cells. Genes Dev *16*, 948-958.

Pall, G.S., Johnson, K.J., and Smith, G.L. (2003). Abnormal contractile activity and calcium cycling in cardiac myocytes isolated from DMPK knockout mice. Physiol Genomics *13*, 139-146.

Pan, X., Roberts, P., Chen, Y., Kvam, E., Shulga, N., Huang, K., Lemmon, S., and Goldfarb, D.S. (2000). Nucleus-vacuole junctions in Saccharomyces cerevisiae are formed through the direct interaction of Vac8p with Nvj1p. Mol Biol Cell *11*, 2445-2457.

Park, S.H., Zhu, P.P., Parker, R.L., and Blackstone, C. (2010). Hereditary spastic paraplegia proteins REEP1, spastin, and atlastin-1 coordinate microtubule interactions with the tubular ER network. J Clin Invest *120*, 1097-1110.

Pearce, L.R., Komander, D., and Alessi, D.R. (2010). The nuts and bolts of AGC protein kinases. Nat Rev Mol Cell Biol *11*, 9-22.

Pinton, P., Giorgi, C., and Pandolfi, P.P. (2011). The role of PML in the control of apoptotic cell fate: a new key player at ER-mitochondria sites. Cell Death Differ *18*, 1450-1456.

Poston, C.N., Krishnan, S.C., and Bazemore-Walker, C.R. (2013). In-depth proteomic analysis of mammalian mitochondria-associated membranes (MAM). J Proteomics *79*, 219-230.

Praefcke, G.J., and McMahon, H.T. (2004). The dynamin superfamily: universal membrane tubulation and fission molecules? Nat Rev Mol Cell Biol *5*, 133-147.

Rambold, A.S., Cohen, S., and Lippincott-Schwartz, J. (2015). Fatty acid trafficking in starved cells: regulation by lipid droplet lipolysis, autophagy, and mitochondrial fusion dynamics. Dev Cell *32*, 678-692.

Ranum, L.P., and Day, J.W. (2004). Myotonic dystrophy: RNA pathogenesis comes into focus. Am J Hum Genet *74*, 793-804.

Reddy, S., Smith, D.B., Rich, M.M., Leferovich, J.M., Reilly, P., Davis, B.M., Tran, K., Rayburn, H., Bronson, R., Cros, D.*, et al.* (1996). Mice lacking the myotonic dystrophy protein kinase develop a late onset progressive myopathy. Nat Genet *13*, 325-335.

Rizzuto, R., Pinton, P., Carrington, W., Fay, F.S., Fogarty, K.E., Lifshitz, L.M., Tuft, R.A., and Pozzan, T. (1998). Close contacts with the endoplasmic reticulum as determinants of mitochondrial Ca2+ responses. Science *280*, 1763-1766.

Roberts, R., Timchenko, N.A., Miller, J.W., Reddy, S., Caskey, C.T., Swanson, M.S., and Timchenko, L.T. (1997). Altered phosphorylation and intracellular distribution of a (CUG)n triplet repeat RNA-binding protein in patients with myotonic dystrophy and in myotonin protein kinase knockout mice. Proc Natl Acad Sci U S A *94*, 13221-13226.

Rojo, M., Legros, F., Chateau, D., and Lombes, A. (2002). Membrane topology and mitochondrial targeting of mitofusins, ubiquitous mammalian homologs of the transmembrane GTPase Fzo. J Cell Sci *115*, 1663-1674.

Romeo, V. (2012). Myotonic Dystrophy Type 1 or Steinert's disease. Adv Exp Med Biol *724*, 239-257.

Rusinol, A.E., Cui, Z., Chen, M.H., and Vance, J.E. (1994). A unique mitochondria-associated membrane fraction from rat liver has a high capacity for lipid synthesis and contains pre-Golgi secretory proteins including nascent lipoproteins. J Biol Chem *269*, 27494-27502.

Salinas, S., Proukakis, C., Crosby, A., and Warner, T.T. (2008). Hereditary spastic paraplegia: clinical features and pathogenetic mechanisms. Lancet Neurol *7*, 1127-1138.

Santel, A., Frank, S., Gaume, B., Herrler, M., Youle, R.J., and Fuller, M.T. (2003). Mitofusin-1 protein is a generally expressed mediator of mitochondrial fusion in mammalian cells. J Cell Sci *116*, 2763-2774.

Santel, A., and Fuller, M.T. (2001). Control of mitochondrial morphology by a human mitofusin. J Cell Sci *114*, 867-874.

Satoh, M., Hamamoto, T., Seo, N., Kagawa, Y., and Endo, H. (2003). Differential sublocalization of the dynamin-related protein OPA1 isoforms in mitochondria. Biochem Biophys Res Commun *300*, 482-493.

Saxena, G., Chen, J., and Shalev, A. (2010). Intracellular shuttling and mitochondrial function of thioredoxin-interacting protein. J Biol Chem *285*, 3997-4005.

Schulz, T.A., and Prinz, W.A. (2007). Sterol transport in yeast and the oxysterol binding protein homologue (OSH) family. Biochim Biophys Acta *1771*, 769-780.

Scorrano, L., Oakes, S.A., Opferman, J.T., Cheng, E.H., Sorcinelli, M.D., Pozzan, T., and Korsmeyer, S.J. (2003). BAX and BAK regulation of endoplasmic reticulum Ca2+: a control point for apoptosis. Science *300*, 135-139.

Shariff, A., Kangas, J., Coelho, L.P., Quinn, S., and Murphy, R.F. (2010). Automated image analysis for high-content screening and analysis. J Biomol Screen *15*, 726-734.

Shiao, Y.J., Lupo, G., and Vance, J.E. (1995). Evidence that phosphatidylserine is imported into mitochondria via a mitochondria-associated membrane and that the majority of mitochondrial phosphatidylethanolamine is derived from decarboxylation of phosphatidylserine. J Biol Chem *270*, 11190-11198.

Shibutani, S.T., and Yoshimori, T. (2014). A current perspective of autophagosome biogenesis. Cell Res *24*, 58-68.

Simmen, T., Aslan, J.E., Blagoveshchenskaya, A.D., Thomas, L., Wan, L., Xiang, Y., Feliciangeli, S.F., Hung, C.H., Crump, C.M., and Thomas, G. (2005). PACS-2 controls endoplasmic reticulum-mitochondria communication and Bid-mediated apoptosis. EMBO J *24*, 717-729.

Singh, R., and Cuervo, A.M. (2011). Autophagy in the cellular energetic balance. Cell Metab *13*, 495-504.

Smirnova, E., Griparic, L., Shurland, D.L., and van der Bliek, A.M. (2001). Dynamin-related protein Drp1 is required for mitochondrial division in mammalian cells. Mol Biol Cell *12*, 2245-2256.

Smirnova, E., Shurland, D.L., Ryazantsev, S.N., and van der Bliek, A.M. (1998). A human dynamin-related protein controls the distribution of mitochondria. J Cell Biol *143*, 351-358.

Song, Z., Chen, H., Fiket, M., Alexander, C., and Chan, D.C. (2007). OPA1 processing controls mitochondrial fusion and is regulated by mRNA splicing, membrane potential, and Yme1L. J Cell Biol *178*, 749-755.

Sonnichsen, B., Koski, L.B., Walsh, A., Marschall, P., Neumann, B., Brehm, M., Alleaume, A.M., Artelt, J., Bettencourt, P., Cassin, E.*, et al.* (2005). Full-genome RNAi profiling of early embryogenesis in Caenorhabditis elegans. Nature *434*, 462-469.

Spang, A. (2009). On vesicle formation and tethering in the ER-Golgi shuttle. Curr Opin Cell Biol *21*, 531-536.

Stefan, C.J., Manford, A.G., Baird, D., Yamada-Hanff, J., Mao, Y., and Emr, S.D. (2011). Osh proteins regulate phosphoinositide metabolism at ER-plasma membrane contact sites. Cell *144*, 389-401.

Subramanian, N., Natarajan, K., Clatworthy, M.R., Wang, Z., and Germain, R.N. (2013). The adaptor MAVS promotes NLRP3 mitochondrial localization and inflammasome activation. Cell *153*, 348-361.

Sugiura, A., Nagashima, S., Tokuyama, T., Amo, T., Matsuki, Y., Ishido, S., Kudo, Y., McBride, H.M., Fukuda, T., Matsushita, N.*, et al.* (2013). MITOL regulates endoplasmic reticulum-mitochondria contacts via Mitofusin2. Mol Cell *51*, 20-34.

Tabak, H.F., Hoepfner, D., Zand, A., Geuze, H.J., Braakman, I., and Huynen, M.A. (2006). Formation of peroxisomes: present and past. Biochim Biophys Acta *1763*, 1647-1654.

Terasaki, M., Chen, L.B., and Fujiwara, K. (1986). Microtubules and the endoplasmic reticulum are highly interdependent structures. J Cell Biol *103*, 1557-1568.

Truong, K., and Ikura, M. (2001). The use of FRET imaging microscopy to detect protein-protein interactions and protein conformational changes in vivo. Curr Opin Struct Biol *11*, 573-578.

Ueda, H., Ohno, S., and Kobayashi, T. (2000). Myotonic dystrophy and myotonic dystrophy protein kinase. Prog Histochem Cytochem *35*, 187-251.

Ueda, H., Shimokawa, M., Yamamoto, M., Kameda, N., Mizusawa, H., Baba, T., Terada, N., Fujii, Y., Ohno, S., Ishiura, S.*, et al.* (1999). Decreased expression of myotonic dystrophy protein kinase and disorganization of sarcoplasmic reticulum in skeletal muscle of myotonic dystrophy. J Neurol Sci *162*, 38-50.

Ungermann, C. (2015). vCLAMPs-an intimate link between vacuoles and mitochondria. Curr Opin Cell Biol *35*, 30-36.

van Herpen, R.E., Oude Ophuis, R.J., Wijers, M., Bennink, M.B., van de Loo, F.A., Fransen, J., Wieringa, B., and Wansink, D.G. (2005). Divergent mitochondrial and endoplasmic reticulum association of DMPK splice isoforms depends on unique sequence arrangements in tail anchors. Mol Cell Biol *25*, 1402-1414.

Vance, J.E. (1990). Phospholipid synthesis in a membrane fraction associated with mitochondria. J Biol Chem *265*, 7248-7256.

Vance, J.E. (2008). Phosphatidylserine and phosphatidylethanolamine in mammalian cells: two metabolically related aminophospholipids. J Lipid Res *49*, 1377-1387.

Vance, J.E. (2014). MAM (mitochondria-associated membranes) in mammalian cells: lipids and beyond. Biochim Biophys Acta *1841*, 595-609.

Vance, J.E., and Tasseva, G. (2013). Formation and function of phosphatidylserine and phosphatidylethanolamine in mammalian cells. Biochim Biophys Acta *1831*, 543-554.

Voss, C., Lahiri, S., Young, B.P., Loewen, C.J., and Prinz, W.A. (2012). ER-shaping proteins facilitate lipid exchange between the ER and mitochondria in S. cerevisiae. J Cell Sci *125*, 4791-4799.

Wansink, D.G., van Herpen, R.E., Coerwinkel-Driessen, M.M., Groenen, P.J., Hemmings, B.A., and Wieringa, B. (2003). Alternative splicing controls myotonic dystrophy protein kinase structure, enzymatic activity, and subcellular localization. Mol Cell Biol *23*, 5489-5501.

Wideman, J.G., Gawryluk, R.M., Gray, M.W., and Dacks, J.B. (2013). The ancient and widespread nature of the ER-mitochondria encounter structure. Mol Biol Evol *30*, 2044-2049.

Wieckowski, M.R., Giorgi, C., Lebiedzinska, M., Duszynski, J., and Pinton, P. (2009). Isolation of mitochondria-associated membranes and mitochondria from animal tissues and cells. Nat Protoc *4*, 1582-1590.

Wozniak, M.J., Bola, B., Brownhill, K., Yang, Y.C., Levakova, V., and Allan, V.J. (2009). Role of kinesin-1 and cytoplasmic dynein in endoplasmic reticulum movement in VERO cells. J Cell Sci *122*, 1979-1989.

Yoon, Y., Krueger, E.W., Oswald, B.J., and McNiven, M.A. (2003). The mitochondrial protein hFis1 regulates mitochondrial fission in mammalian cells through an interaction with the dynamin-like protein DLP1. Mol Cell Biol *23*, 5409-5420.

Youle, R.J., and van der Bliek, A.M. (2012). Mitochondrial fission, fusion, and stress. Science *337*, 1062-1065.

Zhang, A., Williamson, C.D., Wong, D.S., Bullough, M.D., Brown, K.J., Hathout, Y., and Colberg-Poley, A.M. (2011). Quantitative proteomic analyses of human cytomegalovirus-induced restructuring of endoplasmic reticulum-mitochondrial contacts at late times of infection. Mol Cell Proteomics *10*, M111 009936.

Zhang, X.D. (2011). Illustration of SSMD, z score, SSMD*, z* score, and t statistic for hit selection in RNAi high-throughput screens. J Biomol Screen *16*, 775-785.

Zhang, X.D., Lacson, R., Yang, R., Marine, S.D., McCampbell, A., Toolan, D.M., Hare, T.R., Kajdas, J., Berger, J.P., Holder, D.J.*, et al.* (2010). The Use of SSMD-Based False Discovery and False Nondiscovery Rates in Genome-Scale RNAi Screens. Journal of Biomolecular Screening *15*, 1123-1131.

Zhao, X., Alvarado, D., Rainier, S., Lemons, R., Hedera, P., Weber, C.H., Tukel, T., Apak, M., Heiman-Patterson, T., Ming, L.*, et al.* (2001). Mutations in a newly identified GTPase gene cause autosomal dominant hereditary spastic paraplegia. Nat Genet *29*, 326-331.

Zhou, R., Yazdi, A.S., Menu, P., and Tschopp, J. (2011). A role for mitochondria in NLRP3 inflammasome activation. Nature *469*, 221-225.

Zhu, P.P., Patterson, A., Stadler, J., Seeburg, D.P., Sheng, M., and Blackstone, C. (2004). Intra- and intermolecular domain interactions of the C-terminal GTPase effector domain of the multimeric dynamin-like GTPase Drp1. J Biol Chem *279*, 35967-35974.

Zorzano, A., Liesa, M., Sebastian, D., Segales, J., and Palacin, M. (2010). Mitochondrial fusion proteins: dual regulators of morphology and metabolism. Semin Cell Dev Biol *21*, 566-574.

Zunino, R., Schauss, A., Rippstein, P., Andrade-Navarro, M., and McBride, H.M. (2007). The SUMO protease SENP5 is required to maintain mitochondrial morphology and function. J Cell Sci *120*, 1178-1188.